POLITECNICO DI MILANO
DEPARTMENT OF ELECTRONICS, INFORMATION AND BIOENGINEERING
DOCTORAL PROGRAMME IN BIOENGINEERING

A FRAMEWORK FOR THE EVALUATION AND IMPROVEMENT OF HUMAN ERGONOMICS IN HUMAN-ROBOT COLLABORATION

Doctoral Dissertation of:
Marta Lorenzini

Supervisor:
Dr. Ajoudani Arash
Prof. De Momi Elena

Tutor:
Prof. Cerveri Pietro

The Chair of the Doctoral Program:
Prof. Aliverti Andrea

2020 - Cycle XXXII

Abstract

WORK-RELATED MUSCULOSKELETAL DISORDERS (WMSDs) are impairments of the human body structures that are provoked or worsened primarily by work and by the effects of the immediate environment in which work is conducted. WMSDs are the leading cause of disability in four of the six World Health Organisation (WHO) regions, with substantial economic costs and a severe impact on the quality of life. The careful monitoring of workers' exposure to the factors which may contribute to their development is of crucial importance in industrial environments, aiming to lay the foundation of risk prevention and reduction programs. Nevertheless, in the brand-new industrial scenario, featured by frequently varying workflows and unstructured work stations, the traditional view of occupational ergonomics is rather weak and barely applicable. In fact, the most widely used tools are still "pen-and-paper" observational approaches, which need to be carried out in an off-line stage. On the other hand, numerous techniques have been proposed by researchers to estimate humans' physical load, relying on direct measurements collected on the human body through sensors devices. But complex laboratory-based approaches are hardly personalisable and impractical for industrial settings. Accordingly, the scientific objective of this thesis is to fill in this gap, by introducing a novel framework for the evaluation and improvement of human ergonomics, which implements online, personalisable, and reconfigurable strategies to account for workers' ergonomic demands.

The proposed framework entails three main components: the observation layer, the warning layer, and the action layer.

Within the observation layer, data about the humans' motion and the interaction forces they exchange with the environment are measured with fit-for-industry sensor devices, and a subject-specific model of the human body is identified. Their integration enables to define and estimate a human ergonomics monitoring system. The latter is a comprehensive set of indexes to assess humans' physical exposure, accounting online for multiple ergonomic risk factors to the development of WMSDs. Both kinematic and dynamic aspects are addressed, taking into account the whole-body human. To validate the proposed monitoring system, an experimental analysis is conducted on twelve subjects considering three different tasks, which represents typical jobs in manufactur-

ing industries and, additionally, are associated with different potential risk factors. As a result, the ergonomic indexes that better explain the physical load required in each analysed activity are established, confirmed by the outcome of a surface electromyography (sEMG) analysis.
The proposed human ergonomics monitoring system will be addressed in Chapter 4.

Within the warning layer, the levels of the ergonomic risk associated with the estimated indexes are determined. Then, by taking advantage of intuitive and practical feedback interfaces (i.e. visual and vibrotactile), this information is conveyed to the workers to improve their risk-awareness. Both the proposed solutions prove their potential in assisting humans in their occupational activities through corrective feedback interfaces.
The two devised feedback strategies will be presented in Chapter 5.

Within the action layer, an optimisation procedure is adopted to estimate a more ergonomic human body configuration by minimising a selected ergonomic index according to certain constraints. Subsequently, a worker can be facilitated to achieve such an optimal condition by following the guidance of a collaborative robot, thus mitigating the effect of the associated risk factor. The experimental investigations conducted to evaluate the performance of this human-robot collaboration (HRC) framework provide evidence of its capability to reduce the effort on human joints, due to the robot reactive behaviour. Such findings are supported by the results of a sEMG analysis. The proposed strategy shows promising capabilities to reduce humans' exposure to the factors that may determine WMSDs, ensuring workers' well being while enforcing productivity. Therewith, its key strength in the applicability to realistic industrial environments is exhibited.
The HRC framework developed will be presented in Chapter 6.

Contents

Acronyms

2D two-dimensional. 20, 56

3D three-dimensional. 24, 25, 26, 28, 29, 36, 105

ACGIH TLV american conference of governmental industrial hygienists - threshold limit values. 13

AnDy advancing anticipatory behaviors in dyadic human-robot collaboration. 21

ANN artificial neural network. 42, 43, 44

AR augmented reality. 103

ASL Azienda Sanitaria Locale. 36, 44, 54, 58, 67, 109, 120, 123, 128

BSIPs body segment inertial parameters. 21, 30, 31, 42, 131

CoM center of mass. IV, 28, 30, 31, 32, 47, 49, 51, 64, 65, 73, 75, 87, 88, 92, 101

CoP centre of pressure. 21, 23, 28, 29, 30, 31, 32, 33, 34, 37, 38, 42, 43, 44, 45, 46, 51, 52, 53, 54, 65, 67, 68, 105, 109, 110, 111, 112, 117, 119, 120, 122, 131, 134

DHM digital human modelling. 14

DoFs degrees of freedom. 16, 18, 27, 30, 31

EAWS ergonomic assessment worksheet. 4, 13, 14, 17, 20, 67, 73, 96, 97, 102, 132, 133, 135

EMA editor for manual work activities. 14, 15

EMG electromyography. 4, 15, 18, 19, 21, 61, 62, 109

EN European Standards. 3, 12, 14, 96, 105

ERC European Research Council. 21

ERM eccentric rotating mass. 109

F/T forque/torque. 66, 70, 88

FDP force distribution problem. 42, 46

GBD Global Burden of Disease. 2

GDP gross domestic product. 2, 3

GRF ground reaction force. 21, 29, 30, 33, 42, 43, 46, 67, 68, 109, 119, 120, 131, 134

GUI graphical user interface. 28, 135

HAMA hand-arm-movement analysis. 12

HRC human-robot collaboration. II, IV, 6, 7, 107, 115, 116, 117, 119, 120, 121, 123, 124, 125, 126, 127, 129, 130, 131, 133, 134, 135, 136

IMUs inertial measurement units. 25, 26

ISO International Organization for Standardization. 3, 12

LWR Lightweight robot. 120, 123

MAC manual handling assessment charts. 13

MET maximum endurance time. 57

MFA muscle fatigue analysis. 12

MOCA MObile Collaborative robotic Assistant. 127, 128, 129, 130, 134

MPF maximum power frequency. 59, 60, 61, 62, 63

MTM-UAS Methods-Time Measurement - Universal Analyzing System. 96, 102

MVC maximum voluntary contraction. 69, 73, 84, 85, 86, 91, 95

NIOSH National Institute for Occupational Safety and Health. 3, 13

OCRA occupational ripetitive actions. 3, 13

OWAS ovako working posture analysing system. 3, 4, 12

PWM pulse-width modulated. 109

QEC quick exposure check. 12, 13

RAMSIS rechnergestütztes anthropmet-risches mathematisches system zur insassen-simulation. 14, 15

REBA rapid entire body assessment. 4, 12, 15, 17, 20

ROM range of motion. 50, 74, 97, 101

ROS Robot Operating System. 105, 133

RSI repetitive strain injury. 71

RULA rapid upper limb assessment. 4, 12, 13, 15, 16, 17, 20

sEMG surface electromyography. II, 18, 19, 58, 59, 61, 63, 68, 73, 99, 100, 101, 121, 123, 132, 134

SESC statically equivalent serial chain. 21, 23, 30, 31, 32, 34, 37, 42, 43, 44, 51, 54, 67, 68, 109, 111, 120, 131

SMEs small and medium enterprises. 5, 133, 134

SOPHIA socio-physical interaction skills for cooperative human-robot systems in agile production. 21

STA soft tissue artifacts. 25, 27, 35

UDP user datagram protocol. 28

USB universal serial bus. 108

vGRF vertical ground reaction force. 23, 32, 33, 37, 51, 52, 53, 54, 68

VIMS virtual interactive musculoskeletal system. 4, 17

VR virtual reality. 103

WHO World Health Organisation. I, 1

WMSDs work-related musculoskeletal disorders. I, II, 1, 2, 3, 5, 9, 12, 19, 22, 47, 51, 58, 59, 64, 67, 107, 131, 132, 135

CHAPTER 1

Introduction

1.1 Work-related Musculoskeletal Disorders

Work-related musculoskeletal disorders (WMSDs) are impairments of the human locomotor system that are provoked or worsened primarily by work and by the effects of the immediate environment in which work is carried out [1]. As listed in the International Classification of Diseases [2], they comprise more than one hundred and fifty diagnoses that affect the human body structures such as muscles, joints, tendons, ligaments, nerves, bones, and the localised blood circulation system. The majority of WMSDs are cumulative disorders, arising from repeated and prolonged exposure to high but also low-intensity loads induced on the body. These entail lifelong conditions and are associated with ongoing pain and disability. However, WMSDs can also refer to acute traumas, such as sprains, fractures and luxations that may occur during an accident and are short-lived. Some WMSDs, such as carpal tunnel syndrome in the wrist, are characterised by well-established signs and specific symptoms. Other ones are not rigorously defined, because only pain or discomfort exists without evidence of clear symptomatology. The body districts main affected by WMSDs are the back, neck, shoulders and upper limbs, but also disorders in the lower limbs have been reported. Musculoskeletal conditions are typically characterised by pain (often persistent) and restrictions in mobility, dexterity and functional ability. They reduce individual's capacity to work and participate in social roles with associated impacts on mental well-being, and, at a broader level, they undermine the prosperity of communities.

Accurate data on the incidence and prevalence of WMSDs are difficult to obtain, and comparing official statistics across countries is quite complex [3]. However, it is widely recognised that musculoskeletal conditions affect people throughout the life-course in all the regions of the world. As a matter of fact, WMSDs were the leading cause of disability in four of the six World Health Organisation (WHO) regions in 2017 (ranked

second in the East Mediterranean Region and third in the African Region) [4]. According to the Global Burden of Disease (GBD), WMSDs account for the 16% of all years lived with disability and between 20% and 33% of people across the globe live with a painful musculoskeletal condition [5]. A recent report from the United States of America suggests that one American adult in two suffers from musculoskeletal pathologies - the same number of people that live with cardiovascular or chronic respiratory diseases combined [6]. On the other hand, conclusions derived from the 4th European Working Conditions Survey [7] state that about 60 million workers reportedly suffer from WMSDs in Europe. In particular, the 80% of the claimed occupational diseases in Italy in 2018 have been located in the industrial sector, with a WMSDs prevalence of about 65% [8].

Table 1.1: *Most cited physical risk factors associated with WMSDs [9–11].*

Risk factor	Occupational task associated	Possible consequences
High-intensity force exertion	Lifting, carrying, pushing, pulling heavy objects	Acute overloading of the musculoskeletal structures
Repetitive and monotonous movements	Painting, carpentry, shoveling, assembly	Accumulation of local muscle fatigue
Recurrent or sustained awkward postures	Working with heavily bent or twisted trunk, or hands and arms above shoulders	Progressive overloading of the musculoskeletal structures
Localised external pressure	Pressing the body or part of the body (such as the hand) against hard or sharp edges	Damages in superficial tissues and loss of sensitivity
Vibrations (both whole-body and hand-arm)	Working with driller or pneumatic hammer; sitting on a tractor or a forklift	Hand arm vibration: loss of sensitivity Whole-body vibration: dorso-lumbar injuries (e.g. hernia)
Temperature	Any type of task	General worsening of working conditions

WMSDs are a cause of concern not only because of the health effects on individual workers but also for the economic impact on businesses and the extremely heavy charge to companies and healthcare systems. The true extent of WMSDs costs within the workplace is difficult to assess and compare due to the different organisation of insurance systems, the lack of standardised assessment criteria and the questionable validity of reported data [12]. However, considering the results of multiple studies, some insights can be provided. The estimated expenditure associated with WMSDs is among the 0.5% and 2% of gross domestic product (GDP) across the European Union, with costs attributed to lost productivity and absences around 240 billion Euros [13]. In the United States, the indirect and direct costs of WMSDs are equivalent to approxi-

mately 1.4% of GDP (213 billion Dollars) [14]. Instead, the direct and indirect costs of WMSDs to the Canadian economy are estimated at 20 billion Dollars [15].

The causes of WMSDs are usually multifactorial and there are numerous well-established work-related risk factors for the various types of musculoskeletal disorders [16]. These include physical and biomechanical factors, organisational and psychosocial factors, individual and personal factors that may act uniquely or in combination. The ones of major interest in the scope of this thesis are the physical and biomechanical risk factors. The most commonly cited ones are presented in Table 1.1 with some examples of the occupational tasks associated and the possible consequences which may arise in their presence [9–11].

1.2 Human Ergonomics Monitoring and Assessment

The accurate monitoring of workers' exposure to the factors which may contribute to the development of WMSDs has been of crucial importance to both epidemiologists and ergonomists conducting research investigations. In parallel, a growing interest in this respect has been shown by ergonomics practitioners, occupational health physicians, employers, employee representatives, and regulating authorities to lay the foundations of risk prevention and reduction programs in the industrial environment. It is nowadays acknowledged that such programs should be grounded upon ergonomics principles and incorporate the holistic evaluation of all the possible aspects of the work system so that optimal solutions can be achieved [17]. Among the issues which should be addressed, task design, worker/equipment interfaces, individual demands (including motivation), training procedures, work schedule/organization, and legal requirements are the most frequently cited [18].

In this context, a significant number of methods and approaches have been developed in the last decade to assess the exposure to the risks associated with WMSDs, or identifying potentially hazardous tasks or risk factors within a job [17, 19]. Focusing on the industrial scenario, the great majority of tools currently adopted to evaluate workers' ergonomics relies on subjective judgements and systematic observations. The first, in the forms of experts' reports and self-questionnaires, have the benefit of being straightforward to use, applicable to a broad range of occupational situations, and can be conducted for extended periods and long duration. However, subjective ratings are vulnerable to numerous influences and multiple studies have shown that they present too low validity and reliability for a throughout ergonomics evaluation. On the other hand, systematic observations are generally recorded and stored on Pro-forma sheets which are filled in by specialists while assessing the workplace. Many of them have been conceived on the basis of the two most widespread normative which address occupational ergonomics, namely, the International Organization for Standardization (ISO) 11228 and the European Standards (EN) 1005. Alongside such normative, several tools and procedures have been proposed by many researchers to address workers' exposure through an observational approach. The vast majority of them though, analyses a particular manual material activity or a single risk factor and such an high specificity extremely limits their applicability: National Institute for Occupational Safety and Health (NIOSH) index - carrying and lifting; Snook and Ciriello tables - pushing and pulling; occupational ripetitive actions (OCRA) index - low loads at high frequency; ovako

working posture analysing system (OWAS), rapid upper limb assessment (RULA) & rapid entire body assessment (REBA) indexes - posture and movements. In addition, it has been demonstrated that the evaluation outcome for the same task using different indexes may be divergent, and sometimes even contradictory due to a lack of precision and reliability. To provide a consistent and exhaustive unique measure of workers' ergonomic risk, the ergonomic assessment worksheet (EAWS) method has been developed. The EAWS includes different sections focusing on all the essential aspects of workplace evaluation whose corresponding results can be easily compared and integrated. Nevertheless, both EAWS and the other indexes mentioned, must be employed as an off-line procedure after collecting observations/recordings on the analysed activities, which is rather time-consuming and does not provide immediate results. Moreover, the underlying analysis can be carried out only by trained experts. For the above reasons, these so-called "pen-and-paper" techniques are suitable for relatively static and steady jobs but may underestimate the ergonomic risk of more dynamically varying and frequently changing activities, which are becoming increasingly widespread in the current industrial scenario.

Seeking to overcome the drawbacks of the observation-based methods, some investigations have been conducted to combine them with measurements directly collected on the human body by using suitable sensor systems. Algorithms for the automatic completion of RULA, REBA, and to some extent EAWS have been proposed, which mostly rely on different technologies that implement motion-capture systems. Such frameworks represent a major improvement w.r.t. the traditional approach for workers' ergonomics evaluation but, still, they largely focus on the kinematic aspects of the activities while underestimating the influence of dynamic variables as interaction forces, which are generally considered as constant throughout the task.

On the other hand, to take into account the contribution of the external interactions, the moments and forces developed within the body due to their effect must be addressed. To this purpose, direct measurements on the subjects are generally integrated with more or fewer complex models of the human body. Several systems have been developed that adopt detailed biomechanical models of the human musculoskeletal structure to estimate the human dynamic states such as joint reactions (forces and torques) by using inverse dynamics and then optimisation techniques to compute the muscle tensions. Some of these algorithms even gave rise to advanced simulation and analysis software including OpenSim, AnyBody, and virtual interactive musculoskeletal system (VIMS), to cite a few. However, the sophisticated models underneath these approaches require the identification of a huge number of musculoskeletal parameters. Otherwise, they can be obtained by means of anthropometric standards and tables thus the achieved dynamic states are not subject-specific. An alternative solution consists in directly measuring muscle activity using EMG and exploiting empirical models to convert such activity into muscle tensions. Nevertheless, even these models incorporate numerous parameters and the use of EMG is accompanied by several issues: the correct placement of the EMG sensors, an ever-present noise affecting the signal, the disturbances caused by adjacent muscles, the relative movement of the electrodes w.r.t. the measured muscle, and finally, the limitation imposed by the number of available EMG channels. Moreover, both the inverse dynamics and EMG-based techniques, again due to their complexity, are quite computationally expensive and this may undermine the

online applicability of most of them.

In general, the methods that integrate direct measurements collected through sensor technologies with systematic observations or human body models allow an accurate and throughout evaluation of human physical load but they happen to be more suitable for analysis and investigations in laboratory settings than for workers' exposure assessment in a real industrial environment.

Despite that, the adoption of sensors to drive and facilitate the evaluation of human ergonomics has proven to have a high potential and should not be disregarded. The primary requirement in this respect is the choice of devices that pose no hindrance to the humans' movements, enabling them to perform their activities without any constraint or discomfort. Hence, the deployment of wearable and lightweight sensor technologies is of crucial importance. Several commercial solutions are available on the market nowadays, which are easy to set up and calibrate, offer a comfortable fit and can be used for prolonged periods (long battery life). Additionally, a number of them feature online capabilities, showing promising possibilities to be employed by human operators in a real workplace.

To sum up, the tools to assess ergonomic risk factors in the brand-new industrial background, should provide quantitative evaluation and anticipation of the human psychophysical conditions and delivered effort across the working activity. This entails the development of modular fit-for-workplaces sensor technologies and online monitoring systems to account for human kinematic but also dynamic states. Such frameworks should address the varying conditions and demands that feature occupational tasks and adapt to the single worker's specific requirements, filling in the gap between the simplistic traditional ergonomics evaluation procedure, non-scalable and insufficient, and the complex laboratory-based techniques, hardly customisable and impractical for industrial settings. In this respect, the development of online, personalisable and comprehensive strategies to account for human physical exposure to WMSDs would be extremely beneficial.

1.3 Human-Robot Collaboration Frameworks for Lean Production and Services Industry

The current industrial scenario is witness to the rise of an ever-growing number of small and medium enterprises (SMEs). To meet the needs of the contemporary market that is increasingly oriented toward mass customisation, SMEs must implement low-volume and high-mix production processes, which thus require to frequently rearrange workstations and re-schedule the activities of the operators. Ensuring that workers follow ergonomics best practices in such contexts is rather challenging and controversial in terms of economic sustainability [20]. In such contexts, in fact, human operators have to perform in, and interact with environments which vary continuously and dynamically. Consequently, they may be exposed to greater hazards in terms of postures and loads, increasing the already alarming statistics on WMSDs [13]. These latest working conditions make the traditional view of occupational ergonomics, in both the design of workplaces and definition of training procedure, less valid and barely applicable [21]. To address human factors in the current industrial scenario, the tools for the online monitoring of workers' ergonomics should be integrated with highly adaptive and easily

re-configurable systems to take preventive action in the mitigation of the identified risk factors, thus accounting for workers' well-being while ensuring productivity. A possible solution to this issue is offered by the so-called human-robot collaboration (HRC) frameworks, which combine humans' expertise, adaptability and problem-solving capacities with robots precision, endurance and power [22, 23]. In the last decade, the design and development of collaborative robots have become an important trend both in academia and in the industry worldwide. HRC technologies perfectly fit the requirements of the so-called Industry 5.0, which will bring the spotlight back on humans, recognising their predominance over robots in the accomplishment of elaborated and skill-demanding occupational activities [24]. Future industries will need to adapt their work schedule and processes so as to ensure stimulating and healthy working conditions. In this perspective, the robot is no more the substituting agent but is a "smart tool" which supports the workers in their duties, empowers their abilities and reduces their physical effort [22]. In this respect, the development of strategies that guarantee safety and effective effort sharing is one of the key factors to be considered [25]. Nevertheless, current HRC systems address the problem of safety by avoiding accidental collisions and impacts [26, 27] or by simply following dedicated guidelines published in international standards such as ISO/TS 15066 to account for certain force, pressure and velocity limits, given the hardware characteristics [28]. On the contrary, without disregarding the safety aspect, the direct effective interaction of the robot with human co-workers should be exploited to provide them with intelligent physical assistance.

1.4 Objectives and Contributions of the Thesis

In light of the above considerations, the foremost goal of this thesis is the development of an online human ergonomics monitoring system, combined with feedback interfaces and assistive robotic strategies to guide and help humans in performing tasks in the most comfortable and ergonomic body configurations to reduce pain and consequent injuries. The main scientific premises that drive the thesis to achieve this goal can be summarised as follows

- P1. To guarantee a safe interaction and context-aware assistance, robots must monitor online humans' motion and the profile of the interaction forces they exchange with each other and the environment.
- P2. These data can be collected using proper sensor systems. Wearable and lightweight technologies are preferable since they do not add constraints on human mobility and are better suited for industrial environments.
- P3. Integrating the gathered data with a human body model, it is possible to estimate the physical exposure of the humans performing their working activities in terms of ergonomic risk factors (e.g. joint overloading, fatigue, compressive forces).
- P4. With the aim to mitigate human physical exposure and consequently reduce the ergonomic risks, collaborative robots and feedback technologies can provide support and assistance to the workers.

Accordingly, the main contributions of this thesis are:

- C1. A human ergonomics monitoring system to evaluate human kino-dynamic states while categorizing related ergonomic risk factors (this contribution has led to the scientific publications [29–32]).
- C2. Feedback interfaces to alert humans about their physical exposure (this contribution has led to the scientific publications [33, 34]).
- C3. A HRC framework to make the robots guide the movements of the humans toward more comfortable and ergonomic body configurations (this contribution has led to the scientific publications [35–37]).

1.5 Overview of the Framework and Thesis Structure

The overview of the proposed framework is represented graphically in Figure 1.1. Three layers can be distinguished which correspond to the three key components of the procedure for assessing and improving human ergonomics: the observation layer, the warning layer, and the action layer.

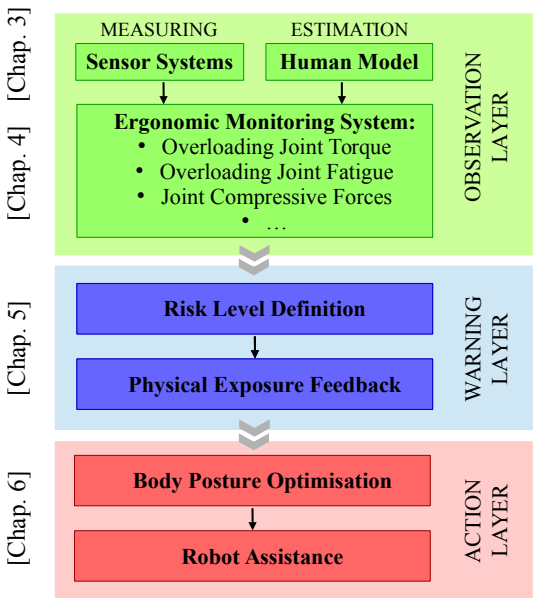

Figure 1.1: *Overview of the proposed framework including the three key components for assessing and improving human ergonomics: the observation layer, the warning layer and the action layer. Each layer will be addressed in a specific Chapter of the thesis as highlighted on the left of the scheme.*

Within the **observation layer**, information about the humans' motion and the forces they exchange with the environment are measured with suitable sensor systems, and a model of the human body is identified. Their integration allows to define and estimate what we refer to as the "ergonomics monitoring system" (C1), namely a comprehensive set of indexes to assess humans' physical exposure during occupational activities which account online for multiple ergonomic risk factors. Both kinematic and dynamic aspects are tackled, taking into account the whole-body. The **warning layer** entails then the definition of the levels of the ergonomic risk associated with the estimated indexes.

Using intuitive and practical feedback interfaces (C2) (e.g. visual and vibrotactile) this information is provided to the humans to alert them about their physical exposure. Finally, a posture optimisation procedure underlies the **action layer**, in which the robot assistance helps humans to reach more ergonomic body configurations to avoid pain and consequent injuries (C3).

Based on this multi-layer structure, this thesis is organised as follows.
In Chapter 2, the state-of-the-art in the monitoring and assessment of human ergonomics in the workplace is presented. In Chapter 3, the sensor technologies to detect human motion and interaction forces profiles are described and the human body model adopted in this thesis is illustrated. Chapter 4 addresses the whole-body online ergonomics monitoring system (observation layer). A detailed explanation of all the indexes defined to assess ergonomic risk factors is provided and, additionally, their validation and comparison with a standard ergonomic tool is outlined. In Chapter 5, two feedback solutions to make humans aware of the level of risk associated with their occupational tasks are introduced (warning layer). Chapter 6 tackles the robotic strategy to guide an individual toward a more ergonomic behaviour determined by a posture optimisation procedure (action layer) with some application scenarios. Finally, Chapter 7 summarises the key points of this thesis highlighting its contribution to the field and discusses future perspectives.

CHAPTER 2

State-of-the-art in Human Ergonomics Monitoring and Assessment

The dramatic health condition of workers employed in manual processing and assembly activities nowadays requires a specific and tailored set of normative and indices to minimise the risks of WMSDs [38]. In contrast with many occupational diseases that have their origin in exposure to particular hazardous agents, most WMSDs are characterised as multifactorial [39]. As already mentioned, findings of scientific research have identified physical, psychosocial/organizational, and individual occupational risk factors, which contribute to the development of WMSDs. Although the importance of workplaces' social and organisational drivers and individual characteristics should not be underestimated, only physical exposure will be addressed here. A range of methods have been developed over the years for the assessment of physical hazards for WMSDs [17] and the objective of this Chapter is to provide an overview of the most widely known and used ones.

The Chapter is organised as follows. Section 2.1 presents the traditional tools used in the industry to assess workers' physical exposure, which mostly rely on observations and subjective judgments. Section 2.2 outlines the more laboratory-based approach to evaluate the physical load by using measurements directly collected on the human body. Section 2.3 introduces some groundbreaking frameworks for WMSDs prevention that attempt to address the needs of the brand-new industrial environment.

2.1 Current Tools in Industry - Subjective and Observational Methods

In one of the earliest studies on the assessment of workload [40], the authors propose that mechanical exposure during physical work should be described by three main dimensions: level/intensity of the force, repetitiveness/frequency of the shifts between

force levels, and duration/time the physical activity is performed. Such dimensions have thereafter established the guidelines for assessing workers' physical effort. However, data should also be recorded for the other important exposure factors, such as postural variation, rate of movement, and vibrations. Adopting the general model proposed in [41], which describes how the working situation induces responses and health effects in the workers, we can distinguish two types of physical exposure: external and internal exposure. The work environment and the actual working method, i.e., the movements and exerted forces that workers with their anthropometrical characteristics exploit to perform a certain activity, are the external exposure. Internal exposure instead refers to the corresponding moments and forces within the human body. On the other hand, earlier reports [39, 40] conventionally categorise the methods to evaluate physical exposure in the following three groups (ordered according to some peculiar features, as represented in Figure 2.1):

- **subjective judgements**: reports from experts or self questionnaires from workers;
- **systematic observations**: collected on-site or afterward from video recordings;
- **direct measurements**: performed at work or during laboratory simulations.

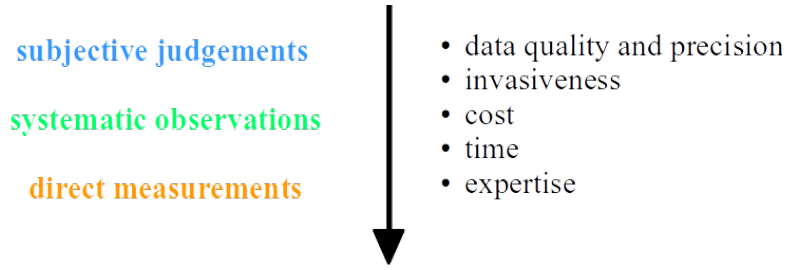

Figure 2.1: *Overview of trade-offs when selecting a method for the assessment of physical exposure.*

Subjective judgements and **systematic observations** are determined to tackle external exposure. The first, in form of experts' reports and self-questionnaire, give only limited insight into the occurrence of tasks and activities. Further information can be obtained from observations, directly on the workplace or at a later stage, analysing video recordings of workers' activities. The vast majority of tools employed in the current industrial scenario to assess workers' ergonomics relies on such two categories that will be covered in the present Section 2.1. A more detailed description will be provided and the methods that they gather will be presented building on some comprehensive reviews [17, 19, 42, 43], in which ergonomics tools were listed, classified, and compared.

On the other hand, **direct measurements** can be employed to estimate both external and internal exposure. In the first case, using mainly motion-capture systems and force sensors, it is possible to obtain large quantities of highly accurate data on a range of exposure variables, which are often combined with observational methods for best results. In the second case, to address internal exposure, direct measurements are generally integrated with more or fewer complex models of the human body. The corresponding category will be addressed in Section 2.2.

Additionally, at the end of the present Section (2.1), a paragraph is dedicated to introducing some examples of commercial software and platforms for the workplace assessment. These platforms basically apply some of the normative and methods presented in this Chapter and provide industries with tools for assessing the ergonomics of their workers as well as other aspects, such as productivity, workplace set-up, and time management.

2.1.1 Subjective Judgements

To assess physical workload, body discomfort, or job stress, it is possible to use self-report methods and collect data directly from the workers, investigating both physical and psychosocial factors. These methods take the form of body map [44] (see Figure 2.2a), rating scales [45, 46] (see Figure 2.2b), questionnaires or interviews [47–50] and checklists [51–54].

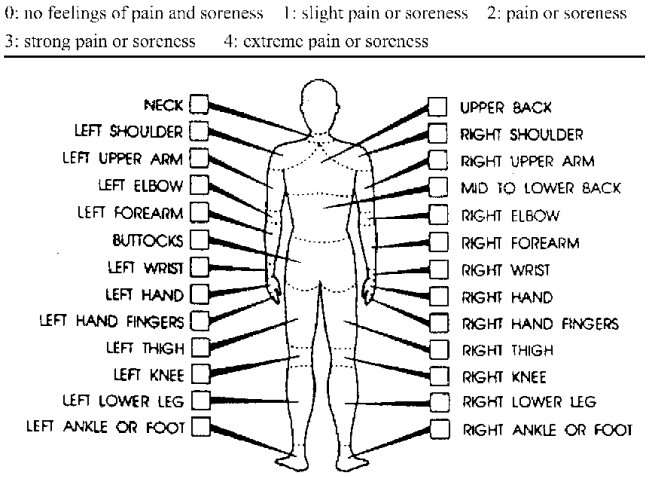

(a)

Rating	Descriptor
0	Rest
1	Very, Very Easy
2	Easy
3	Moderate
4	Somewhat Hard
5	Hard
6	-
7	Very Hard
8	-
9	-
10	Maximal

(b)

Figure 2.2: *(a) Corlett's body map for body map discomfort score [44]. (b) the original Borg CR10 Scale® [46] used to measure the perception of intensity of any experience.*

Almost all the strategies for subjective judgements developed up to now are built on the basis of the above-mentioned earliest attempts. Traditionally, data were collected using written means but more recent innovations include self-evaluations through video film recordings or the use of web-based questionnaires. These tools are important because ergonomists need to concentrate on the feeling of the workers. Some authors even state that "If the person tells you that he/she is loaded and effortful, then he/she is loaded and effortful whatever the behavioural and performance measures may show" [55]. These methods, which are based on subjective judgements, have the benefit of being straightforward to use, applicable to a wide range of work situations, and can be performed for extended periods and long duration. In addition, they are appropriate for surveying great numbers of subjects at comparatively low cost. As a result, the data sets obtained (with multiple subjects and extended recording-time) are rather large, ensuring that the information collected is representative of the occupational groups being investigated. Nevertheless, subjective ratings are vulnerable to many influences and several studies have shown that they have too low validity [56] and reliability [50] in relation to the needs for ergonomic interventions. Moreover, difficulties with self-

reports may arise from varying levels of worker literacy, comprehension, or question interpretation.

2.1.2 Systematic Observations

To systematically record workplace exposure to be assessed by an observer and stored on Pro-forma sheets, several methods have been developed. Most of them have been conceived on the basis of the two most relevant and widespread normative which tackle the ergonomic assessment issue, namely the ISO 11228 and the EN 1005. These norms aim to establish ergonomic recommendations to ensure operators' health. They include different sections, which focus on different aspects of the analysis of manual handling activities. The first section of ISO 11228 (ISO 11228-1) and the second section of EN 1005 (EN 1005-2) attempt to define specific limits for repetitive and non-repetitive manual lifting and carrying of objects whose weight is 3 kg or more, taking into account multiple aspects of the performed task: intensity, frequency, and duration. ISO 11228-2 and EN 1005-3 analyse the impact of pushing and pulling actions on the whole musculoskeletal system aiming to identify potential risks in relation to the weight of the object and the type of tools used. ISO 11228-3 and EN 1005-5 assess the tasks involving low loads that are handled at high frequency. Finally, ISO 11226, which is the extension of ISO 11228, and EN 1005-4 present the guidelines adopted to assess workers' body postures during a manufacturing or an assembly activity.

As stated above, in parallel with these standards, in the last decades many researchers proposed useful tools and approaches to assess the ergonomics of working conditions. The postures and movements of the worker can be carefully evaluated by a bunch of indicators, which cover the whole body both considering the upper and lower limbs as well as the spine, neck and head. Posturegram [57], Posture targeting [58], OWAS [59], RULA [60] (see Figure 2.3a), hand-arm-movement analysis (HAMA) [61], PLIBEL (a method assigned for the identification of ergonomics hazards) [62], quick exposure check (QEC) [63] (see Figure 2.3b and 2.3c) and REBA [64] are pen-and-paper[1] based observational techniques that are mainly posture-based. They are relatively inexpensive to carry out, and the postural assessments can be made in several different workplaces without disrupting the workers. The main issue with these techniques is that the intermittent recording procedures lack precision and thus reliability. Besides, no general guidelines are available to control and evaluate the trade-off between repeated and prolonged exposure and the criteria for determining the optimum number of observations are still unclear. For these reasons, the application of pen-and-paper based observational methods has been restricted to relatively static jobs, where body postures are held for long periods, or the body movement follows a simple pattern that is repeated during work.

Even if work posture is found to be an important factor associated with WMSDs in some body regions, other workplace factors such as load/force, repetition, duration of movement, vibration, and their interaction/combination have to be considered for the physical exposure assessment. Similar to these techniques for posture analysis, there is muscle fatigue analysis (MFA) [65]. In this approach, each body part is scaled into four effort levels according to its working position, but even to the duration of the ef-

[1]These methods are called "pen-and-paper" since they were applied by using written means at the time they were created. However, at present, the electronic version of the worksheets are available for practitioners of ergonomics.

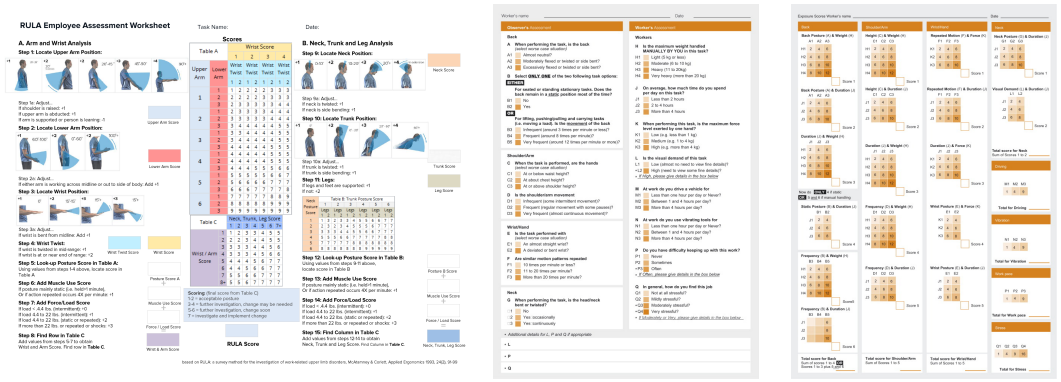

(a) (b) (c)

Figure 2.3: *(a) rapid upper limb assessment (RULA) [60] worksheet and quick exposure check (QEC) [63] assessment form (b) and scoring form (c), respectively.*

fort and the frequency. Considering lifting and carrying loads, NIOSH equations [66] are adopted to define the suggested load weight limit to be lifted by human operators considering the worker gender, the forces exerted on the spine structure and the calories consumed during the effort. Mechanical exposure can then be evaluated with respect to intensity (or magnitude), repetitiveness and duration even with the Strain Index, the american conference of governmental industrial hygienists - threshold limit values (ACGIH TLV) [67], LUBA (an assessment technique for postural loading on the upper body based on joint motion discomfort and maximum holding time) [68] and manual handling assessment charts (MAC) [69]. Snook and Ciriello [70] proposed a detailed procedure to assess the exerted force to perform pushing and pulling activities taking into account the weight of the handled object, the frequency, and duration of the action as well as the actual distance of pushing and pulling. Finally, there are methods that focus on the evaluation of actions performed at high frequency with low loads and consider even the recover time like OCRA, a concise index for the assessment of exposure to repetitive movements of the upper limb [71]. Although these indices are more comprehensive and have been widely adopted both by practitioners and researchers, they present several limitations. First, it has been demonstrated that the evaluation results for the same task using different indices are divergent, and sometimes even contradictory because of a lack of precision and reliability. Second, subjective variability can influence the evaluation results, even when using the same observational method for the same task. Finally, they do not provide a consistent and overall measure of the ergonomic risk. In fact, every index focuses on a specific manual material activity, despite an operator generally performs multiple activity types during a shift or a cycle time. In view of this, the EAWS method [72] has been developed to provide a unique and exhaustive ergonomic analysis. The EAWS is made of four different sections (see Figure 2.4) that focus on each specific aspect of manual material activities. Specifically, the sections cover: postures and movements, action forces, manual material handling, and upper limb, respectively. A great strength of this approach is the comparability of the results of each section and the possibility to integrate their outcomes. This enables a comprehensive risk evaluation that includes every biomechanical risk to which an operator may be exposed during a working task. In fact, EAWS provides one score for each section and also a final score can be computed, which summarises the analy-

sis outcomes. Such scores are all shown in a traffic light scheme (green, yellow, red) according to Machinery Directive 2006/42/EC (EN 614), making their interpretation straightforward and easy to use.

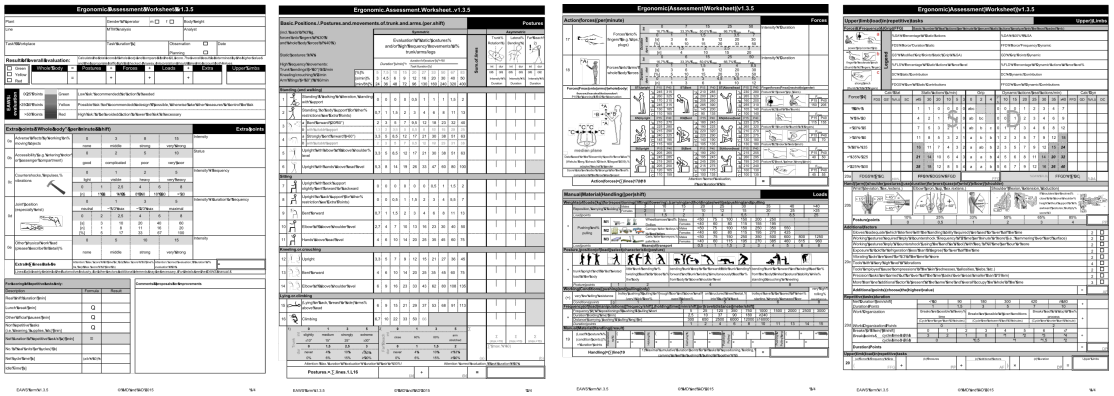

Figure 2.4: *EAWS sections: section 0 - header/overall evaluation/extra points, section 1 - posture and movements, section 2 and 3 - action forces/manual material handling, section 4 - upper limbs.*

Nevertheless, both EAWS and the other indexes mentioned, must be employed as an off-line procedure after collecting observations/recordings on the analysed activities (or when performing simulations of the workplace), which is rather time-consuming and does not provide immediate results. Furthermore, the dynamic aspects of the tasks are considered to a limited extent (e.g., interaction forces are considered constant throughout the task). Finally, all the required analyses can be carried out only by trained experts.

2.1.3 Commercial Software for Ergonomics Assessment

There is a significant number of software and platforms that provide the industries with tools for assessing the ergonomics of their workers as well as other aspects, namely, productivity, workplace set-up, and time management. Two categories of software can be distinguished:

1. **Software for simulations:** editor for manual work activities (EMA), digital human modelling (DHM) in production ergonomics (Human builder, Jack, rechnergestütztes anthropmet-risches mathematisches system zur insassensimulation (RAMSIS) which translates as computer-aided anthropometrical mathematical system for occupant simulation);

2. **Software for direct assessment of real workplace:** ErgoPlus, HumanTech, Kinetica Labs, Cority, ErgoWeb, ScaleFit;

3. **Software with both possibilities**: MTM-Ergonomics, NextGen Ergonomics.

On the other hand, the above-mentioned software can be distinguished on the basis of their capability to address kinetic and dynamic aspects of workers' activities and to be applied online in the workplace or as an off-line procedure. The categorisation made accordingly is represented in Figure 2.5.

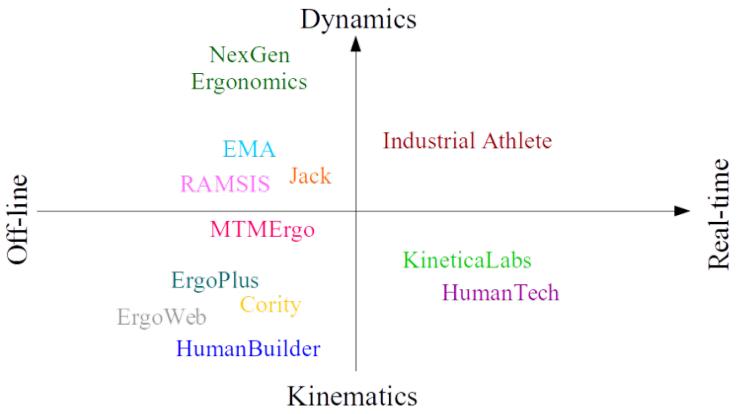

Figure 2.5: *Overview of the available commercial software for ergonomics assessment categorised on the basis of their capabilities.*

Ergoplus, ErgoWeb, HumanBuilder and Cority provide ergonomics evaluations with traditional tools (such as REBA and RULA), which are based on human kinematics only. EMA, RAMSIS, Jack, and MTM-Ergonomics offer the possibility to take into account in the evaluation procedure weights and forces applied during the workers' activities (thus also dynamic aspects). However, they all need the user to specify such weights/forces manually, which are then considered to be constant throughout the whole task. Finally, NextGen Ergonomics includes measurements with EMG sensors and force sensors, thus, it considers the actual interaction forces exerted during a task. Nevertheless, all these software conduct ergonomics analysis in an off-line phase on the basis of recorded data or by means of their companies' support team observations. Only Kinetica Labs and HumanTech present a more straightforward approach: they allow the user to collect data with the video camera of any mobile device and they perform ergonomics evaluations in few minutes thanks to a sensor-less video-based motion-capture system. But this is not still an online evaluation and the estimated kinematic and kinematic variables are not accurate.

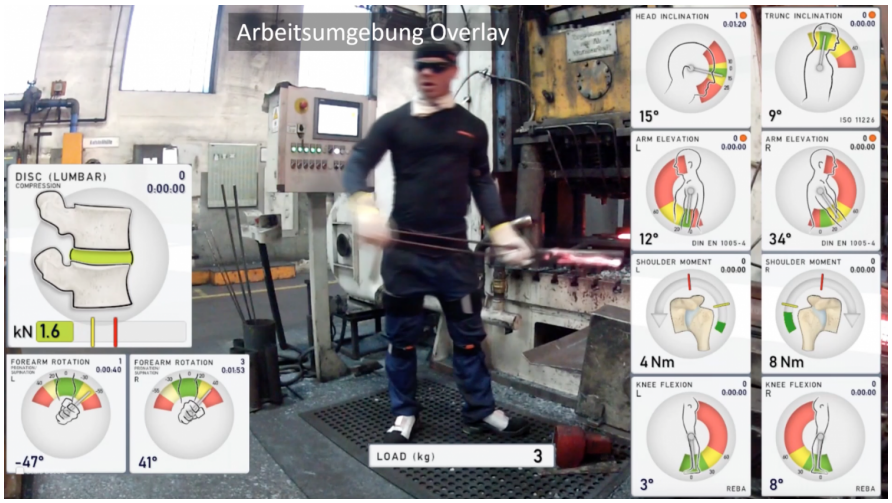

Figure 2.6: *Snapshot of Industrial Athlete software, provided by ScaleFit.*

Only the recently-introduced software Industrial Athlete, provided by ScaleFit (see Figure 2.6), offers an online workplace analysis on-site conducting ergonomic assessments according to international standards and considering also the monitoring of loads and forces involved in the working tasks. Notwithstanding this, there is a lack of tools that offer an online ergonomics evaluation considering even interaction forces exerted during occupational activities. However, several researches are currently investigating in this direction.

2.2 Laboratory-based Approaches - using Direct Measurements

With the objective to facilitate the assessment of exposure variables in the workplace, in the last decade, an extensive number of researchers have focused their effort in developing techniques relying on sensor systems that directly collect measurements on the human body. As mentioned at the beginning of Section 2.1, direct measurements can be employed to both tackle external and internal physical exposure. In this Section, some cases in point of research studies conducted to this end will be presented.

2.2.1 Direct Measurement for External Exposure

To monitor humans' physical external exposure, as defined in Section 2.1, several investigations have been carried out in which mainly motion-capture data are successfully combined with observational methods (described in Section 2.1).

In [73], the authors first employ a magnetic motion-capture technology to evaluate by means of the RULA method the activities that an operator perform in a virtual environment. A similar investigation is conducted in [74] but replacing the magnetic technology with a marker-based optical system. By using instead inertial sensors, a biomechanical model of the upper body is developed in [75] (see Figure 2.7a), to enable the real-time ergonomic assessment of manual tasks in an industrial environment. A major

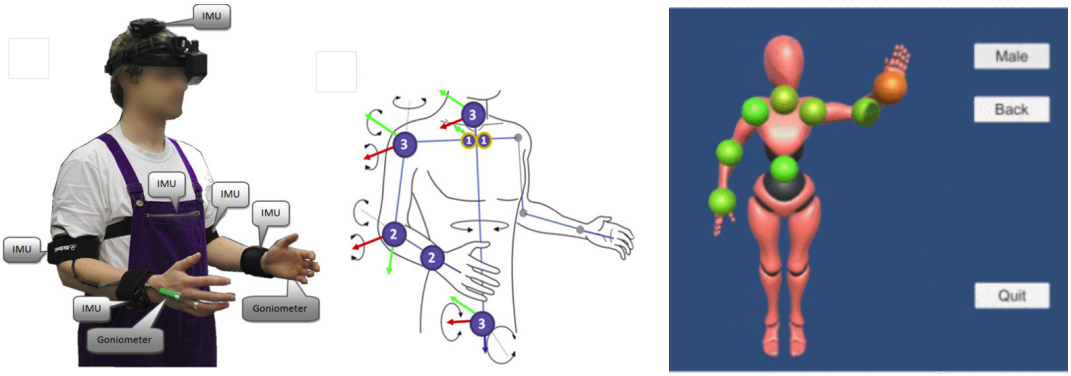

(a) (b)

Figure 2.7: *(a) On-body sensor network employed in [75] composed of inertial sensors coupled with goniometers (left) and underlying biomechanical model of the upper body (right) with rotation axes for local body frames, and degrees of freedom (DoFs) of each joint. (b) Screenshots of the graphical interface developed in [76] to alert the user about the level of risk of the body posture according to REBA scoring.*

improvement in this direction is constituted by the introduction of optical marker-less

motion-capture systems, due to their reduce cost, ease of use and the absence of cumbersome suits and markers. A range camera is employed in [77] for human posture analysis and ergonomic categorisation. The low-cost and portable Kinect camera was used in [78] for assessing assembly operations and in [79] for lifting/lowering tasks. This last study provides also the validation of a skeleton data correction, comparing the postures detected by Kinect with ground-truth data. All the above-mentioned studies implement ergonomic assessment using RULA but alternative tools have been proposed in combination with direct measurements. In [76] the REBA worksheet is filled in automatically and online by taking advantage of an optical marker-based motion-capture. A graphical interface was also developed here (see figure 2.7b) to inform the user about the ergonomics evaluation results. The REBA is also considered in [80], to determine the optimal posture of the human during a human-robot collaborative task.

Alternatively, the EAWS method is adopted in [38] to provide the automatic assessment of the ergonomic risk in manual manufacturing and assembly activities employing a network of marker-less depth cameras. The automatic completion of the EAWS is also the objective of the authors in [81], which develop an activity recognition algorithm based on supervised learning.

All the frameworks just introduced represent a significant improvement with respect to the traditional approach for workers' ergonomics evaluation since they offer the possibility to automatize and perform online the procedure described in Section 2.1. Nevertheless, such methodologies are rather detailed and complex thus their computerised version may be susceptible to errors. Furthermore, as previously said, they largely focus on the kinematic aspects of the tasks while underestimating the influence of dynamic variables as interaction forces, which are generally considered as constant throughout the task.

2.2.2 Direct Measurement for Internal Exposure

To address humans' physical internal exposure, namely, the moments and forces developed within the body while performing a task, direct measurements are generally integrated with more or fewer complex models of the human body.

Several algorithms have been proposed for estimating muscle tensions and joint loads using detailed models of the musculoskeletal system. One of the most well-know is the algorithm underlying the open-source software "OpenSim" [82] (see Figure 2.8a). This platform allows to create dynamic simulations of movement that integrates off-the-shelf models describing the anatomy and physiology of the elements of the neuromusculoskeletal system and the mechanics of multi-joint movement. Consequently, it provides the estimation of meaningful variables such as muscle and joint forces, which are difficult to be measured experimentally. Similar capabilities are offered by the simulation software "Anybody" [83], which is capable of analysing the musculoskeletal architecture of humans or other animals as rigid-body systems. Hence, standard methods of multi-body dynamics (i.e. inverse kinematics and inverse dynamics) can be applied but integrating in the model reasonable representation of the muscle geometry and the recruitment pattern of the muscles. Both OpenSim and AnyBody can be fed with recordings of the human movements as well as contact forces which are collected while performing activities that require to be analysed. An analogous package is VIMS [84].

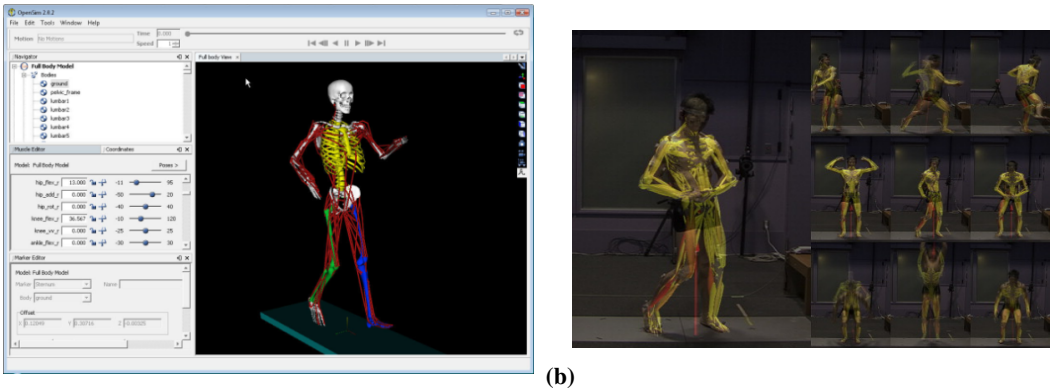

(a) (b)

Figure 2.8: *(a) Snapshot of the open-source software OpenSim [82] (b) Visual feedback presented to the user during real-time estimation and visualization of muscle tensions in [85].*

Besides the massive studies behind the development of these platforms, there are also some minor works in which muscle models are proposed to account for physical exposure. In [86], an approach to compute musculoskeletal loading is presented to predict both synergistic and antagonistic muscle activity. In [87], three different musculotendon models are introduced and compared to simulate musculotendon dynamics. Muscle energy consumption is instead tackled in [88] using a phenomenological model in conjunction with a simple Hill-type [89] model for muscle contraction. In [90], algorithms developed in robotics for multi-body systems are exploited to address human somatosensory information using a motion-capture system. Finally, a model of the lower limb is developed in [91] to study the influence of bi-articular muscles on the force distribution and joint loads during walking, using optoelectronic motion tracking.

All the above-mentioned platforms and methodologies account for joint reactions (forces and torques) by using inverse dynamics and then optimisation techniques to compute the muscle tensions. Nevertheless, due to the actuation redundancy (the number of muscles is greater than the number of degrees of freedom (DoFs) of the system) a desired motion in terms of joint torques can be achieved by an infinite number of activation patterns of the muscles. It is therefore impossible to obtain precise muscle tension information only from motion data. Another drawback is that the complex musculoskeletel models underlying require the identification of a large number of parameters [92]. Alternatively, they can be obtained by means of anthropometric standards and tables [93, 94] thus they are not subject-specific.

An alternative solution is to directly measure muscle activation using EMG and exploit empirical models [89, 95] to convert such activation into muscle tensions. Some emblematic examples follows.
The long-term monitoring of low back physical exposure and cumulative compression by using an EMG-based technique is tackled in [96]. In [97], EMG measured in the back and shoulders is evaluated as an indicator of peak and cumulative workload. In addition, its relationship with injury indicators and other workload measurements is explored. In [98], muscle force and joint load are estimated specifically for the knee using a EMG-driven approach while the lumbar spine is addressed in [99]. sEMG is employed as stand alone acquisition tool for ergonomic purposes in [100]. Finally, muscle tension estimation by means of optical motion-capture and EMG measurements

is enriched with a visual feedback interface (see Figure 2.8b) in [85], where a musculoskeletal human model overlays the images recorded from a standard video camera.

Nevertheless, even EMG-based approaches incorporate numerous parameters and the use of EMG presents several drawbacks. Firstly, correct placement of the EMG sensors is quite difficult. Secondly, EMG signals, especially those obtained by non-invasive sEMG measurements, are inevitably affected by various noise signals or artifacts [101] and often mixed up with disturbances from other muscles. Thirdly, the relative movement of the electrodes with respect to the measured muscle during the sEMG measurements in dynamic conditions makes their estimates questionable and may lead to incorrect conclusions [102]. In addition, EMG information are strictly limited by the number of available EMG channels and finally, many EMG-based approaches are conceived for specific body parts.

Furthermore, again due to their complexity, both inverse dynamics and EMG-based techniques are rather computationally expensive and this affects the online capabilities of most of them.

To sum up Section 2.2, several sensor technologies can be used to collect direct measurements on the human body to be integrated with observational methods or human body models aiming to assess physical exposure. However, when considering this approach some disadvantages must be taken into account. Firstly, the attachment of sensors directly to the subject may result in discomfort and possibly lead to changes or even limitations in workers' behaviour. Secondly, the high data generation capacity of many of these systems may be considered impractical by several practitioners due to the time required for the analysis and interpretation of the data. In addition, direct measurement systems require a considerable initial investment to purchase the equipment, as well as the resources necessary to cover the costs of maintenance and employment. Finally, highly trained and skilled technical staff is needed to ensure their effective operation. In conclusion, they look more suitable for analysis and investigations in laboratory settings than for workers' activities assessment in an industrial environment.

Despite that, the adoption of sensors to drive and facilitate the evaluation of human ergonomics has proven to have a high potential and should not be disregarded.

2.3 The need for Online, Personalisable, and Flexible Technologies

Today's manufacturing industries must meet the demands of the contemporary market, and fulfill its customisation needs with high-mix low-volume production processes [103]. Subsequently, industrial procedures must adapt to constantly varying workflows, which require the workers to frequently change tasks and switch between different work stations. In such dynamically changing environments, the workers may be exposed to greater ergonomic risks in terms of body postures and load, threatening to raise the already alarming incidence of WMSDs [13]. In such a context, the traditional view of occupational ergonomics to ensure workers' well-being is less valid and hardly applicable [21]. As previously discussed, the vast majority of tools employed in the current industrial scenario to account for workers' exposure relies on pen-and-paper based techniques. Besides their electronic versions are available, these methods require complex and time-consuming procedures, which can be implemented only off-line at a later stage. Moreover, only trained specialists can carry out the analysis. Different

strategies have been proposed by the research community, addressing the automatic completion of a portion of these worksheets (i.e. RULA, REBA and EAWS). However, to our knowledge, these solutions are still confined to laboratory settings. Furthermore, it should be reminded that, in general, the dynamic aspects of workers' task execution (e.g. complex physical interactions) are underestimated by such observational techniques. With the view to overcoming this limitation, the integration of measurements collected directly on the workers with human body models represents a promising perspective. However, finding the best trade-off in terms of the human model complexity as well as the suitable number, cost, and invasiveness of the sensor systems is a challenging task. Moreover, anatomic model-based approaches usually make use of human anthropometric standards and tables thus they are not subject-specific and are characterized by a high level of uncertainty.

In the brand-new industrial background, the tools to evaluate human physical exposure should entail modular fit-for-workplaces sensor technologies and online human kino-dynamic states monitoring systems. Such frameworks should address the varying activities involved in the working process and adapt to an individual's specific demands, filling in the gap between the simplistic traditional ergonomics monitoring, non-scalable and insufficient, and the complex laboratory-based approaches, hardly customisable and impractical for industrial settings. For these reasons, many researches have recently focused their effort on developing online, personalisable and comprehensive strategies to account for human physical ergonomic risk factors. Some promising examples of these innovative approaches are introduced hereafter.

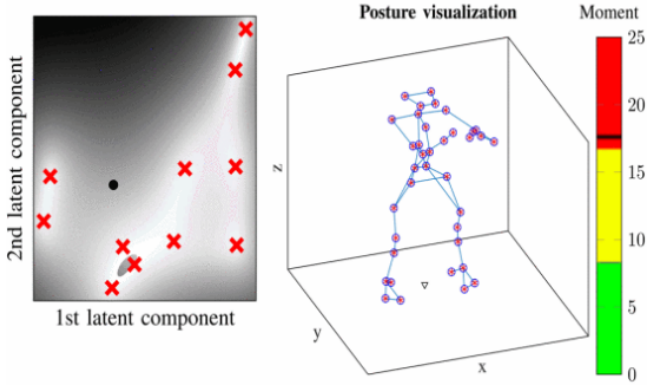

(a)

Indicator definition	Equation
Joint normalized position (RA, LA, B, L)	$\frac{1}{N_j}\sum_{i=1}^{N_j}\left(\frac{q_i - q_i^{neutral}}{q_i^{max} - q_i^{neutral}}\right)^2$
Joint normalized torque (RA, LA, B, L)	$\frac{1}{N_j}\sum_{i=1}^{N_j}\left(\frac{\tau_i}{\tau_i^{max}(t)}\right)^2$
Joint velocity (RA, LA, B, L)	$\frac{1}{N_j}\sum_{i=1}^{N_j}\dot{q}_i^2$
Joint acceleration (RA, LA, B, L)	$\frac{1}{N_j}\sum_{i=1}^{N_j}\ddot{q}_i^2$
Joint power (RA, LA, B, L)	$\frac{1}{N_j}\sum_{i=1}^{N_j}\mid \dot{q}_i\,\tau_i \mid$
Kinetic energy	$\frac{1}{2}\boldsymbol{\nu}^T M \boldsymbol{\nu}$
Velocity transmission ratio (right hand, left hand)	$\left[\mathbf{u}^T (J M^{-1} L^2 M^{-1} J^T)^{-1}\mathbf{u}\right]^{\frac{1}{2}}$
Force transmission ratio (right hand, left hand)	$\left[\mathbf{u}^T (J M^{-1} L^{-2} M^{-1} J^T)\mathbf{u}\right]^{\frac{1}{2}}$
Head dexterity	$\frac{\sigma_{min}}{\sigma_{max}}$
Balance stability margin	$\frac{1}{N_b}\sum_{i=1}^{N_b} d_i^2$
Dynamic balance	$\frac{\|\mathbf{v}_{CoP}\|}{d}$

(b)

Figure 2.9: *(a) Latent space representation for a 2D task (a plane) with eleven data point inputs shown as red crosses, these are the simulated values from a musculoskeletal model with Anybody [83]. On the right, a visualization of the posture associated with the latent point, shown as a black dot on the left figure, and the corresponding max joint moment on the color bar as a line. [104] (b) Ergonomic indicators for evaluating biomechanical demands in manual activities in [105] (find here the details of the equations).*

In [104], the authors propose the optimisation of "contextual ergonomics models" to successfully reduce the muscle activation of subjects performing a drilling task. The presented models are gaussian process latent variable models, which are trained off-line with detailed musculoskeletal simulations but can be employed in a low-dimensional

latent space (see Figure 2.9a), ensuring online capabilities. Multiple ergonomic indicators are defined in [105] (see Figure 2.9b), which are capable of quantifying exhaustively and concisely the physical demands endured by a worker when executing various manual activities. The objective here is to orient the design of a collaborative robot but the proposed set of variables, due to their ease of computation, may be employed to implement an online ergonomics assessment. These approaches tackle exhaustively both the kinematic and dynamic aspects of the workers' activities and can operate online with practical sensor systems but still lack a fundamental aspect, which is the ability to include subject-specific features. In fact, the development of personalisable human models has been the topic of recent European projects such as H2020 socio-physical interaction skills for cooperative human-robot systems in agile production (SOPHIA) [106] and the European Research Council (ERC) project Ergo-Lean [107], where this thesis have directly contributed to. These two projects aim to create new human-state monitoring frameworks (e.g., see [31,32,108]) that are capable of estimating human kino-dynamic states during work. In another European project, advancing anticipatory behaviors in dyadic human-robot collaboration (AnDy) [109], a novel sensor suit called AnDySuit, has been developed, capable of measuring online human whole-body dynamics. The big data sets collected with the AnDySuit can be used to generate ergonomic and anticipatory models which are then employed online by collaborative robots to adapt their control, ensuring a more efficient and ergonomic interaction. In particular, the control framework introduced in [110], proposed a method to link ergonomics targets such as muscular effort and body posture to human kinematic and dynamic quantities such as joint torque and joint angles/velocities. The approach of employing the principles of humanoid robotics to model human kinematics, dynamics and effort shows promising opportunities for humans' physical exposure assessment. In fact, the computational cost would be significantly lower than the one characterising detailed musculoskeletal models, ensuring online[2] capabilities. Furthermore, the sensor systems required to address the human kino-dynamic states in this view can be limited to light-weight and wearable devices for motion-capture and force detection since there is no need for high accuracy. Impractical acquisitions using EMG sensors can be avoided as well.

With the purpose to pursue this idea, a novel technique for the online estimation of the joint torque variations in humans is introduced in [108] (which has been the theoretical departure point of this thesis). The method is based on the deviations of the centre of pressure (CoP) and ground reaction force (GRF) in the presence of an external load applied on the human body and provides an intuitive and easy to use index for human physical load while performing quasi-static heavy manipulation tasks. The statically equivalent serial chain (SESC) technique is employed here to obtain the CoP estimation, which provides the identification of subject-specific body segment inertial parameters (BSIPs), tailoring the estimated quantities and thus accounting for workers' individual features. In a later work [31], the cumulative effect of joints overloading is addressed aiming at the evaluation of joint fatigue during repetitive activities in which, instead, light payloads are involved. Since only the effect of the external load has been tackled so far, this thesis, above all, will focus on integrating the above-mentioned

[2]It is worth to remind here that the term "online" is different from "real-time". The latter enforces limits on time latency that can be ensured only following specific technological requirements while the first simply means that responses are given in a timely manner, without timely relationship enforcing them.

estimators in a comprehensive set of indexes which takes into account the multiple ergonomic risk factors to the development of WMSDs.

CHAPTER 3

Material and Methods

In this Chapter, the materials and methods adopted in this thesis are presented. Section 3.1 addresses the sensor technologies selected to collect data about human motion and the interaction forces he/she exchanges with the environment. In Section 3.2, the human modeling bases are addressed. It is important to underline here that all the models and methods employed in this thesis have been conceived in view of their application and usage in an industrial environment. Hence, they are aimed at a simplified - not simplistic - approach that focuses on fast identifiability of the models and online capabilities of the methods, respectively. The solutions proposed here were built starting from the development of the overloading joint torque index proposed in [108], which will be discussed in detail in Section 4.2. Its computation required a model of the human whole-body CoP and the knowledge of the contact point of the external load applied on the human body, which causes the joint overburden. Based on that, Section 3.2 is organised as follows. First, the simplified model used to represent the human biomechanical structure as a multi-body system is described. Next, the SESC technique [111] to obtain a reduced-complexity model of the whole-body CoP is introduced. In addition, two approaches to extend the human model are proposed: an online method to detect and locate the application point of the external load and a learning technique to estimate the human feet vertical ground reaction force (vGRF) and CoP to encompass the double-support. For the latter two approaches, also an experimental validation is provided. [1]

[1] Parts of this Chapter have been published in [29, 32]

3.1 Human Tracking Tools: Wearable and Lightweight Sensor Systems

To monitor workers' physical exposure during their occupational activities, the use of wearable and lightweight sensor technologies is of crucial importance. Wearable systems, in fact, pose no hindrance to the humans' movements, allowing them to carry out their tasks without any constraints or discomfort. Furthermore, unlike laboratory-based equipment that demands a dedicated controlled area, wearable sensors can be used in most environments. They are easily transportable, usually not requiring any stationary units (e.g. transmitter, receiver, or cameras) [112], and they can be used for prolonged periods of time (long battery life). Additionally, they are, in general, easy to set up, calibrate and use, and do not require highly skilled operators. Finally, it is worthwhile to mention within the aim of this thesis that a number of them feature online capabilities.

The sensor systems adopted for the purposes of this thesis are:

- An inertial-based motion-capture suit, the Xsens MVN Biomech suit, commercialised by Xsens Technologies B.V. (headquarters: Enschede, Netherlands);
- a Kistler force plate, commercialised by Kistler Holding AG (headquarters: Winterthur, Switzerland);
- the OpenGo sensor insoles, commercialised by Moticon GmbH (headquarters: Munich, Germany);

While the Xsens suit and the Moticon insoles have been selected in view of the above considerations, the Kistler force plate is employed for validation purposes (a deeper discussion will follow in this Section). A brief description of these devices, illustrating their main features and highlighting their merits, follows in this Section.

3.1.1 Motion-capture Suit

The measurement of the human whole-body motion is achieved using the Xsens MVN Biomech suit [113]. This motion-capture system is based on inertial sensors located on the human body, which measure the acceleration, velocity, and magnetic field of the body segments on three orthogonal axes. These data are then processed to obtain a reasonable representation of the human movements and postures [114].

Extensive literature exists that reviews and compares different motion-capture technologies [115, 116], even specifically in the field of robotics [117] and occupational ergonomics [118]. The most common alternative to inertial devices for the monitoring of human motion is offered by the optical motion-capture systems. This technology utilises data that is captured from image sensors to triangulate the three-dimensional (3D) position of a subject between two or more cameras, calibrated to provide overlapping projections. Marker-based technologies (e.g. Optitrack™by NaturalPoint Inc., Vicon by Vicon Motion Systems Ltd) exploit active or passive markers displaced in specific parts of the human body. They can reach a high level of accuracy but their set-up is rather complex and time-consuming. In addition, the markers must be mounted on cumbersome suits or directly on the body thus becoming uncomfortable and even constrictive for the user. This major drawback is overcome by the latest advance in motion-capture, namely marker-less optical systems (using e.g. Kinect by Microsoft,

RealSense™by Intel®, Roboception by Roboception GmbH), which frees the operator to perform his activities without wearing any suit nor having sensors located on the body. Nevertheless, this technology relies on the images collected by depth cameras that are processed by computer vision algorithms which, despite becoming increasingly sophisticated over time, still present a limited accuracy. Moreover, optical systems in general suffer from visibility issues due to the occlusions and the limited range of cameras. As a result, inertial motion-capture seems to be the best solution to be adopted in real industrial environments. Specifically, the Xsens suit can be employed in a broad variety of scenarios, just ensuring to remain within the range of the wireless network. The users are not forced to limit their movements to a specific measurement volume and it is not necessary to place or install any fixed infrastructure. The set-up of the system, including calibration, is in fact very fast (less than 10 minutes) and rather easy to deploy. However, a disadvantage of this technology is that it does not ensure an accurate absolute position of the limbs due to a positional drift which compounds over the recording time.

In addition, it is worth mentioning one of the main contemporary issues in 3D motion analysis, which affects all the technologies just described, now commonly referred to as the soft tissue artifacts (STA). The marker/sensors whose recorded trajectories are used to reconstruct the human motion are placed directly on the skin or on a dedicated suit. Due to the interposed soft tissues or the movement of the suit w.r.t. the body, they are not rigidly fixed to the underlying bones. Hence, the local mobility of these markers/sensors leads to errors that, in some cases, are of the same order of magnitude as the motions at the joints being investigated [119].

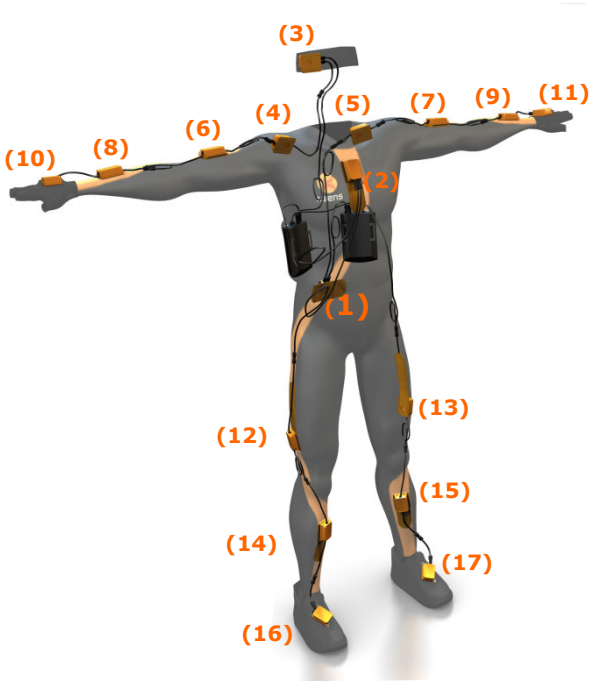

Figure 3.1: *Wearable lycra suit provided by Xsens embedding seventeen IMUs with their relative labels [120]. Also mounting straps are available as the mounting system to support the sensors, keeping the same locations on the body. In this thesis, this second option has been mainly used for greater practicality.*

Going into details, the MVN Biomech suit, depicted in Figure 3.1, is provided with seventeen miniature inertial measurement units (IMUs) called MTx/MTw. IMUs integrates rate gyroscopes to measure 3D angular velocities, accelerometers to measure 3D accelerations (including gravity), magnetometers to measure 3D earth magnetic field, as well as atmospheric pressure using a barometer. Both a lycra suit or mounting straps are available as mounting system to support the sensors (MTx and MTw respectively). While MTx require a cable system, MTw are wireless trackers (see Figure 3.2). In this thesis, the second option (involving MTw) has been mainly used for greater practicality. The specifications about MTw are listed in Table 3.1.

Table 3.1: *Xsens IMUs specifications [120]*

Specification	Numerical Value
Sampling rate[2]	1000 Hz
Operating Voltage	4.5 – 30 V
Power consumption	350 mW
Operating temperature range	$-40 to + 85$ °C
Gyroscopes bias stability	20 deg/h
Timing accuracy	10 $10^{-6} s$
Static accuracy (roll/pitch)	< 0.5 deg
Static accuracy (heading)	< 1 deg
Dynamic accuracy	2 deg RMSE
Angular resolution	0.05 deg

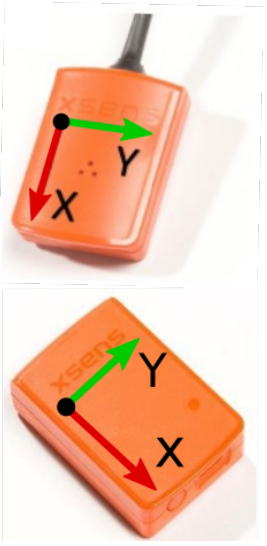

	Link	*IMUs*
Trunk	*Pelvis*	(1)
	L5	
	L3	
	T12	
	T8	(2)
Head	*Neck*	
	Head	(3)
Arm	*Shoulder*	(4)-(5)
	UpperArm	(6)-(7)
	ForeArm	(8)-(9)
	Hand	(10)-(11)
Leg	*UpperLeg*	(12)-(13)
	LowerLeg	(14)-(15)
	Foot	(16)-(17)
	Toe	

Figure 3.2: *On the left, Xsens IMUs are shown: MTx on the top and MTw on the bottom respectively. The table on the right depicts the set of links for human model with the relative parent joints and associated sensors.*

The system runs in real-time with a maximum update rate of 240 Hz for MTx and 60 Hz for MTw, respectively. In order to estimate the variations of the body links orientation and position, gyroscope and accelerometer signals are continuously updated and

[2]Maximum IMUs update rate depends on amount of IMUs used.

integrated within a biomechanical model of the human body (detailed information can be found in [120]). The Xsens human model includes twenty-three segments (pelvis, L5, L3, T12, T8, neck, head, and right and left shoulder, upper arms, fore arms, hands, upper legs, lower legs, feet and toes) linked together by twenty-two joints with three DoFs. The seventeen IMUs are attached to such body segments as indicated in the Table on the right of Figure 3.2. The origins of the joints are defined in the centre of the functional axes with the directions of the $x-y-z$ axes being related to functional movements (see the left side of Figure 3.3).

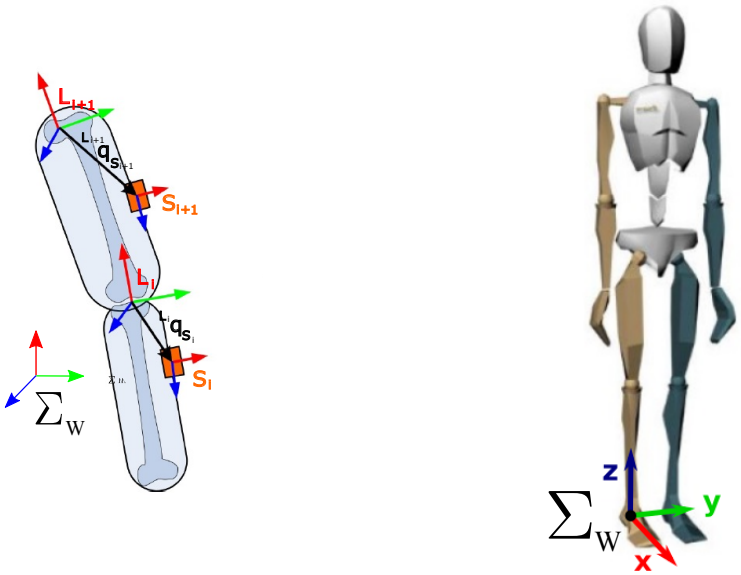

Figure 3.3: *On the left, orientation and position of the sensors w.r.t. the link frames. S_i is the sensor frame, L_i is the link frame, ${}^{L_i}q_{S_i}$ is the quaternion that express the transformation between the sensor and the link. [113] On the right, Xsens model of a subject performing N-pose. The global frame Σ_W is also highlighted. [120]*

When a sensor is attached to the human body, the initial transformation between the sensor and the body segment on which is located is unknown. Moreover, assessing the distances between body segments by numerical integrating the accelerations is pretty difficult. To tackle this issue and express the body segment kinematics in a global frame, a calibration procedure must be performed. During this process, the orientation of the sensors w.r.t. the segments (see the left side of Figure 3.3) and the relative distances between joints in a-priori known body configuration are determined. The subject must keep this configuration, called N-pose, depicted on the right side of Figure 3.3, during the whole calibration phase. After the calibration procedure, all the sensors' positions and orientations can be estimated by integrating the gyroscope data and double integrating the accelerometer data in time. Then, to achieve six full DoFs tracking of the subject, the information coming from the sensors is translated to body segments using the above-mentioned biomechanical model and the sensor pose w.r.t. the body segment, found in the calibration step. It should be pointed out that the uncertainty of the joint position and rotation increase throughout time, due to the sensor noise related to skin and STA. However, the resulting error is compensated by using the joint measurement updates, exploiting the knowledge that two segments are on average connected but with

statistical uncertainty. In addition, a Kalman filter is used to correct the kinematics for both the drift and the uncertainty of the joint position. Summing up, the Xsens MVN Biomech suit provides the 3D position, velocity, acceleration, orientation, angular velocity, and angular acceleration of all the twenty-three body segments w.r.t. a global (earth-fixed) coordinate system Σ_W[3] (illustrated in Figure 3.3). Then, the Euler angles ZXY (flexion/extension, abduction/adduction, internal/external rotation) are extracted for all the twenty-two joints. Additionally, the positions and the trajectories of some points of interest, the anatomical landmarks, are provided in the links frames. These points are not measured directly as in traditional optical motion-capture systems but estimated by using the measured segment kinematics in combination with the anatomical model. The center of mass (CoM) 3D position is also computed, based on the segment poses together with a body mass distribution model. The software provided with the system, MVN Studio is an easy-to-use graphical user interface (GUI) and allows the visualization of the subject movements in real-time and from previous recordings. Data streaming through user datagram protocol (UDP) connection is also available.

3.1.2 Force Sensors

To measure the reaction forces that the human exchanges with the ground and to compute the position of the human CoP, suitable instrumentation for collecting force/pressure data is required. In this thesis, two alternative devices have been adopted for this purpose: a force plate and sensor insoles.

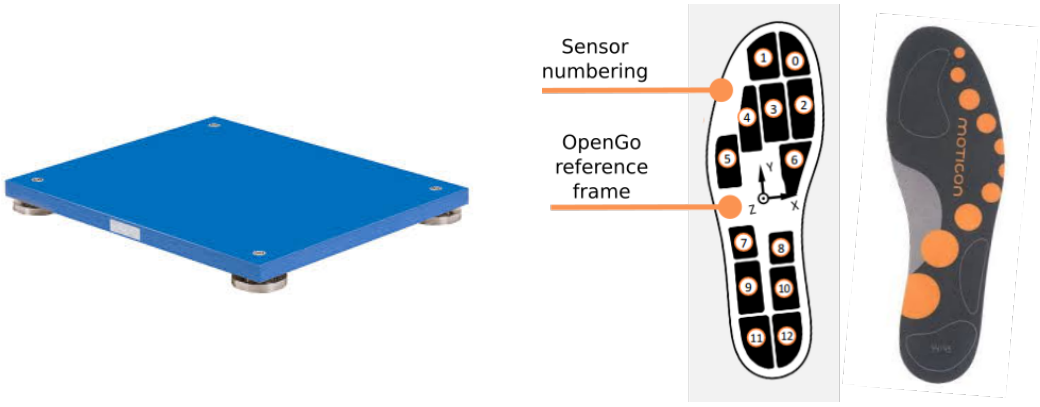

Figure 3.4: *Kistler multicomponent force plate Type 9260AA (left) and OpenGo sensor insoles (right).*

The force plate is a Kistler multicomponent force plate Type 9260AA and is depicted on the left of Figure 3.4. The corresponding specifications are listed in Table 3.2. This device is designed specifically for use in gait and balance analysis. Rather than having to be mounted on a frame like conventional force plates, it can simply be used on a flat surface and, due to its low weight, it is easily portable. Hence, it has the benefit of being conveniently relocated in different places within the experimental area or even moved to different experimental areas. Despite the very wide measuring range (see Table 3.2), the Kistler force plate ensures a high accuracy and linearity over the entire spectrum of applications and guarantees overload protection both for static

[3]The Xsens suit global frame Σ_W is adopted as the human model global frame which will be defined in Section 3.2.1.

Table 3.2: *Kistler force plate specifications [121]*

Specification	Variable	Numerical Value
Natural frequency	$f_n(x, y)$	≈ 400 Hz
	$f_n(z)$	≈ 200 Hz
Dimensions		$600 \times 500 \times 50$ mm
Measuring range	F_x, F_y	$-2.5 \dots 2.5$ kN
	F_z	$0 \dots 5$ kN
Overload	F_x, F_y	$-3/3$ kN
	F_z	$0/8$ kN
Linearity	% FSO	$< \pm 0.5$
Hysteresis	% FSO	< 0.5
Crosstalk	$F_x <-> F_y$	$< \pm 2.5$ %
	$F_x, F_y -> F_z$	$< \pm 2.5$ %
	$F_z -> F_x, F_y$	$< \pm 0.5$ %
Max CoP error	a_x	≈ 2 mm
	a_y	≈ 2 mm
Operating temperature range		$10 \dots 50$ °C
Weight		8.6 kg

and impulse loads. These last two features in particular, make this force plate a reliable mean to obtain a ground truth for the human GRF and CoP. In fact, within this thesis it is mainly used when a new proposed method must be assessed and validated. Nevertheless, force platforms severely reduce human mobility by its very definition. Therefore, once a properly validated technique requires to be applied in real industrial environments, alternative solutions are needed.

To this end, the OpenGo fully integrated sensor insoles by Moticon GmbH have been considered in this thesis. The corresponding pressure sensor specifications are listed in Table 3.3. These insoles measure the plantar pressure distribution, total loads,

Table 3.3: *OpenGo sensor insoles specifications.*

Specification	Value
Principle	capacitive
Quantity	13 sensors per insole
Coverage	≈ 50 %
Range	$0.0 - 40.0$ N/cm^2
Output resolution	7 bit
Sampling frequency[4]	$5, 10, 25, 50, 100$ Hz

and acceleration of the foot. The CoP and the total force are not provided directly but they can be calculated based on the sensor data. OpenGo are easily wearable (they have to be placed inside the shoes) and completely wireless thus they do not impose any restriction on the wearers' mobility. As shown in Figure 3.4, thirteen capacitive pressure sensing pads are included in the devices, along with a 3D accelerometer. To improve the reliability of the information measured, a supplementary mechanical part has been developed [34], consisting of a thin and flexible surface placed as an additional attachment on the top of the OpenGo. The designed part presents some protuberances

[4]OpenGo sampling rate depends on the amount of sensing pads used.

on the lower surface that match the centres of the capacitive pressure sensing pads, enabling a more effective distribution of the user body weight over the insole. This expedient allows increasing significantly the accuracy of the measured data.

It should be noted that, using OpenGo sensor insoles, it is possible to achieve only the single foot CoP. Then, the whole-body CoP vector $\mathbf{C}_P = [C_{Px} \quad C_{Py}]^T \in \mathbb{R}^2$ in the global frame (which will be defined in Section 3.2.1) can be calculated as

$$\mathbf{C}_P = \frac{f_L \cdot \mathbf{C}_{P,L} + f_R \cdot \mathbf{C}_{P,R}}{f_L + f_R}, \tag{3.1}$$

where f_L and f_R are the GRF of left and right foot, respectively and $\mathbf{C}_{P,L}$ and $\mathbf{C}_{P,R}$ are the CoP of left and right foot, respectively, transformed from their local frame and expressed in the global frame.

3.2 Human Dynamic Modeling Bases

In this Section, the human modeling basis on which this thesis is grounded and developed are addressed.

3.2.1 Human Body Model

As illustrated in Fig. 3.5, the human body in this thesis is modelled as a floating-based sequence of rigid links interconnected by revolute joints. The pelvis frame is set as the human base frame Σ_0 and it is attached to the inertial frame Σ_W, which represents the global frame, through six virtual DoFs. Each link has a mass, m_i, (with link index $i \in [1 \quad \cdots \quad n_i]$) and the total mass M is represented by the sum of the link masses, i.e., $M = \sum m_i$. $\boldsymbol{x_0} \in \mathbb{R}^3$ and $\boldsymbol{\theta}_0 \in \mathbb{R}^3$ are the position and the orientation of the base frame Σ_0, respectively. The position vector of the CoM for each link, $\boldsymbol{c}_i \in \mathbb{R}^3$, is represented w.r.t. the local frame Σ_i. $\boldsymbol{d_i} \in \mathbb{R}^3$ is the link length vector w.r.t. the previously connected link local frame Σ_{i-1}. The rigid links are articulated through n_j revolute joints, and the angular position of those joints is denoted as $\boldsymbol{q}_h = [q_1 \quad \dots \quad q_{n_j}]^T \in \mathbb{R}^{n_j}$. The generalized coordinate of the system is defined by $\boldsymbol{q} = [\boldsymbol{x}_0^T \quad \boldsymbol{\theta}_0^T \quad \boldsymbol{q}_h]$.

3.2.2 Whole-Body Centre of Pressure Model

The traditional approach to estimate the CoM of the human body consists in measuring the subjects' pose and making use of the anthropometric heuristic data [93,94] proposed in the literature to approximate the mass and composition of each limb. Nevertheless, the information in these anthropometric tables was compiled for a given population thus it does not accurately represent any individual. Age, gender and fitness level may affect the error of the CoM estimation [122]. A methodology for the real-time identification of the full BSIPs from motion and contact force was proposed in [123], which addresses subject-specific parameters. Alternatively, a reduce-complexity approach, called the SESC technique, was introduced in [111] to obtain the human BSIPs based on the work in [124]. The SESC parameters can then be employed to achieve a subject-specific estimation of the whole-body CoM. As a result, the whole-body CoP estimation can thus be accomplished, both in static and dynamic conditions.

It has been proved in [111] that the whole-body CoM position of any branched chain (e.g. the human body with arms and legs) is equivalent to the end-effector position of

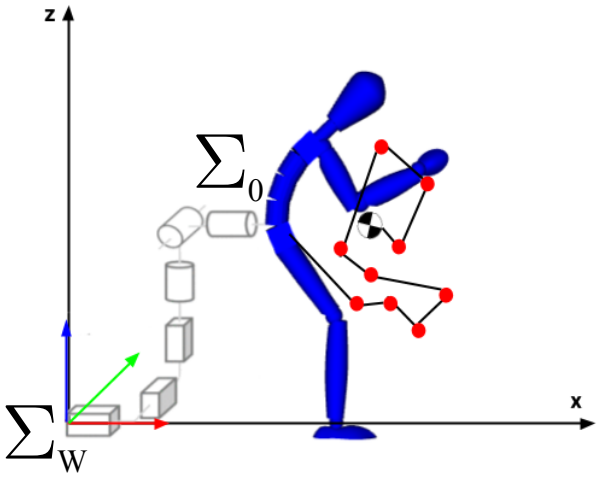

Figure 3.5: *A sagittal floating-base model of the human body. The SESC to estimate the CoM position is attached to the base frame Σ_0 and represented by a red and black dot-dash chain with the computed CoM. The transformation from the inertial frame Σ_W to the base frame Σ_0 with six virtual DoFs is depicted as well.*

a virtual chain known as the SESC. Its structure can be set up by using the static and geometric parameters (i.e. mass, length and CoM of each link) of the original chain as

$$\boldsymbol{\phi}_i = \frac{1}{M}\left[m_i \mathbf{c}_i + \sum^{n_i}\left(\mathbf{d}_{i+1}\sum_{l=i}^{L} m_l\right)\right]. \tag{3.2}$$

where n_i is the number of local frame and L is the last local frame in each branch. As a result, the CoM of the original structure in the global frame Σ_W, denoted as $\mathbf{C}_M$, can be obtained through a forward kinematics operation and modelled as

$$\mathbf{C}_M = \mathbf{x}_0 + \mathbf{B}\boldsymbol{\Phi}, \tag{3.3}$$

where $\mathbf{x}_0$, as previously said, is the position of Σ_0, matrix $\mathbf{B} = \begin{bmatrix}\mathbf{A}_0 & \cdots & \mathbf{A}_n\end{bmatrix} \in \mathbb{R}^{3\times 3(n+1)}$ contains i-th link rotation matrices $\mathbf{A}_i \in SO(3)$ w.r.t. Σ_W. Matrix $\boldsymbol{\Phi} = \begin{bmatrix}\boldsymbol{\phi}_0^T & \cdots & \boldsymbol{\phi}_n^T\end{bmatrix}^T \in \mathbb{R}^{3(n+1)}$ includes the vector of SESC parameters $\boldsymbol{\phi}_i \in \mathbb{R}^3$, which refers to the unknown BSIPs of the human.

The identification of the parameter vector $\boldsymbol{\Phi}$ can be accomplished by writing Equation 3.3 in a regressor form as

$${}^0\mathbf{C}_M = \mathbf{C}_M - \mathbf{x}_0 = \mathbf{B}\boldsymbol{\Phi}, \tag{3.4}$$

where ${}^0\mathbf{C}_M$ is the CoM represented in Σ_0. The rotation matrices in $\mathbf{B}$ and the human base frame position vector $\mathbf{x}_0$ are achieved, in this thesis, by means of the motion-capture system outlined in Subsection 3.1.1. On the other hand, the CoM vector cannot be collected directly from any sensor technology. However, it is possible to obtain the ground-projected CoM, which corresponds to the CoP in the static condition, using measuring instruments for the ground reaction forces. Therefore, the whole-body CoP vector $\mathbf{C}_P = \begin{bmatrix}C_{P|x} & C_{P|y}\end{bmatrix}^T \in \mathbb{R}^2$ w.r.t. the Σ_W is achieved using the devices introduced in Subsection 3.1.2.

Expressed as in 3.4, the identification of the SESC parameters can be considered as a classical least-squares problem and it can be solved using the stacked matrices $\mathbf{B}$ and vectors ${}^{0}\mathbf{C}_{P}$ (the CoP represented in Σ_0.) for a set of p human poses defined as $\mathbf{W} \in \mathbb{R}^{2p\times 3(n+1)}$ and $\mathbf{\Omega} \in \mathbb{R}^{2p\times 1}$, respectively. The vector of the identified $\hat{\mathbf{\Phi}} \in \mathbb{R}^{3(n+1)}$ can then be estimated as

$$\hat{\mathbf{\Phi}} = \mathbf{W}^{+}\mathbf{\Omega}, \tag{3.5}$$

where $\mathbf{W}^{+} = \left(\mathbf{W}^{T}\mathbf{W}\right)^{-1}\mathbf{W}^{T}$ is the Moore-Penrose generalised inverse.

In static conditions, the CoP can be computed by projecting the whole-body CoM estimated by (3.3) with the identified SESC parameters (3.5) onto the x-y plane. Conversely, when considering dynamic conditions, the position of CoP w.r.t. the CoM can be obtained by using the differences between the angular momentum variations and the acceleration about the CoM [93, 125]. However, given that the angular momentum of the CoM is negligible for a rotationally stable body resting on a flat ground surface, we can obtain the estimated CoP vector $\hat{\mathbf{C}}_P$ on the contact surface as

$$\hat{\mathbf{C}}_P = \begin{bmatrix} \hat{C}_{P|x} \\ \hat{C}_{P|y} \end{bmatrix} = \begin{bmatrix} \hat{C}_{M|x} \\ \hat{C}_{M|y} \end{bmatrix} - \frac{\hat{C}_{M|z}}{\ddot{\hat{C}}_{M|z} + g} \begin{bmatrix} \ddot{\hat{C}}_{M|x} \\ \ddot{\hat{C}}_{M|y} \end{bmatrix}, \tag{3.6}$$

where g is gravitational constant, $\hat{\mathbf{C}}_M$ is the estimated CoM vector from the SESC, and $\ddot{\hat{C}}_{M|x}$, $\ddot{\hat{C}}_{M|y}$ and $\ddot{\hat{C}}_{M|z}$ are the linear accelerations of the CoM. Hence, to estimate the CoP of the human body, the second derivative of the CoM vector and g alone can be considered. Additionally, the Kalman filtering approach can be used to compute the acceleration of the CoM vector [126].

It should be noted that the SESC technique reaches an accuracy of the CoM estimation comparable to the one achieved by the classical models that are based on articulated chains [122, 127]. Furthermore, since it is based on a geometrical reconstruction of the CoM, the observability of the CoM position is complete [128]. Finally, a great strength of this method is that, due to its principled simplification approach, it can be applied online [129].

3.2.3 External Load Localisation

In [32], a novel method to detect and locate the contact point of an external load applied on the human body was introduced. The proposed technique relies on a torque equilibrium condition on the human sagittal plane, which involves a whole-body CoP model, identified by using the SESC method described in Subsection 3.2.2, along with the measured CoP and the vGRF. A statistical analysis approach is then integrated in the procedure to increase the accuracy of the estimation (affected by sensor noise and uncertainties in the model) to the extent required for industrial applications. The contact point localisation capability of the proposed approach is tested through a simulation study using Simscape Multibody™. Then, an experimental analysis is conducted on two human subjects to investigate its performance in realistic settings, considering three different application points of a load applied on the participants' body.

Contact Point Localisation Method

To achieve the contact point location of an external load applied on the human body, it is possible to consider a torque equilibrium condition, which can be approximated

by an equivalent mechanical system performing quasi-static movements. Assuming a generic force vector $\mathbf{F}$ that acts on a rigid body system, the result of the interaction is the joint torque vector $\mathbf{T}$ defined as

$$\mathbf{T} = \mathbf{x}_p \times \mathbf{F}, \tag{3.7}$$

where $\mathbf{x}_p$ represents the contact point vector. In case of multiple interaction forces, several torques act on the body simultaneously. If the body stays at rest, it means that such torques are balanced and there is no net torque ($\mathbf{T}_{net} = 0$) acting on the body which thus is said to be in an equilibrium condition. Considering likewise the

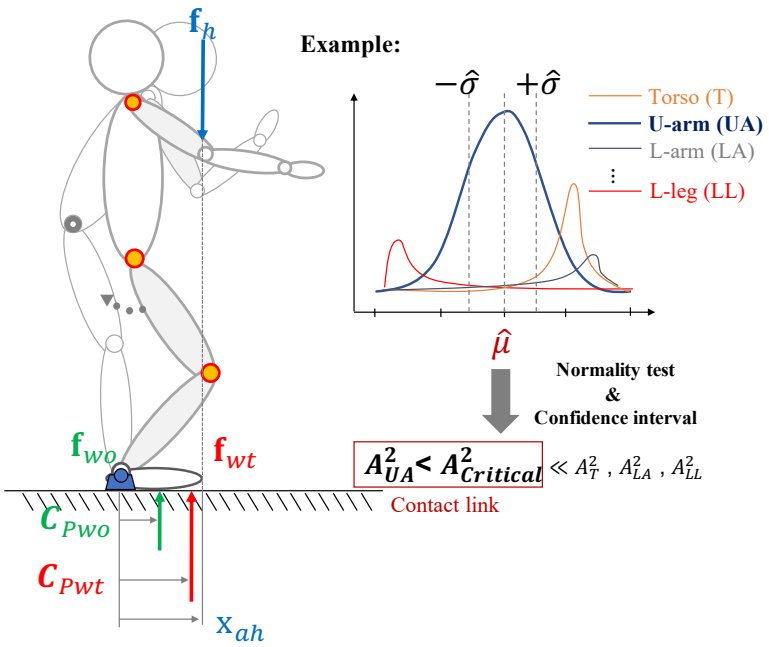

Figure 3.6: *The overall procedure to detect the contact point combining a torque equilibrium condition and statistical analysis approach.*

interaction forces acting on the body on the left side of Figure 3.6, a torque is produced by an external load and the equilibrium condition can be described as

$$\mathbf{C}_{P_{wt}} \times \mathbf{f}_{wt} = \mathbf{C}_{P_{wo}} \times \mathbf{f}_{wo} - \mathbf{x}_{a_h} \times \mathbf{f}_h, \tag{3.8}$$

where $\mathbf{C}_{P_{wt}}$ and $\mathbf{C}_{P_{wo}}$ are the body CoP in the loaded and not loaded condition, respectively. $\mathbf{f}_{wt}$ is the vGRF vector applied at $\mathbf{C}_{P_{wt}}$, which is obtained by the sum of the body weight and the external load, while $\mathbf{f}_{wo}$ represents the body weight alone. $\mathbf{f}_h$ refers then to the load that is applied at the contact point $\mathbf{x}_{a_h}$. By making the assumption of a single load applied on the body thus a unique contact point, the latter can be defined as $\mathbf{f}_h = -(\mathbf{f}_{wt} - \mathbf{f}_{wo})$. Taking into account that on a flat surface - that commonly characterises industrial work spaces - the vGRF is substantially higher than the tangential components of the GRF, such components can be neglected and the vGRF can then be expressed by the human body weight, which is acting on the projected CoP position [130]. Therefore, by projecting all the forces onto the ground, the equilibrium equation of the torques about a pivot (i.e. ankle joint) for the human in the sagittal

plane, can be written as

$$\mathrm{x}_{a_h|x} = \frac{C_{P_{wt}|x}\mathbf{f}_{wt} - C_{P_{wo}|x}\mathbf{f}_{wo}}{(\mathbf{f}_{wt} - \mathbf{f}_{wo})}, \tag{3.9}$$

where $\mathrm{x}_{a_h|x}$ is the x-coordinate of the application point of the external load (i.e. contact point). The whole-body CoP vector $\mathbf{C}_{P_{wo}}$ is obtained with the SESC technique presented in Subsection 3.2.2 while the CoP vector $\mathbf{C}_{P_{wt}}$ can be measured by using a suitable sensor system (see Subsection 3.1.2).

At this point, the location of the contact point must be determined. First, the link which includes the contact point must be identified. Next, the position of the contact point on such a link must be estimated. The procedure employed in this study will be presented hereafter and the corresponding pseudocode is illustrated in algorithm 1.

Algorithm 1 Detection of contact point position.

procedure CONTACTPOINT($\mathrm{x}_{a_h|x}$)
  Initialize: $n^j \leftarrow 0,\ j = 1, \ldots, k$
    $N \leftarrow 0$
  while true **do**
    for $j = 1 \rightarrow k$ **do**
      $\mathrm{x}^j_{a_h|y} \leftarrow \pi_\perp(\mathrm{x}_{a_h|x}) \cap \overbrace{link}^{j}$ ▷ *compute the intersection*
      if $\mathrm{x}^j_{a_h|y} \neq 0$ **then**
        $\mathrm{X}^j_{a_h}[n^j] \leftarrow {}^{link}\mathrm{x}^j_{a_h,i}$
        $n^j \leftarrow n^j + 1$
      $\hat{\mu}^j \leftarrow \textsc{Mean}(\mathrm{X}^j_{a_h})$ ▷ *compute the sample mean*
      $\hat{\sigma}^j \leftarrow \textsc{Std}(\mathrm{X}^j_{a_h})$ ▷ *compute the sample standard deviation*
      if $n^j > 50$ **then**
        $A^{2,j} \leftarrow$ using (3.12)
        if $A^{2,j} < A^2_{critical}$ **then** ▷ *contact point link found*
          $N \leftarrow j$
    if $N \neq 0$ **then**
      $\delta^N_m \leftarrow$ using (3.13)
      if $\delta^N_m < \delta_{m,threshold}$ **then** ▷ *contact point position found*
        break
  return $\hat{\mu}_N$

First of all, the algorithm starts establishing whether it exists the point of intersection between $\pi_\perp(\mathrm{x}_{a_h|x})$, which is the perpendicular line passing through $\mathrm{x}_{a_h|x}$, and a j-th link segment $\overbrace{link}^{j}$ (with link index $j \in [1 \quad \cdots \quad k]$). It should be noted that it is possible to find multiple candidates for the load application point on y-axis ($\mathrm{x}_{a_h|y}$), in the event that the perpendicular line $\pi_\perp(\mathrm{x}_{a_h|x})$ intersects along its path more than one link. Every time an intersection point ${}^{link}\mathrm{x}^j_{a_h}$ w.r.t. Σ_{link} is computed for a j-th link, its measurement is collected and stored in the j-th link corresponding vector $\mathrm{X}^j_{a_h}$. Then, to identify the best candidate, i.e. the contact point which approaches the most probable value, the mean value of the data set in $\mathrm{X}^j_{a_h}$ is considered and a statistical hypothesis test for normality is implemented. It is important to underline here that the estimation of the load contact point obtained by using (3.9), is based on the measurements gathered with sensor devices thus some disturbances due to sensors noise must be taken into account.

Additionally, the humans' natural ever-present movement generates some artifacts (e.g. STA [113], the motion of fabric sensors w.r.t the body in suit-based sensing technologies [131]) which inevitably affects the estimation procedure. To model the resulting error, the Gaussian model is broadly used in inertial body tracking [132, 133] as well as in the analysis of human motion [134]. Likewise, the data set built in the procedure just explained can be characterised as [135, 136]

$$\mathrm{X}^{j}_{a_h} \sim \mathcal{N}(\hat{\mu}^{j}, \hat{\sigma}^{2,j}), \tag{3.10}$$

where $\hat{\mu}^{j}$ and $\hat{\sigma}^{j}$ are the mean value and the standard deviation of $\mathrm{X}^{j}_{a_h}$, respectively, and $\mathcal{N}$ denotes the normal (i.e. Gaussian) distribution. Therefore, in this study, the approach to identify a contact point from an approximate probability distribution is assumed to rely on the normality assumption. The one-sided Anderson-Darling test [137] is implemented online to this end. Prior to the test, the element $\mathrm{x}^{j}_{a_h,i}$ of $\mathrm{X}^{j}_{a_h}$ for $i = 1, ..., n^{j}$ must be sorted such that $\mathrm{x}^{j}_{a_h,1} \leq \mathrm{x}^{j}_{a_h,2} \leq ... \leq \mathrm{x}^{j}_{a_h,n^{j}}$ and standardised as

$$\mathrm{s}^{j}_{i} = \frac{\mathrm{x}^{j}_{a_h,i} - \hat{\mu}^{j}}{\hat{\sigma}^{j}}. \tag{3.11}$$

First, a sufficient number of samples must be collected until the condition $n^{j} > 50$[5] is satisfied. Then, test statistic $A^{2,j}$ for the j-th link can be defined as

$$A^{2,j} = -n^{j} - \sum_{i=1}^{n^{j}} \frac{2i-1}{n^{j}} \left[\ln\left(F(\mathrm{s}^{j}_{i})\right) + \ln\left(1 - F(\mathrm{s}^{j}_{n^{j}+1-i})\right) \right]. \tag{3.12}$$

where F is the standard normal cumulative distribution function and ln is the natural logarithm. Whether $A^{2,j}$ goes beyond a pre-defined critical value, the hypothesis of normality is rejected with some significance level. The critical values depends on the significance level and on the number of samples, and can be found in [138]. Accordingly, the first link whose sample of contact points exhibits a value of $A^{2,j}$ under the critical value $A^{2}_{critical}$, it is selected as the contact point link N (see Figure 3.6). This is in compliance with the expectation that the data set underlying the estimated contact point must be normally distributed. Once the contact point link is identified, the contact point position ${}^{link}\mathrm{x}^{N}_{a_h}$ w.r.t. Σ_{link} must be computed. At this stage, to establish if enough accuracy is reached by the collected sample or not, a method to monitor the estimated range of the desired parameter (i.e. contact point) is needed. Due to the normality assumption previously made, the confidence interval of the sample mean can be used for this purpose. By definition, a confidence interval provides an estimated range of values which is likely to include an unknown population parameter, the estimated range being calculated from a given sample [139]. Since the mean of the sample of the contact point link $\hat{\mu}^{N}$ is considered to be equal to the estimated contact point position ${}^{link}\mathrm{x}^{N}_{a_h}$, the magnitude of its confidence interval gives an estimate of the accuracy of the contact point computation. As soon as this confidence interval falls below a pre-defined threshold $\delta_{m,threshold}$, the sample mean $\hat{\mu}^{N}$ is established as the contact point position. The confidence interval of the mean δ^{N}_{m} is determined as

$$\delta^{N}_{m} = \pm \mathrm{z}^{*} \frac{\hat{\sigma}^{N}}{\sqrt{n^{N}}} \quad \text{such as} \quad -\mathrm{z}^{*} \frac{\hat{\sigma}^{N}}{\sqrt{n^{N}}} \leq \hat{\mu}^{N} \leq +\mathrm{z}^{*} \frac{\hat{\sigma}^{N}}{\sqrt{n^{N}}}, \tag{3.13}$$

[5] The choice of the threshold for the number of samples to be collected is related to the selection of the critical value of $A^{2,j}$ (further details will follow in this Section).

where z^* is a critical value which expresses the confidence level of the interval. The critical values for computing the confidence intervals depends on the significance level and can be found in [140].

Experimental Analysis

The experimental analysis to validate the proposed contact point detection technique is presented hereafter. First, a simulation study is conducted with Simscape Multibody™ (formerly SimMechanics™), a multibody simulation environment for 3D mechanical systems developed and commercialised by MathWorks, Inc. (Natick, Massachusetts, USA). Next, experiments on two human subjects using data collected with sensor systems are performed as a proof-of-concept, to test the detection capability of the technique in real settings considering three different application points of an external load. The whole experimental procedure was carried out in accordance with the Declaration of Helsinki and the protocol was approved by the ethics committee Azienda Sanitaria Locale (ASL) Genovese N.3 (Protocol IIT_HRII_001).

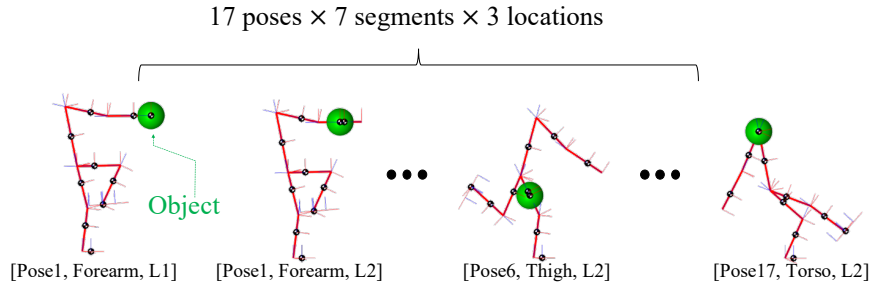

Figure 3.7: *Some examples of the body configurations and the object placement conditions employed for the contact point estimation in the simulation performed with SimMechanics™ and the proposed technique.*

Simulation experiments were destined and developed to evaluate the *feasibility* of the proposed technique in the localisation of an external load on the body links in different body configurations. A total of 357 conditions (17 poses ×7 segments ×3 locations) were simulated to investigate the accuracy of the method in detecting the contact points. In Figure 3.7, a few of these cases are presented as an example. These simulations were indeed to figure out the expected performance of the proposed technique, prior to the experimental analysis that revealed the effective capabilities in a real environment. The simulation was conducted using a personal computer with an Intel Core i7, CPU 2.50 GHz processor, 16.0 GB 1600 MHz RAM and for integration, a ode15s solver was employed. The state variables (e.g. joint angles) were collected from a SimMechanics™ model. On the other hand, $\boldsymbol{C}_p$ and $\boldsymbol{f}$ of the human model (see Equation 3.8) were obtained by means of a virtual force plate, which was located at the bottom of the foot link. To consider feasible and realistic human postures, the data to simulate the body configurations were measured through the Xsens MVN Biomech suit described in Subsection 3.1.1. For each body configuration, three fixed points (proximal, central, distal) on each one of the seven links considered (forearm, upper arm, torso, left thigh, left shank, right thigh, and right shank) were assumed to be, one by one, the load application point. In each of these $17 \times 7 \times 3$ conditions, the estimated

and measured CoP and vGRF were simulated and the contact point was achieved as explained in the previous paragraph. It should be noted that, in the simulation study, the contact point link was assumed to be known thus only the estimation error of the proposed technique was assessed.

Figure 3.8: *Overview of the experimental setup. All the sensors involved in the experiment are illustrated on the left. The three different body locations in which a weight was placed to simulate the external load are illustrated on the right.*

For the experiments on human subjects, two healthy volunteers, one female and one male, labeled as subject 1 and subject 2, respectively, (age: 28 and 34 years; mass: 50 and 76 kg; height: 171 and 178 cm) were involved in the experimental session. A written informed consent was obtained for both of them. The Xsens MVN Biomech suit presented in Subsection 3.1.1 was used to track the whole-body motion. On the other hand, the whole-body CoP and vGRF were collected using the Kistler force plate presented in Subsection 3.1.2. The experimental setup is depicted on the left side of Figure 3.8. The experimental procedure included an off-line calibration experiment and a validation experiment.

In the calibration experiment, the subjects were asked to hold twenty-five static postures to build a proper input data set for the CoP model estimation by means of the SESC technique presented in Subsection 3.2.2. During the data collection, the postures were chosen arbitrarily by the subjects, but with the requirement to vary the orientations of each body link as much as possible in between, to gather variables as linearly-independent as possible. The movements were constrained to the sagittal plane since a human sagittal model is considered in this study. Accordingly, both the estimated and measured CoP employed were projected onto such a plane for the computations. Once the SESC parameters were identified off-line, they could be employed to estimate

online the human whole-body CoP in any body configuration.

For the validation experiment, the subjects were required to perform three sessions. In each session, a 4 kg weight was placed in one of the three pre-selected positions on the human body - hands, mid-forearms, and mid-upper arms - as shown in Figure 3.8, distributed equally on the two limbs (2 kg for each one). The measured linear position of the contact points in the corresponding link frame Σ_{link}, considered to be the real ones, were respectively: 0.31 m w.r.t forearm frame Σ_{FA}, 0.14 m w.r.t Σ_{FA} and 0.22 m w.r.t upper arm frame Σ_{UA}. Once the load was placed, the subjects were asked to move freely in the sagittal plane in a quasi-static way and perform symmetrical movements with both the upper and lower limbs for the entire duration of the experiment. Meanwhile, the contact point x_{a_h} was detected using the proposed algorithm 1. A significance level of 0.05 (5%) was selected to set both the Anderson-Darling test critical value and the z^* value to compute the confidence interval. The corresponding values are given in Table 3.4 along with the confidence interval threshold, which was set arbitrarily (a further discussion about the value of $\delta_{m,\text{threshold}}$ follows above). For each

Table 3.4: *Anderson-Darling test critical value, z^* value and confidence interval threshold according to a significance level of 0.05 (5%)*

$A^2_{\textbf{critical}}$	$\mathbf{z}^*$	$\delta_{m,\textbf{threshold}}[m]$
0.735	1.96	0.01

experimental condition, the percentage errors between the real and the estimated linear positions of the contact point w.r.t Σ_{link} were computed and the time needed to detect the contact point was measured.

Results

The results of the simulation study to estimate the contact point position using the proposed technique are shown in Figure 3.9. The colored bars represent the mean value among all the simulated body configurations of the contact point computed through the proposed technique, in the proximal (blue), central (orange), and distal (yellow) location on the link, respectively, for each link. The considered links are forearm (FA), upper arm (UA), torso (T), left thigh (LT), left shank (LS), right thigh (RT), right shank (RS). The black line superimposed on the bars represents the maximum and minimum error of the contact point position estimation between all the body configurations. In each condition, the percentage errors between the expected and the computed contact point were calculated and the mean and the standard deviation values, computed among all the contact point positions and body configurations, were obtained for each link. Specifically, the results of such computations are: $17.53\% \pm 20.56\%$ for the forearm, $0.95\% \pm 2.71\%$ for the upper arm, $7.18\% \pm 21.44\%$ for the torso, $2.47\% \pm 8.98\%$ for the left thigh, $0.62\% \pm 0.85\%$ for the left shank, $2.32\% \pm 10.07\%$ for the right thigh and $4.35\% \pm 14.68\%$ for the right shank, respectively. Since static body postures were considered in the simulation study, a simple computation of the contact point using (3.9) and the knowledge about the contact link were sufficient to accurately identify the contact point position $\mathrm{x}^N_{a_h}$. Nevertheless, as previously explained, a criterion to identify the contact link must be set without a priori knowledge thus the Anderson-Darling normality test is employed. Moreover, to ensure a good level of accuracy with

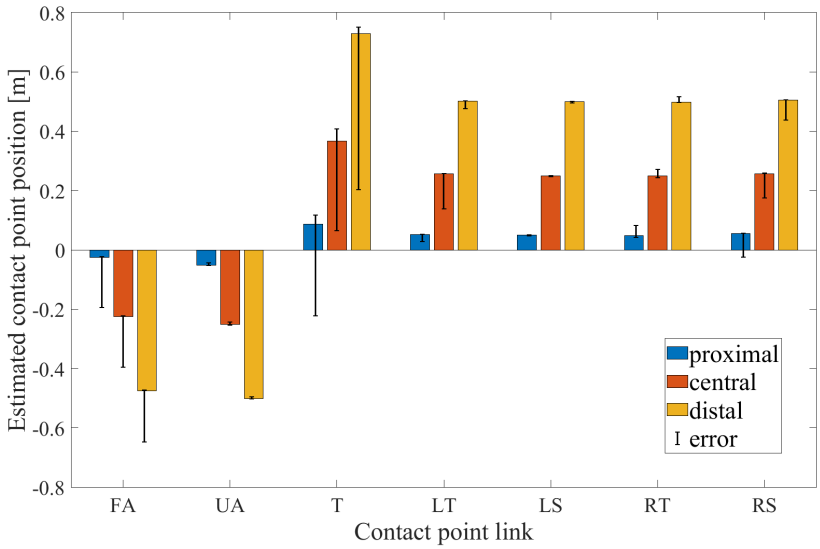

Figure 3.9: *The results of the contact point estimation using SimMechanics™ and the proposed technique in the forearm (FA), upper arm (UA), torso (T), left thigh (LT), left shank (LS), right thigh (RT), right shank (RS) links, are illustrated in error bar plots.*

real data, which are inevitably affected by artifacts and noise, the concept of confidence level δ_m is introduced.

The results of the the validation experiment on human subjects are hereafter presented. The percentage error of the contact point positions and the time needed to estimate it, in each experimental condition, are illustrated in Table 3.5, for subject 1 and subject 2, respectively.

Table 3.5: *Results of the validation experiment. The percentage error of the contact point positions and the time needed to estimate it are shown for both subject 1 and 2.*

Subject	Experimental condition	Percentage error	Estimation time
1	Hands	1.022%	9.4 s
	Mid-forearms	20.92%	16.1 s
	Mid-upper arms	11.15%	14.4 s
2	Hands	1.17%	16.0 s
	Mid-forearms	48.04%	27.2 s
	Mid-upper arms	16.05%	17.5 s

The changes of $A^{2,N}$ and δ_m^N during the contact point detection phase, on the y-axis and on the x-axis respectively, are shown in Figure 3.10 for subject 1 (first row) and subject 2 (second row), respectively, in each experimental condition, namely considering a load applied on the hands (left column), mid-forearms (middle column) and mid-upper arms (right column). The red square represents the starting point while the green square represents the instant in which the contact point is detected. The blue dashed lines represent the thresholds for $A^{2,N}$ and $|\delta_m^N|$, namely A^2_{critical} (horizontal line) and $|\delta_{m,\text{threshold}}|$ (vertical line), respectively. The contact point link is selected as soon as $A^{2,N} < A^2_{\text{critical}}$ meaning that the hypothesis of normality for the data set of the contact

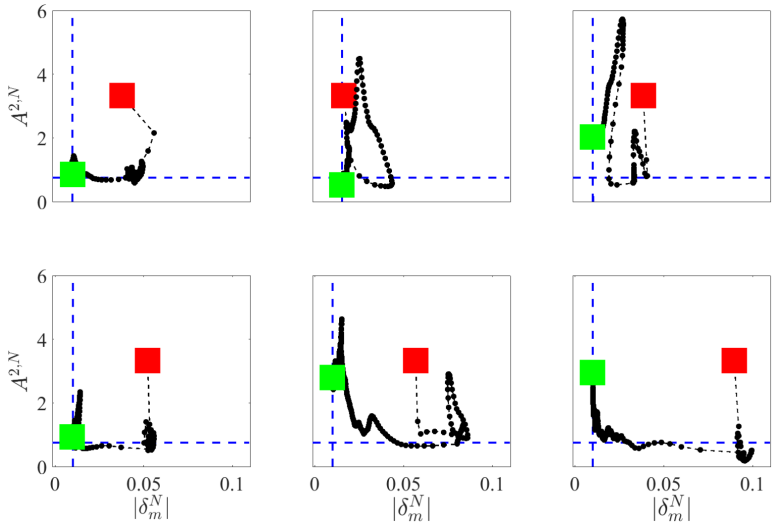

Figure 3.10: *Results of the validation experiment: the profiles of A^2 and δ_m, on the y-axis and on the x-axis respectively, computed and monitored over the experiment for subject 1 (first row) and subject 2 (second row), in each experimental condition, for the correspondent contact point link: hands (left column), mid-forearms (middle column) and mid-upper arms (right column). The red square represents the starting point while the green square represents the instant in which the contact point is detected. The blue dashed lines represent the thresholds for $A^{2,N}$ and $|\delta_m^N|$, namely $A^2_{critical}$ (horizontal line) and $|\delta_{m,threshold}|$ (vertical line), respectively.*

point link can be accepted. Nevertheless, the contact point link is not changed even if the value of $A^{2,N}$ return beyond the threshold. In fact, it should be noted that in some cases, in the end point, $A^{2,N} > A^2_{\text{critical}}$. The contact point position is then found when the value of $|\delta_m^N|$ is under the threshold $|\delta_{m,\text{threshold}}|$. This means that the confidence level of the mean value is included within the pre-defined threshold. In all the experimental conditions, even if the condition $n^j > 50$ was satisfied and values $A^{2,j}$ were computed also for other candidate links, the link that satisfies first the condition $A^{2,N} > A^2_{\text{critical}}$ was always the actual contact point link. Finally, typical results of the correlation between the choice of $\delta_{m,\text{threshold}}$ and estimation time are shown in Figure 3.11. By setting a higher threshold, the contact point position could be found faster, nevertheless, with a larger confidence interval thus with less accuracy. Hence, $|\delta_{m,\text{threshold}}|$ has been set equal to 0.01 m as a good compromise between time and accuracy.

Discussion

In the simulation study, results indicated that the estimation error of the contact point position, computed between all the body configurations considered, was significantly low in most of the links. However, some exceptions were found for the torso and the forearm. This is most likely due to a failure in computing the intersection between the perpendicular line passing through $\mathrm{x}_{a_h|x}$ and the link segment. In fact, when the vertical projection lies slightly beyond the link end-point, the contact position can not just be detected and this leads to a misleading increment of the percentage error. Accordingly, we can state that the proposed method is able to accurately estimate the contact point position in most of the cases, with a low chance of failure occurring in extreme conditions (i.e. in the proximity of the link end-points). An analysis of the performance

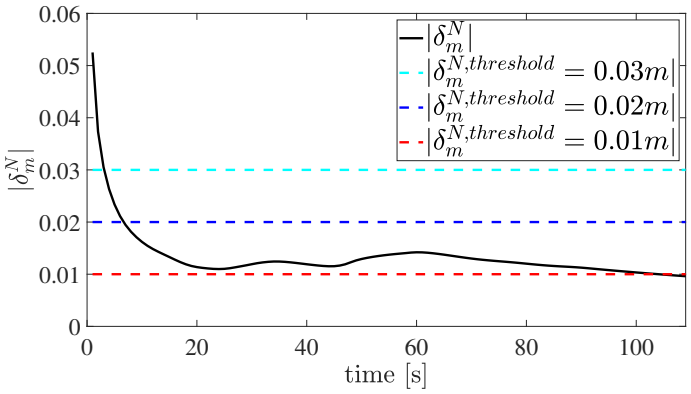

Figure 3.11: *Illustrative trend of δ_m^N during the validation experiment represented with varying values of $\delta_{m,threshold}$. By setting a higher threshold, the contact point position could be found faster, nevertheless, with a larger confidence interval thus with less accuracy.*

of the proposed method in real settings indicated that some factors, such as movement artifacts (that are present even during quasi-static motion) and the noise introduced by sensor systems, could affect the accuracy of the estimation. To compensate for this effect in this work, a statistical analysis approach was introduced with the aim to improve the accuracy of the estimation. As a result, in the validation experiment, the link was correctly identified for all three experimental conditions for both the subjects, and the localisation accuracy is deemed acceptable to the extent of the industrial applications addressed in this thesis. Furthermore, the time needed to detect the contact point was less than half a minute thus the 'industrial-fast' detection capacity of the proposed system is demonstrated. Accordingly, the proposed method shows a promising potential to quickly detect the contact point position. It should be pointed out that, due to the assumption of quasi-static, sagittal, and symmetric movements and the capability of the method to work only with vertical forces, the proposed framework can be deployed in certain specific industrial tasks, which are quite numerous (lifting, carrying, pick and place in the sagittal plane, etc.).

3.2.4 Extension to Bipedal Models

The SESC technique described in Subsection 3.2.2 allows to identify a model of the human whole-body CoP. Hence, it can be employed to represent the human biomechanical system as a planar serial chain that includes only one GRF. The development of this reduced model to a bipedal one, thus including the reaction forces exchanged by both feet with the ground, would enable the tracking of human states in a wider work space, broadening the potential applications to more realistic and complex scenarios. To this end, a method to estimate the feet CoP and GRF, during double-support, on the basis of the whole-body CoP and the total GRF is required. Nevertheless, the computation of physically feasible contact forces to match a desired net contact wrench, known as the force distribution problem (FDP), is known to be an under-determined problem. In fact, when the full BSIPs are not available, it is not possible to obtain analytically the feet CoP and GRF.

In the robotics community, several authors addressed this issue using constrained optimisation methods that employed sub-optimal solutions by applying simplifying assumptions [141, 142]. A specific objective - the tangential force [143], contact force norms [144], ground force magnitudes [141], and ankle torques [142] - was selected on the basis of the context or the application targeted and the corresponding objective function was then minimised. Similarly, an optimisation procedure was proposed in [145] to solve the force distribution problem (FDP) during human gait. Nevertheless, these optimisation approaches require to establish a-priori which strategy a human is going to use to perform a task, which may be a huge presupposition. Alternatively, the concept of "Smooth Transition Assumption" was introduced in [146], involving a smooth function that is adjusted for the double-support phase between the uniquely determined values of the GRF components of the single-support phase. However, this method is specifically developed for gait analysis. On the other hand, more recent works showed the potential of neural networks in predicting GRF and CoP during different human motions as gait [147] and standing/sitting/squatting actions [148].

Accordingly, the aim of [29] is to propose a novel approach to solve the un-determinacy of the FDP for the human. A relation is built which connects the whole-body GRF and CoP to the feet GRF and CoP, directly on the basis of the data measured on the human subjects. A synergistic method is then developed to combine the information enclosed in the SESC model for the whole-body CoP estimation with the ability of learning techniques to implicitly detect complex nonlinear relationships between variables.

The corresponding procedure is shown in Figure 3.12. In an off-line phase, a large dataset is built to implement the proposed method. Using external sensor systems, sets of measurements of the human whole-body pose along with CoP and GRF are collected upon a large number of static postures. Firstly, this dataset is used to identify the CoP model with the SESC technique (see Subsection 3.2.2). Next, to design and train a feed-forward ANN employed for solving the FDP. Once the proposed synergistic model is identified, it can be used online to obtain the feet CoP and GRF estimation. An experimental analysis is conducted on five subjects to investigate its capabilities.

Learning Technique to Estimate Feet Centres of Pressure

Prior to using this technique, the whole-body CoP model using the SESC technique presented in Subsection 3.2.2 must be identified. Then, to manage the double-support

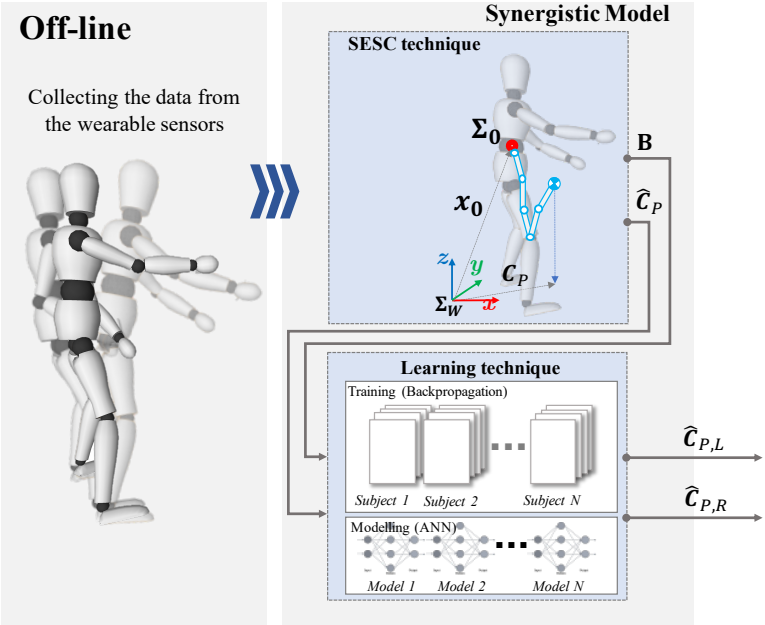

Figure 3.12: *The procedure for estimating the feet GRF and CoP using the synergistic model.*

indeterminacy and thus the case in which n_f is equal to 2 in (4.4), the multi-layer ANN technique is employed. The feet GRF and CoP are estimated using as inputs the whole-body CoP estimated by the SESC model and body configurations measured with a motion-capture system. This consideration is to reduce the amount of modeling uncertainty that is expected to be learned by the ANN. Supporting this choice, it has been shown that supervised multi-layer ANN with the proper input data and non-linear activation functions are capable of representing accurate approximations and mappings [149]. Specifically, a feed-forward ANN with one hidden layer including a sufficient number of neurons can fit any finite input-output mapping problem [150]. To achieve the best results possible, different combinations of training functions, numbers of neurons in the hidden layer, and sets of input data are tested. As regards the input data, the whole-body $\hat{\mathbf{C}}_P$ from the SESC model, the orientation matrix of the simplified human model $\mathbf{B}$ and the pelvis, the left foot and the right foot positions are ultimately employed for the training and the validation. As regards the structure, a feed-forward ANN is built, which is composed of one hidden layer containing four neurons with a non-linear activation function and an output layer with a linear function. The network is trained with the target data (e.g. the measured feet CoP using a suitable pressure sensor) using the weights and bias values according to Levenberg-Marquardt optimisation. Consequently, by using the proposed synergistic model, the feet CoP $\hat{\mathbf{C}}_{P,R}$ and $\hat{\mathbf{C}}_{P,L}$ can be estimated online. In addition, deriving from (3.1), the distribution gain ζ can be obtained for each foot as

$$\begin{bmatrix}\zeta_L & \zeta_R\end{bmatrix} = \begin{bmatrix}\left|\frac{\hat{\mathbf{C}}_P - \hat{\mathbf{C}}_{P,R}}{\hat{\mathbf{C}}_{P,L} - \hat{\mathbf{C}}_{P,R}}\right| & \left|\frac{\hat{\mathbf{C}}_P - \hat{\mathbf{C}}_{P,L}}{\hat{\mathbf{C}}_{P,R} - \hat{\mathbf{C}}_{P,L}}\right|\end{bmatrix}. \tag{3.14}$$

where ζ_L and ζ_R are the distribution gains for the left and the right foot, respectively. Reminding that $\sum_i \zeta_i = 1$ it is possible to compute the gain related to one foot and then subtract its value from 1 to obtain the gain related to the other foot.

Experimental Analysis

The experimental analysis to validate the proposed learning technique is presented hereafter. The whole experimental procedure was carried out in accordance with the Declaration of Helsinki and the protocol was approved by the ethics committee Azienda Sanitaria Locale (ASL) Genovese N.3 (Protocol IIT_HRII_001). Five healthy male volunteers (age: 28.6 ± 4.3 years; mass: 84.7 ± 10.7 kg; height: 182.2 ± 2.9 cm) [6] were recruited in the experimental session. A written informed consent was obtained after explaining the experimental procedure. Each subject was asked to wear the Xsens MVN Biomech suit presented in Subsection 3.1.1 and the OpenGo sensor insoles presented in Subsection 3.1.2) and then required to hold two hundred static postures for the data collection. During the acquisition, the body configurations were chosen by each subject arbitrarily but with the requirement to change the orientations of each segment and the position of the feet CoP as much as possible in between, to obtain variables as linearly-independent as possible. A large number of postures collected along with their variability are necessary to build a suitable set of input data for the parameters identification of the proposed synergistic model.

Results

Table 3.6 presents the means and the standard errors of the position of the CoP with respect to the Σ_W to evaluate the performance of the SESC technique implemented with the selected sensor systems.

Table 3.6: *Means and standard errors of the position between the whole-body CoP measured using the OpenGo sensor insoles, and the CoP estimated by the identified SESC model. The errors are computed for each subject on the x-axis and on the y-axis across two hundred postures.*

Subject	CoP errors (m)	
	$C_{P_x,L}$	$C_{P_y,L}$
1	1.34* ± 0.04*	1.33* ± 0.04*
2	1.57* ± 0.04*	1.34* ± 0.04*
3	1.45* ± 0.04*	1.56* ± 0.04*
4	1.76* ± 0.05*	1.70* ± 0.05*
5	1.83* ± 0.05*	1.40* ± 0.05*

*All the values in the table are multiplied by 10^{-2}

This position error was computed in x- and in y-direction for all the two hundred postures performed by five subjects. We compared $\mathbf{C}_{P_{wt}}$ and $\hat{\mathbf{C}}_{P_{wo}}$ positions, computed with (3.1) using data measured by the OpenGo sensor insoles and estimated by the SESC model, respectively, without the effect of external forces. The mean position error was $1.83 \times 10^{-2} m$ in the x-direction and $1.40 \times 10^{-2} m$ in the y-direction across all postures for the subject with the worst results. Hence, the SESC CoP estimate using the OpenGo sensor insoles has an equivalent performance as the literature-based one with high-end sensors [122], providing solid evidence on the accuracy of the online CoP model.

For the training of the ANN we used one hundred sixty static poses (around 80% of the whole data set) which were in fact adopted as the training set. Then, forty postures

[6] Subject data is reported as: mean ± standard deviation.

were used as the validation set to examine the network performance (around the other 20% of the whole data set). In Figure 3.13 the results for one subject are presented, showing the profile of the x coordinate of the CoP w.r.t. the Σ_W, measured with the OpenGo sensor insoles (red line) and estimated by means of the proposed method (blue line) both for the left (upper chart) and for the right (lower chart) foot.

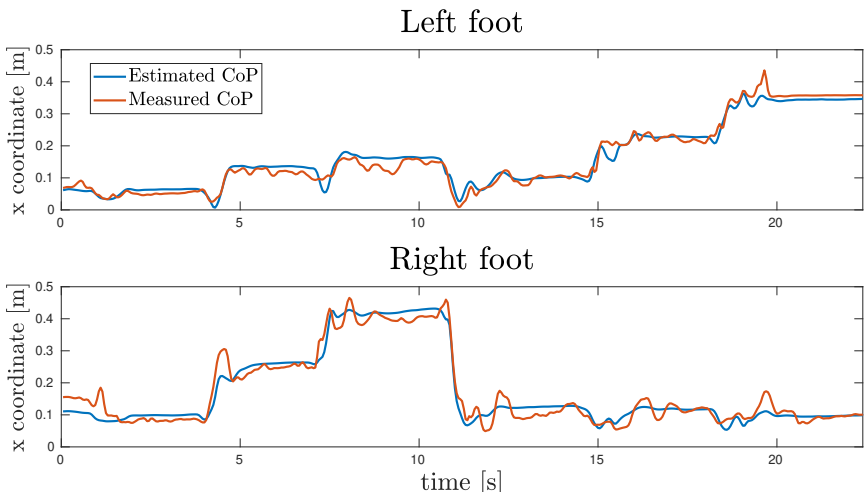

Figure 3.13: *X coordinate of the position of the CoP measured (red line) using the OpenGo sensor insoles and estimated (blue line) by the synergistic method, for the left foot (upper chart) and for the right foot (lower chart). The feet CoP position errors are expressed in the inertial (global) frame.*

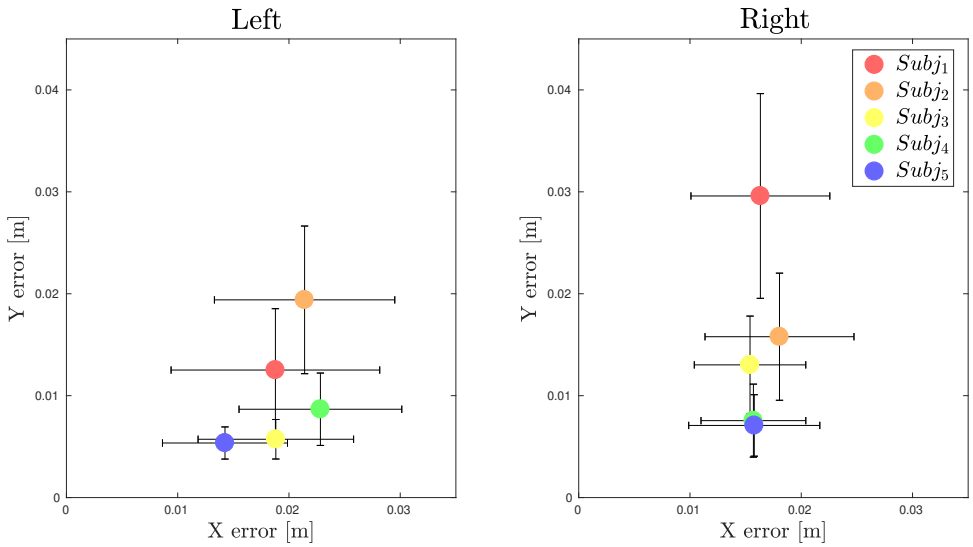

Figure 3.14: *Graphical representation of the means and standard errors of the position for the left foot (left chart) and for the right foot (right chart) between the feet CoP measured using the OpenGo sensor insoles and the feet CoP estimated by the synergistic method. The feet CoP position errors are expressed in the inertial frame and computed for each subject on the x-axis and on the y-axis across forty postures.*

Figure 3.14 is a graphical representation of the means and the standard errors of the position between the feet CoP w.r.t. the Σ_W, measured and estimated. These errors

were computed for each subject on the x-axis and on the y-axis for the left foot and for the right foot across the postures of the validation set.

Discussion

The magnitude of the error was uniform between the subjects, demonstrating that the proposed synergistic approach can deal with varying patterns of movement and human body models with different inertial parameters. The consistency of the error in the x and y directions and the level of accuracy achieved were suitable for the extent required by the industrial scenarios addressed in this thesis. The results proved that the proposed synergistic model is capable of solving the un-determinacy of the FDP for the human and provided promising evidence on its capabilities to achieve the feet CoP and GRF estimation in an online stage. The choice to use a neural network to solve the FDP was due to the ability of such techniques to learn multi-input multi-output non-linear systems, and to the fact that finding a nonlinear approximation by hand would not have been feasible considering the large input-output dimension. The training of several prototypes of neural networks with different numbers of layers attributed the best performance to the single-layer neural network.

CHAPTER 4

Human Ergonomics Monitoring System

In view of the considerations made in Section 2.3, the foremost objective of this thesis is to define an online human ergonomics monitoring system, which can provide on the fly, just as the workers are performing their tasks, a comprehensive set of indexes that account for multiple ergonomic risk factors (e.g. awkward postures, mechanical overloading of the body, repetition frequency, etc.) and thus enable the assessment of a broad range of manual material activities typically conducted in industrial environments. Unlike the traditional approaches that focus particularly on the kinematic variables, this thesis places a great emphasis on the dynamic aspects of the tasks (i.e. forces or torques acting on and inside the body), which may contribute significantly to the development of WMSDs. Accordingly, kinematic variables such as joint angles, velocities, and accelerations are integrated with overloading torque, fatigue, and power, human CoM potential energy, and compressive forces (by taking advantage of some estimated indicators which were investigated and developed in previous studies) to establish an exhaustive method for the assessment of physical exposure in the workplace. Furthermore, to provide subject-specific values for such indicators, this thesis has focused on the development of personalisable and re-identifiable human models.

As mentioned in Section 1.5, this Chapter will address the first block of the framework proposed in this thesis (see Figure 1.1): the observation layer. In Figure 4.1, the observation layer is emphasised with its key elements. Integrating the data about human motion and interaction forces, measured through suitable **sensor systems** (presented in Section 3.1) within a **human model** (presented in Section 3.2), it is possible to estimate the physical exposure of the humans performing their working activities in terms of ergonomic risk factors (e.g. joint overloading, fatigue, compressive forces). Hence, the human **ergonomics monitoring system** can be defined as a set of indexes, which from now on will be referred as "ergonomic indexes" and are expressed as $\boldsymbol{\omega}_h(\mathbf{q}) \in \mathbb{R}^{n_j}$,

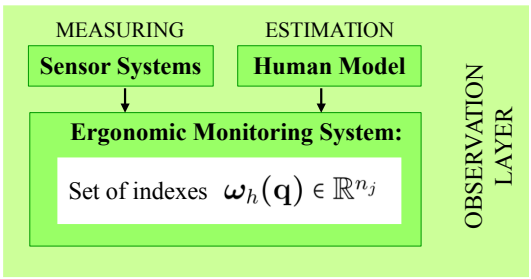

Figure 4.1: *First block of the framework proposed in this thesis for the assessment and improvement of human ergonomics: the observation layer (see Section 1.5).*

where $\mathbf{q}$ refers to the generalized coordinate of the system and n_j is the number of the joints (see Section 3.2.1). Such indexes, with the corresponding equation, scope, and the ergonomic risk factor that each one of them seeks to address are listed in Table 4.1 and will be presented in detail in this Chapter.

Table 4.1: *The proposed set of "ergonomic indexes" to assess human kino-dynamic states taking into account multiple ergonomic risk factors. The corresponding scope - kinematics or dynamics - and equation are included for each of them.*

SCOPE	INDEX	EQUATION	RISK FACTOR
Kinematics	**Joint Displacement**	$\boldsymbol{\omega}_1(\mathbf{q}) = \frac{\lvert\mathbf{q}_h\rvert}{\mathbf{q}_h^{\max} - \mathbf{q}_h^{\min}}$	Awkward body postures
	Joint Velocity	$\boldsymbol{\omega}_2(\mathbf{q}) = \frac{\dot{\mathbf{q}}_h}{\dot{\mathbf{q}}_h^{\max}}$	Abrupt and sudden efforts
	Joint Acceleration	$\boldsymbol{\omega}_3(\mathbf{q}) = \frac{\ddot{\mathbf{q}}_h}{\dot{\mathbf{q}}_h^{\max}}$	High-intensity forces due to inertia
Dynamics	**Overloading Joint Torque**	$\boldsymbol{\omega}_4(\mathbf{q}) = \frac{\Delta\boldsymbol{\tau}_s}{\Delta\boldsymbol{\tau}^{\max}}$	Mechanical overburden of the musculoskeletal stucture
	Overloading Joint Fatigue	$\boldsymbol{\omega}_5(\mathbf{q}) = \frac{\boldsymbol{\tau}^F(t)}{\boldsymbol{\tau}^{F,\max}(t)}$	Repetitive and monotonous movements
	Overloading Joint Power	$\boldsymbol{\omega}_6(\mathbf{q}) = \frac{\mathbf{P}}{\mathbf{P}^{\max}} = \frac{\dot{\mathbf{q}}_h \Delta\boldsymbol{\tau}_s}{\dot{\mathbf{q}}_h^{\max} \Delta\boldsymbol{\tau}^{\max}}$.	Mechanical overburden of the musculoskeletal stucture
	CoM Potential Energy	$\boldsymbol{\omega}_7(\mathbf{q}) = \frac{\Delta E_P}{\Delta E_P^{\max}} = \frac{\Delta C_M \lvert z}{\Delta C_M \lvert z^{\max}}$	Awkward body postures
	Compressive Forces	$\boldsymbol{\omega}_8(\mathbf{q}) = \frac{\mathbf{f}_C}{\mathbf{f}_C^{\max}}$	Mechanical overburden of the musculoskeletal stucture

Section 4.1 addresses the variables related to joint kinematics (i.e. joint displace-

ment, joint velocity, and joint acceleration). Section 4.2 introduces the "overloading joint torque", originally proposed in [108] which accounts for the torque variations induced on the human joints by an external load. In Section 4.3 the fatigue model introduced in [31] to evaluate the cumulative effect of the overloading torque induced on the joints over time, namely "overloading joint fatigue", is presented. Section 4.4 tackles the "overloading joint power" and the potential energy associated with the human CoM. Finally, in Section 4.5, a tool for the assessment of the direct effect of an external force on the human joints [151] is proposed. For the overloading joint torque and the overloading joint fatigue (indexes $\mathbf{w}_4$ and $\mathbf{w}_5$, respectively) some experimental results of their application are also provided. [1]

In addition, in Section 4.6, an experimental analysis conducted on twelve subjects to validate the proposed set of indexes as a human ergonomics monitoring system is presented.

[1] Parts of this Chapter have been published in [31, 32]

4.1 Joint Kinematic Variables

4.1.1 Joint Displacement

The first index $\boldsymbol{\omega}_1(\mathbf{q})$ is the joint displacement, which is considered as the distance from the mechanical joint limit, and can be defined as

$$\boldsymbol{\omega}_1(\mathbf{q}) = \frac{|\mathbf{q}_h|}{\mathbf{q}_h^{\max} - \mathbf{q}_h^{\min}},$$

where $\mathbf{q}_h = [q_1 \ \dots \ q_{n_j}]^T \in \mathbb{R}^{n_j}$ is the joint angles vector, $|\mathbf{q}_h|$ is the vector including its absolute values, $\mathbf{q}_h^{\max}$ and $\mathbf{q}_h^{\min}$ are the vector including the joints upper and lower boundaries and n_j is the number of joints. The values of $\mathbf{q}_h^{\max}$ and $\mathbf{q}_h^{\min}$ can be found in literature [152].

The aim of monitoring the joint displacement is to detect wherever the body configurations that a worker is adopting to perform his/her occupational activities are not ergonomic. In fact, certain specific human postures have proven to be a potential cause of injuries and musculoskeletal diseases [153]. For example, long-lasting activities involving trunk inclination may cause degenerative disorders in the lumbar region, especially if the task is conducted over a period of many years. Furthermore, keeping inconvenient body configurations for a long duration is connected with long-term activation of muscles that may result in muscular fatigue and a significant and harmful reduction in blood circulation. Such unfavourable postures are mostly related to specific sections of the human range of motion (ROM) which should be avoided (e.g. in proximity to the maximum limits). Hence, the joint displacement index $\boldsymbol{\omega}_1(\mathbf{q})$ offers a straightforward method to identify them, thus preventing all the associated negative effects. It should be noted that the time factor is not considered in $\boldsymbol{\omega}_1(\mathbf{q})$ so far, but it will be investigated in future studies on this topic.

4.1.2 Joint Velocity

The second index $\boldsymbol{\omega}_2(\mathbf{q})$ is the joint normalised angular velocity and it can be defined as

$$\boldsymbol{\omega}_2(\mathbf{q}) = \frac{\dot{\mathbf{q}}_h}{\dot{\mathbf{q}}_h^{\max}},$$

where $\dot{\mathbf{q}}_h \in \mathbb{R}^{n_j}$ is the joint velocities vector, $\dot{\mathbf{q}}_h{}^{\max}$ is the vector including the joints maximum velocities and n_j is the number of joints. The values of $\dot{\mathbf{q}}_h{}^{\max}$ can be found in literature [154].

As reported by some researchers, when assessing dynamically varying activities, the direct measurement of human motion - in terms, for example, of joint velocity and acceleration - can provide more relevant information than posture analysis for the ergonomics risk of the low back [155] and wrist [156, 157]. Joint velocities, in particular, are suggestive of eventual abrupt movements that may be frequently associated with sudden and acute efforts potentially leading to severe injuries. Accordingly, by means of the joint velocity index $\boldsymbol{\omega}_2(\mathbf{q})$, such hazardous situations can be detected.

4.1.3 Joint Acceleration

The third index $\boldsymbol{\omega}_3(\mathbf{q})$ is the joint normalised angular acceleration and it can be defined as

$$\boldsymbol{\omega}_3(\mathbf{q}) = \frac{\ddot{\mathbf{q}}_h}{\ddot{\mathbf{q}}_h^{\max}},$$

where $\ddot{\mathbf{q}}_h \in \mathbb{R}^{n_j}$ is the joint accelerations vector, $\ddot{\mathbf{q}}_h^{\max}$ is the vector including the joints maximum accelerations and n_j is the number of joints. The values of $\ddot{\mathbf{q}}_h^{\max}$ can be obtained experimentally, by estimating directly their value on the individuals.

As mentioned above, joint accelerations have already been investigated as a method to assess the risk factors to the development of WMSDs [158, 159]. As a matter of fact, the forces induced inside the human body are affected by the joint accelerations as biomechanically explained by Newton's second law, force = mass × acceleration. When high accelerations are in place, such forces may lead to the potential overload of musculoskeletal tissues, thereby causing internal stresses, or compressing the nerves, thus increasing the risk of injuries. This can happen when the subjects perform actions that require high accelerations to be accomplished in an efficient way (e.g. hammering). With the aim to recognise the risk associated with such scenarios, the joint acceleration can be tracked by means of the corresponding index $\boldsymbol{\omega}_3(\mathbf{q})$.

4.2 Overloading Joint Torque

In [108], a technique to account online for the torque variations induced on the human main joints by an external load, defined as the "overloading joint torques" was originally proposed. The method is based on the displacement of the CoP, computed from the difference between an estimated one and a measured one. The estimated CoP can be obtained, in static conditions, by projecting the whole-body CoM estimated by taking advantage of the SESC technique presented in Subsection 3.2.2. Besides, when considering dynamic conditions, the position of CoP with respect to the CoM can be computed using 3.6. On the other hand, the measured CoP can be collected using a suitable sensor system.

If no interactions of the human with the external environment (or with a tool/object) occur, the estimation of the CoP vector $\hat{\mathbf{C}}_{P_{wo}}$ obtained with the model is comparable to the measured one $\mathbf{C}_{P_{wt}}$. On the other hand, whether an external load is applied on the human body, the estimated and the measured CoP vectors differ. Hence, the overloading joint torque vector can be estimated accordingly, by using the CoP displacement vector. The human body model described in Subsection 3.2.1 is employed here for this purpose.

The human joint torque vector $\boldsymbol{\tau}_{wo}$ with no external load except the human body weight can be computed by using $\hat{\mathbf{C}}_{P_{wo}}$ and the vGRF vector $\mathbf{f}_{wo}$ as

$$\mathbf{S}^T\boldsymbol{\tau}_{wo} = \boldsymbol{\tau}_b - \sum_{i=1}^{n_f} \mathbf{J}_{\hat{\mathbf{C}}_{P_{wo},i}}(\mathbf{q})^T\mathbf{f}_{wo,i}. \tag{4.1}$$

Similarly, the torque vector $\boldsymbol{\tau}_{wt}$, which takes into account the effect of eventual external loads, can be computed by using $\mathbf{C}_{P_{wt}}$ and the vGRF vector $\mathbf{f}_{wt}$ as

$$\mathbf{S}^T\boldsymbol{\tau}_{wt} = \boldsymbol{\tau}_b - \sum_{i=1}^{n_f} \mathbf{J}_{\mathbf{C}_{P_{wt},i}}(\mathbf{q})^T\mathbf{f}_{wt,i} - \sum_{j=1}^{n_h} \mathbf{J}_{a_h,j}(\mathbf{q})^T\mathbf{f}_{h,j}, \tag{4.2}$$

where $\boldsymbol{\tau}_b \in \mathbb{R}^{n+6}$ is equal to $\mathbf{M}(\mathbf{q})\ddot{\mathbf{q}} + \mathbf{C}(\mathbf{q}, \dot{\mathbf{q}})\dot{\mathbf{q}} + \mathbf{G}(\mathbf{q}) \in \mathbb{R}^{n+6}$. $\mathbf{f}_{wo}$ and $\mathbf{f}_{wt}$ are the vGRF vectors applied at the CoP of each foot without and with considering the effect of external loads. Hence, they can be deemed as the weight of the human body and the weight measured by a suitable sensor system, respectively. n_f is the number of contact forces exchanged with the ground. $\mathbf{f}_h$ refers to the interaction forces that are applied at the contact points $\mathbf{a}_h$, excluding the feet contacts. n_h is the number of contact points where the external forces are applied. In addition, $\mathbf{S} = \begin{bmatrix}\mathbf{0}_{n\times 6} & \mathbf{I}_{n\times n}\end{bmatrix} \in \mathbb{R}^{n\times(n+6)}$ is the actuation matrix and $\mathbf{J}_{p_i}(\mathbf{q})$ is the contact Jacobian at the point $\mathbf{p}_i$ (e.g. positions of the feet CoP, application point of an external load) with respect to Σ_W. The relation between the vGRF variation $\Delta\mathbf{f}_{w,i} = \mathbf{f}_{wt,i} - \mathbf{f}_{wo,i}$ and the interaction force $\mathbf{f}_h$ can be defined as

$$\Delta\mathbf{F} = \sum_{i=1}^{n_f} \Delta\mathbf{f}_{w,i} = -\sum_{j=1}^{n_h} \mathbf{f}_{h,j}. \tag{4.3}$$

At this point, deriving from (4.1), (4.2) and (4.3), the overloading joint torque vector can then be defined as

$$\begin{aligned}\Delta\boldsymbol{\tau}_s &= \mathbf{S}^T(\boldsymbol{\tau}_{wt} - \boldsymbol{\tau}_{wo}) \\ &= \sum_{j=1}^{n_h} \mathbf{J}_{a_{hj}}(\mathbf{q})^T \eta_j \Delta\mathbf{F} - \sum_{i=1}^{n_f} \left(\mathbf{J}_{\Delta C_{Pi}}(\mathbf{q})^T \mathbf{f}_{wt,i} + \mathbf{J}_{\hat{C}_{P_{wo}i}}(\mathbf{q})^T \zeta_i \Delta\mathbf{F}\right),\end{aligned} \tag{4.4}$$

with $\mathbf{J}_{\Delta C_{Pi}} = \mathbf{J}_{C_{P_{wt}i}} - \mathbf{J}_{\hat{C}_{P_{wo}i}}$ is the Jacobian of the CoP displacement. It is worthwhile noticing that $\boldsymbol{\tau}_b$ does not affect the overloading joint torque vector $\Delta\boldsymbol{\tau}_s$ in any body configuration because the external load effect is included in $\Delta\boldsymbol{\tau}_s$ itself. Due to this consideration, the number of parameters to be identified for the human model [160] are considerably reduced. $0 \le \zeta_i, \eta_j \le 1$ are the distribution gains for vGRF and interaction forces, respectively, which can be computed knowing the body configuration [161,162] (N.B. $\sum_i \zeta_i = 1$, $\sum_j \eta_j = 1$ is a necessary condition). As a result, the fourth index $w_4(\mathbf{q})$ is the joint normalised overloading torque and it can be defined as

$$\boldsymbol{\omega}_4(\mathbf{q}) = \frac{\Delta\boldsymbol{\tau}_s}{\Delta\boldsymbol{\tau}^{\max}}$$

where $\Delta\boldsymbol{\tau}^{\max}$ is the vector including the maximum values of the human joint torque. The tuning and personalisation of the maximum torque values in $\Delta\boldsymbol{\tau}^{\max}$ are based on experiments on subjects. Increasing torque profiles are applied on the selected body joints, one at a time, until the subjects start to feel discomfort. In such a specific instant, the resulting torque values are estimated (based on the applied force and the lever arm) and compared to the ones extracted from literature [70, 163, 164]. If these values are comparable, the experimental ones are used as the maximum torque values. If the differences is significant, the "safest" choice, i.e., the smallest value for the maximum torque, is chosen.

As mentioned above, the overloading joint torque estimates the overload induced on the human joints by an external load. As a result, the corresponding index $\boldsymbol{\omega}_4(\mathbf{q})$ can be employed to account for the mechanical overburden of musculoskeletal structures induced by the weight of a tool or object. It should be pointed out that this method takes into account only the vertical component of external forces thus it can be deployed in a

certain class of industrial tasks, which nevertheless, are quite numerous (lifting/lowering, carrying, pick and place, etc.).

4.2.1 Experimental Application of the Method

The second objective of [32] was to apply the proposed method, which allows to identify the contact point of an external load applied on the human body (see Subsection 3.2.3), to the estimation of the overloading joint torque. In fact, the assumption of a fixed and predefined contact point (i.e. the human hand/s holding an object) was made so far within the procedure to estimate $\Delta\boldsymbol{\tau}_s$, as it was originally developed in [108]. Hence, its integration with an online contact point localisation method would enable to extend the potential of the overloading joint torque technique, by improving its flexibility to varying interaction conditions in realistic industrial settings.[2] In this Subsection, the experimental analysis conducted on two human subjects as a proof-of-concept, to investigate such an integration, is presented. First, the contact point position was localised on the subjects' bodies. Then, the overloading joint torques induced by the external load were computed accordingly using a slight variant of the procedure described above.

Overloading Joint Torque Method Extension

Let us resume Equation 4.2 in which the overloading torque vector $\boldsymbol{\tau}_{wt}$, considering the effect of any external force, is computed by using $\mathbf{C}_{P_{wt}}$ and the vGRF vector $\mathbf{f}_{wt}$ as

$$\mathbf{S}^T\boldsymbol{\tau}_{wt} = \boldsymbol{\tau}_b - \sum_{i=1}^{n_f}\mathbf{J}^T_{C_{P_{wt}{}^i}}\mathbf{f}_{wt,i} - \sum_{j=1}^{n_h}\mathbf{J}^T_{a_{hj}}\mathbf{f}_{h,j}, \tag{4.5}$$

where n_f is the number of contact forces exchanged with the ground. $\mathbf{f}_{wo}$ and $\mathbf{f}_{wt}$ are the vGRF vectors applied at the CoP without and with the effect of external forces. $\mathbf{f}_h$ represents the weight of the object/tool that is applied at the contact point $\mathbf{x}_{a_h}$ and n_h is the number of contact points where the external loads are applied. A single contact point $n_h = 1$ is considered here. While the contact Jacobians at the CoP vectors $\mathbf{J}_{C_P}$ have fixed parameters, the Jacobian $\mathbf{J}_{a_h}$ at the contact points $\mathbf{x}_{a_h}$ varies, depending on which body link the load is applied to and on the application point position of the load in such a body link, so it is a function of $\mathbf{q}$ and $\mathbf{x}_{a_h}$. Conversely, in the procedure described above (Section 4.2), the Jacobian $\mathbf{J}_{a_h}$ was fixed like $\mathbf{J}_{C_P}$. Then, deriving from (4.1) and (4.2), the overloading joint torques can be defined as

$$\Delta\boldsymbol{\tau}_s = \mathbf{S}^T(\boldsymbol{\tau}_{wt} - \boldsymbol{\tau}_{wo}) = -\mathbf{J}^T_{a_h}\mathbf{f}_h + \sum_{i=1}^{n_f}\left(\mathbf{J}^T_{\hat{C}_{P_{wo}{}^i}}\zeta_i\mathbf{f}_h - \mathbf{J}^T_{\Delta C_{Pi}}\mathbf{f}_{wt,i}\right), \tag{4.6}$$

with the Jacobian of the CoP displacement defined as $\mathbf{J}_{\Delta C_{Pi}} = \mathbf{J}_{C_{P_{wt}{}^i}} - \mathbf{J}_{\hat{C}_{P_{wo}{}^i}}$.

Experimental Analysis

Two healthy volunteers, one female and one male, labeled as subject 1 and subject 2, respectively, (age: 28 and 34 years; mass: 50 and 76 kg; height: 171 and 178 cm)

[2] A video showing the whole procedure to detect online the contact point and estimate the joints physical load is available at `https://youtu.be/uqide04oABk`.

were recruited in the experimental analysis. A written informed consent was obtained for both of them. To monitor the human whole-body motion, the Xsens MVN Biomech suit presented in Subsection 3.1.1 was employed, while the whole-body CoP and vGRF were measured using the Kistler force plate presented in Subsection 3.1.2. The whole experimental procedure was carried out in accordance with the Declaration of Helsinki and the protocol was approved by the ethics committee ASL Genovese N.3 (Protocol IIT_HRII_001). The experimental setup is depicted in Figure 4.2.

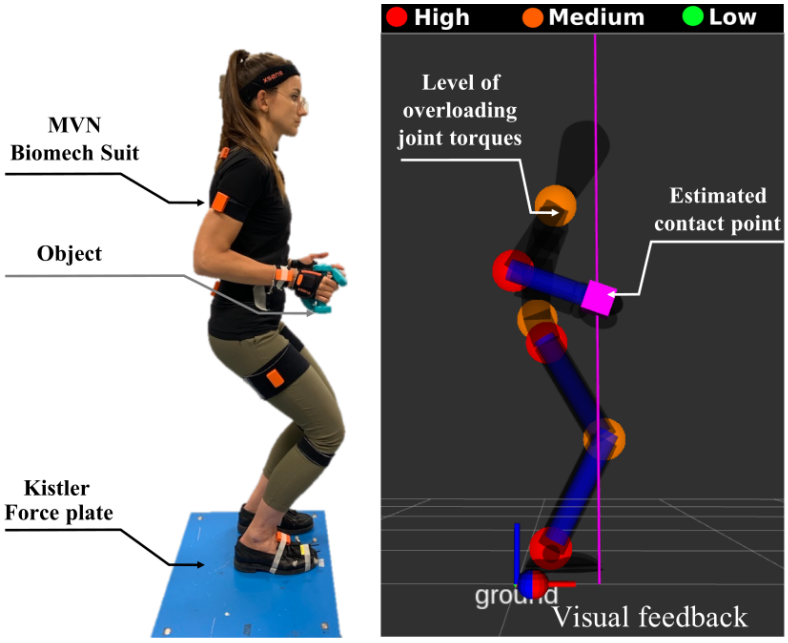

Figure 4.2: *Overview of the experimental setup. All the sensors and the object involved in the experiment are shown on the left. The visual feedback that was provided to the subjects is illustrated on the right, showing the current status: the estimated contact point and the level of the joints overloadings.*

For purposes of the experiment, the subjects were asked to move freely in the sagittal plane in a quasi-static way and perform symmetrical movements with the upper and lower limbs while holding a 5 kg box. The movements were constrained to the sagittal plane since a human sagittal model was considered. The experimental session was divided into two phases. In the first phase, the contact point x_{a_h} was detected using the procedure explained in Subsection 3.2.3. A significance level of 0.05 (5%) was selected to set both the Anderson-Darling test critical value and the z^* value to compute the confidence interval. Accordingly, A^2_{critical} was equal to 0.735, z^* was equal to 1.96 and $\delta_{m,\text{threshold}}$ was equal to 0.01 m, respectively. In the second phase, once the contact point position was found, the overloading torque vector on the human main joints was computed using (4.4), by varying the contact point Jacobian $\mathbf{J}_{a_h}$ depending on the contact point position $\mathbf{x}_{a_h}$ estimated. To compute the whole-body CoP model, needed for the computation of the overloading joint torques, the SESC parameters, identified specifically for the recruited subjects in previous experimental analysis, were employed. During the experiment, the participants were provided with visual feedback (see Section 5.1) showing the current body configuration, the position of the estimated contact point, and the overloading torque on the more meaningful joints, as illustrated in the right side of Figure 4.2.

Results

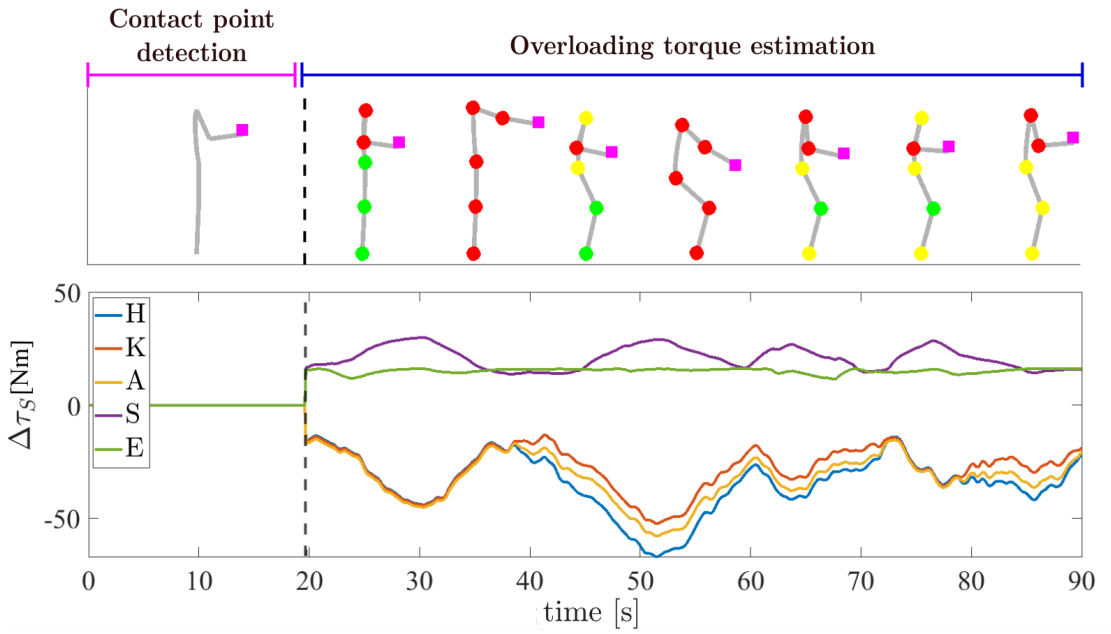

(a) *Results for subject* 1.

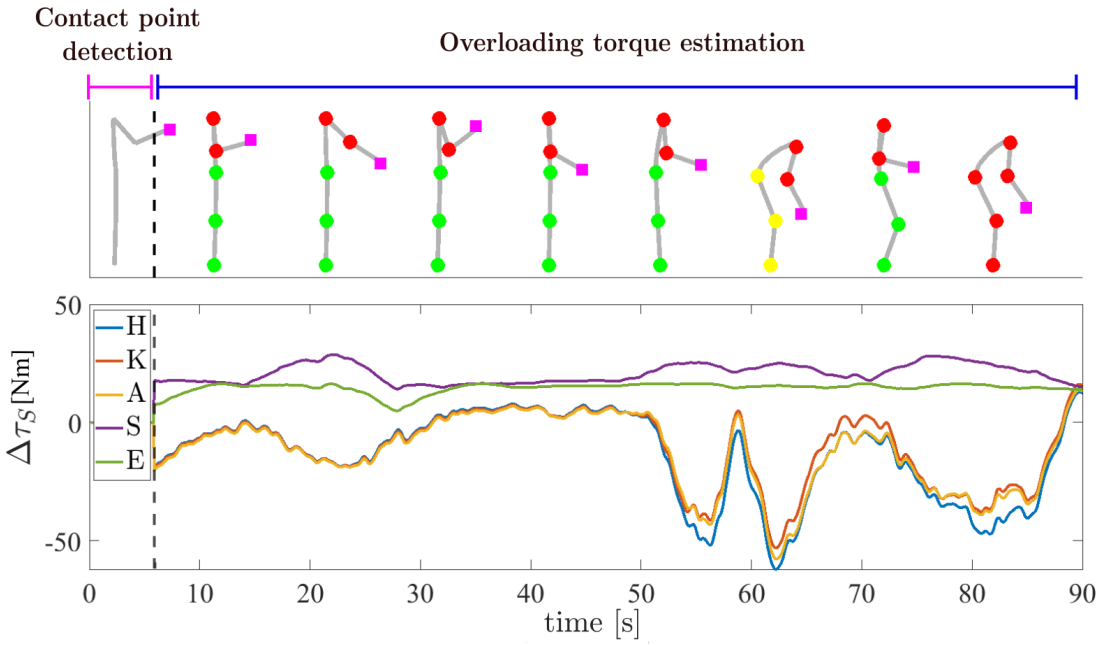

(b) *Results for subject* 2.

Figure 4.3: *Results of the experimental application of the contact point detection method in the estimation of the overloading joint torques. For subject* 1 ***(a)*** *and for subjects* 2 ***(b)****, respectively, the human posture in some illustrative instants throughout the experiment (upper graph) are represented. The overloading torques induced by the external load are displayed in the form of spheres superimposed on the stick-model, color-coded to denote a high (red), medium (yellow) or (low) level. Their trend is also illustrated (lower graph) in the human main joints: hip (H), knee (K), ankle (A), torso (T), shoulder (S) and elbow (E).*

In Figure 4.3 the results of the demonstration experiments are illustrated for subject 1 (Figure 4.3a) and for subject 2 (Figure 4.3b), respectively. As explained in the previous paragraph, the experiment was divided into two phases: the contact point detection and the overloading joint estimation. A black dotted line separates the two phases in the plots. For each subject, two graphs are reported. In the upper one, the two-dimensional (2D) stick-model of the human is depicted in some illustrative body configurations throughout the experiment. Only during the second phase, the overloading joint torques, which are computed based on the contact point estimated in the first phase, are displayed in the form of spheres superimposed on the stick-model, color-coded to denote a high (red), medium (yellow) or (low) level of joint overloading. Details about how the three levels of the ergonomic index are determined will be provided in Section 5.1. The contact point position is depicted as well through a pink square. This information was provided online to the subject by means of the graphical interface during the experiment. The percentage error of the contact point positions and the estimation time are: 5.04% and 19.60 s for subject 1 and 9.83% and 5.80 s for subject 2, respectively. In the lower graph, the overloading torque values for the human main joints: hip (H), knee (K), ankle (A), torso (T), shoulder (S), and elbow (E) are shown. In the first phase, before the black dotted line, the values are zero since the contact point is not found yet while in the second phase, after the black dotted line, it is possible to compute them. As explained in the previous paragraph, only symmetrical movements were performed in this experiment thus the information of the two legs and arms is considered to be equal.

Discussion

For both subjects 1 and 2, the link including the contact point was correctly identified and the localisation accuracy is considered acceptable to the extent of the industrial applications addressed in this thesis. Accordingly, it is possible to assume that the overloading torque computed on the basis of the estimated contact points are good indicators for the mechanical overburden of the human body structures while performing activities with an external load.

4.3 Overloading Joint Fatigue

For the mitigation of risks associated with repetitive and monotonous lightweight tasks, the overloading joint torque method presented in Section 4.2 would not be suitable. In fact, the overloading torques induced by a light payload (e.g. a lightweight tool) are low/moderate and the associated risk of joint injuries is not significant. On the other hand, even if the instantaneous overloading torques are not high, the building up of their effect on the joints over a protracted period of time could become hazardous. Accordingly, the focus of [31] was to develop a whole-body fatigue model to evaluate the cumulative effect of the overloading torque induced on the joints throughout time by light payloads. In addition, since the perception of fatigue is expected to be subject-specific, an index called fatigue ratio K is considered in the model, which is computed experimentally. The less the subjects can support a load, the greater the fatigue ratio K and the quicker the accumulation of joint fatigue.

Fatigue and Recovery Model

The proposed overloading joint *fatigue model* is based on the model proposed in [42] and represented by an RC circuit with zero initial charge state, which is mathematically modelled by a differential equation. However, in [42] the fatigue ratio K was considered as a constant and set equal to 1 while it is estimated experimentally in the presented model. The overloading joint fatigue of the i-th joint τ_i^F at a time instant t can be defined as

$$\tau_i^F(t) = \Delta\tau_i^{\max}\left(1 - e^{\int_0^T -K_i \frac{\Delta\tau_i(t)}{\Delta\tau_i^{\max}} \mathrm{d}t}\right), \tag{4.7}$$

where $\Delta\tau_i^{\max}$ is the maximum joint overloading for the i-th joint, K_i is the fatigue ratio for the i-th joint (see next section for details), and $\Delta\tau_i(t)$ is the overloading torque for the i-th joint at a time instant t, computed as explained in Section 4.2.

Along with the overloading joint fatigue model, a *recovery model* should also be modelled to describe how the force generation capacity is recovered during rest periods. The recovery model can be defined as

$$\tau_i^F(t) = \tau_i^{\max} - (\tau_i^{\max} - \tau_i^{F_0})e^{-R_i t}, \tag{4.8}$$

where $\tau_i^{F_0}$ is the initial value of the overloading fatigue and R_i is the recovery ratio for the i-th joint, which is set to $2.4K_i$ in accordance with other works on recovery models found in literature [165, 166].

In the new proposed overloading joint fatigue and recovery models, we assume that the relationship between the models is represented by the threshold $\tau_i^{\text{th}} = 0.33\Delta\tau_i^{\max}$. The model can then be defined as

$$\tau_i^F(t) = \begin{cases} \text{Fatigue model} & \text{if } \Delta\tau_i(t) > \tau_i^{\text{th}} \\ \text{Recovery model} & \text{otherwise} \end{cases}.$$

Fatigue Ratio Identification

Since fatigue is strictly related to the individual's physical capacity and feelings, the fatigue ratio K_i must be subject-specific and can be identified experimentally, for each i-th joint. To obtain this ratio, we consider the overloading fatigue model in static conditions, resulted from a constant overloading joint torque in a fixed body configuration. A time interval T_F is defined, similarly to the maximum endurance time (MET) presented in [167], by the period from the beginning of the trial to the time instant at which joint overloading fatigue reaches the current overloading torque $\Delta\bar{\tau}_i$ at joint i. Hence:

$$\tau_i^F(t) = \Delta\tau_i^{\max}\left(1 - e^{-K_i|\Delta\bar{\tau}_i|T_F}\right) = \Delta\bar{\tau}_i, \tag{4.9}$$

where $|\Delta\bar{\tau}_i|$ is the normalised current overloading joint torque, defined as $\Delta\bar{\tau}_i/\Delta\tau_i^{\max}$. Consequently, the fatigue ratio K_i is obtained from the measured T_F in (4.9) as

$$K_i = -\frac{\ln(1 - |\Delta\bar{\tau}_i|)}{|\Delta\bar{\tau}_i|T_F}. \tag{4.10}$$

The fatigue ratio K_i is computed for each i-th joint since the strength exerted by each joint varies and thus the fatigue occurs in different timings.

As a result, the fifth index $\boldsymbol{\omega}_5(\mathbf{q})$ is the joint normalised overloading fatigue and it can be defined as

$$\boldsymbol{\omega}_5(\mathbf{q}) = \frac{\boldsymbol{\tau}^F(t)}{\boldsymbol{\tau}^{F,\max(t)}}.$$

where $\boldsymbol{\tau}^{F,\max}$ is the vector including the maximum values of the human joint fatigue and can be estimated experimentally. The accumulation of local joint fatigue due to external load, which can be monitored by means of $\boldsymbol{\omega}_5(\mathbf{q})$, can result from repetitive actions with lightweight tool/objects protracted over long periods of time. On the other hand, repetitive and monotonous movements are among the most frequently cited risk factors associated with WMSDs, in both experimental science and epidemiologic investigations [168]. Hence, the overloading fatigue index can be another beneficial indicator of humans' physical exposure in the workplace.

4.3.1 Experimental Application of the Method

In this Subsection, the experimental analysis carried out on ten subjects to validate the overloading fatigue model proposed in [31] is presented. First, the procedure for the identification of the fatigue ratio, K_i is described. Next, the outcome of the overloading fatigue model is evaluated by means of a sEMG signal analysis in static conditions. Finally, the capability of the model to monitor online the progression of fatigue is presented for ten subjects performing a painting task with a lightweight tool. Accordingly, three experimental sessions can be distinguished: the model identification, the offline validation, and the online validation. It should be noted that, since tools with a known mass and inertial properties were considered in this experimental analysis, the overloading joint torques were estimated by means of the extended algorithm developed in [169] which enables to perform the computations without the need for external (force/pressure) sensors.

Experimental Setup

Ten healthy volunteers, seven males and three females, (age: 30.1 ± 3.8 years; mass: 65.5 ± 29.5 kg; height: 176.2 ± 5.2 cm) [3] were recruited in the experimental analysis. A written informed consent was obtained after explaining the experimental procedure. The whole experimental procedure was carried out in accordance with the Declaration of Helsinki and the protocol was approved by the ethics committee Azienda Sanitaria Locale (ASL) Genovese N.3 (Protocol IIT_HRII_001).

For the model identification experiment, to determine K_i by means of (4.10), the subjects had to keep a defined position until they were able to support a load without changing even minimally the body configuration. In this way, it was possible to assume that the overloading joint torque $\Delta\bar{\boldsymbol{\tau}}$, which is a function of the body configuration and external load, was constant throughout the experiment. The time interval, defined as T_F, since the subjects started holding the load till when they were no longer able to

[3] Subject data is reported as: mean ± standard deviation.

support it, i.e. when they reached a high level of fatigue, was measured. Firstly, the fatigue ratio K_s was computed for the shoulder joint, given the value of the correspondent overloading joint torque $\Delta\bar{\tau}_s$ in the selected body configuration. To this aim, the subjects were asked to stand and hold a 1.5 kg weight (corresponding to the weight of the painting tool) with the dominant hand, having the arm raised at a $90°$angle with the torso and the elbow slightly bent, the other arm by their side. Then, the fatigue ratio for the other joints K_i could be obtained proportionally, on the basis of the ratio between the maximum overloading joint torque for the shoulder $\Delta\tau_s^{\max}$ and the maximum overloading joint torque for the i-th joint $\Delta\tau_i^{\max}$.

For the off-line validation experiment, the outcome of the proposed overloading fatigue model was compared to physiological fatigue expressed as the variations of the maximum power frequency (MPF) of some significant sEMG signals. In fact, muscle fatigue during submaximal, i.e. isometric contractions, has been shown to be accompanied by decreases in the MPF [170]. Six sEMG sensors were placed on the arm of each subject, specifically on the following muscles: the anterior deltoid (AD), the posterior deltoid (PD), the biceps (BC), the triceps (TC), the brachioradialis (BR) and the extensor carpi ulnaris (EC). To monitor the whole-body motion the subjects were asked to wear the Xsens MVN Biomech suit presented in Subsection 3.1.1. Then, they were required to assume the same body configuration described above (for the fatigue ratio identification experiment) and to perform three trials: to hold the 1.5 kg weight without changing the defined position for three different time interval, respectively 90, 60 and 30 seconds, with the necessary rest time in between. During these trials, the sEMG signals were measured and the overloading joint fatigue was estimated. Prior to the analysis, the sEMG signals were filtered (passband: 1-500 Hz) to remove movement artifacts. Linear regression was then used to extract from the sEMG data the linear model for the MPF, in accordance with studies for sEMG-based fatigue analysis in literature [171, 172]. Both the MPF and the overloading fatigue time series were normalised over time to correspond to the same number of samples for the sake of comparison and the overloading fatigue values were normalised between 0 and 1. It should be pointed out that MPF gives a fatigue estimation at the muscle level while the overloading fatigue model is expressed at the joint level thus a direct comparison between the two variables is not possible. However, their similarities in the percentage of decrement/increment and in the trend can be assessed.

For the online validation experiment, since the aim of the overloading fatigue model is to estimate the risk associated with repetitive lightweight tasks in real-life environments, a typical scenario in the manufacturing industry was selected, namely manual spray painting, which has proven to result in a high incidence of WMSDs [173]. Hence, the capability of the overloading fatigue model to monitor online the progression of fatigue exhibited during manual spray painting was assessed. The subjects, wearing the Xsens suit, were asked to hold a 1.5 kg spray gun with their dominant hand and stand in front of a car bumper (the object which needed to be painted) placed approximately at the height of their torso. Next, following a set of sound signals which dictated a specific timing, they were asked to simulate the painting action with a spray gun in eight predefined points on the car bumper (i.e. P1, P2,$\cdots$, P8), in accordance with a specific order (see Fig. 4.4). After the starting signal, the subjects had to process each point for approximately 15 seconds and, as soon as they heard another sound signal, they

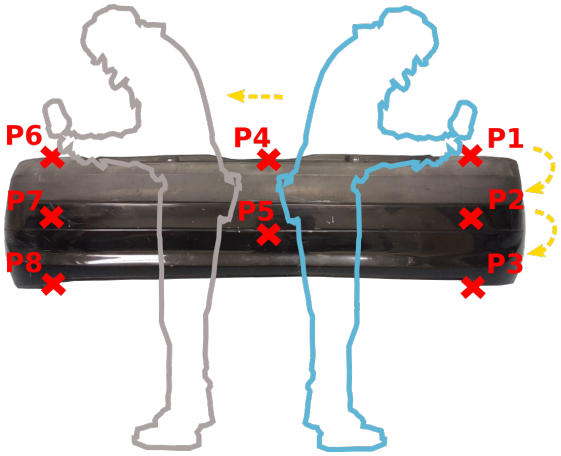

Figure 4.4: *Experimental setup for the online validation experiment of the proposed fatigue model. The subjects were asked to hold a* 1.5 *kg spray gun with their dominant hand and stand in front of a car bumper (the object which needed to be painted) placed approximately at the height of their torso. Next, following a set of sound signals which dictated a specific timing, they were asked to simulate the painting action with a spray gun in eight predefined points on the car bumper (i.e. P1, P2,⋯, P8), in accordance with a specific order.*

were asked to change body configuration to pass to the subsequent point as quickly as possible. The overloading fatigue in the crucial human joints was estimated throughout the experiment for all the subjects and its values were normalised between 0 and 1. Subjects' motion was constrained to the sagittal plane since a human sagittal model is considered in this study. In addition, given that the movements of the leg were almost symmetric, the overloading torques on the joints of the legs were assumed to be equal in the right and in the left one.

Results

The results of the off-line validation experiment are shown in Figure 4.5 for one selected subject. The first line of graphs is related to the variables representative for the shoulder, i.e. the MPF decrement in the AD and PD muscles and the estimated normalised overloading fatigue $|\tau_S^F|$ in the shoulder joint. The second line of graphs, instead, is related to the variables representative for the elbow, i.e. the MPF decrement in the BC and in the TC muscles and the estimated normalised overloading fatigue $|\tau_E^F|$ in the elbow joint. The MPF trend in the BR and in the EC muscles, in retrospect, were considered not significant for the analysis. The mean and the standard deviation of the decrement ratio for both the MPF and the overloading fatigue between all the ten subjects in the three experimental conditions were computed. A t-test was performed and it resulted that all the analysed data come from a normal distribution at the 1% significance level hence the mean and the standard deviation were considered as good indicators for the analysis. Considering all the subjects, the results for the shoulder joint are presented in Table 4.2 while the results for the elbow joint are presented in Table 4.3.

The results of the online validation experiment are illustrated in Figure 4.6 and 4.7. In Figure 4.6a the profile of the angles in all the main joints (hip (H), knee (K), ankle (A), shoulder (S), and elbow (E)) exhibited by one subject throughout the experiment are depicted. In Figure 4.6b, the normalised overloading torque $|\Delta\boldsymbol{\tau}|$ (left side) and

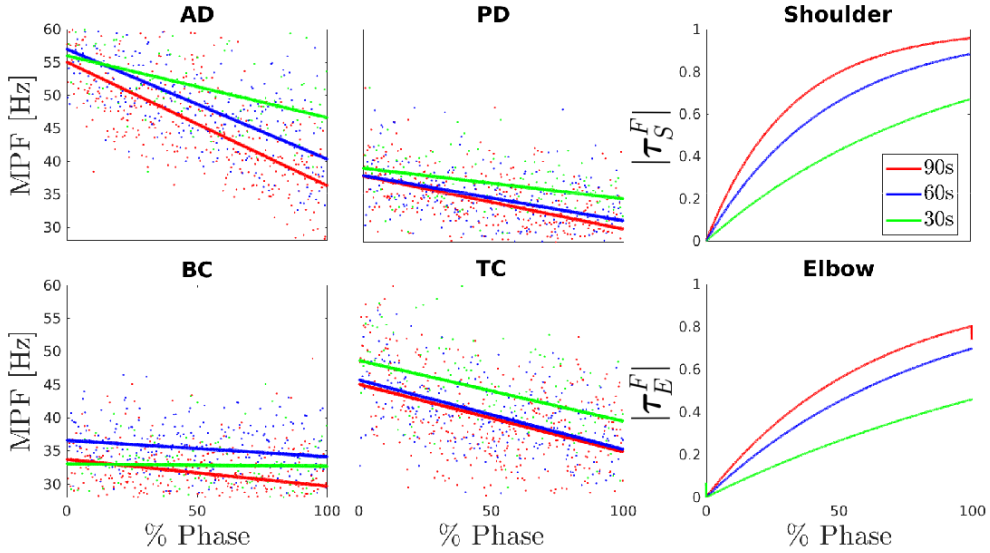

Figure 4.5: *Trend of the the MPF of the sEMG signals measured in the anterior deltoid (AD), posterior deltoid (PD), biceps (BC) and triceps (TC) muscles and trend of the overloading joint fatigue estimated in the shoulder and in the elbow throughout 3 different trial lasting* 90, 60 *and* 30 *seconds respectively, for one subject.*

Table 4.2: *Mean and standard deviation computed between ten subjects of the MPF of the EMG signals measured in the anterior deltoid (AD) and posterior deltoid (PD) muscles and of the overloading joint fatigue estimated in the shoulder in three trials lasting* 90, 60 *and* 30 *seconds, respectively.*

Period	EMG % dec.		Fatigue % inc.
	AD	PD	Sho
90s	24.92±10.08	20.06±8.74	94.42 ± 10.38
60s	16.45±12.71	15.73±9.78	87.48±14.24
30s	6.90±9.65	4.02±9.02	65.32±14.56

the normalised overloading fatigue $|\boldsymbol{\tau}^F|$ (right side) are presented in the shoulder (S) and in the elbow (E) - the joints more at risk for this specific task - for one subject. These graphs show how the trend of the overloading fatigue varied depending on the value of the overloading torque: if $|\Delta\boldsymbol{\tau}|$ was over the threshold, $|\boldsymbol{\tau}^F|$ increased while it decreased under the threshold since the recovery mode was initiated. In Figure 4.7 the mean and the standard deviations of the joint overloading torque (left side) and of the fatigue (right side), respectively, computed between all the ten subjects are displayed in all the main joints (hip (H), knee (K), ankle (A), shoulder (S) and elbow (E)). It is evident that the trend of the overloading torque was very similar between the subjects since the timing of the task was fixed and the body configurations chosen by the subjects were very similar. The overloading fatigue, instead, is more variable since it depends on the subject-specific fatigue ratio K.

Table 4.3: *Mean and standard deviation computed between ten subjects of the MPF of the EMG signals measured in the biceps (BC) and triceps (TC) muscles and of the overloading joint fatigue estimated in the elbow for three trials lasting* 90, 60 *and* 30 *seconds, respectively.*

Period	EMG % dec.		Fatigue % inc.
	BC	TC	Elb
90s	8.27±7.50	19.48±5.20	57.03 ± 8.13
60s	4.47±9.80	14.81±7.58	46.43±8.45
30s	-0.34±6.91	6.21±8.54	31.97±8.77

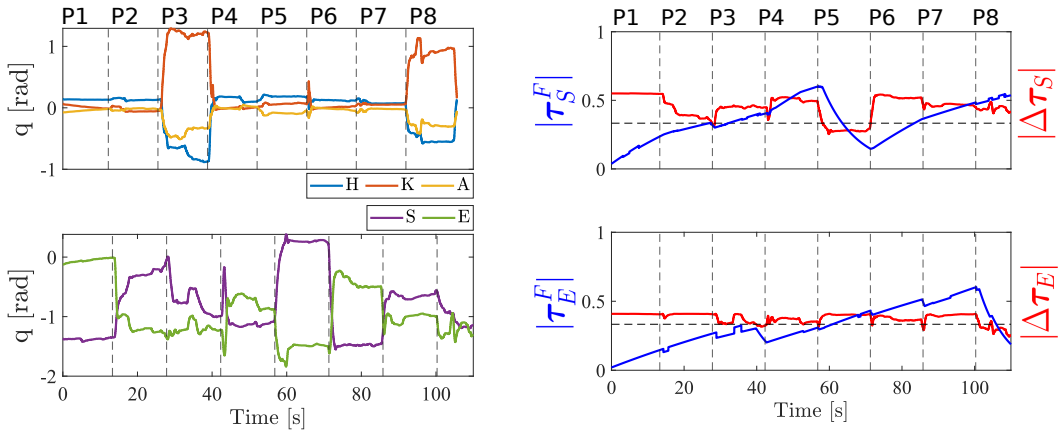

(a) **(b)**

Figure 4.6: *(a) joint angles profiles in the main body joints: hip (H), knee (K), ankle (A), shoulder (S) and elbow (E) for one subject. (b) overloading joint torque (red line) and overloading joint fatigue (blue line) estimated in the shoulder (S) and in the elbow (E) for one subjects.*

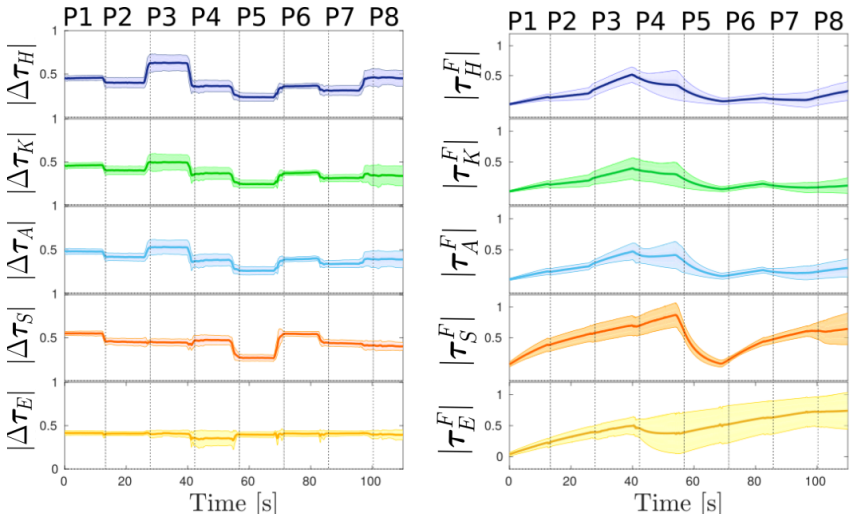

Figure 4.7: *Mean and standard deviation of the overloading joint torque (left side) and of the overloading joint fatigue (right side) computed between ten subjects in the main body joints: hip (H), knee (K), ankle (A), shoulder (S) and elbow (E).*

Discussion

In this paragraph, the results of the off-line validation experiment are first discussed and then the outcome of the online validation experiment is addressed.

In Figure 4.5 it is possible to observe that, as expected, a longer trial corresponds to a greater decrement of the sEMG signals MPF in all the considered muscles. Correspondingly, the overloading fatigue model is able to reproduce the same trend but, clearly, in the opposite way, since the progression of fatigue is described through an increasing function in the proposed method. For all the subjects, an increment trend comparable to the decrement trend of the sEMG signals MPF, in the three experimental conditions, is demonstrated. In view of the above, the overloading fatigue model shows promising capabilities to account for the accumulation of physiological fatigue throughout time. It should be pointed out that the performance of the proposed approach was tested by executing isometric, i.e. constant length (static) muscle contractions because sEMG measurements can be considered far more reliable in such conditions and can be used for evaluations. Nevertheless, as previously said, in dynamic conditions sEMG estimations are questionable while the proposed model has the potential to be employed even in the dynamic case, i.e. when the subject moves to perform a task or applies different forces at hand.

On the other hand, the results of the online validation experiment highlight the benefit, introduced by the proposed fatigue model, of addressing the cumulative effect of the overloading torque throughout time. Considering the elbow joint in Figure 4.6b as an example, the overloading torque value remained moderate and almost constant over the entire duration of the task thus it did not represent a potential source of risk. Conversely, the overloading fatigue took into consideration its cumulative contribution and, after some time, increased significantly, proving its capability to identify the hazards associated with fatigue progression while performing repetitive tasks involving light payloads.

4.4 Energy-related Variables

4.4.1 Overloading Joint Power

The sixth index $\boldsymbol{\omega}_6(\mathbf{q})$ is the joint normalised overloading power which can be defined as

$$\boldsymbol{\omega}_6(\mathbf{q}) = \frac{\mathbf{P}}{\mathbf{P}^{\max}} = \frac{\dot{\mathbf{q}}_h \Delta\boldsymbol{\tau}_s}{\dot{\mathbf{q}}_h{}^{\max} \Delta\boldsymbol{\tau}^{\max}}.$$

where $\Delta\boldsymbol{\tau}_s$ is the overloading joint torque vector, $\Delta\boldsymbol{\tau}^{\max}$ is the vector including the corresponding maximum values, $\dot{\mathbf{q}}_h$ is the joint velocity vector and $\dot{\mathbf{q}}_h{}^{\max}$ is the vector including the joints maximum velocities. Based on human joint power, several procedures can be found in the literature with the aim to estimate the physical effort needed during gait [174, 175] but also to detect potential risk in manual material handling [99]. Overloading joint power is different from joint power in his classical conception since the overloading joint torques (which takes into account only the effect of an external load) and not the net joint torques are employed in the computation. Nevertheless, it is considered worthwhile to investigate also $\boldsymbol{\omega}_6(\mathbf{q})$ as a further possible indicator of the physical expenditure during occupational activities.

4.4.2 Delta CoM Potential Energy

In [176], the change in potential energy of human body masses was employed as a measure of performance within an optimisation-based approach to model human motion. Based on that, the "delta CoM potential energy" index was developed. The potential energy for the CoM of the human body can be obtained by multiplying the height of the CoM, thus the z-coordinate, by the force of gravity and the human body mass. However, such a quantity is not evaluated directly but rather its variation between different body configurations is considered. Accordingly, two potential energies are defined: $E_P^0 = mg^T C_M^0|z$ which is associated with a neutral and natural body configuration and $E_P = mg^T C_M|z$ which is associated with the current one. Hence, delta CoM potential energy can be defined as

$$\Delta E_P = E_P - E_P^0 = Mg\Delta C_M|z = Mg(C_M|z - C_M^0|z),$$

where M is the mass of the subject, g is the gravity acceleration and $\Delta C_M|z$ is the variation of the z-coordinate of the CoM, with $C_M^0|z$ the CoM in the neutral posture and $C_M|z$ the CoM in the current one. Such a quantity provides the degree of deviation of the the posture of the subjects from a neutral and convenient body configuration. Hence, to some extent, it is capable to monitor the risk associated with awkward and unfavourable postures, which, as noted above, are a major contributor to the development of WMSDs. Accordingly, the seventh index $\boldsymbol{\omega}_7(\mathbf{q})$ is the normalised delta CoM potential energy and it can be defined as

$$\boldsymbol{\omega}_7(\mathbf{q}) = \frac{\Delta E_P}{\Delta E_P^{\max}} = \frac{\Delta C_M|z}{\Delta C_M|z^{\max}}.$$

where ΔCoM_z^{max} is the maximum displacement of the CoM height (z-coordinate) and it can be estimated experimentally. It should be noted that only the vertical movement of the human CoM is taken into account by this index. Nevertheless, the horizontal

deviations of the CoM (strictly related to the CoP) are thoroughly evaluated by the overloading joint torque and by the other associated indexes.

4.5 Compressive Forces

With the aim to account for the balanced inward ("pushing") forces that result from the interaction of the human with the environment or objects, a new index was proposed in [151]. In particular, the concept of the proposed "compressive forces" was conceived to overcome the limitations of the overloading joint torque index. In fact, there are certain body configurations or task-dependent force profiles (magnitude and direction) that are characterised by negligible joint torques but considerable compressive forces, which may be harmful to the musculoskeletal system. For instance, this happens with body configurations at the edge of the human reachability map, like the one represented in Figure 4.8, where interaction forces present short lever arm but significant compressive potential on the joints. Additionally, the compressive force index takes into account

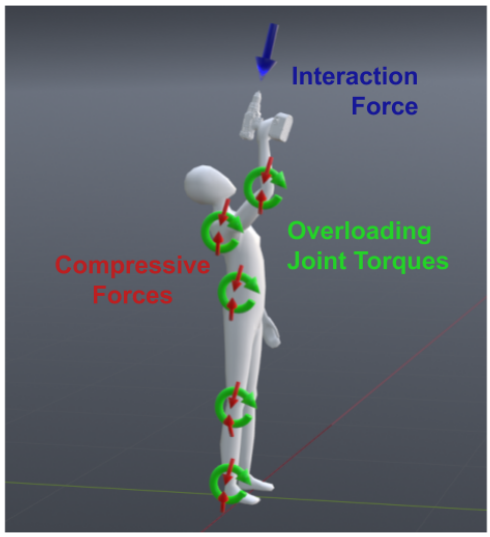

Figure 4.8: *Explanatory body configuration in which interaction force profiles (magnitude and direction) may result in negligible joint torques due to a small lever arm but can induce high compressive forces at the human joints.*

all the components of the external force, in contrast with the overloading joint torque which is based only on the objects' gravitational load.

To address these so called compressive forces, a free-body diagram approach was considered that account for the direct effect on the body of an external forces applied at the end-effector, in accordance with Newton's third law. Hence, the effect of an external force $\mathbf{f}_h \in \mathbb{R}^3$, applied at the human end-effector, on a body joint i can be computed as

$$\mathbf{f}_{C,i} = \mathbf{R}_0^i \mathbf{R}_W^0 \mathbf{f}_{h,\mathrm{EE}}, \tag{4.11}$$

where $\mathbf{R}_i^0 \in SO(3)$ expresses the orientation of frame Σ_0 relative to frame Σ_i and $\mathbf{R}_W^0 \in SO(3)$ expresses the orientation of frame Σ_W relative to frame Σ_0 (see Section 3.2.1 for details about the human model adopted in this thesis). $\mathbf{f}_h$ can be measured

with a suitable forque/torque (F/T) sensor. It should be noted that compressive forces, as defined here, are not intended as biomechanics-related variables but rather are the result of geometric considerations.

Based on the above, the eighth index $\boldsymbol{\omega}_8(\mathbf{q})$ is the joint normalised compressive force and it can be defined as

$$\boldsymbol{\omega}_8(\mathbf{q}) = \frac{\mathbf{f}_C}{\mathbf{f}_C^{\max}}$$

where $\mathbf{f}_C$ is the compressive force vector and $\mathbf{f}_C^{\max}$ is the vector including the corresponding maximum values, which can be found experimentally.

4.6 Validation of the Human Ergonomics Monitoring System

To validate the human ergonomics monitoring system developed in this Chapter, an experimental analysis was conducted on twelve subjects considering three different tasks that represent typical occupational activities in manufacturing industries and, additionally, are associated with different potential risk factors to the development of WMSDs. While the subjects were performing such activities, their whole-body motion and the forces they exchanged with the environment were measured. Then, the set of proposed ergonomic indexes was computed in an off-line phase. It should be underlined that, as previously said, the proposed indexes are conceived to perform an online evaluation. However, in this study, they are computed a posteriori for the sake of a thorough analysis. The outcome of the proposed indexes is investigated to establish their link with the main ergonomic risk factor such as mechanical overloading of the body structures or monotonous actions repetitiveness. To provide a benchmark of the effective physical effort required for the tasks, muscle activity is monitored throughout the whole duration of the experiments. In addition, a comparison is made with the ergonomic risk scores resulting from the EAWS [72], which are a well-recognised and exhaustive method to evaluate workers' physical exposure. The corresponding analysis and computations are carried out in collaboration with Fondazione Ergo (headquarters: Varese, Italia).

The reasoning underlying this experimental analysis is expressed with the objective to offer the proposed human monitoring system as a possible tool to assess human ergonomics, with the added groundbreaking benefit of an online and subject-specific evaluation.

4.6.1 Experimental Analysis

In this section, the experimental analysis conducted on human subjects to validate the proposed ergonomics monitoring system is presented. Firstly, a calibration experiment was performed to identify the subject-specific whole-body CoP model by means of the SESC technique presented in Section 3.2.2. Next, three different tasks were performed by each participant with the aim to simulate, in the laboratory settings, occupational activities which are commonly carried out by workers in the current industrial scenario. Such tasks were selected to encompass the most significant risk factors in the workplace: mechanical overloading of the body joints, variable and high-intensity interaction forces, and repetitive and monotonous movements. Accordingly, lifting/lowering of a heavy object, drilling, and painting with a lightweight tool were considered, respectively, in this study. While the subjects were carrying out such activities, the data regarding the whole-body motion and the forces exchanged with the environment (both GRF and interaction forces at the end-effector) were collected. Lastly, the full set of ergonomics indexes (see Table 4.1) to the assessment of human whole-body kino-dynamic states was estimated in an off-line phase. The whole experimental procedure was carried out in accordance with the Declaration of Helsinki and the protocol was approved by the ethics committee ASL Genovese N.3 (Protocol IIT_HRII_001). Twelve healthy volunteers, eight males and four females, (age: 28.9 ± 3.5 years; mass: 69.3 ± 13.5 kg; height: 173.9 ± 6.8 cm)[4] were recruited in the experimental analysis. A written informed consent was obtained after explaining the experimental procedure.

[4] Subject data is reported as: mean ± standard deviation.

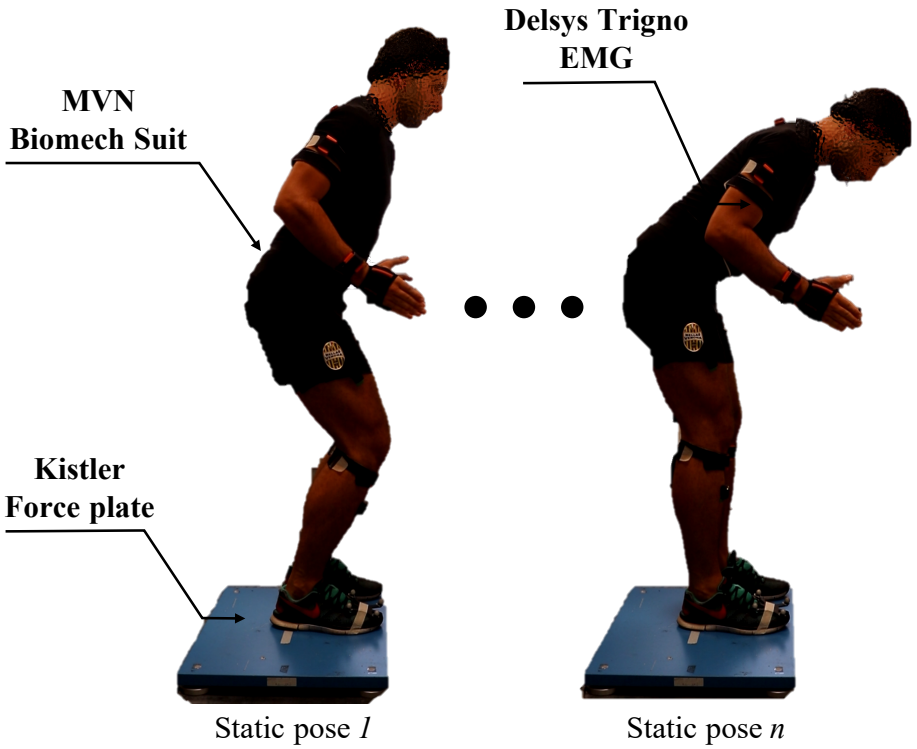

Figure 4.9: *Overview of the experimental setup. All the sensors involved in the experiments are illustrated. For the calibration experiments, they were asked to hold twenty-five static postures.*

For the calibration experiment, the subjects were asked to wear the Xsens MVN Biomech suit, presented in Subsection 3.1.1, to track the whole-body motion and to stand on the Kistler force plate, presented in Subsection 3.1.2, to measure the whole-body CoP and vGRF. The experimental setup is depicted in Figure 4.9. Then, they were asked to hold twenty-five static postures to build the input data set required for the SESC parameters identification, following the procedure presented in Subsection 3.2.2. During the acquisition, the body configurations were selected arbitrarily by the subjects, but with the requirement to vary the orientations of the body segments as much as possible in between, to collect data as linearly-independent as possible. The subjects were required to the extent possible to restrict their movements to the sagittal plane since a human sagittal model is adopted in this thesis. Accordingly, both the estimated and measured human CoP were projected onto such a plane for the sake of computations. Once the SESC parameters were identified for each participant, they could be used to achieve the subject-specific whole-body CoP estimation in any body configuration.

For the validation experiments, the subjects were asked to wear the Xsens MVN Biomech suit and to stand on the Kistler force plate, to track the whole-body motion and the CoP and GRF, respectively. In addition, ten sEMG sensors were placed on the body of each subject to measure muscle activity as a reference to the effective physical effort required for the tasks. Specifically, the following muscles were analysed: the

Anterior Deltoid (AD), the Posterior Deltoid (PD), the Biceps Brachii (BC), the Triceps Brachii (TC), the Trapezius Descendens (TR), the Erector Spinae (ES), the Gluteus Maximus (GM), the Rectus Femoris (RF), the Biceps Femoris (BF) and the Tibialis Anterior (TA). As in the calibration experiment, the subjects were required to bound their movements to the sagittal plane. Accordingly, the selection of the muscles was made considering the ones more involved in flexion/extension movements. Prior to the experiment, the maximum voluntary contraction (MVC) exerted by each muscle was recorded for all the participants with the aim to normalise the muscle activity. Then, the subjects were required to perform the three selected tasks to simulate industrial occupational activities.

These tasks are illustrated in the next paragraphs and the corresponding procedure and experimental setup as well as the rationale for the selection are provided. Note that, for all the tasks, a trial is referred to as a work cycle. Additionally, a final paragraph presents the processing performed on the data collected during the experiments.

Task 1: Lifting/Lowering a Heavy Object

As explained in Section 1.1, many disorders and injuries that affect the musculoskeletal system are mainly provoked by the mechanical overload of biological structures such as muscles and joints. The potential overload of tissues results from high-intensity forces or torques which act on and within the human body. Among the occupational activities that coincide with high mechanical requirements, one of the most commonly performed in manual manufacturing industries is the handling/carrying of heavy objects. The detrimental effect of mechanical overload primarily depends on the magnitude of the force required to accomplish it. Accordingly, the lifting/lowering of boxes characterised by different weight (thus demanding different effort) was the selected task to evaluate the overburden of body structures as an ergonomics risk factor. To reproduce such a task, the scenario represented in Figure 4.10 was defined.

The subjects had to place their feet in a pre-defined position (on the force plate), 0.5 m far from the wall, and keep them there for the whole duration of a work cycle. The task consisted in lifting/lowering a box on a shelving (with shelves 0.3 m long) and put it/take it at/from three different height levels that where located under the human knees (V1, 0.6 m w.r.t. the floor), at the level of the pelvis (V2, 1.15 m w.r.t. floor) and over the shoulder (V3, 1.7 m w.r.t. floor), respectively. Specifically, the subjects had to pick up the box from the floor, put it on the selected height, keep the position for 3 seconds (without supporting the weight of the box), and then pick up again the box and put it on the floor. The weights of the boxes were 2.5, 5, and 10 kilograms, respectively. During a work cycle, all the possible combinations of box weight/height level were considered in a randomized order. The sequences of the nine box weight/height level combinations (ordered from 1 to 9) to be performed within each work cycle are specified in Table 4.11. The subjects were required to perform three work cycles and between one work cycle and the following, there was a resting period of 2 minutes.

Task 2: Drilling

As mentioned in the previous paragraph, the load affecting the musculoskeletal system during working activities depends mainly on the magnitude of the force exerted/experienced by workers. Nevertheless, other factors can contribute to its intensification,

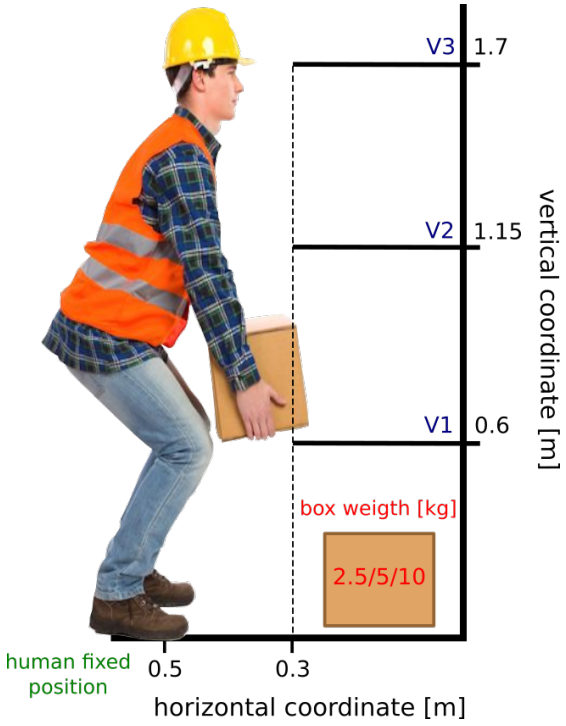

Figure 4.10: *Scenario for ergonomics assessment while performing a lifting/lowering task with a heavy object.*

Figure 4.11: *The sequences of the nine box weights × height levels combinations (ordered from* 1 *to* 9*) to be performed within each work cycle for task 1.*

Trial 1		Height		
		V1	V2	V3
Weight	2.5 Kg Box	1	7	3
	5 Kg Box	9	4	5
	10 Kg Box	6	8	2

Trial 2		Height		
		V1	V2	V3
Weight	2.5 Kg Box	9	4	2
	5 Kg Box	1	8	7
	10 Kg Box	3	6	5

Trial 3		Height		
		V1	V2	V3
Weight	2.5 Kg Box	6	3	9
	5 Kg Box	5	8	2
	10 Kg Box	7	4	1

namely the direction of the force, its variability over time, and the postural demands required to develop it. Accordingly, to assess concurrently these determinants the drilling of panels located in different position and orientations in the work space was selected as the second task, and the scenario represented in Figure 4.12 was defined for this purpose.

The subjects had to place themselves in the same configuration defined for task 1. The task consisted in drilling three wood panels that are located in three different positions (D1, D2, D3) on a shelving, highlighted in green in Figure 4.12. The holes, made with the driller, had to be performed approximately in the points where the red crosses (x) are depicted. Specifically, the three points to be drilled are located at the following horizontal and vertical coordinates: $(0.15, 1.7)$ m, $(0.0, 1.3)$ m and $(0.15, 0.6)$ m respectively. During a work cycle, each point had to be drilled for 10 seconds, in the sequence D1, D2, D3, with a break of approximately 5 seconds in between. Throughout the whole duration of the task, the interaction forces developed at the hand/tool interface were measured. For this purpose, the subjects had to keep the driller through a dedicated handle, which was connected to a F/T sensor (see the left side of Figure

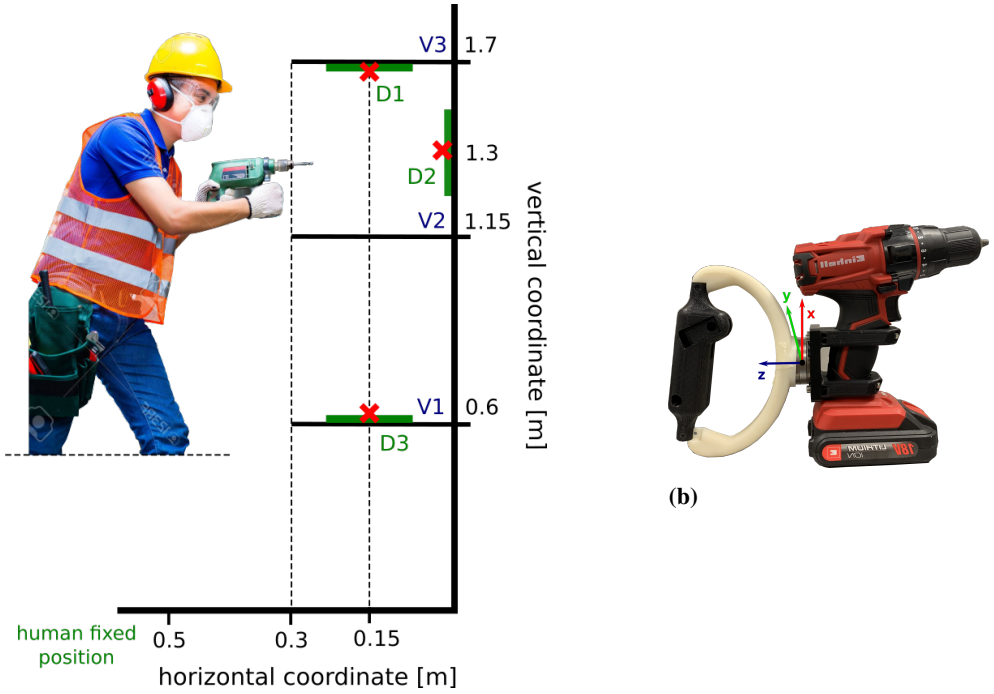

(a) **(b)**

Figure 4.12: *(a) Scenario for ergonomics assessment while performing a drilling task. (b) The tool employed for the task: a driller connected to a F/T sensors and supported by a dedicated handle. The F/T sensor frame is also highlighted.*

4.12). The tool (driller+handle) had to be used with only the dominant hand while the other arm had to be kept stationary along the body. The weight of the full tool was 2.5 kg. The subjects were required to perform three work cycles and between one work cycle and the following, there was a resting period of 2 minutes. The work cycles were all performed following the same procedure.

Task 3: Painting with a Lightweight Tool

An other of the most frequently cited contributors to musculoskeletal failures is represented by monotonous and repetitive manipulations protracted over long periods of time. In fact, repetitive actions with light-weight objects may result in the accumulation of local muscle fatigue, which can cause severe injuries [177, 178]. The pain felt in muscles, nerves, and tendons caused by repetitive movements and overuse can be described with the general term repetitive strain injury (RSI) and mostly affects the upper body structures.

Accordingly, a spray painting task with a lightweight spray gun was selected to evaluate the risk of RSI and the scenario represented in Figure 4.13 was defined.

The subjects had to place themselves in the same configuration defined for the previous tasks. The task consisted in painting two helmets along their whole surface (the surface accessible at best considering the positioning of the helmets) with a spray-gun. The helmets were hanging from a hook at two different height levels (V2, V3) that are 1.15 m and 1.7 m respectively. During a work cycle, the subjects had to spray each helmet (first the one located at V3, next the one located at V2) moving smoothly and

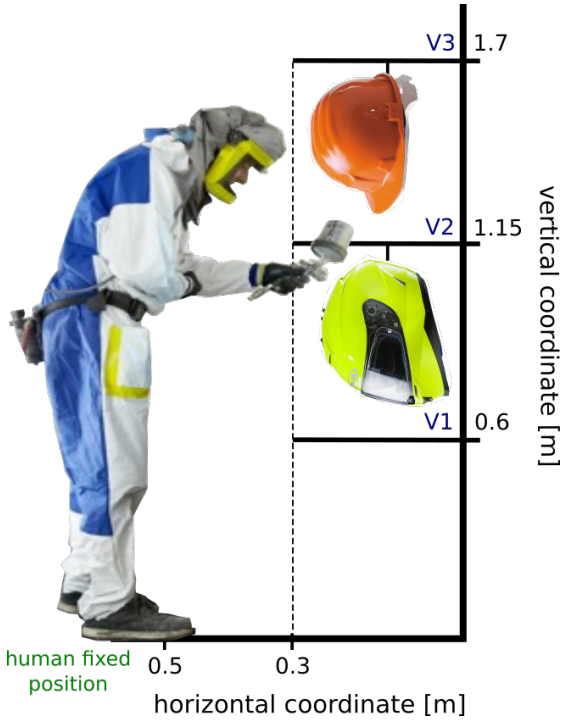

Figure 4.13: *Scenario for ergonomics assessment while performing a spray painting task.*

slowly the spray-gun in proximity to the helmet: from the top to the bottom for 10 seconds, then from to the bottom to the top for 10 seconds and finally again from the top to the bottom for 10 seconds. In total, each helmet has to be painted for 30 seconds, with a break of 5 seconds approximately in between. The subjects were required to perform three work cycles and between one work cycle and the following, there was a resting period of 2 minutes. The work cycles were all performed following the same procedure.

Data Processing

For all the tasks described above, for all the related trials (work cycles), and for all the twelve subjects, the full set of ergonomic indexes proposed in this thesis (see Table 4.1) to the assessment of human whole-body kino-dynamic states was estimated. For task 1 and task 2, the most significant events throughout the execution of the tasks were identified and data were cut accordingly, with the aim to extract the data sections of interest to the analysis. Specifically, for each trial of Task 1, nine data sections corresponding to a lifting action and nine data sections corresponding to a lowering action were extracted (due to the three box weights $\times$ the three height levels experimental conditions). On the other hand, three data sections corresponding to a drilling action were extracted for each trial of task 2. For task 3, no cutting was performed in any of the trials. In fact, the repetitiveness of movements and actions over time and thus the build-up of the effects of physical exposure was analysed in this case. Subsequently, the data of each action for trials 1 and 2 and the full data of task 3 were normalised over time to 101 frames (0 – 100% of the action or task progression) for the sake of comparison. The latter operations were performed for all twelve subjects. Finally, the data were

averaged among the three trial for each subject and then, among the twelve subjects. The sEMG signals for all the ten muscles were first filtered (pass band: 1-500 Hz) to remove movement artifacts. Then, they were rectified and normalised using the MVC values previously recorded for each subject.

4.6.2 Results

In this Subsection, the results of the validation experiments are presented for all the three selected tasks performed by twelve subjects. A specific paragraph is dedicated to the outcome of the analysis carried out using the EAWS method.

Task 1: Lifting/Lowering a Heavy Object

In Figures from 4.14 to 4.20 some of the proposed ergonomic indexes are presented for task 1. Both the lifting (red lines) and lowering (blue lines) actions are illustrated considering all the three box weights, namely 2.5 (a - first row), 5.0 (b - second row), and 10.0 kg (c - third row) and the three height levels, namely low (dashed lines), mid (dotted lines) and high (solid lines). The mean values computed among the twelve subjects (in turn averaged among the three trials) for the overloading torque $|\Delta\boldsymbol{\tau}|$, the overloading power $|P|$, the angle $\mathbf{q}$, the velocity $|\dot{\mathbf{q}}|$ and the acceleration $|\ddot{\mathbf{q}}|$ are represented in the human main joints. Specifically, each Figure corresponds to a joint: hip (H - Figure 4.14), knee (K - Figure 4.15), ankle (A - Figure 4.16), back (B - Figure 4.17), shoulder (S - Figure 4.18), elbow (E - Figure 4.19), and wrist (W - Figure 4.20). The standard deviation values computed among the twelve subjects are also highlighted for $|\Delta\boldsymbol{\tau}|$ and $|P|$. The just mentioned ergonomic indexes are selected for task 1 since they are expected to provide more relevant information for the purpose of physical exposure assessment in relation to the specifications of the task itself. In fact, since considerable mechanical overloading of the body is envisaged during lifting/lowering of a heavy load, overloading joint torque and overloading joint power will be analysed. In addition, the full joints kinematics (i.e., angles, velocities and accelerations) and the CoM potential energy are examined. Note that all the quantities presented are normalised with respect to their maximum value as defined in Chapter 4 except the joint angles for whom the raw value is given for the sake of the analysis.

At the hip level, no significant differences can be observed on the whole. $|\Delta\tau_H|$ and $|P_H|$ values show similar trends and both remain in the lower half of the plot for all the box weight and height level conditions. q_H increases following the height level condition from low to high, but is almost equal among different boxes weights. As expected, only flexion is performed and in a similar way for all the experimental conditions. $|\dot{q}_H|$ shows different profiles among the experimental conditions but its maximum value is approximately the same. $|\ddot{q}_H|$ is quite constant in the lifting phase except for a peak at the end of the action at low height level for all the box weight conditions. In the lowering phase, more variable trends can be noted among the experimental conditions. However, maximum acceleration values are quite low and similar to each other.

At the knee level, $|\Delta\tau_K|$ and $|P_K|$ values are generally higher than at the hip level. Among different height levels they don't show meaningful differences but, from 2.5 to 10.0 kg of the box weight, an increment, more pronounced for $|\Delta\tau_K|$, can be observed in both the lifting and lowering phase. q_K is almost equal for all the experimental conditions except a slight decrement for low height level. As at the hip level, only

flexion is always performed with no particular variations. $|\dot{q}_K|$ shows a sort of M-shaped profile and its maximum value is approximately the same in all the experimental conditions, a bit lower than at the hip level. $|\ddot{q}_K|$ tends to increase in the lifting phase and to decrease in the lowering phase and, as at the hip level, maximum values do not show significant magnitudes.

At the ankle level, $|\Delta\tau_A|$ exhibits an increase from 2.5 to 10.0 kg of the box weight as at the knee level and similarly, there are no significant differences among height levels. A comparable behaviour is shown by $|P_A|$ but less prominent. q_A presents comparable values and limited ROM for all the experimental conditions. As regards $|\dot{q}_A|$ and $|\ddot{q}_A|$, the observations done at the knee level can be repeated.

At the back level, a substantial rise in $|\Delta\tau_B|$ with increasing weight of the box can be noted, together with a moderate one with increasing height level. As a result, very high values of overloading are reached in some conditions, especially with 10.0 kg. $|P_B|$ is overall quite low, except a small increment for the 10 kg box condition. No significant flexion can be observed from q_B. Its ROM grows from low to high height levels. Both $|\dot{q}_B|$ and $|\ddot{q}_B|$ are rather low and steady among all the experimental conditions.

At the shoulder level, $|\Delta\tau_S|$ exhibits trends similar to those at the back level, increasing considerably with the box weight and less with the height level. Accordingly, also at the shoulder level, significant values of overloading are achieved and mostly for the 10.0 kg box weight condition. $|P_B|$ is overall low but it presents a peak at the end of the actions which increases both with the box weight and the height level. As for the previous joints, q_S ROM increases with the height level and its trend does not vary significantly among different experimental conditions. $|\dot{q}_S|$ maximum values are higher than at the knee, ankle, and back level and comparable to those at the hip level. The profiles are similar among the experimental conditions. $|\ddot{q}_S|$ tends to increase in the lifting phase and to decrease in the lowering phase and maximum values are not meaningful as at the knee and ankle level.

At the elbow level, what was said as regards the shoulder level can be basically repeated. The only exception is that $|\Delta\tau_E|$ seems to be higher for the mid height level than for the high height level for all the box weight conditions. In addition, it should be noted that q_E, as q_K, at the knee level approaches the ROM boundaries and tends to grow over the course of the actions.

At the wrist level, $|\Delta\tau_W|$ do not show meaningful differences among height levels but present a considerable growth with increasing box weight and thus high values of overloading can be observed, as for the back, shoulder, and elbow. On the whole, $|P_W|$ is low, except for a slight increment for the 10 kg box weight condition. q_W and $|\dot{q}_W|$ do not exhibit relevant peculiarities since q_W ROM is limited and $|\dot{q}_W|$ is globally low and approximately steady. On the other hand, $|\ddot{q}_W|$ shows quite variable profiles among the different experimental conditions and is significantly higher than for all the other joints.

To recap, $|\Delta\boldsymbol{\tau}|$ in the lower body presents overall a moderate value. No meaningful differences can be observed among different height levels but a modest rise can be noted with increasing box weights. On the other hand, $|\Delta\boldsymbol{\tau}|$ in the upper body (back + arm) shows substantial growth with increasing weight of the box and an appreciable growth also with increasing height level. At the elbow level, $|\Delta\tau_E|$ exhibits a higher value for the mid height condition. Most likely, for the high height condition, the load was sup-

ported mostly by the shoulder thus the effort in the elbow do not increase. No relevant information is provided by $|P|$ in general, except for some peaks that increase with both the box weight and height level conditions, noticeable at the shoulder and elbow level. Considering $\mathbf{q}$, the most remarkable ROM and maximum values are presented at the knee and at the elbow level, to a small extent at the hip level. The values of $|\dot{\mathbf{q}}|$ are globally moderate and steady among different experimental conditions and the same reasoning is valid for the values of $|\ddot{\mathbf{q}}|$, excluding the more considerable accelerations exhibited at the wrist level.

In Figures 4.21, 4.22 and 4.23 the muscle activity in the leg, in the back and in the arm, respectively, is presented for task 1. Both the lifting (dark green lines) and lowering (light green lines) actions are illustrated considering all the three box weights, namely 2.5 (first row), 5.0 (second row) and 10.0 kg (third row) and the three height levels, namely low (dashed lines), mid (dotted lines) and high (solid lines). The mean and standard deviation values computed among the twelve subjects (in turn averaged among the three trials) are represented. Specifically, the muscles analysed are: the Rectus Femoris (RF), the Biceps Femoris (BF) and the Tibialis Anterior (TA) for the leg, displayed in Figure 4.21; the Trapezius Descendens (TR), the Erector Spinae (ES) and the Gluteus Maximus (GM) for the back, displayed in Figure 4.22; the Anterior Deltoid (AD), the Posterior Deltoid (PD), the Biceps Brachii (BC) and the Triceps Brachii (TC) for the arm, displayed in Figure 4.23, respectively.

The leg muscles globally show a moderate activity and similar profiles among all the different experimental conditions. The only exception is the BF that presents noticeable growth with increasing box weight. It should be noted that similar behaviour is exhibited by the $|\Delta\boldsymbol{\tau}|$ in the lower body joints. The back muscles activity overall augment with increasing box weight. TR, in particular, presents considerable growth also with increasing height level. A very similar trend is visible in the arm muscles, more notably in the AD and BC, to a less extent in the TC, which is generally not very active. As for the lower body, the muscles of the back and of the arm basically reflect the pattern of $|\Delta\boldsymbol{\tau}|$ in the upper body joints.

In Figure 4.24, The CoM potential energy is depicted. No significant differences can be observed, neither to vary box weight or to vary height levels.

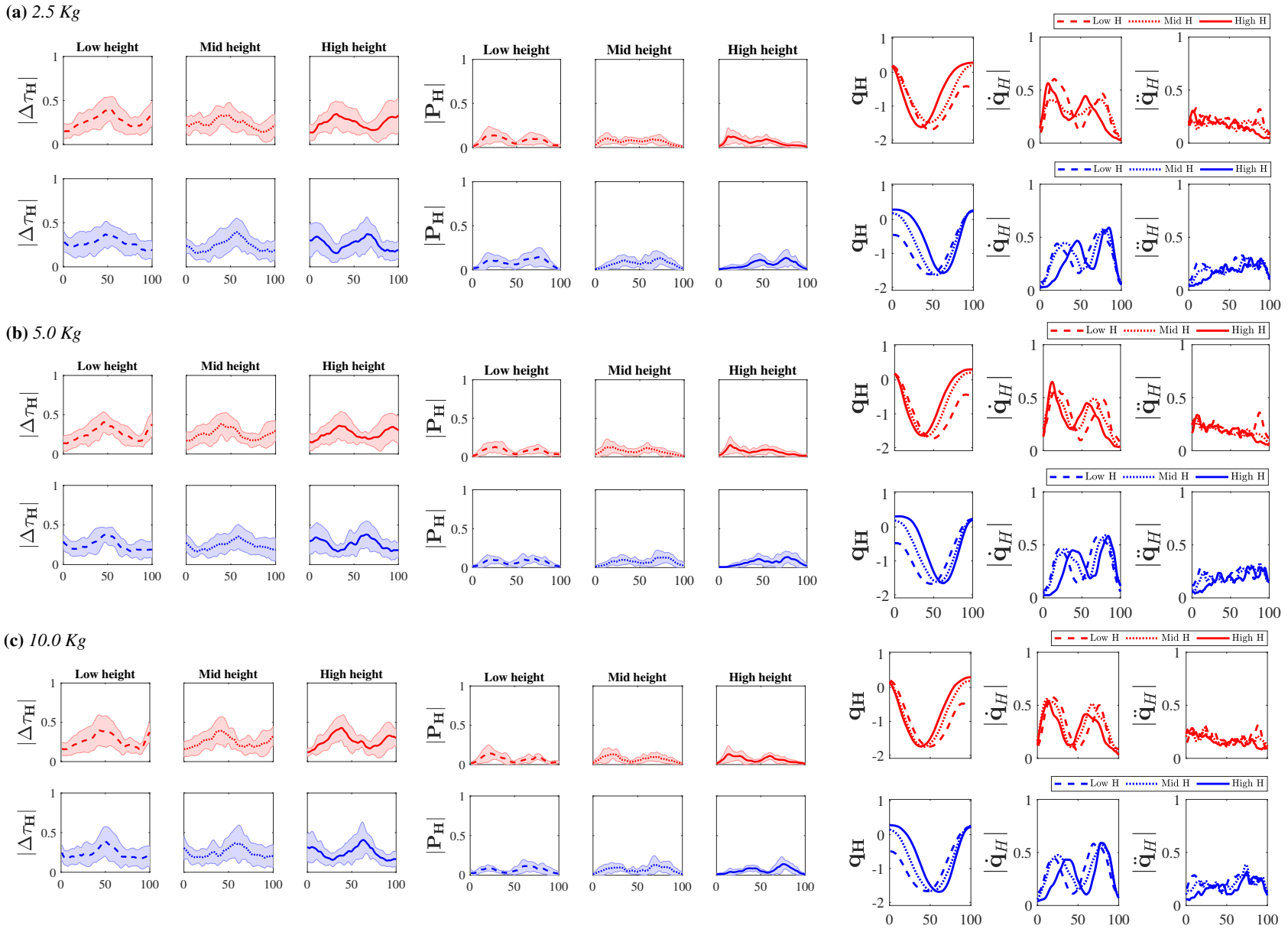

Figure 4.14: *Task 1: overloading torque $|\Delta\tau|$, overloading power $|P|$, angle $\mathbf{q}$, velocity $|\dot{\mathbf{q}}|$ and acceleration $|\ddot{\mathbf{q}}|$ in the **hip** while lifting (red lines) and lowering (blue lines) a box of 2.5 (a), 5.0 (b), and 10.0 (c) kg at three different height levels, namely low (dashed lines), mid (dotted lines), high (solid lines). The mean among twelve subjects (among three trials for each one) is represented. The standard deviation is also highlighted for $|\Delta\tau|$ and $|P|$.*

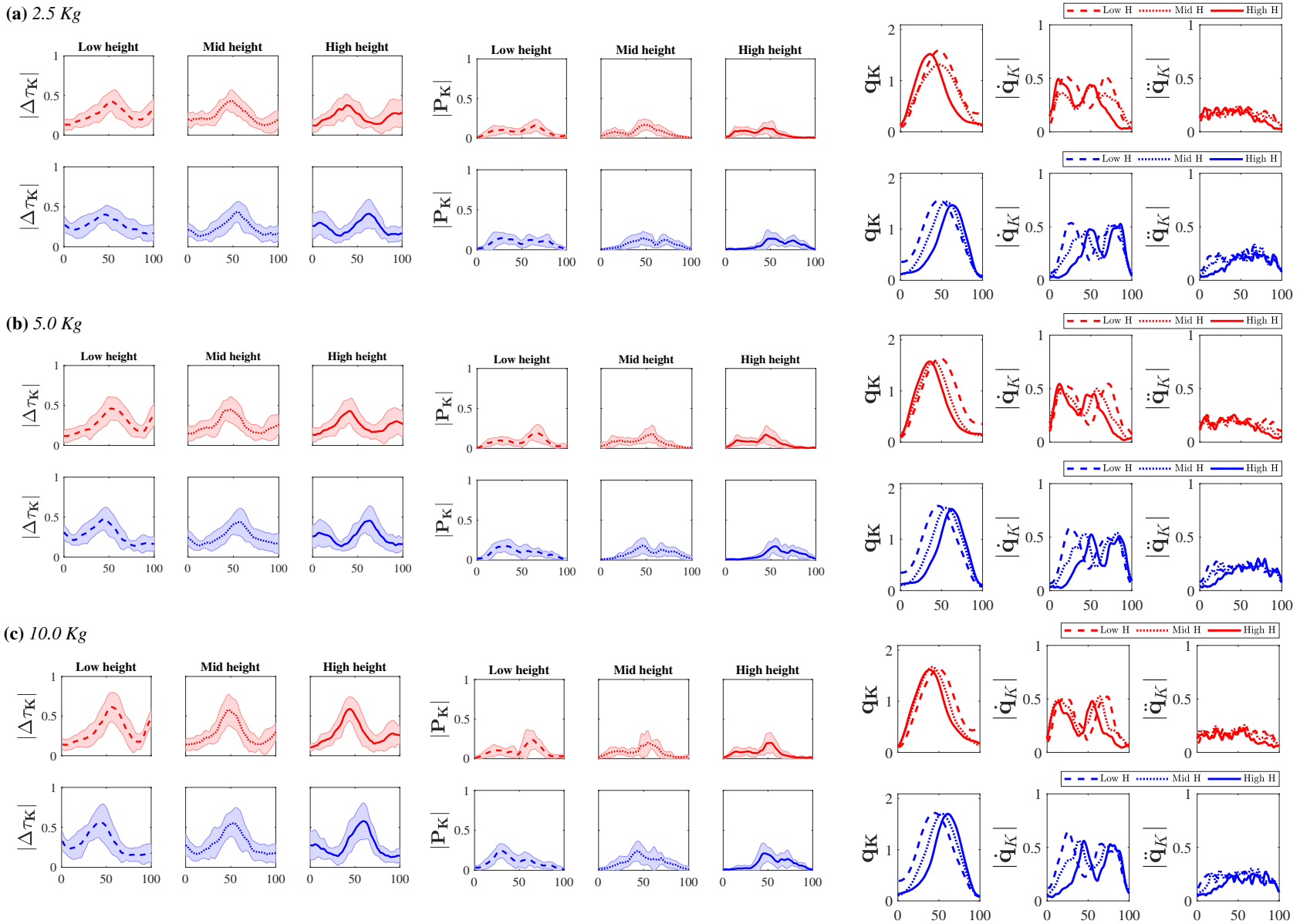

Figure 4.15: *Task 1: overloading torque $|\Delta\tau|$, overloading power $|P|$, angle $\mathbf{q}$, velocity $|\dot{\mathbf{q}}|$ and acceleration $|\ddot{\mathbf{q}}|$ in the **knee** while lifting (red lines) and lowering (blue lines) a box of 2.5 (a), 5.0 (b), and 10.0 (c) kg at three different height levels, namely low (dashed lines), mid (dotted lines), high (solid lines). The mean among twelve subjects (among three trials for each one) is represented. The standard deviation is also highlighted for $|\Delta\tau|$ and $|P|$.*

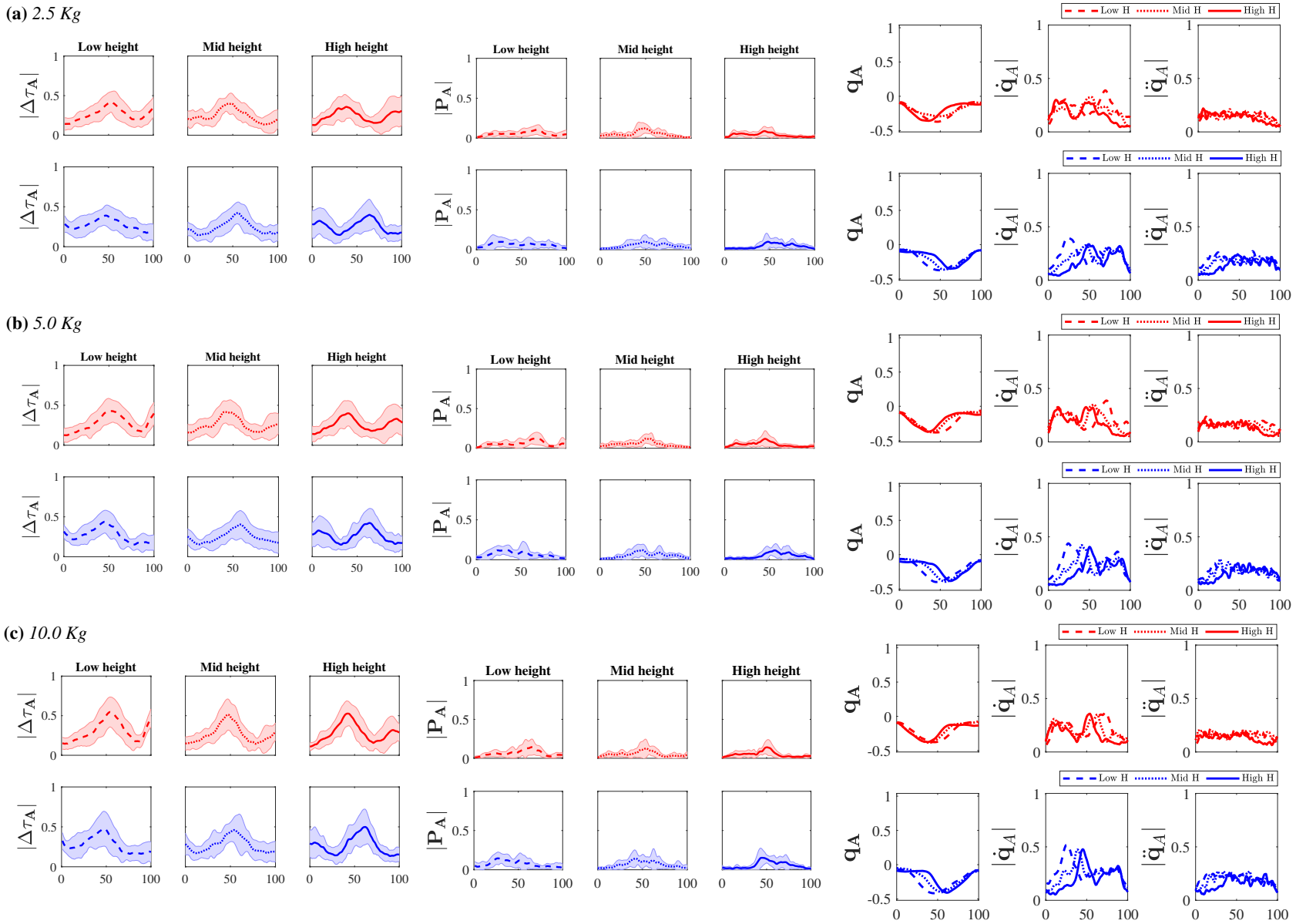

Figure 4.16: *Task 1: overloading torque $|\Delta\tau|$, overloading power $|P|$, angle $\mathbf{q}$, velocity $|\dot{\mathbf{q}}|$ and acceleration $|\ddot{\mathbf{q}}|$ in the **ankle** while lifting (red lines) and lowering (blue lines) a box of 2.5 (a), 5.0 (b), and 10.0 (c) kg at three different height levels, namely low (dashed lines), mid (dotted lines), high (solid lines). The mean among twelve subjects (among three trials for each one) is represented. The standard deviation is also highlighted for $|\Delta\tau|$ and $|P|$.*

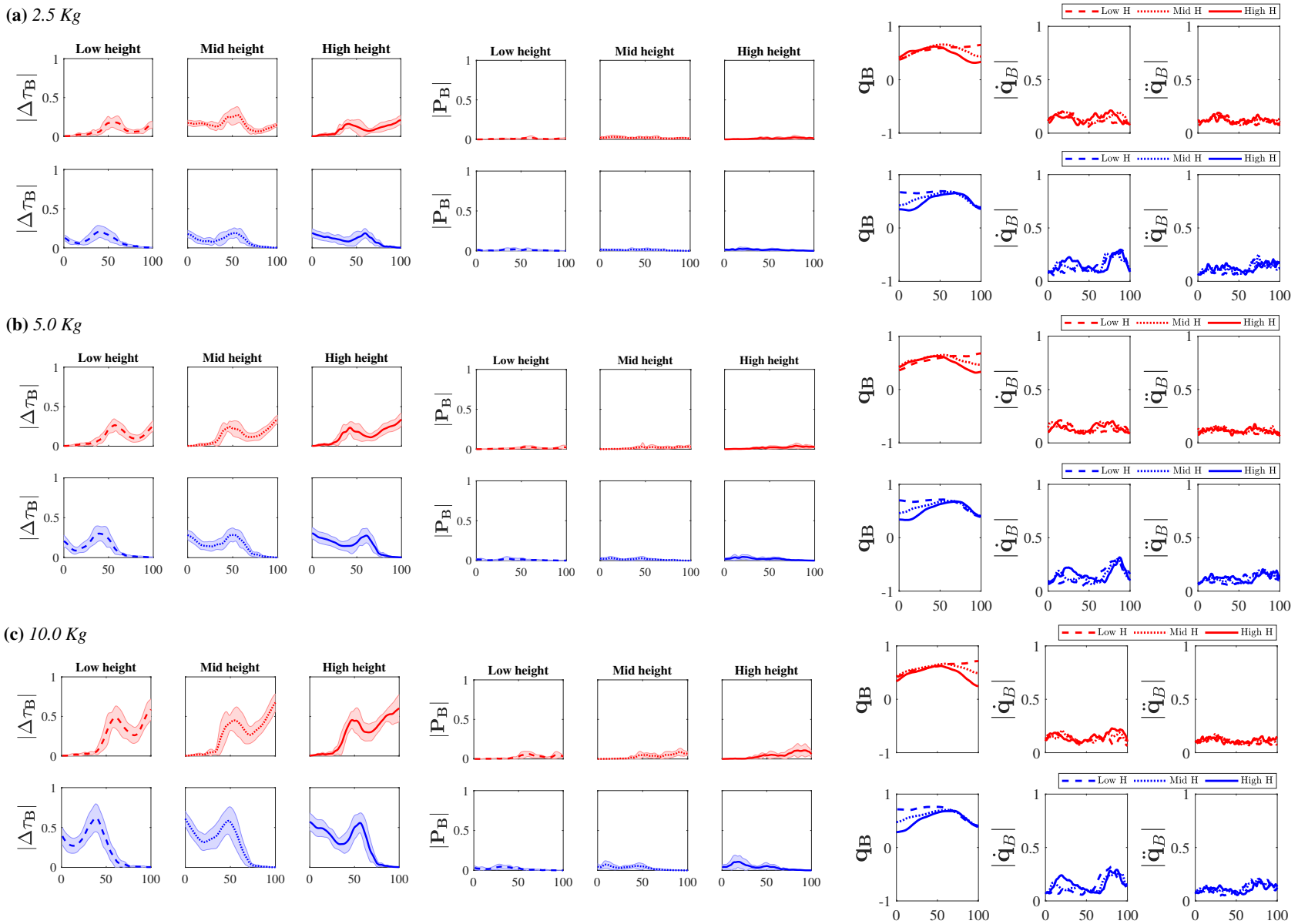

Figure 4.17: *Task 1: overloading torque $|\Delta\tau|$, overloading power $|P|$, angle $\mathbf{q}$, velocity $|\dot{\mathbf{q}}|$ and acceleration $|\ddot{\mathbf{q}}|$ in the **back** while lifting (red lines) and lowering (blue lines) a box of 2.5 (a), 5.0 (b), and 10.0 (c) kg at three different height levels, namely low (dashed lines), mid (dotted lines), high (solid lines). The mean among twelve subjects (among three trials for each one) is represented. The standard deviation is also highlighted for $|\Delta\tau|$ and $|P|$.*

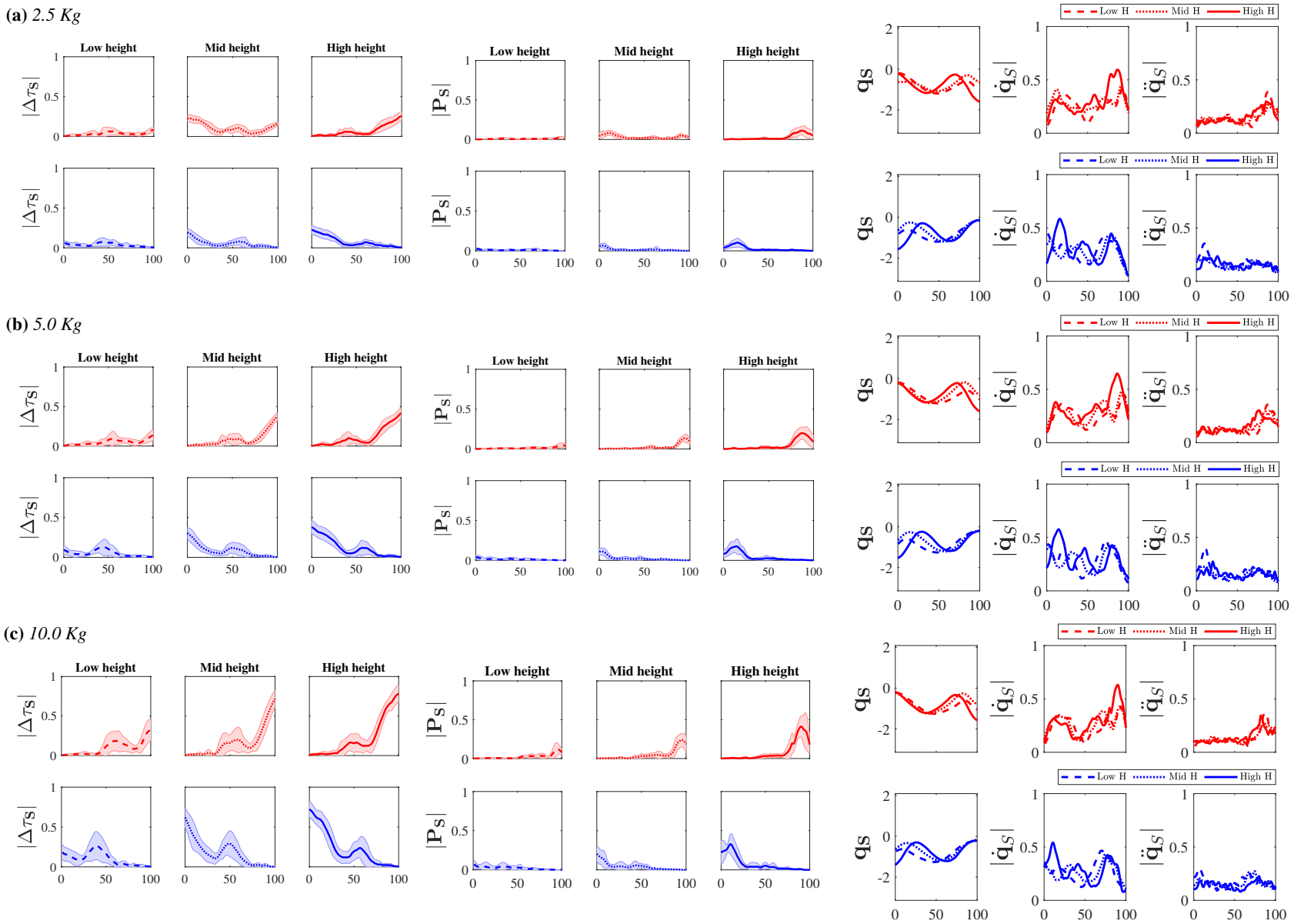

Figure 4.18: *Task 1: overloading torque $|\Delta\tau|$, overloading power $|P|$, angle $\mathbf{q}$, velocity $|\dot{\mathbf{q}}|$ and acceleration $|\ddot{\mathbf{q}}|$ in the **shoulder** while lifting (red lines) and lowering (blue lines) a box of 2.5 (a), 5.0 (b), and 10.0 (c) kg at three different height levels, namely low (dashed lines), mid (dotted lines), high (solid lines). The mean among twelve subjects (among three trials for each one) is represented. The standard deviation is also highlighted for $|\Delta\tau|$ and $|P|$.*

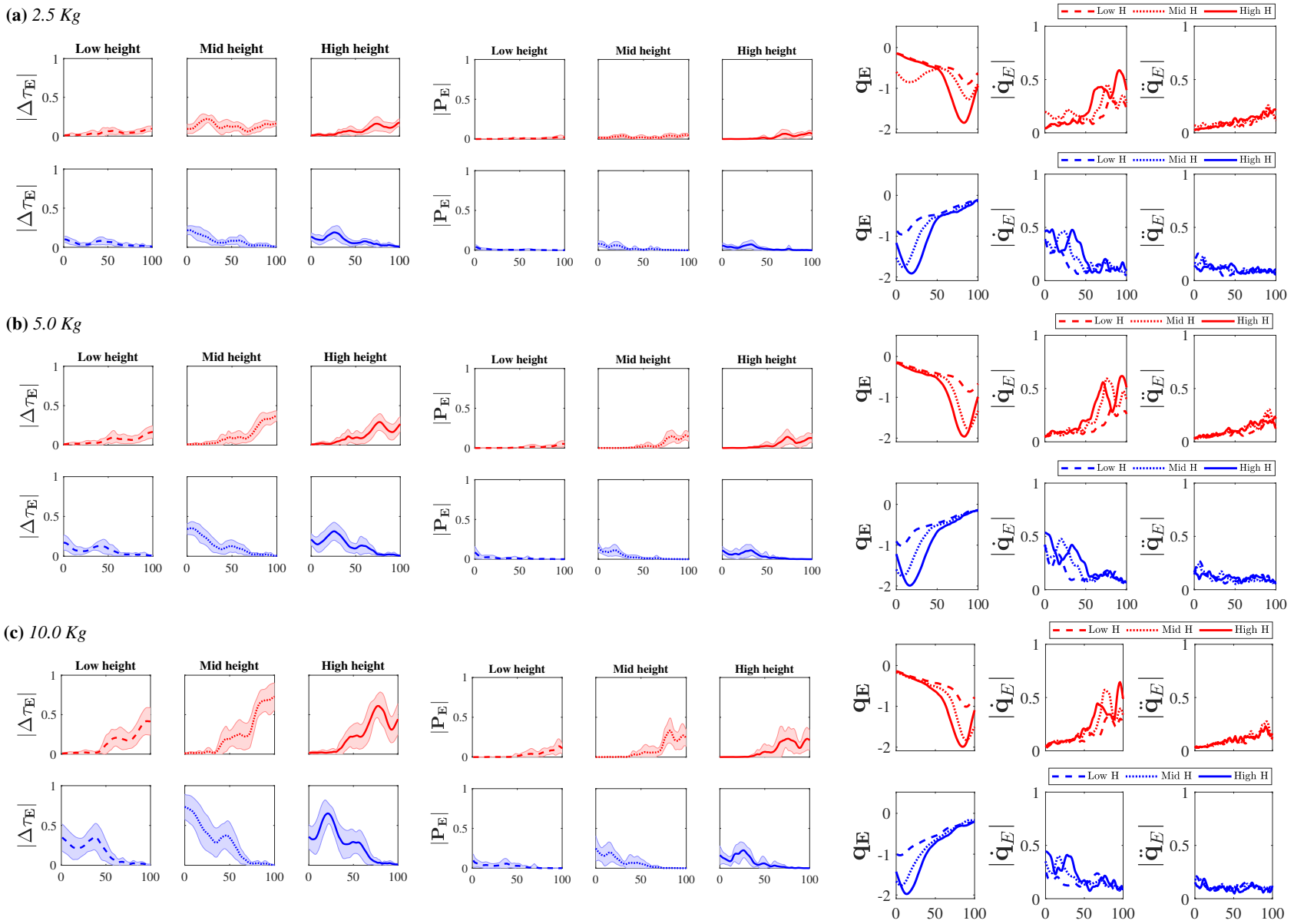

Figure 4.19: *Task 1: overloading torque $|\Delta\tau|$, overloading power $|P|$, angle $\mathbf{q}$, velocity $|\dot{\mathbf{q}}|$ and acceleration $|\ddot{\mathbf{q}}|$ in the **elbow** while lifting (red lines) and lowering (blue lines) a box of 2.5 (a), 5.0 (b), and 10.0 (c) kg at three different height levels, namely low (dashed lines), mid (dotted lines), high (solid lines). The mean among twelve subjects (among three trials for each one) is represented. The standard deviation is also highlighted for $|\Delta\tau|$ and $|P|$.*

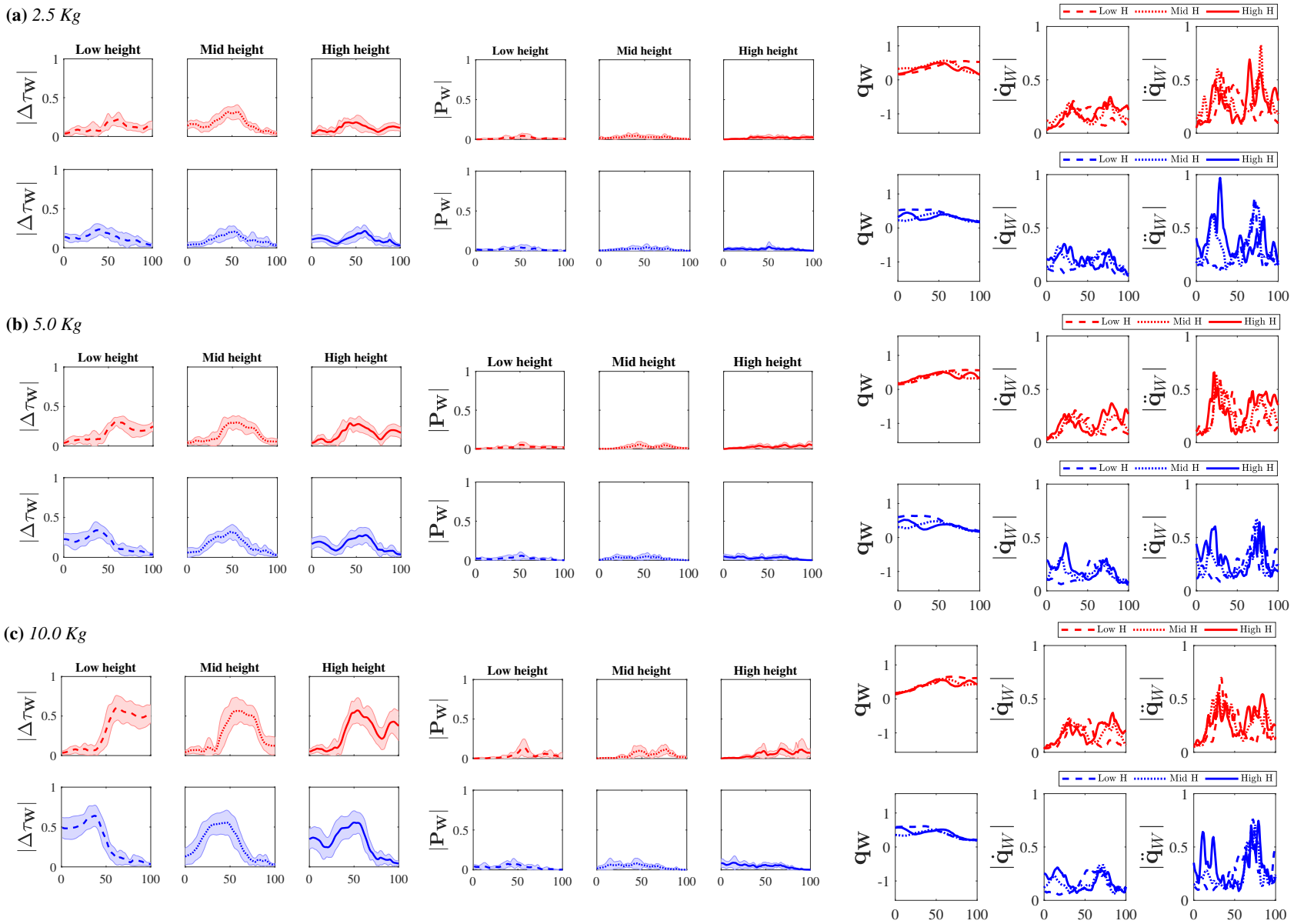

Figure 4.20: *Task 1: overloading torque $|\Delta\tau|$, overloading power $|P|$, angle $\mathbf{q}$, velocity $|\dot{\mathbf{q}}|$ and acceleration $|\ddot{\mathbf{q}}|$ in the **wrist** while lifting (red lines) and lowering (blue lines) a box of 2.5 (a), 5.0 (b), and 10.0 (c) kg at three different height levels, namely low (dashed lines), mid (dotted lines), high (solid lines). The mean among twelve subjects (among three trials for each one) is represented. The standard deviation is also highlighted for $|\Delta\tau|$ and $|P|$.*

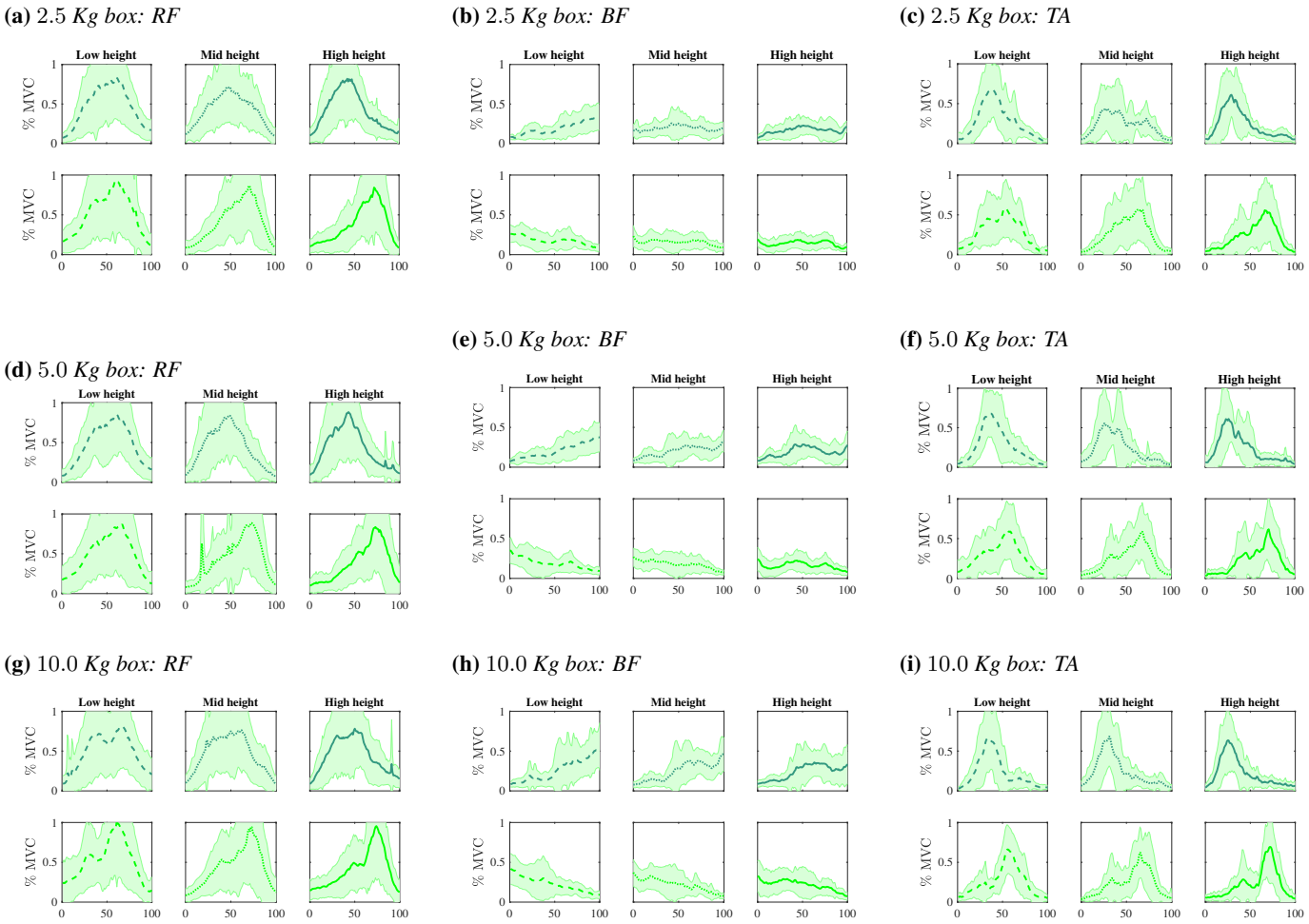

Figure 4.21: *Task 1 - muscle activity expressed as % of the MVC in the **leg** muscles (RF, BF, TA) while lifting (dark green lines) and lowering (light green lines) a box of* 2.5 *(first row),* 5.0 *(second row), and* 10.0 *(third row) kg at three different height levels, namely low (dashed lines), mid (dotted lines), high (solid lines). The means and the standard deviations among twelve subjects (among three trials for each one) are represented.*

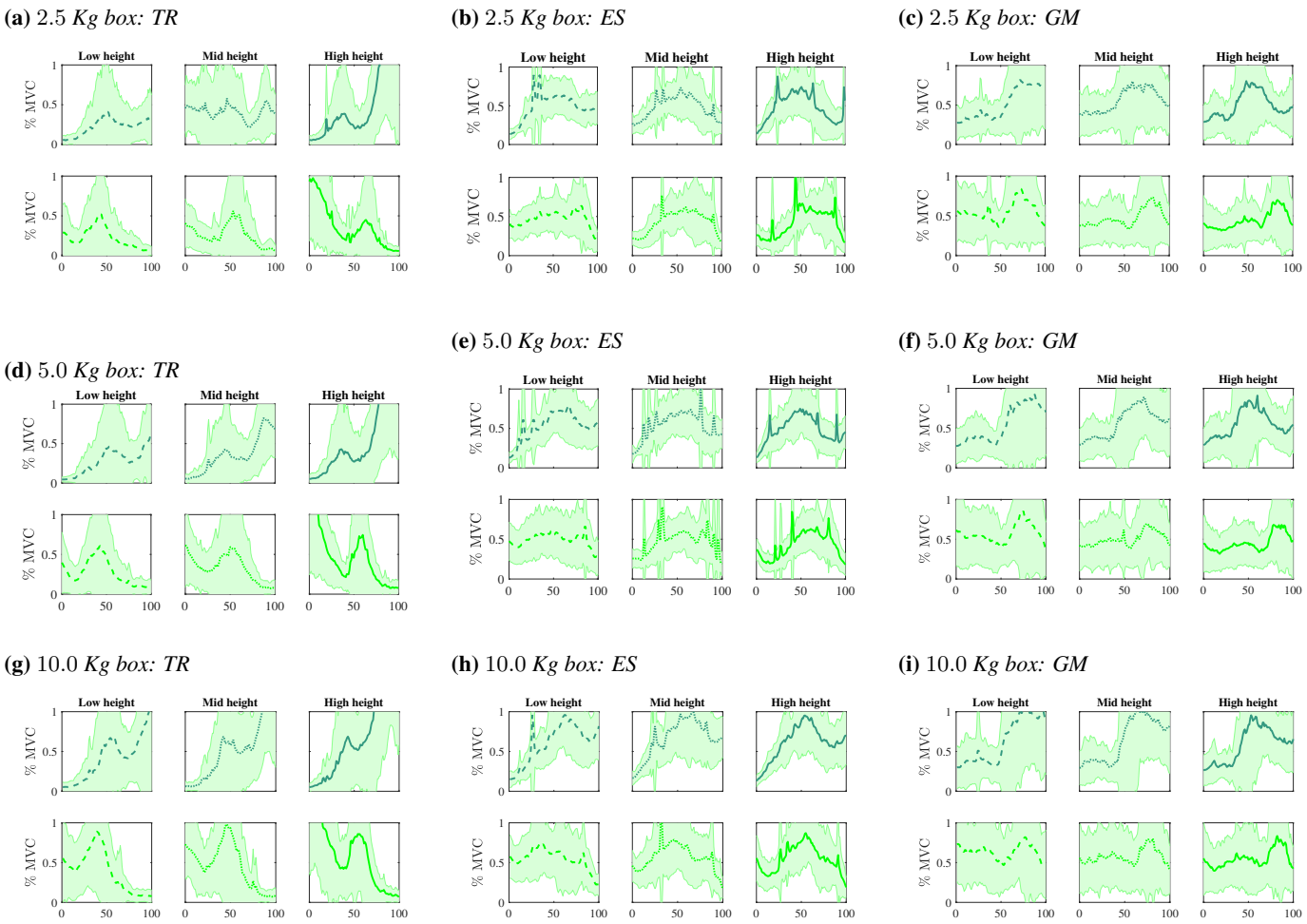

Figure 4.22: *Task 1 - muscle activity expressed as % of the MVC in the **back** muscles (TR, ES, GM) while lifting (dark green lines) and lowering (light green lines) a box of* 2.5 *(first row),* 5.0 *(second row), and* 10.0 *(third row) kg at three different height levels, namely low (dashed lines), mid (dotted lines), high (solid lines). The means and the standard deviations among twelve subjects (among three trials for each one) are represented.*

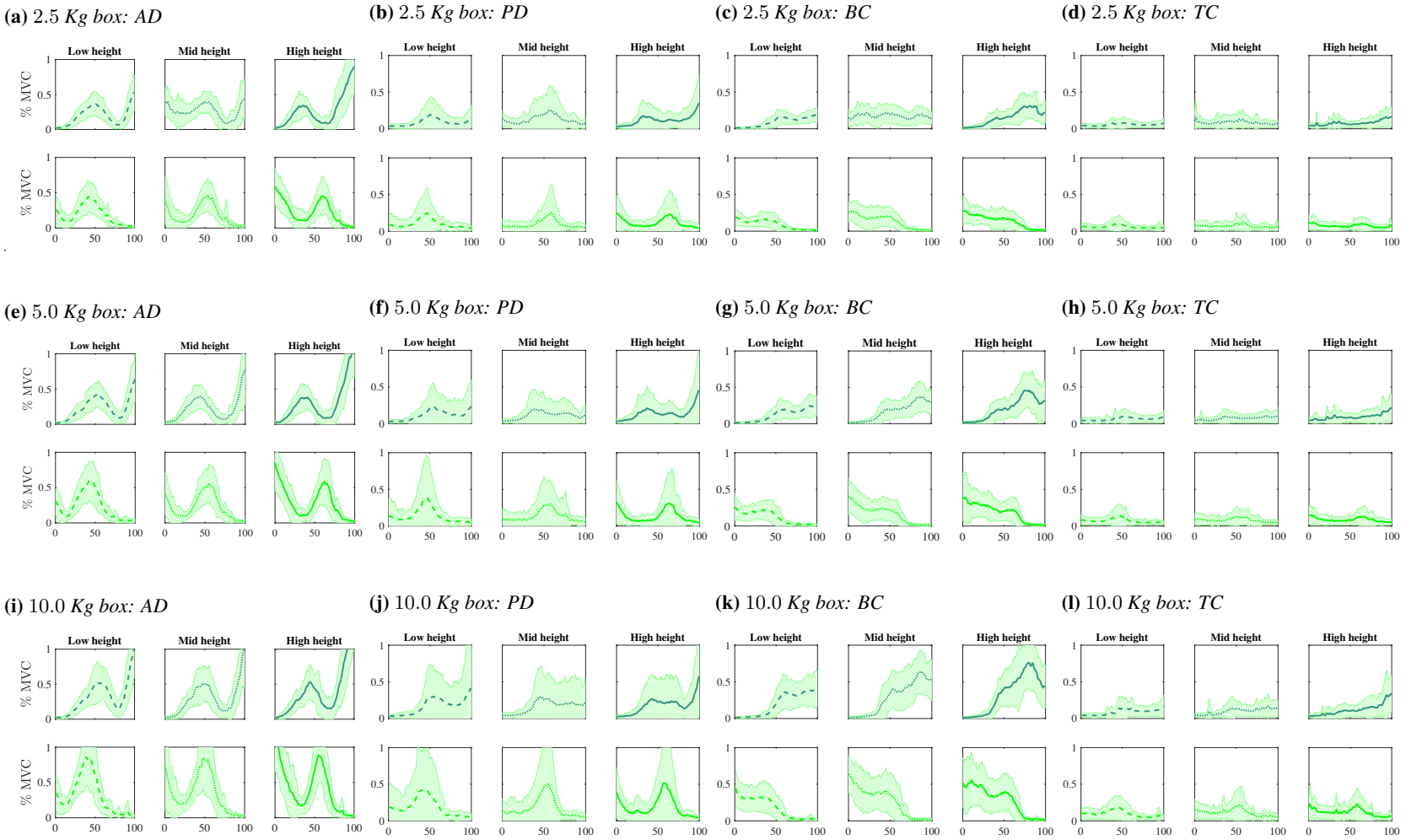

Figure 4.23: *Task 1 - muscle activity expressed as % of the MVC in the **arm** muscles (AD, PD, BC, TC) while lifting (dark green lines) and lowering (light green lines) a box of* 2.5 *(first row),* 5.0 *(second row), and* 10.0 *(third row) kg at three different height levels, namely low (dashed lines), mid (dotted lines), high (solid lines). The means and the standard deviations among twelve subjects (among three trials for each one) are represented.*

Figure 4.24: *Task 1 - CoM potential energy variations while lifting (red lines) and lowering (blue lines) a box of* 2.5 *(a),* 5.0 *(b),* 10.0 *(c) kg at three different height levels (low, mid, high). The means and the standard deviations among twelve subjects (among three trials for each one) are represented.*

Task 2: Drilling

In Figure 4.25, the overloading joint torques and the compressive forces are presented for task 2. As for task 1, only the quantities which are expected to provide more relevant information for the purpose of physical exposure assessment with respect to the type of task, are selected among the proposed ergonomics indexes. In fact, while drilling, different factors can contribute to stress the musculoskeletal system (i.e., the magnitude, the direction, and the variability of the force exerted/experienced by the subjects) that can be addressed by the selected indexes. Neither the joint kinematics nor CoM potential energy are presented since they do not show meaningful variations throughout the task, in line with the fact that subjects were basically steady. All the three drilling actions, corresponding to the three different positions (D1, D2, D3) of the panels to be drilled, are illustrated. The mean and the standard deviation values computed among the twelve subjects (in turn averaged among the three trials) for overloading torque $|\Delta\boldsymbol{\tau}|$ (yellow lines) and the compressive force $|\mathbf{f_C}|$ (purple lines) are represented in the human main joints. Specifically, each Subfigure corresponds to a joint: hip (H) in (a), knee (K) in (b), ankle (A) in (c), back (B) in (d), shoulder (S) in (e), elbow (E) in (f), wrist (W) in (g). Observing Figure 4.25 on the whole, it is evident that both $|\Delta\boldsymbol{\tau}|$ and $|\mathbf{f_C}|$ are quite steady over the task progression, in accordance with what stated above. $|\Delta\boldsymbol{\tau}|$ is quite low in the lower body and even less significant in the upper body, with no meaningful differences among drilling locations in any joints. On the other hand, $|\mathbf{f_C}|$ shows substantially higher values and more variability between joints and experimental conditions. At the hip level, $|\mathbf{f_{C,H}}|$ presents comparable values in D2 and D3 and a higher value in D1. At the knee level, no relevant differences can be observed between D1, D2, and D3. At the ankle level, $|\mathbf{f_{C,A}}|$ is considerable in D1 and shows a slight decrement in D2 and a further one in D3. At the shoulder level, the same trend as at the back level can be noted for $|\mathbf{f_{C,S}}|$ while at the elbow level, the exact opposite behaviour is exhibited by $|\mathbf{f_{C,E}}|$. Finally, at the wrist level, $|\mathbf{f_{C,E}}|$ is lower in D2 while higher comparable values can be observed in D1 and D3. To recap, the overloading joint torque $|\Delta\boldsymbol{\tau}|$ does not seem to provide relevant information about the physical effort required for the task. Most likely, this is due to the fact that the overloading joint torque, as it is defined, considers only the gravitational component of the force thus the weight of the tool. Since while drilling the tool is partially supported by the drilled interface, such a component is not significant during this specific task. Accordingly, $|\Delta\boldsymbol{\tau}|$ is overall not significant. On the other hand, the compressive force takes into account all the components of the external force induced on the human end-effector. In fact, this information is provided by the F/T sensor mounted purposely on the driller. As a result, $|\mathbf{f_C}|$ enables to estimate the effect of the external force on the human body structure considering all its contributing factors (i.e. magnitude, direction, variability). In fact, remarkable differences can be distinguished among different experimental conditions and at different joint levels.

In Figures 4.26 the whole-body muscle activity is presented for task 2. For all the three drilling actions, corresponding to the three different positions (D1, D2, D3) of the panels to be drilled, the mean and standard deviation values computed among the twelve subjects (in turn averaged among the three trials) are illustrated. Specifically, each Subfigure corresponds to an analysed muscle: the Rectus Femoris (RF) in (a), the Biceps Femoris (BF) in (b), the Tibialis Anterior (TA) in (c), the Trapezius Descendens

(TR) in (d), the Erector Spinae (ES) in (e), the Gluteus Maximus (GM) in (f), the Anterior Deltoid (AD) in (g), the Posterior Deltoid (PD) in (h), the Biceps Brachii (BC) in (i) and the Triceps Brachii (TC) in (j).

As regards the leg muscles, RF shows significant activity in D1, low activity in D2, and moderate activity in D3. The activity in BF is overall not very high. In TA a meaningful but decreasing activity can be observed in D1 while low values are presented in the other conditions. Hence, likewise for $|\mathbf{f_C}|$ in the lower body joints, the higher effort is generally found in D1. As regards the back muscles, TR shows comparable activities in D1 and D2 and lower activity in D3. ES is moderately active in D1 and less active in D2 and D3 while GM globally presents decent values although the standard deviation is quite high. No particular similarities can be found with the trend of $|\mathbf{f_C}|$ in the back joint. The most meaningful activity among the arm muscles is exhibited by AD with considerable activity in D1, moderate activity in D2 but a low activity in D3. Such a trend corresponds to the trend of $|\mathbf{f_C}|$ in the shoulder, which can be also correlated to the muscle activity in TR. Both PD and BC do not show meaningful activities except for a slight increment in D3 for PD. TD is a little more active, mostly in D2. As for the back, no particular similarities can be found between the trend of muscle activity and compressive forces in the upper body with the only exception of the shoulder. However, it is expected that the external force repartition over the joints cannot be easily related to more sophisticated physiological quantities such as muscle activity.

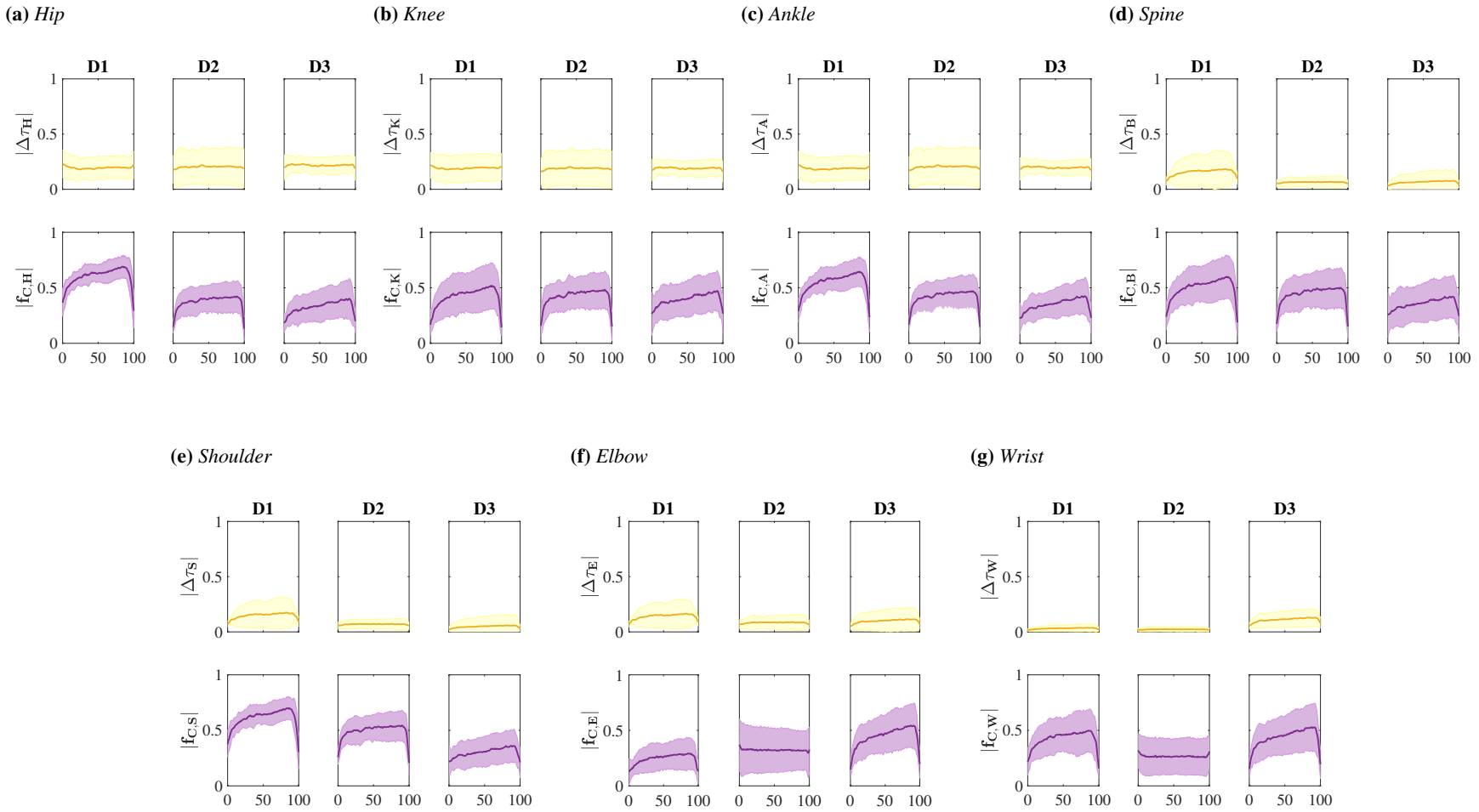

Figure 4.25: *Task 2 - overloading torques (yellow lines) and compressive forces (purple lines) in the main joints (hip, knee, ankle, spine, shoulder, elbow, wrist) while drilling three panels that are located in three different positions (high, mid, low) on a shelving. The means and the standard deviations among twelve subjects (among three trials for each one) are represented.*

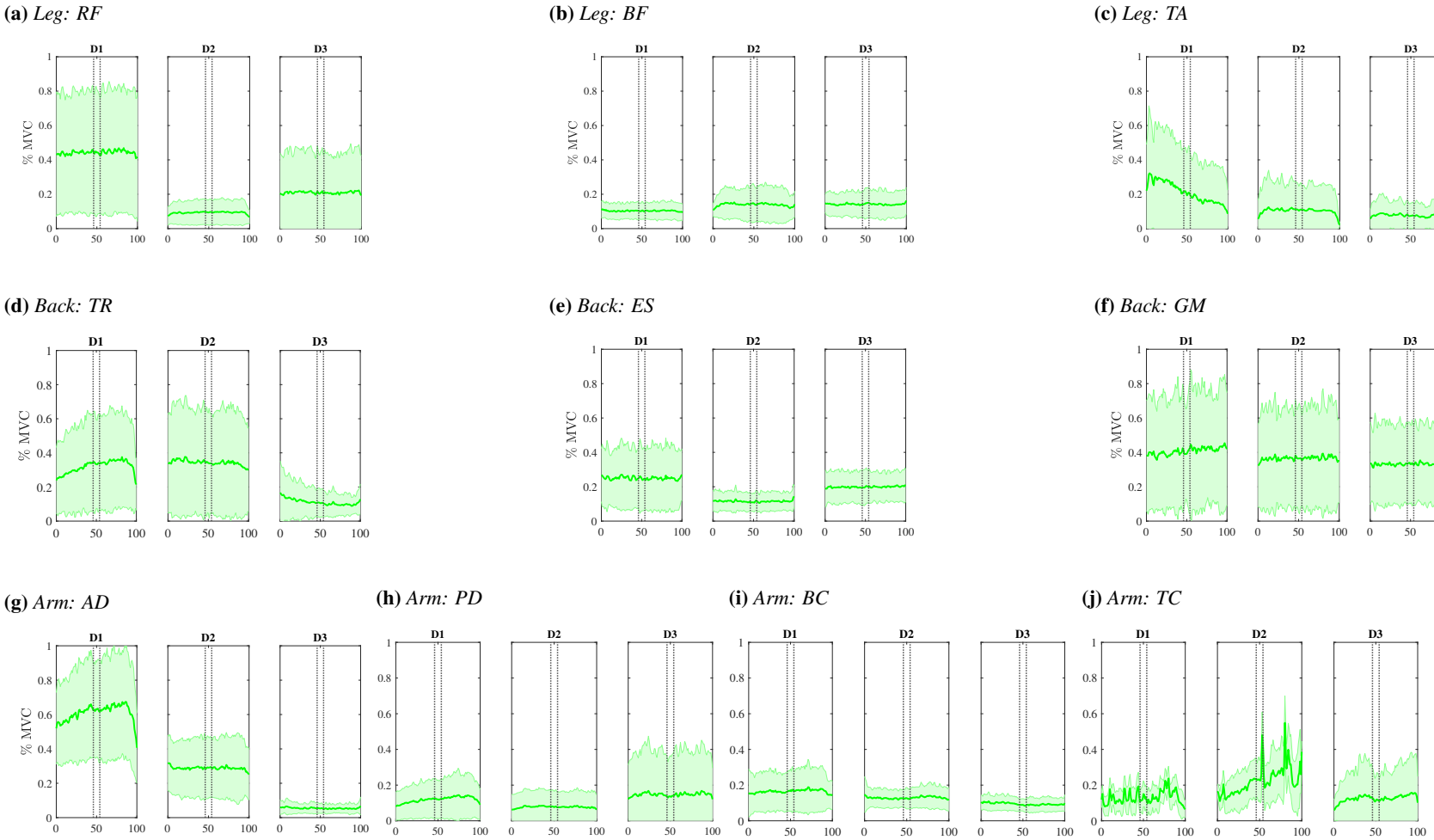

Figure 4.26: *Task 2 - muscle activity expressed as % of the MVC in the selected muscles (AD, PD, BC, TC, TR, ES, GM, RF, BF, TA) while drilling three panels that are located in three different positions (D1, D2, D3) on a shelving. The means and the standard deviations among twelve subjects (among three trials for each one) are represented.*

Task 3: Painting with a Lightweight Tool

In Figure 4.27, the overloading joint fatigue and the overloading joint torque are presented for task 3. The overloading fatigue is expected to be the ergonomic index that better represents the effect on the human body of light but repetitive efforts protracted for a long duration. The overloading torque is illustrated to highlight the relevance of taking into account its cumulative effect over time even if its instantaneous value is not significant. As for task 2, neither the joint kinematics nor CoM potential energy are presented since they do not show meaningful variations throughout the task, in line with the fact that subjects were basically steady. As previously said, for task 3 no specific actions were selected within its execution, the full-time series is considered. However, the two phases of the task, corresponding to the two helmets to be painted, are distinguished on the plots by means of vertical dashed lines (which actually indicate the time breaks in between). The mean and the standard deviation values computed among the twelve subjects (in turn averaged among the three trials) for overloading fatigue $|\boldsymbol{\tau}_F|$ (pink lines) and overloading torque $|\Delta\boldsymbol{\tau}|$ (light blue lines) are represented in the human main joints. Specifically, in Subfigure (a) the lower body joints are illustrated, namely hip (H), knee (K), and ankle (A), while in Subfigure (b) the upper body joints are illustrated, namely back (B), shoulder (S), elbow (E), wrist (W), respectively.

At the lower body level, the trend of $|\Delta\boldsymbol{\tau}|$ and $|\boldsymbol{\tau}_F|$ is very similar among all the joints. $|\Delta\boldsymbol{\tau}|$ in the leg, in the knee, and in the ankle present a low value that becomes higher in the second phase of the task. Correspondingly, $|\boldsymbol{\tau}_F|$ grows slowly in the first phase while increases faster in the second phase. However, $|\boldsymbol{\tau}_F|$ do not achieve significant values, in accordance with the fact that $|\Delta\boldsymbol{\tau}|$ values in the second phase are more meaningful but oscillating. At the upper body level, analogous profiles are exhibited in the back and in the shoulder. $|\Delta\tau_B|$ and $|\Delta\tau_S|$ show quite high values in the first phase and moderate/low values in the second phase. As a result, $|\tau_{F,B}|$ and $|\tau_{F,S}|$ increase very quickly in the first phase achieving also extremely high values and drop in the second phase. At the elbow level, $|\Delta\tau_E|$ is moderate in the first phase and slightly minor in the second phase thus $|\tau_{F,E}|$ increase slowly in the first phase and decrease in the second phase, respectively. On the contrary, at the wrist level, $|\Delta\tau_W|$ is not significant in the first phase and grows in the second phase leading to an increment in $|\tau_{F,W}|$. What is not evident observing these results but it should be underlined, it is that the overloading fatigue model is extremely sensitive to the threshold which has been set to distinguish among fatigue and recovery phase. This explains why the increment of $|\boldsymbol{\tau}_F|$ can be very fast or a bit slower for similar values of $|\Delta\boldsymbol{\tau}|$.

In Figures 4.28 the whole-body muscle activity is presented for task 3. As for the ergonomic indexes, the full task is considered and the two phases are indicated on the plots by means of vertical dashed lines. The mean and standard deviation values computed among the twelve subjects (in turn averaged among the three trials) are represented. Specifically, in Subfigure (a) the lower body muscles are illustrated, namely the Rectus Femoris (RF), the Biceps Femoris (BF) and the Tibialis Anterior (TA); in Subfigure (b) the back muscles are illustrated, namely the Trapezius Descendens (TR), the Erector Spinae (ES) and the Gluteus Maximus (GM); in Subfigure (c) the upper body muscles are illustrated, namely the Anterior Deltoid (AD), the Posterior Deltoid (PD), the Biceps Brachii (BC) and the Triceps Brachii (TC).

As regards the leg muscles, the activity of RF and TA, and to a lesser extent of

BF, is lower in the first phase and higher in the second phase, always quite oscillating. Accordingly, the trend of the lower muscles activity is comparable to the trend of $|\Delta\boldsymbol{\tau}|$ and $|\tau_F|$ in the lower body joints. As regards the back muscles, TR is more active in the first phase and less active in the second one while ES shows the exact opposite behaviour. The activity of GM is moderate and quite constant throughout the whole task. No particular similarities can be found with the trend of $|\Delta\boldsymbol{\tau}|$ and $|\boldsymbol{\tau}_F|$ in the back joint. As regards the arm muscles, AD and TC exhibit significant activity in the first phase and lower activity in the second phase thus their trend is comparable to the one of $|\Delta\boldsymbol{\tau}|$ and $|\boldsymbol{\tau}_F|$ in the shoulder and in the elbow. On the other hand, PD and BC are overall a little active throughout the whole task.

(a) *Lower body: hip, knee, ankle*

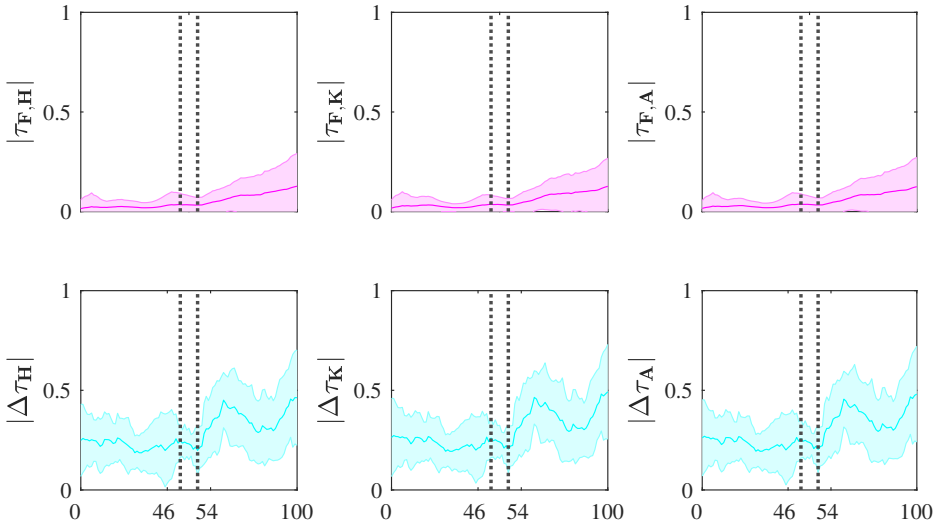

(b) *Upper body: spine, shoulder, elbow, wrist*

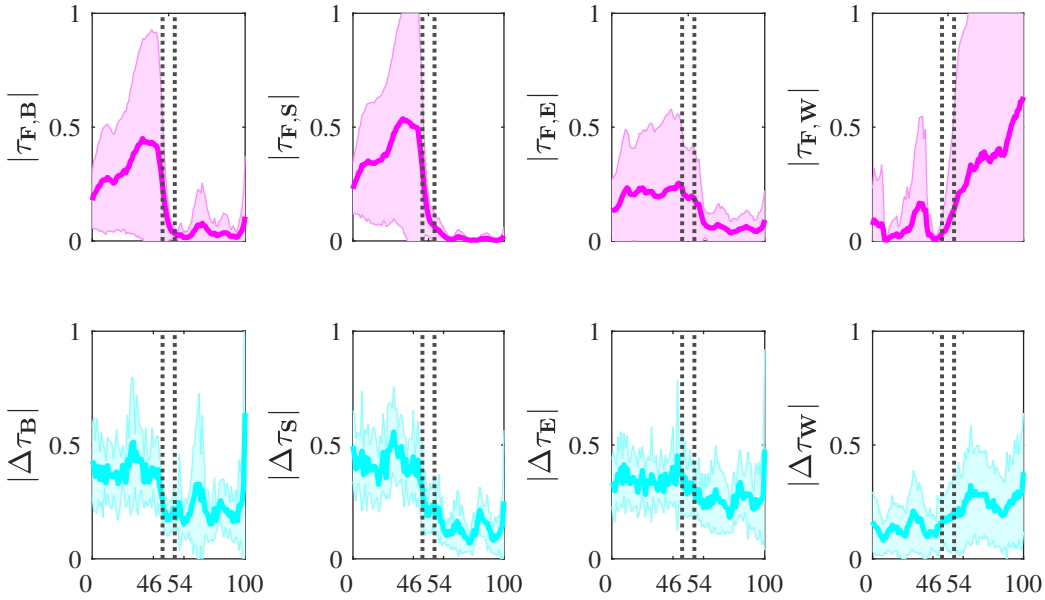

Figure 4.27: *Task 3 - overloading fatigue (pink lines) and overloading torque (light blue lines) in the main joints (hip, knee, ankle, spine, shoulder, elbow, wrist) while painting with a lightweight spray-gun. The means and the standard deviations among twelve subjects (among three trials for each one) are represented.*

(a) *Leg: RF, BF, TA*

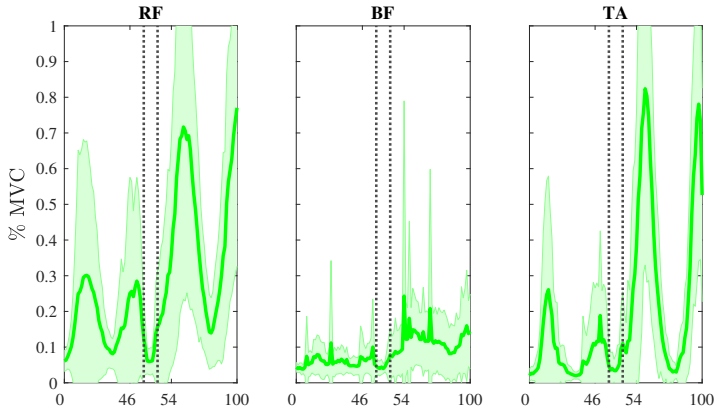

(b) *Back: TR, ES, GM*

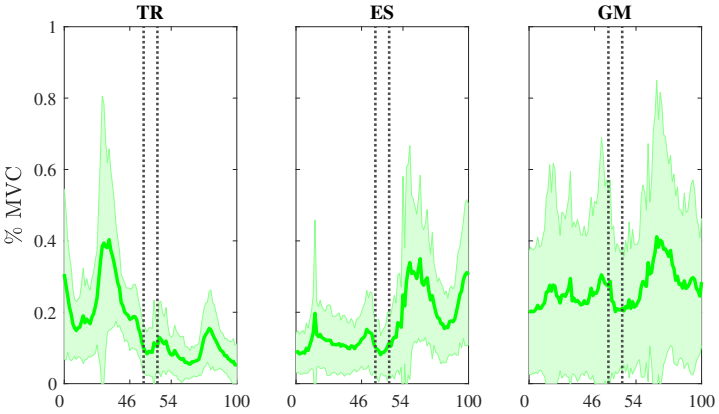

(c) *Arm: AD, PD, BC, TC*

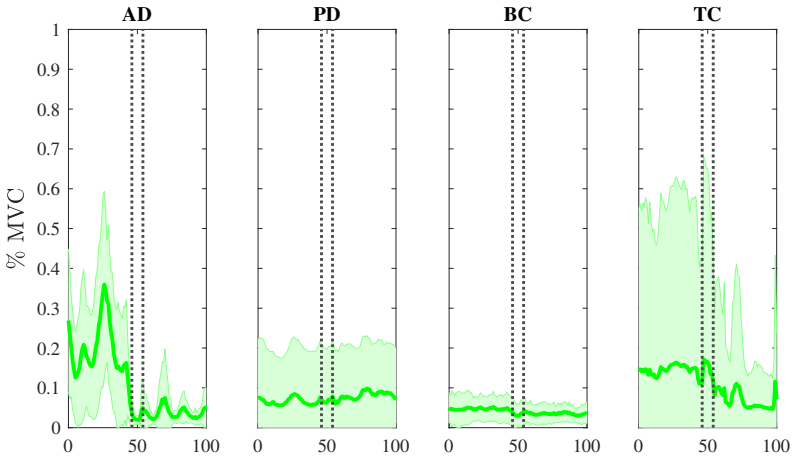

Figure 4.28: *Task 3 - muscle activity expressed as % of the MVC in the selected muscles (AD, PD, BC, TC, TR, ES, GM, RF, BF, TA) while painting with a lightweight spray-gun. The means and the standard deviations among twelve subjects (among three trials for each one) are represented.*

Ergonomics Assessment with the EAWS

To assess the potential of the proposed ergonomics monitoring system, its outcome was compared with the ergonomic risk scores provided by a well-recognised and widely used tool to evaluate workers' physical exposure, namely the EAWS method [72]. Since the EAWS method requires a quite complex and sophisticated procedure and a priori specific knowledge of typical industrial processes, the corresponding analysis and computations were conducted in collaboration with Fondazione Ergo (headquarters: Varese, Italia). It should be noted that to perform EAWS analysis for the simplified activities considered in the present experimental investigation, several assumptions have been made to contextualise them in a real workplace. For instance, since the level of performance of the recruited subjects was not realistic compared to an actual worker, the task timing was defined according to standard base time using the Methods-Time Measurement - Universal Analyzing System (MTM-UAS) method [179]. In fact, in the industrial environment, it is necessary to quantify work with respect to a regulatory level of performance [180]. As explained in Section 2.1, the EAWS enable a comprehensive and unique ergonomic risk evaluation. In fact, four different sections that focus on each specific aspect of manual material activities are included and their results can be integrated into a combined score presented in an intuitive traffic light scheme (green, yellow, red) according to the Machinery Directive 2006/42/EC (EN 614). Accordingly, the evaluation of the three occupational tasks considered in this experimental analysis (i.e., lifting/lowering, drilling, and painting) by means of the EAWS method resulted in a total score for each of them, indicative of the associated ergonomics risk level. The EAWS score was computed for each trial of every task and then the mean value among the resulting score was computed. This procedure was repeated for all the twelve subjects. As a result, each subject presented a EAWS final score for each task. It should be noted that for task 1 three different ratings were computed, considering the box weight conditions in a separate way. The mean and the standard deviation values which were finally computed among all the subjects and the corresponding risk level are illustrated in Table 4.4.

Table 4.4: *Mean and standard deviation[6] computed among twelve subjects of the EAWS final scores for all the task considered in the experimental analysis.*

Task	Activity	Condition	EAWS Final Score	Risk level[5]
1	lifting/lowering	2.5 Kg box	$38.8 \pm 1.2^{\dagger\dagger}$	Moderate
		5.0 Kg box	$41.7 \pm 1.7^{\dagger\dagger}$	Moderate
		10.0 Kg box	$48.7 \pm 6.9^{\dagger\dagger}$	Moderate
2	drilling		$23.1 \pm 5.0^{\dagger}$	Low
3	painting		$14 \pm 0.0^{\dagger}$	Low

For task 1, the inter-subject variability of the EAWS score only depends on the worker gender, i.e. the male and the female subjects, respectively, have the exact same rating among them. This was due to the level of risk associated with the box weight which was indeed gender-specific. It can be noted that, as expected, the EAWS score

[6]The risk level associated with the EAWS score is determined as follows: the range $0 - 25$ points corresponds to a low risk (†), the range $25 - 50$ points corresponds to a moderate risk (††) and a value > 50 points corresponds to a high risk, respectively.

of the lifting/lowering task grows with increasing box weight. Looking at the mean among the subjects, the risk level associated is moderate (††) for all the experimental conditions. Nevertheless, considering the 10 kg box one, the EAWS score is quite close to the higher threshold (> 50) and the standard deviation equal to 6.9 suggests that for some subjects the risk level turns into high. It should be observed that the growing trend of the risk level with the box weight was likewise identified by the proposed human ergonomics monitoring system. For task 2, each trial of each subject exhibits a rather different EAWS score since the maximum value (worst condition) of the force exerted while drilling was taken into account. Similarly, as for the last experimental condition in task 1, the rating is quite close to the mid threshold (> 25) and presents a significant standard deviation (5.0). Thus, the risk level considering the mean value is low (†) but for some subjects it turns into moderate. On the other hand, for task 3, the EAWS score was exactly the same for each subject, leading to a standard deviation equal to 0.0 In fact, neither the gender nor other individual factors influenced the evaluation of this specific activity but only the task timing. The risk level associated is then low for all the subjects, abundantly within the low part of the range.

4.6.3 Discussion

To assess, on the whole, the results of the experimental analysis presented in this Section, the outcome of the proposed ergonomic indexes has been resumed in the aggregated polar plots illustrated in Figures 4.29, 4.30 and 4.31 for task 1, task 2 and task 3, respectively. For task 1, a plot for each experimental condition (box weight, height level) is provided. For task 2, three plots corresponding to the three different positions (D1, D2, D3) of the panels to be drilled are shown. For task 3, two plots are considered to represent the two phases, i.e. the two helmets to be processed, of the painting activity.

Each plot includes eight axes to correspond to the eight ergonomic indexes listed in Table 4.1. For each index, the maximum normalised values of the action/phase are exhibited for all the considered joints, specifically: hip (H), knee (K), ankle (A), back (B), shoulder (S), elbow (E) and wrist (W). To highlight the scope of the ergonomic indexes, two separate areas are enhanced on the polar plots: the pink area encompasses the indexes accounting for kinematic aspects while the light blue area encompasses the indexes accounting for dynamics aspects.

Let us consider the plots in Figure 4.29, relative to task 1. Focusing on the pink area, which comprises the indexes accounting for the kinematics aspects, it can be noted that the highest values are reported by ω_1 i.e. the joint displacement index. As already observed, at the hip, knee, and elbow level the joint angles approach the boundaries of the ROM to a slight different extent among the experimental conditions, suggesting that the subjects could have been required to adopt potentially unfavourable postures to execute this specific task. As regards ω_2, the values are gathered approximately in the middle of the range and no meaningful differences in joint velocities can be found among the different experimental conditions. Similarly, as shown by ω_3, comparable joint accelerations are exhibited by the subjects, even varying the conditions, with values in the lower half of the index range for all the joints. Interestingly, the only exception is the acceleration at the wrist level which presents rather high values. Since the variations of wrist acceleration have proven to correlate with ergonomic risk factor in the

workplace [181], this data acquire certain importance for the purposes of the current analysis.

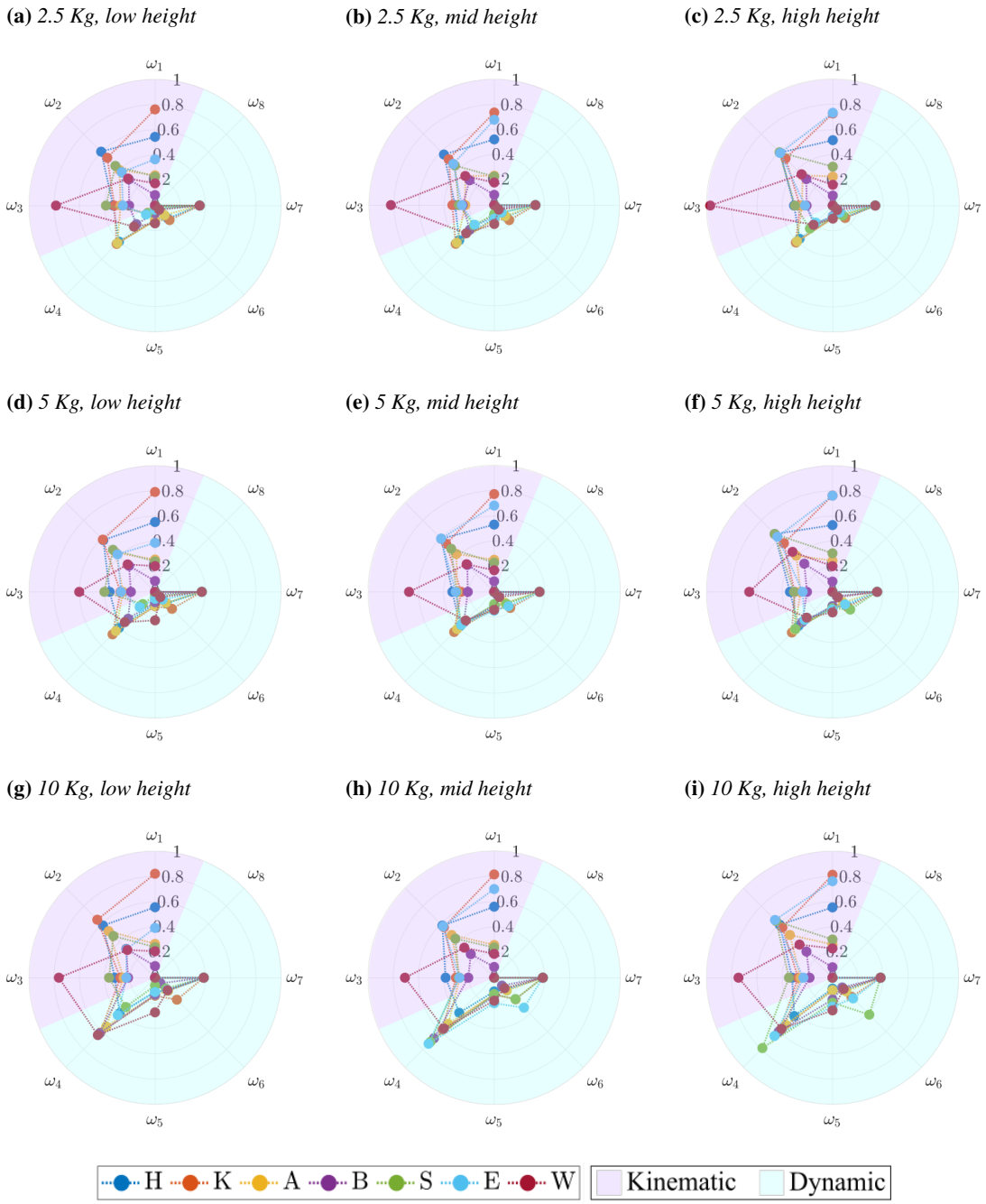

Figure 4.29: *Polar plots to represent the overall outcome of the proposed ergonomic indexes for task 1. For each experimental condition, i.e. box weight and height level, the maximum normalised values of each index over the trial are illustrated in the human main joints: hip (H), knee (K), ankle (A), back (B), shoulder (S), elbow (E) and wrist (W).*

On the other hand, focusing on the light blue area of the polar plots, which covers the indexes accounting for the dynamics aspects, it can be noted that the more relevant

information is provided by ω_4, the overloading joint torque index. ω_5 and ω_6 remain generally low and steady among the different experimental conditions, ω_7 (which is actually joint-independent) is slightly higher but likewise without considerable variations. ω_8 cannot just be estimated due to the absence of full knowledge about interaction forces for this task. Conversely, the overloading joint torque index exhibits a clear growth with increasing box weight and to a small extent with increasing height level. Hence, it is possible to state that ω_4 is able to account for the varying ergonomic risk posed by different experimental conditions considering the lifting/lowering of a heavy object. Furthermore, its trend is comparable to the muscle activity one, measured through sEMG, in most of the considered muscles, providing proof of its capability to address human physical effort. Specifically, the percentage increase of the muscle activity between the 2.5 kg box and the 5.0/10.0 kg boxes (averaged among height levels which showed less significant variations) is 51.3/112.9 % in the AD, 33.4/115.9 % in the PD, 67.9/175.1 % in the BC, 9.1/69.3 % in the TC, 49.8/143.5 % in the TR and 27.1/90.1 % in the ES, 13.2/33.5 % in the GM, 23.8/57.6 % in the RF, respectively [7]. The muscle activity in BF and TA instead is approximately constant among different experimental conditions.

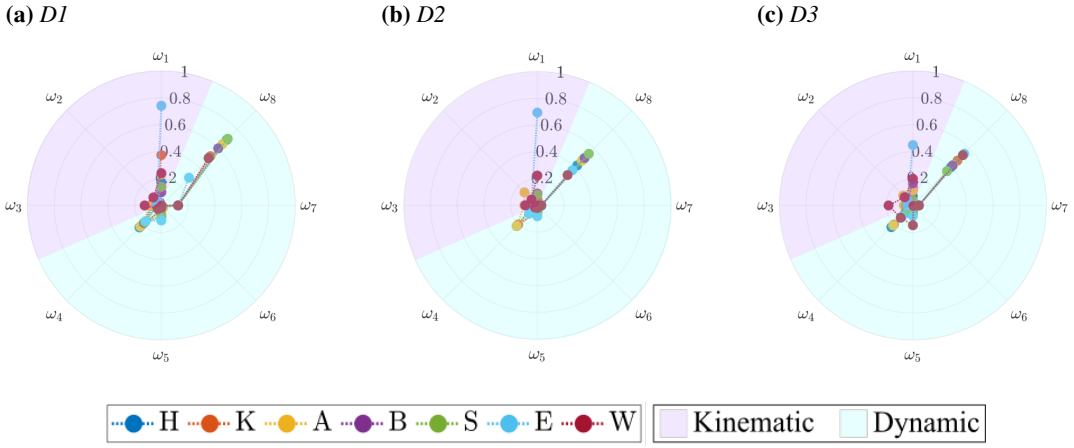

Figure 4.30: *Polar plots to represent the overall outcome of the proposed ergonomic indexes for task 2. For each experimental condition, i.e. the positions (D1, D2, D3) of the panels to be drilled, the maximum normalised values of each index over the trial are illustrated in the human main joints.*

Let us then observe the plots relative to task 2, illustrated in Figure 4.30. Considering the indexes accounting for the kinematics aspects (pink area), it can be noted that either ω_1, ω_2 and ω_3 show low values in all the experimental conditions, except the joint displacement at the elbow level (in line with the task requirements), meaning that kinematics variables are not significantly predictive of the ergonomics risk associated with this specific activity. This is consistent with the fact that the subjects were basically steady throughout its whole duration. On the other hand, considering the indexes accounting for the dynamics aspects, the predominance of ω_8 over the other indexes is clearly noticeable. The compressive forces index is overall far higher than all the other indexes and presents a certain increment in D1 with respect to D2 and D3, most likely

[7] The reported values of sEMG are the ones exhibited by the muscles in the same instant in which the maximum value of the compared index ω, which is shown in the polar plots, was found.

due to the fact that in D1 the gravitational component of the external force was greater because of the tool weight. Similarly, the sEMG signals display more significant values in D1 than in the other two conditions in several muscles, meaning that ω_8 correlates to muscle activity to some extent. Specifically, the percentage increase of the muscle activity between D2/D3 and D1 is $130.3/1153.1$ % in the AD, $32.2/93.0$ % in the BC $6.3/267.7$ % in the TR, $112.7/24.1$ % in the ES, $3.5/18.9$ % in the GM, $358.7/106.1$ % in the RF and $47.6/85.2$ % in the TA, respectively. The muscle activity in PD was 86.7 % lower in D2 but in 14.9 % in D3 than in D1, probably due to the task requirements. The same explanation can be given for the muscle activity in TC, which is highest in D3, lower in D2, and even less significant in D1. Accordingly, it is possible to state that ω_8 is capable to reveal the physical load associated with the considered drilling activity.

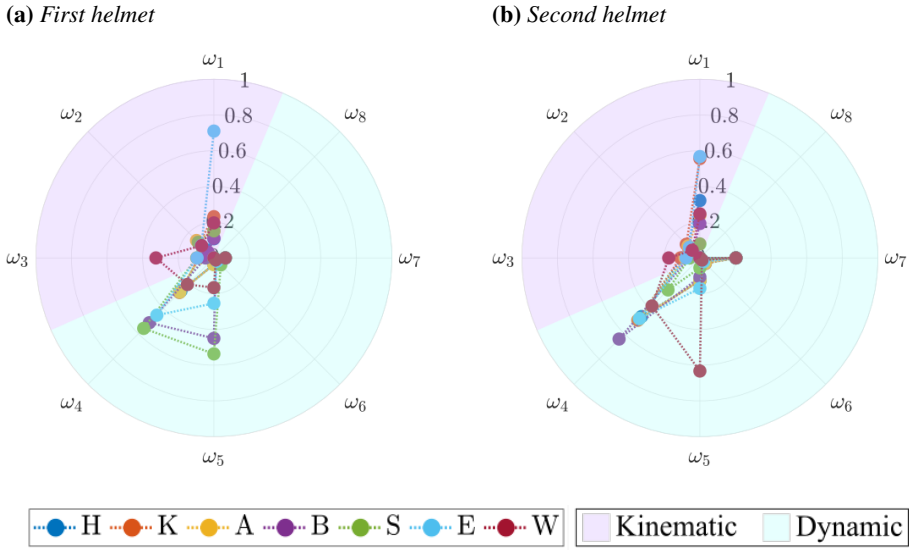

Figure 4.31: *Polar plots to represent the overall outcome of the proposed ergonomic indexes for task 3. For each phase of the task, i.e. one of the two helmets to be painted, the maximum normalised values of each index over the phase are illustrated in the human main joints.*

Lastly, let us focus on the plots depicted in Figure 4.31, relative to task 3. Considering the kinematics-related variables (pink area), it can be observed that rather meaningful values are shown by ω_1 at the elbow and knee level, to a lesser degree at the hip level, meaning that potentially risky body configurations could have been adopted by the subjects to accomplish the task. On the other hand, ω_2 and ω_3 are altogether very low thus bearing no information for the purposes of the ergonomics assessment. Similarly as in task 1, the only exception is the acceleration of the wrist that, as already mentioned, may be suggestive of potential hazards. Considering then the dynamics-related variables, it is evident that the most relevant indexes to explain the physical exposure of the task are ω_4 and ω_5, in comparison with all the other indexes which are basically negligible. Moreover, the trend of the muscle activity is comparable to the one displayed by both the overloading torque and fatigue in the lower body and in the arm, giving further evidence of the capability of ω_4 and also ω_5 to account for human effort. Specifically, the raising of the overloading torque and fatigue in the legs between the first and the second phase is accompanied by a percentage increase of muscle ac-

tivity of 348.5 % in the RF, 177.5 % in the BF, and 624.5 % in the TA. Conversely, the overloading torque and fatigue in the arms are reduced between the first and the second phase but still matching the activity in most of the muscles with a percentage decrement of 78.2 % in the AD, 15.2 % in the BC, 48.8 % in the TC and 42.9 % in the TR. Nevertheless, by adopting the polar plot representation, which takes into account the maximum values of the mean among twelve subjects, it is not possible to appreciate the benefit introduced by the overloading fatigue index to address the cumulative effect of the overloading torque. In fact, it should be reminded that considerable standard deviation values are exhibited by $\boldsymbol{\omega}_5$.

In view of the above, some conclusive remarks can be drawn for the human ergonomics monitoring system introduced in this Chapter. As regards kinematics-related variables, the most beneficial index in assessing physical exposure is represented by $\boldsymbol{\omega}_1$. The joint displacement index allows to detect wherever the human current body configuration lays within specific sections of the human ROM which should be avoided (e.g. in proximity to the maximum limits). Hence, by monitoring how often and how long these body configurations are maintained, it is possible to determine if a potential ergonomic risk exists. As a matter of fact, joint kinematics in general has extensively been used in the analysis of human movement and joint angles, in particular, have widely been employed to identify human awkward or unfavourable postures while performing work activities. Concerning joint velocities and accelerations, no significant information is offered by $\boldsymbol{\omega}_2$ and $\boldsymbol{\omega}_3$ in the context of this experimental analysis, excluding the rather significant accelerations exhibited by the wrist, which should be taken into account since they have been demonstrated to correlate with occupational risks. Nevertheless, the three tasks considered were quite steady and regular and did not require the development of significant speeds and accelerations. Hence, the joint velocity and acceleration indexes should be investigated more thoroughly.

As regards dynamics-related variables, a specific index has been identified that better explains the physical load required in each considered task, supported by the outcome of the sEMG analysis. Specifically, the overloading joint torque index $\boldsymbol{\omega}_4$ is the more promising mean to account for the mechanical overburden of the body structures in tasks involving the handling of heavy objects (task 1). Instead, considering task in which all the components of the interaction forces at the hand/tool interface are relevant - not only the gravitational one - (task 2), the joint compressive forces index $\boldsymbol{\omega}_8$ has proven to be more predictive of the risk associated with dynamically varying interaction forces. In fact, in these cases, the overloading joint torque may underestimate the hazard. Finally, to account for fatigue accumulation while executing repetitive and monotonous prolonged activities (task 3) the overloading joint fatigue index $\boldsymbol{\omega}_5$ happens to be more valuable since it takes into consideration the cumulative effect of the risk and not the instantaneous one. However, as already mentioned, the sensitivity of the overloading fatigue model to thresholds must be further investigated. Additionally, concerning the overloading joint power index $\boldsymbol{\omega}_6$ and the CoM potential energy index $\boldsymbol{\omega}_7$ similar observations can be made. Not remarkable or not easily interpretable information appears to be provided by such variables but this may be due to the fact that, as already noticed, no considerable velocities or unexpected movements were required to accomplish the analysed tasks. Conversely, regular, smooth, and constant-speed actions were repeated. Hence, the potential of both the indexes should be investigated

more deeply while conducting more dynamically varying jobs, likewise for ω_2 and ω_3.

Ultimately, a comparison should be made between the proposed set of ergonomic indexes and the EAWS. It is critical to note that EAWS are conceived and usually applied in real industrial scenarios. On the contrary, for the sake of this experimental analysis, they have been adopted with simplified activities that were designed to simulate occupational tasks and were conducted during experiments in laboratory settings. Accordingly, several assumptions have been made to contextualise such simplified tasks in the workplace which was intended to be replicated. Bearing in mind the above, it should be observed that EAWS happens to be subject-specific only to a certain degree. For task 1, only the gender was taken into account to compute the final score, i.e. the male and the female subjects present the same rating among them. For task 3, the exact same score is assigned to all the subjects, since its estimation is mainly based on the task timing, which is set according to standard base time using the MTM-UAS method [179]. The inter-subject variations are instead more significant for task 2 since the maximum force exerted in each trial by each subject was considered. However, it is possible to state that the set of ergonomic indexes proposed in this thesis pays much more attention to the individual's behaviours and demands while performing a potentially risky task. In fact, it is based on a subject-specific model of the human body. In addition, the EAWS analysis consists in a rather complex and articulated procedure that can be conducted only in an off-line phase and, according to the author of this thesis, to some extent is affected by the subjective opinions of the expert who carries out the analysis. Due to the current ongoing technological developments, an accessible and easy-to-use version of EAWS will be probably available soon. Nevertheless, this method seems still to lack a full evaluation of all the dynamics aspects underlying the execution of occupational tasks. In light of the above, the integration of a well-recognised tool for the human ergonomics assessment in the workplace as the EAWS with the proposed human ergonomics monitoring system would allow a more comprehensive and thorough analysis of the whole range of risk factors associated with occupational activities, taking equally into account the relative kinematics and dynamics aspects and addressing workers' specific requirements.

CHAPTER 5

Feedback interfaces for Situational Awareness

To continuously encourage humans to avoid awkward body postures or unfavourable physical loading conditions, appropriate warning modalities are an essential requirement. By using intuitive and practical feedback interfaces the workers can be informed about the excessive overburden of the body structure and thus guided towards more ergonomic and convenient working conditions. With the aim to improve human risk-awareness, multiple different technologies (e.g. visual, auditory, and haptic) can be exploited.

In the last decade, an increasing interest has been aroused by augmented reality (AR) [182]. Several commercial systems for AR (as well as virtual reality (VR)) were developed (e.g. Oculus Rift by Oculus VR, Hololens by Microsoft, Tango by Google) and proposed as a promising tool to improve workers' ergonomics [183]. Nevertheless, recent research has shown that the implementation of AR for industrial applications is challenging [184]. Visual displays may be disadvantageous in terms of the cognitive load in some specific applications [185], and may limit the natural field of view of the workers. Furthermore, despite the constant advances in the field, these devices still present several technological and perceptual limitations: obtrusiveness of the equipment, need for frequent recalibrations, general discomfort if used for long periods of times, and low luminance of the micro-displays, to cite a few [186].

Audio devices were also considered as a form of ergonomic intervention. In particular, in [187] the Spineangel by Movement Metrics Ltd was developed to monitor trunk posture during daily activities and to supply audio feedback to the wearer whenever specific postural thresholds were exceeded. However, due to the always-working machinery, the industrial settings are generally very noisy and audio modalities may be ineffective in such contexts.

To reliably provide feedback even in boisterous workplaces, sensory substitution

techniques such as vibrotactile interfaces were proposed and their effectiveness has been validated in a range of applications: human navigation [188, 189], posture awareness [190] and posture control in rehabilitation [191]. In particular, in [192] a method to drive the position of the human through a vibrotactile device was introduced in a human-robot collaboration context. Similarly, visual feedback was considered to reduce hazardous postural behaviours [193, 194] and even then integrated in human-robot interaction frameworks [76]. Nevertheless, the above-mentioned solutions provide feedback that only contains kinematic information, neglecting equally valuable aspects as the physical loading on the joints, or just focus on specific body parts.

To tackle these issues, two feedback solutions were proposed within the purposes of this thesis: a graphical interface to provide visual feedback and a vibrotactile device as a sensory substitution modality. The latter, especially, offers the huge benefit of being wearable and wireless thus it can assist the users within a broad area and allow them to act freely in the work space without the need to focus on any specific spot. The graphical interface is one of the main contributions of this thesis. For the development of the vibrotactile device, the author of this thesis just acted as a minor collaborator, however, it is considered worthwhile to include the related work here. A description of these two approaches, illustrating their main features and highlighting their merits, follows in Section 5.1 and in Section 5.2, respectively. [1]

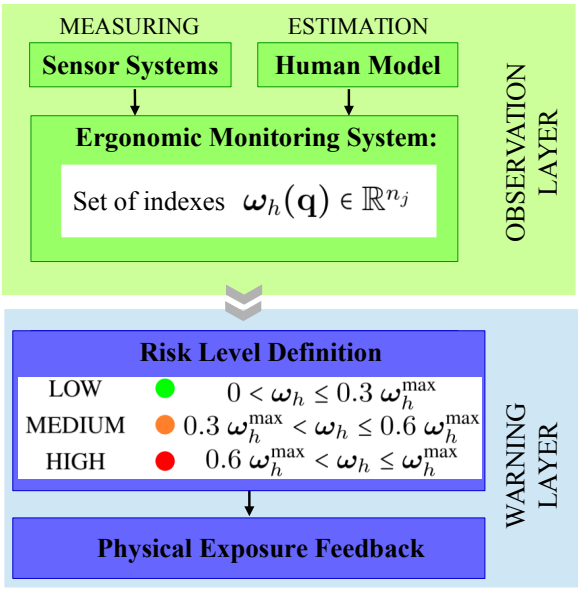

Figure 5.1: *Second block of the framework proposed in this thesis for the assessment and improvement of human ergonomics: the warning layer (see Section 1.5). The warning layer follows the observation layer addressed in Chapter 4.*

As mentioned in Section 1.5, this Chapter will hence address the second block of the framework proposed in this thesis (see Figure 1.1): the warning layer. In Figure 5.1, the warning layer is emphasised with its key elements. Once the set of indexes to account

[1] Parts of this Chapter have been published in [33, 34]

for the human ergonomic risk factors has been defined within the observation layer, criteria to set their level must be established. Considering a generic ergonomics index $\boldsymbol{\omega}_h(\mathbf{q}) \in \mathbb{R}^{n_j}$, as introduced in Chapter 4, three classes can be defined to categorise the associated level of hazard, as illustrated in Table 5.1.

Table 5.1: *Step-wise scheme for ergonomic index levels.*

Ergonomics index level	Control threshold
LOW	$0 < \boldsymbol{\omega}_h \leq 0.3\ \boldsymbol{\omega}_h^{\max}$
MEDIUM	$0.3\ \boldsymbol{\omega}_h^{\max} < \boldsymbol{\omega}_h \leq 0.6\ \boldsymbol{\omega}_h^{\max}$
HIGH	$0.6\ \boldsymbol{\omega}_h^{\max} < \boldsymbol{\omega}_h \leq \boldsymbol{\omega}_h^{\max}$

The purpose of defining a number of specific levels is to make the ergonomic indexes accessible to the feedback interfaces. In fact, the three classes defined in Table 5.1 are adopted to color-code a graphical mean and to set the degree of vibration for the visual interface and for the vibrotactile device, respectively.

5.1 A Graphical Interface for Visual Feedback

The main focus of [34] was to propose an intuitive graphical interface to make humans aware of potentially risky body configurations while being exposed to external loads. By means of a dedicated screen, both dynamic and kinematic meaningful information on the whole body can be provided online to the user, as illustrated in Figure 5.2. The Robot Operating System (ROS) 3D visualizer RViz[2] is employed for displaying purpose.

Kinematic data refer to the current body configuration of the user, depicted by using a virtual simplified model of the human system that consists of a branched structure of rigid bodies. The position of the human CoP can be represented as well, whether estimated or measured. The dynamic information is expressed in terms of overloadings induced on the human joints by an external load using the method described in 4.2. The estimated overloading joint torques are illustrated with spheres superimposed on the human body model and located in the main joints (hip, knee, ankle, shoulder, elbow). As anticipated above, the level of the index selected to be displayed by the graphical interface is color-coded to denote a high (red), medium (orange), or low (green) value which corresponds to the ergonomic risk associated. This traffic light scheme has been recognised by the Machinery Directive 2006/42/EC (EN 614) and enables a straightforward interpretation and ease of use of the indexes. The three levels of the overloading joint torque are hence determined as explained in in Table 5.1, considering the overloading joint torque $\Delta\boldsymbol{\tau}$ as the ergonomics index $\boldsymbol{\omega}_h$.

As shown in Figure 5.2, different tools/objects can be represented and thus distinguished through a different color/shape in the graphical interface. Depending on their weight, the external load induced on the human body varies and thus the estimation procedure of the overloading joint torques can be tuned accordingly. In each row of the Figure, three different postures are depicted, passing from a high-risk condition, denoted by considerable values of the overloadings on the joints, to a more safe and comfortable one in which the physical effort is minimised, as suggested by the lower

[2] http://wiki.ros.org/rviz

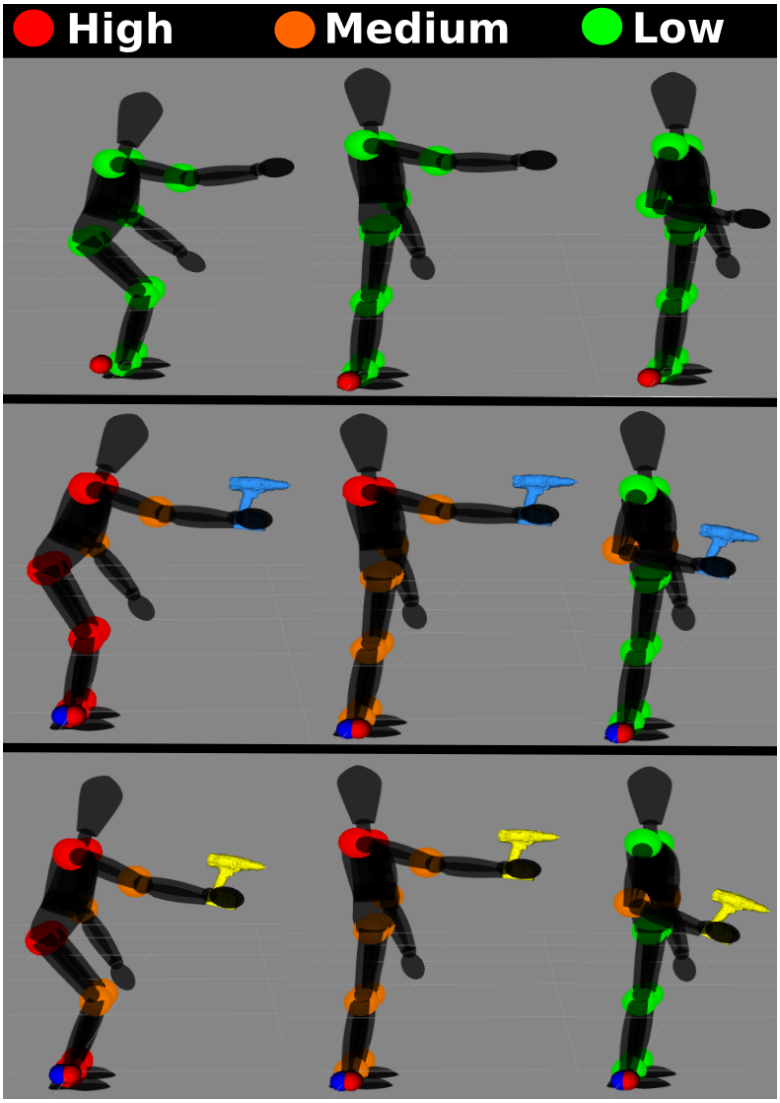

Figure 5.2: *An overview of the graphical interface: in each row, the human is represented in three different body configurations, without any tool in the first row and with two different tools in the second and third row, respectively. The level of overloading joint torque is color-coded to denote a high, medium, or low value, and illustrated in the main joints of the human body.*

values of the overloadings. Regarding the first row, it shows the human operating without any tool and thus without the effect of any external load. Hence, the overloading on the joints is always low. The second and the third row, instead, depict the human operating with two different types of tools, respectively.

To sum up, the proposed graphical interface can help the users to learn and achieve more ergonomic configurations during industrial job duties. Even though it was originally proposed to report the level of the overloading joint torque (Section 4.2), it can be reset to provide the user with information about the level of other alternative ergonomic indexes. For example, in [31], in lieu of the overloading torques, their cumulative effect over time, defined as overloading fatigue and explained in Section 4.3 was illustrated in the human main joints. In Subsection 6.2.2 further details will be provided about its use in this respect.

Furthermore, its functionalities can be extended to represent much other valuable information for the purpose of ergonomics monitoring and improvement. In [32] a method was presented to detect and locate an external load exerted on the human (as mentioned in Section 4.2) and the graphical interface is exploited to depict, among other information, the estimated load application point on the human body.

In addition, the proposed graphical interface was combined with the HRC framework which will be presented in Chapter 6, in the context of several studies [29, 31, 35] to provide the human subjects with further guidance to perform their task. In this respect, some experimental results of the visual interface's capability to give intuitive and beneficial feedback to workers can thus be found in Section 6.2.

5.2 ErgoTac: a Vibrotactile Feedback Device

Opting for vibrotactile devices as a feedback modality for the improvement of human ergonomics guarantees stable, smooth, and intuitive ways to make the humans aware of the hazards connected to excessive loading on the musculoskeletal structure or inconvenient body postures, thus preventing the development of WMSDs.

With the aim to improve human risk-awareness in the execution of heavy or repetitive industrial tasks, in [33] a novel wireless and wearable vibrotactile technology called "ErgoTac" was introduced. The proposed device provides online whole-body feedback to humans with the information about excessive overloading of body joints by applying appropriate tactile stimuli, and drive them towards more ergonomic physical exposure conditions. A user study on ten human subjects was performed to validate the approach. While performing a lifting task with a heavy object, the subjects were required to reconfigure their body posture by following the vibrotactile feedback guidance so as to reduce the effort on the joints. Statistical analysis is included in the experimental results which prove the potential of ErgoTac in assisting the workers in their occupational activities.

5.2.1 Specifications of ErgoTac

The developed device ErgoTac, depicted in Figure 5.3, is designed as a wireless vibrotactile feedback interface that can be located in proximity to the most meaningful joints of the human body to alert the user about the level of the overloading joint torques, whose computation is addressed in 4.2. By following the provided stimuli, the body

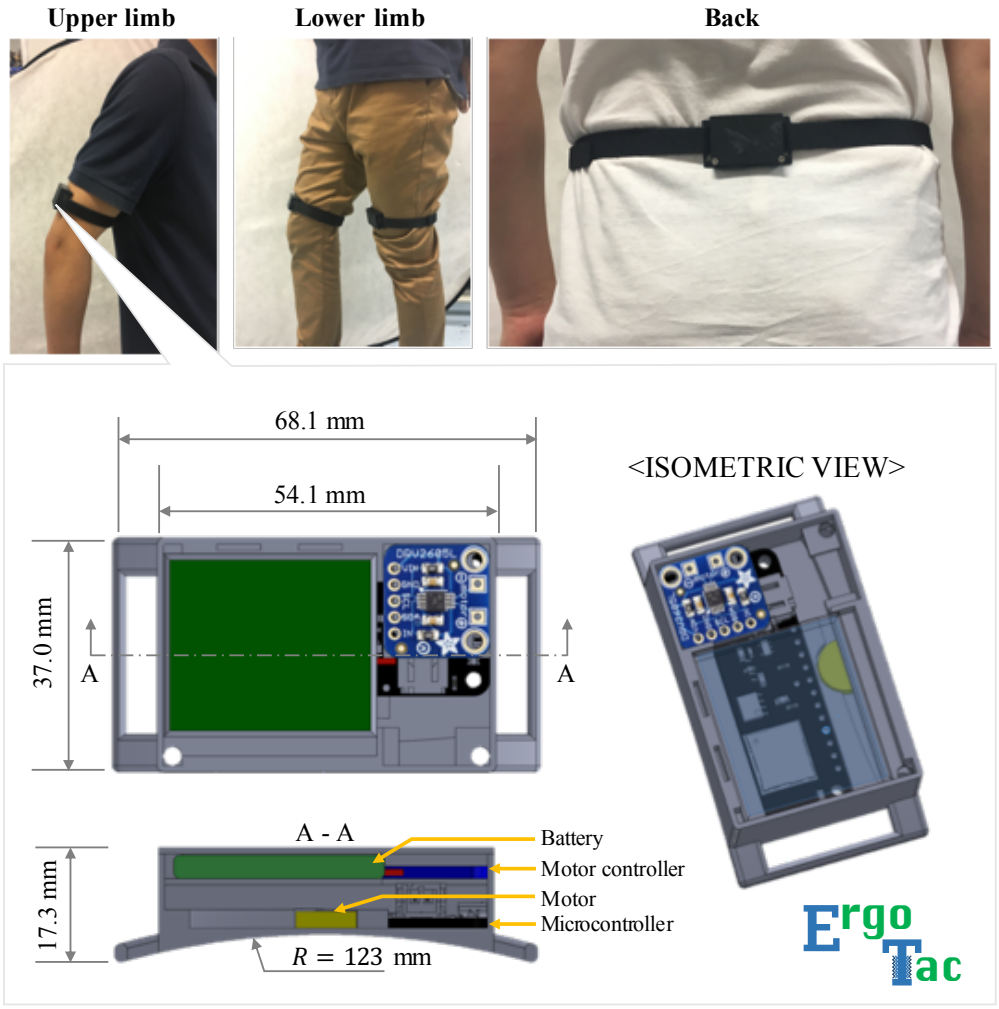

Figure 5.3: *The specifications and components of the developed wearable vibrotactile feedback device ErgoTac which can be worn on the upper limb (left), lower limb (middle), or even on the back (right).*

configuration can be modified attempting to reduce the vibrations and thus to minimize the effect of an external load on the joints. As a result, more ergonomic postures can be achieved. Considering the industrial environment as the primary target, the wearability and handiness of the hardware components are major requirements in the designing process. In view of this, the weight and dimensions of ErgoTac are 28 g and 68.1 mm ×37.0 mm ×17.3 mm, respectively. Its case is realised in lightweight plastic by means of a 3D printer. To be adaptable to the shapes of the human body, the bottom surface of the device is slightly curved and practical stretchable bands are used to attach it to the body segments (e.g. thigh, upper arm, etc.). Then, to further ensure the portability of the device, Bluetooth low energy which uses 2.4 GHz spectrum wireless protocol has been integrated with a portable microcontroller (Adafruit Feather M0 Bluefruit). Since wireless communication supports multi-point connections, multiple ErgoTac can be connected simultaneously. To control the single feedback device, an RF-module (nRF51 Dongle, Nordic Semiconductor) is connected to the user side via a universal serial bus (USB) and an area of 10 m can be covered. Moreover, to avoid impractical wiring, the battery is placed inside the box. A small size Lithium-polymer battery

with a rated voltage of 3.7V and a capacity of 300 mAh is selected as a trade-off between size and power. Battery life is approximately 3 hours. Finally, to control the intensity of the vibrotactile stimulation, pulse-width modulated (PWM) drive signals are employed. On the other hand, a mini eccentric rotating mass (ERM) vibration motor is used to generate the vibrotactile effect. The corresponding rated voltage of 3.7 V allows a frequency which is approximately 121 Hz thus is sufficient to stimulate the human skin for the considered purpose [195].

5.2.2 Integration with the Observation Layer

The aim of ErgoTac is to drive the users toward body configurations in which the overloading joint torques, estimated as explained in Section 4.2, are minimised. For this reason, the strength of the vibrotactile feedback is tuned to reflect the level of the overloading effect in certain specific joints. As a result, the users can modify their movements looking for lower stimuli that correspond to minor efforts in performing their task, thus preventing potential injuries. Accordingly, three different levels have been selected for the amplitude of the vibration (high, medium, and low) and associated with the overloading joint torque levels as explained in in Table 5.1, considering the overloading joint torque $\Delta\boldsymbol{\tau}$ as the ergonomics index $\boldsymbol{\omega}_h$.

The selected feedback amplitude is transmitted online to ErgoTac to activate the motor and the PWM duty cycle is controlled with a sensitivity level of 30%, 60% or 100% to produce a low, medium, or high vibration, respectively. To make the user easily distinguish the different levels of vibrations, a considerably different frequency of the ERM vibration motor is considered for each of them.

5.2.3 Experimental Setup

The experimental setup is shown in Figure 5.4. To track human motions, the Xsens suit, presented in Section 3.1 was used. To measure the GRF and CoP, the Kistler force plate presented in Section 3.2 was used. Five ErgoTac devices were located on the human body, specifically onto the upper-arm, the forearm, the pelvis, the thigh, and the shank. The stimulation induced on such body segments corresponded to the overloading level computed on the shoulder, elbow, hip, knee, and ankle, respectively. Muscle activity was measured in the whole body for the entire duration of the task, using the Delsys Trigno Wireless system to collect EMG signals. Specifically, four muscles were considered: anterior deltoid (AD), biceps (BC), L5 paraspinal (L5) and lateral gastrocnemius (LG) with the aim to assess the capability of the proposed approach to reduce human physical loading. The whole experimental procedure was carried out in accordance with the Declaration of Helsinki and the protocol was approved by the ethics committee ASL Genovese N.3 (Protocol IIT_HRII_001). Ten healthy subjects, nine males and one female, (age: 28.9 ± 3.2 years; mass: 76.4 ± 8.5 kg; height: 1.80 ± 0.04 m)[3] were recruited in the experimental analysis. A written informed consent was obtained after explaining the experimental procedure. First, the human model of each subject was identified by using the SESC technique (presented in Section 3.2) during an off-line calibration phase. The subjects were required to wear the MVN Biomech suit and stand on the Kistler force plate and then to perform two hundred different static

[3] Subject data is reported as: mean ± standard deviation.

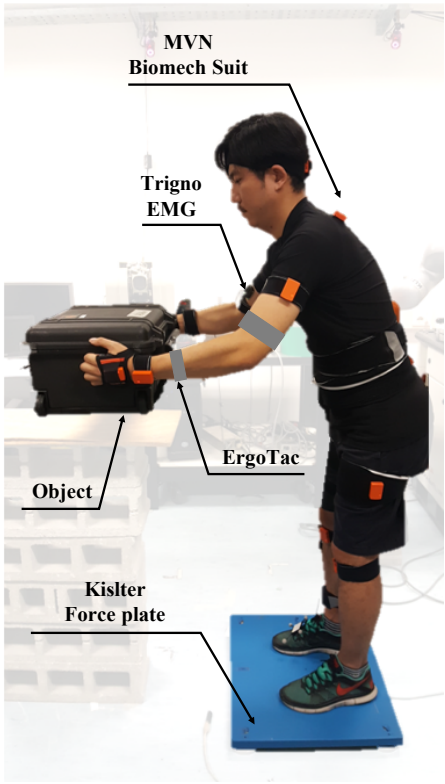

Figure 5.4: *Overview of the experimental setup. All the sensor systems involved in the experiment and the vibrotactile devices are illustrated.*

body configurations to collect a sufficient dataset for the model parameters identification. The CoP model thus estimated was then used during in an online phase to address overloading joint torques. Among the industrial tasks which are usually associate with high risk of musculoskeletal injuries, the lifting task is one of the most cited [163, 196] thus it was selected for the experimental analysis. Accordingly, all the subjects were asked to hold a heavy object (mass: 5.7 kg) and handle it using both hands. Prior to the experiment, all the subjects were trained to distinguish the three levels of vibrations and thus the degree of joint overloadings. Three sequential phases were included in the experimental session: the box lifting (3 sec.), the box handling by following vibrotactile feedback via ErgoTac - changing online the body configuration while attempting to reduce the level of the stimuli and thus the degree of the joint overloading - and, finally, the termination of the motion as soon as the lowest vibrotactile feedback possible was sensed in most of the devices. Throughout the whole task, the subjects were constrained to keep the object at a predefined height that was set at the beginning of the session. The experimental conditions consisted in fact in three different heights of the object: 0.3m, 0.6m, and 0.9m, respectively. A different trial was conducted for each one of them thus three trials for each subject were conducted. To validate the capability of the proposed device in guiding the user toward the reduction of the overloading joint torque by means of the vibrotactile stimuli, the muscle activity recorded at the beginning and at the end of the task was compared for all the subjects. Statistical differences were also tested using a post-hoc t-test with Bonferroni correction. The level of statistical significance was set to 0.05.

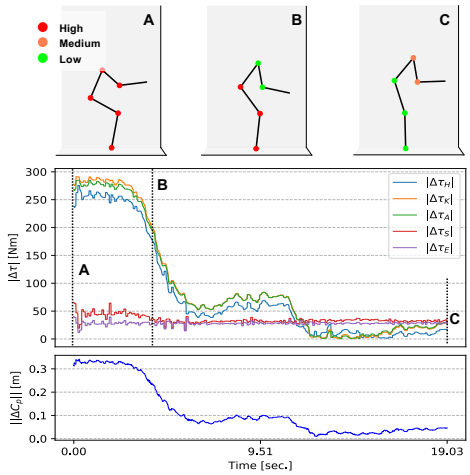

(a) *Condition 1 (height = 0.3m)*

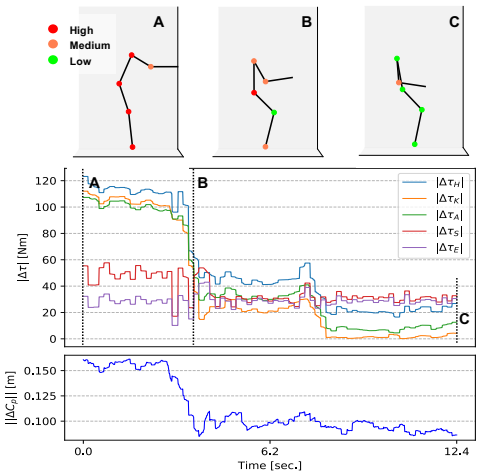

(b) *Condition 2 (height = 0.6m)*

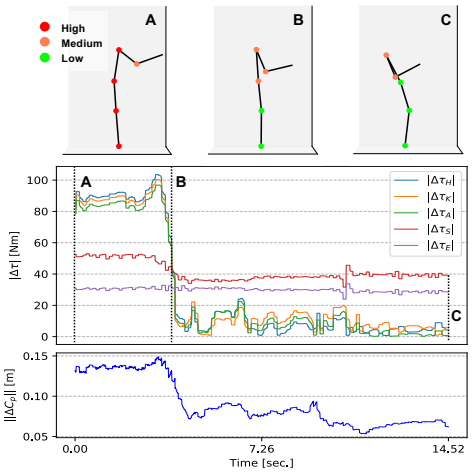

(c) *Condition 3 (height = 0.9m)*

Figure 5.5: *Results of vibrotactile feedback experiments with ErgoTac. The amplitude of the feedback (upper figures) is high in phase (A), then the human pose is adjusted following the stimuli toward phase (C) in which the amplitude is minimised. The overloading joint torques (second plot from top) in the human joints are reduced and the displacement of the CoP (bottom plot) likewise decreases between* $\hat{\mathbf{C}}_P$ *(SESC) and* $\mathbf{C}_P$ *(force plate).*

5.2.4 Results

Figure 5.5 illustrates the experimental results considering the three different experimental conditions (constrained height of the object) of one selected subject, taken as an example. Different sequences of movements to reach the final configuration were exhibited by the ten participants thus make an average of their outcomes was not possible. The first row depicts three body configurations in certain instants during the task. The vibrotactile feedback amplitude for each joint is highlighted through color-coded spheres superimposed on the stick-model of the human. This information was provided online to the subjects during the experiments. Phase (A), which corresponds to the box lifting phase, is characterised by a high-risk body configuration, thus the ErgoTac clearly provided the most significant level of stimuli to alert the user about the danger. Phase (B) corresponds to the mid-phase while re-configuring the posture by following

the ErgoTac guidance. The final phase (C) corresponds to the minimisation of the risk of joint overloadings when the lowest amplitude of vibrotactile feedback was reached. The plots in the second row show the estimated overloading joint torque in the main joints (H: hip, K: knee, A: ankle, S: shoulder, E: elbow) while the plots in the last row illustrate the displacement of the CoP computed between the measured and estimated vectors, respectively. The average time needed to complete the task among all the ten subjects for each experimental condition was: 19.92 ± 8.53 s (condition 1), 17.08 ± 7.43 s (condition 2), and 23.50 ± 18.16 s (condition 3), respectively.

In Table 5.2 the overall experimental results are presented. The reduction rate of the overloading joint torque in each joint and the corresponding variations of the muscle activity (filtered and normalised), respectively, were averaged across the subjects for each condition. It should be noted that body configurations in the final phase after re-configuring due to the vibrotactile feedback, were not the same for all subjects.

Table 5.2: *Experimental results for ten subjects. The results are separated according to the three experimental conditions for the overloading joint torque (SH: shoulder, EL: elbow, HP: hip, KN: knee, AK: ankle) and muscle activity (AD: anterior deltoid, BC: biceps, L5: L5 paraspinal, LG: lateral gastrocnemius). The decrement ratio of data is reported as: mean (standard error of the mean).*

Index		Condition 1	Condition 2	Condition 3
Overloading joint torque [Nm]	SH	26.73 (6.38)	38.71 (7.97)	30.33 (4.05)
	EL	8.89 (8.09)	5.86 (5.56)	1.29 (3.80)
	HP	64.49 (7.75)	61.09 (8.54)	58.32 (9.51)
	KN	70.87 (9.41)	56.76 (10.18)	59.27 (9.37)
	AK	70.87 (9.13)	58.67 (9.32)	57.87 (9.62)
Muscle activity [%]	AD	81.26 (6.86)	96.62 (0.51)	80.38 (8.60)
	BC	6.00 (31.79)	29.27 (10.66)	33.17 (10.57)
	L5	45.03 (8.79)	53.72 (4.43)	60.69 (6.17)
	LG	20.98 (28.40)	50.68 (10.82)	63.48 (6.00)

Figure 5.6 shows the box plots for the overloading joint torque and muscle activity corresponding to the data collected in phase (A) (blue box plots) and in phase (C) (green box plots), respectively, for all the subjects. The values of the overloading joint torque in the shoulder, hip, knee, and ankle joint estimated in phase (A) were significantly higher than in phase (C) considering the overall conditions. On the other hand, the overloading joint torque reduction in the elbow joint was not meaningful. The differences were, respectively, 2.12±1.61 Nm (p =.23) in condition 1, 1.48±1.21 Nm (p =.27) in condition 2 and 0.68±0.65 Nm (p =.34) in condition 3 and they were sta-

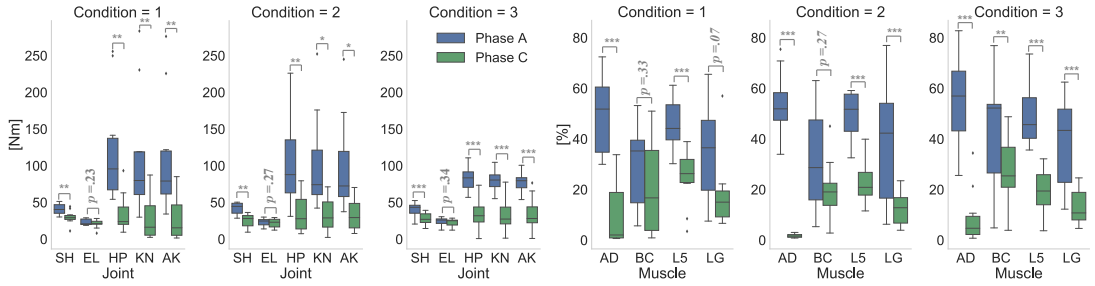

(a) *Overloading joint torque* **(b)** *Muscle activity*

Figure 5.6: *Statistical results of the joint overloading and the muscle activity for ten subjects during the experiments with ErgoTac. The joints overloading (SH: shoulder, EL: elbow, HP: hip, KN: knee, AK: ankle) of most of the joints resulted in phase (A) are significantly greater than phase (C), except the EL joint. Most of muscles activity (AD: anterior deltoid, BC: biceps, L5: L5 paraspinal, LG: lateral gastrocnemius) showed a significant difference between phase (A) and phase (C), except in the BC (condition 1 and 2) and LG (condition 2). Asterisks indicate the level of statistical significance after post-hoc t-tests: *p <.05, **p <.01 and ***p <.001*

tistically not significant. Similarly, the muscle activity measured on the AD and L5 displayed a considerable difference between phase (A) and phase (C). On the contrary, the muscle activity measured in LG in condition 1, and the muscle activity measured in BC in condition 1 and 2 showed statistically not significant results. In all the other conditions, the differences of the muscle activity in the same muscles were instead statistically significant. Specifically, as regards LG the variation was: 17.09 ± 8.03 Nm (p = .07) in condition 1, as regards BC the variation was: 8.18 ± 7.56 Nm (p = 0.33) in condition 1 and 11.92 ± 5.32 Nm (p = .27) in condition 2.

5.2.5 Discussion

Observing the results of the overloading joint torques in the different phases, it is possible to state that, due to vibrotactile feedback guidance, the overloading torques in the joints throughout the task exhibit an overall reduction. As shown in Table 5.2, the corresponding decrement was 44.37%, 44.22%, and 41.41% in each experimental condition, respectively. The majority of the joints presented significantly lower overloading joint torques in the final phase, excluding the elbow joint. Since a constraint on the height of the object was imposed for the task, most likely the elbow joint had a major role than the other joints in accomplishing the task thus it reconfigured differently. The results also indicate that the reduction rate of the overall muscle activity was 38.32%, 57.57% and 59.43% in each experimental condition, respectively. In particular, the variations in DT and L5, which belong to the most common areas of human injuries (i.e. lumbar spine), exhibit meaningfully lower muscle activity in the final phase. The muscle activity in BC and LG had increased or slightly reduced but not as much as in the other joints. Following the same reasoning done for the overloading joint torque, the activity of these muscles was most likely connected to the task constraint of maintaining the object at the same height as well as balancing the body during the task. However, it is possible to affirm that the workload generally decreased under the task constraints, and steady external forces were distributed into the joint minimising the overloading effect, by re-configuring the human pose according to the guidance of the vibrotactile feedback.

Experimental results provided first evidence on the capability of the proposed online feedback device and method to achieve more ergonomic behaviours while performing the desired industrial tasks. It is worth mentioning that humans could also recognize the overloading effect on the joints by means of their own kinesthetic feedback. Nevertheless, most of the time the associated risk is underestimated and thus neglected. This is one of the reasons why many work-related health issues are experienced every year in industrial environments. In addition, some tasks require a constant but low level of overloadings that may be negligible for the workers on the spot, but it has considerable effects over longer periods. Therefore, a warning interface to make humans aware of all the inappropriate working conditions can make a major contribution in reducing work-related risks.

CHAPTER 6

A Human-Robot Collaboration Framework to Guide the Humans toward More Ergonomic Postures

In the current industrial background, to address workers' ergonomic demands while ensuring productiveness and efficiency, highly adaptable and quickly re-configurable systems with online data processing capabilities are required. As already mentioned in Section 1.3, a promising solution in this respect, is offered by collaborative robots, which can put their precision, endurance, and power at the service of workers. However, in order to guarantee human safety, such robotic assistants are usually programmed to avoid accidental collisions and impacts but seldom conceived to enter in direct contact with humans to offer effective help.

With the aim to take advantage of the intelligent physical support of the robot to mitigate workers' ergonomic risks, an HRC control approach was originally proposed in [129] to guide the human toward more convenient behaviour in a co-manipulation task. Within the context of this thesis, the application and extension of this HRC framework has been addressed to different extents [29, 31, 197] and it will be presented in Section 6.2. As mentioned in Section 1.5, this Chapter will indeed cover the third block of the framework proposed in this thesis (see Figure 1.1): the action layer. In Figure 6.1, the action layer is emphasised with its key elements.

Once the set of indexes to account for the human ergonomic risk factors has been defined within the observation layer, and their level of risk has been established in the warning layer, preventive action must be taken to mitigate their effect. Accordingly, assuming to consider only one specific ergonomic index at a time, wherever its level of risk is medium/high ($\boldsymbol{\omega}_h > 0.3\boldsymbol{\omega}_h^{\max}$), an optimisation procedure is triggered to estimate more ergonomic working conditions. Essentially, the selected ergonomic index is

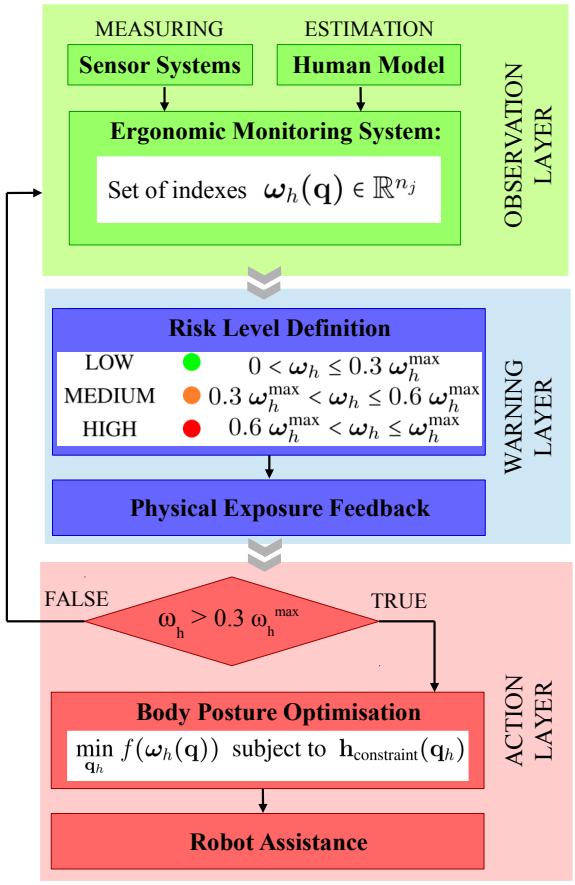

Figure 6.1: *Third block of the framework proposed in this thesis for the assessment and improvement of human ergonomics: the action layer (see Section 1.5). The action layer follows the observation layer addressed in Chapter 4 and the warning layer addressed in Chapter 5.*

minimised according to certain specific constraints and the human body configuration in terms of $\mathbf{q}_h$ (the joint angles vector, see Subsection 3.2.1), which satisfies at best all the requirements, is obtained as a result. Such a body configuration is considered to be more ergonomic since it minimises the effect of the risk factor associated with the selected index. In addition, by introducing a collaborative robot as a further actor in the working task execution, the human can be facilitated to achieve more ergonomic conditions by following its guidance. In fact, assuming a co-operation or co-manipulation [1] activity, the trajectory of the robot end-effector can be adjusted to drive the worker from a risky body configuration to the estimated optimal one.

This Chapter is organised as follows. Section 6.1 describes the online optimisation procedure just mentioned to estimate more ergonomic human body postures. In Section 6.2, some applicative examples of the HRC framework addressed in this Chapter are presented.[2] First, its implementation to human bipedal models is illustrated. Next, its extension by means of a trigger mechanism based on human physical fatigue thresholds

[1] Co-operation activities are referred, for example, to those tasks in which the robot is holding an object and the human is operating on it with or without a tool (drilling, polishing, screwing, etc.) while co-manipulation tasks are referred, for example, to the co-sharing or handover of objects between the human and the robot.

[2] Parts of this Chapter have been published in [29, 31, 197]

is introduced. In addition, the case study of a multi-human and mobile-robot collaborative team is provided.

6.1 Body Posture Optimisation Procedure

The aim of the anticipatory robot assistance is to encourage the human partner to perform the collaborative task in a more efficient way, i.e. adopting behaviours that avoid the excessive overloading of body tissues. In this view, an online optimisation procedure can be implemented to estimate ergonomic human postures, given the information about human movements and external forces profiles, the task objectives and its constraints. To achieve such an optimal body configuration, the minimisation of any selected index, accounting for an ergonomic risk factor, must be performed in the joints that are subject to potential injuries. Accordingly, the optimisation problem can be designed by setting as the objective function the sum of the weighted norms of the ergonomic index, which is function the human joint angles vector $\mathbf{q}_h$, subject to nonlinear inequality constraints

$$\min_{\mathbf{q}_h} f(\mathbf{q}_h) = \frac{1}{2}\sum_{i=1}^{n_j} \lambda_i |\omega_i(\mathbf{q_h})|^2, \tag{6.1}$$

$$\text{subject to: } \mathbf{q}_{\text{min}} \leq \mathbf{q}_h \leq \mathbf{q}_{\text{max}}, \tag{6.2}$$

$$\mathbf{h}_{\text{stable}}(\mathbf{q}_h) \leq 0, \tag{6.3}$$

$$\mathbf{h}_{\text{share}}(\mathbf{q}_h) \leq 0, \tag{6.4}$$

$$\mathbf{h}_{\text{Manipulability}}(\mathbf{q}_h) \leq 0, \tag{6.5}$$

where $\omega_i(\mathbf{q})$ is the i-th joint ergonomic index, selected among the ones listed in Table 4.1 (excluding joint kinematics indexes), λ_i is a weight associated with the joint i, and $\mathbf{h}$ are inequality box constraints.

All the weights ($\lambda > 0$) per optimisation cycle are computed by $|\omega_i/\omega_{\text{max}_i}|$ and kept fixed, with ω_i and ω_{max_i} representing the actual ergonomic index value at the beginning of optimisation and its maximum value at the i-th joint, respectively. The weights λ_i are introduced to set priorities between the joints, namely to pay more attention within the quadratic optimisation process to those ones which were more prone to risks. As an instance, $\omega_i \approx \omega_{\text{max}_i}$ means that that the i-th joint is subject to a higher hazard thus it should get the highest priority via $\lambda_i \approx 1$ with respect to the other joints.

Several constraints have been considered in the proposed optimisation process and they will be all illustrated hereafter. However, within the applicative examples of the HRC framework that are addressed in Section 6.2, just some of them are usually selected at a time. Accordingly, the details about the specific constraints adopted for each approach will be provided case to case.

To ensure that the body configuration resulting from the optimisation is feasible and safe, (6.2) expresses a boundary condition on the joint angles, which are restricted within the human body joint physiological limits, represented by lower ($\mathbf{q}_{\text{min}}$) and upper ($\mathbf{q}_{\text{max}}$) boundaries. The second constraint is associated with postural stability. A set of inequality constraints is considered in (6.3) to ensure that the position of CoP exists only within the convex hull of the contact points (i.e. within the support polygon of

feet). Accordingly, the inequality constraint (6.3) can be formulated as

$$\mathbf{h}_{\text{stable}}(\mathbf{q}_h) := \hat{\mathbf{C}}_{P_{wo}}(\mathbf{q}_h) - \text{conv}\{\boldsymbol{p}_{F|j}^{x,y}\} \leq 0, \tag{6.6}$$

where $\hat{\mathbf{C}}_{P_{wo}}(\mathbf{q}_h)$ is the CoP model as explained in Subsection 3.2.2, $\text{conv}\{\boldsymbol{p}_{F|j}^{x,y}\}$ is the convex hull including each possible j-th contact point $\boldsymbol{p}_F^{x,y}$ and it can be computed through the forward kinematic of the feet. Next, (6.4) expresses an inequality constraint related to the shared space between the human and the robot. Wherever a co-manipulation task is considered, the position of the co-manipulated object is constrained not only within a maximum distance from the human base but also a maximum distance from the robot base, to ensure a feasible and convenient working area for both the operators. Consequently, the inequality constraint (6.4) can be defined as

$$\mathbf{h}_{\text{share}}(\mathbf{q}_h) := \begin{cases} \boldsymbol{p}_{obj}(\mathbf{q}_h) - \boldsymbol{p}_{H|th} \leq 0, \\ -(\boldsymbol{p}_{obj}(\mathbf{q}_h) - \boldsymbol{p}_{R|th}) \leq 0, \end{cases} \tag{6.7}$$

where $\boldsymbol{p}_{R|th}$ and $\boldsymbol{p}_{H|th}$ are the position threshold considering the robot and the human work space, respectively, and $\boldsymbol{p}_{obj}(\mathbf{q}_h)$ is the co-manipulated object's position. All of them are computed using forward kinematics. Both the thresholds and the object's position are represented in the base frame, hence, the constraint should be represented within the shared Cartesian work space. Finally, the constraint in (6.5) is connected to the endpoint manipulability of the human arm. It is well-recognised that humans typically adjust the configuration of their body and limbs tending to maximise both the kinematic and dynamic aspects according to the given tasks and environmental conditions [198]. In robotics, the classical quantity used to account for the kinematic and dynamic properties of a robot end-effector is the manipulability, which notices how well the end-effector can produce velocity or force in different directions of the Cartesian space [199]. This concept can be applied also to humans. The directions of the best velocity and force axes can be obtained from the eigenvectors and the eigenvalues of human arm Jacobian $\mathbf{J}_a(\mathbf{q}_a) \in \mathbb{R}^{m \times l}$, where m is the size of Cartesian space and l is the number of considered joints in the arm, included in q_a, which is the joint angles vector specific to the arm. The manipulability can be geometrically represented as an ellipsoid at the level of the end-effector, whose radius in a specific direction refers to the capability to generate velocity/force. To provide an example, let us consider a specific task that requires an object/tool to be manipulated in a complex way. Such a task would probably involve a generation of force/velocity at the end-effector which is almost equal in all the directions of the Cartesian space. Hence, the configuration of the arm should be adjusted seeking to keep the end-effector where the endpoint manipulability ellipsoid is isotropic.

In view of the above considerations, the position of an object/tool - being manipulated by the human or co-manipulated by a human and a robot - can be also constrained by the human arm endpoint manipulability. Accordingly, the inequality constraint (6.5) can be defined as

$$\mathbf{h}_{\text{Manipulability}}(\mathbf{q}_h) := w_{\text{min}} - |\det(\mathbf{J}_a(\mathbf{q}_a))| \leq 0, \tag{6.8}$$

where w_{min} is the manipulability threshold. If $w_{\text{min}} = 1$, the algorithm will search for the optimal minimum ergonomic index within human arm endpoint positions, where the

manipulability ellipsoid is isotropic. In other cases, it will search within some region around isotropy. The application of all the constraints just presented in the optimisation process guarantees the stability and safety of both the partners in the collaboration task.

Once the human optimal body configuration is computed using (6.1), it is expressed in the Cartesian space along with the current human body configuration, by applying forward kinematics. Then, the difference between the two configurations can be employed to compute the trajectory for the robot end-effector. To achieve safe and adaptive interaction between the human and robot, a Cartesian impedance controller is generally employed to control it, setting the translational and the rotational stiffness to 1500 N/m and 150 Nm/rad in all axes, respectively. These values provide a reasonable trade-off between the trajectory tracking performance and end-effector compliance. Then, by following the guidance of the robot, humans can be facilitated to achieve more ergonomic and convenient body configurations.

6.2 Experimental Application of the HRC Framework

In this Section, some applicative examples of the online optimisation procedure just explained, to improve workers' ergonomics within HRC contexts, are provided.

6.2.1 Toward the Extension of the Work Space

The synergistic model presented in Subsection 3.2.4 to estimate the human feet GRF and CoP, was originally proposed in [29] to extend the overloading joint torque estimation procedure presented in Subsection 4.2. In fact, the latter could be so far applied to human biomechanical models represented by planar serial chains that include only one GRF. Its extension to bipedal models by means of the synergistic model, and thus the computation of the overloading joint torque for both the legs, would allow the tracking of human states in a wider work space, broadening the applications of the technique to more realistic and complex scenarios.

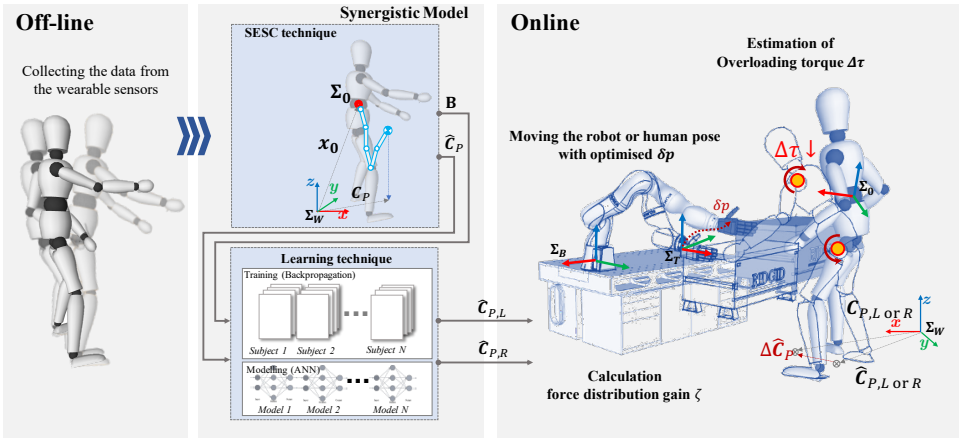

Figure 6.2: *The overall procedure for estimating the feet GRF and CoP using the synergistic model (left), and reducing the overloading joint torque during HRC in the online phase (right).*

The capability of the synergistic model to enable the online estimation of the overloading joint torques encompassing double-support, was investigated in a human-robot

load sharing task. The overall procedure, which complements the off-line step introduced singularly in Subsection 3.2.4, is illustrated in Fig. 6.2. Two main parts can be distinguished: the off-line and the online phase. The off-line phase corresponds to the stage already addressed in Subsection 3.2.4 to estimate the human feet GRF and CoP combining the SESC method with a learning technique. In the online phase, the overloading torques induced on the main human joints while manipulating a heavy object in collaboration with a robot were first computed. Next, the robot end-effector trajectory was optimised to minimise such overloadings, by considering the human, the robot, and the task constraints. Being assisted by the robot, the subject could then change the body configuration to achieve a more ergonomic and comfortable condition. The experimental analysis conducted to evaluate the online performance of the synergistic model within the HRC framework will be addressed in detail in this Subsection.

Experimental Setup

The experimental setup is illustrated in Figure 6.3. The whole experimental procedure was carried out in accordance with the Declaration of Helsinki and the protocol was approved by the ethics committee Azienda Sanitaria Locale (ASL) Genovese N.3 (Protocol IIT_HRII_001). One healthy subject (age: 30 years; mass: 76.5 kg; and height: 1.78 m) was asked to wear the MVN Biomech suit and the OpenGo sensor insoles (see Section 3.1). The external object (width: 0.33 m; depth: 0.56 m; height: 0.23 m; mass: 8 kg) was grasped from one side by the human hands and from the other side by the Pisa/IIT Softhand [200] which was attached to a KUKA Lightweight robot (LWR). The points of interaction of the human with the object were assumed to be located at the end of the forearm links and a symmetric distribution ratio among them was considered. Accordingly, in Equation (4.4) (see Section 4.2) the values of η_j were set to 0.5 for both the left and right hand while the values of ζ_j were computed using (3.14) (see Section 3.2.4). For the purpose of the experiment, the subject had to achieve the load sharing task with the robot in a way that optimised the working conditions while considering the task constraints and prevent any excessive load on the human body joints. To this end, the optimisation process described in Section 6.1 was adopted. As already mentioned, the ergonomic index selected to be minimised was the overloading joint torque. On the other hand, the constraints considered in the procedure were the joint angles boundary condition (6.2), the postural stability condition (6.3) and the human-robot shared space condition (6.4). As a result of the optimisation, during the HRC task, the subject being assisted by the robot was induced to move the object and to modify his body configuration so as to reach more ergonomic loading conditions. In addition, to make the subject aware of several meaningful information and to provide him with further guidance to perform the task, the graphical interface presented in Section 5.1 was adopted. The level of the overloading estimated on the main joints and the current body configuration along with the optimal one were shown to the subject throughout the whole experiment, as depicted in the low part of Figure 6.3.

Results

Figure 6.4 illustrates the results of HRC experiment. The first row depicts three specific body configurations adopted by the subject while performing the task: the unoptimised (A), in motion (B) and optimised (C) posture, respectively. The overloading

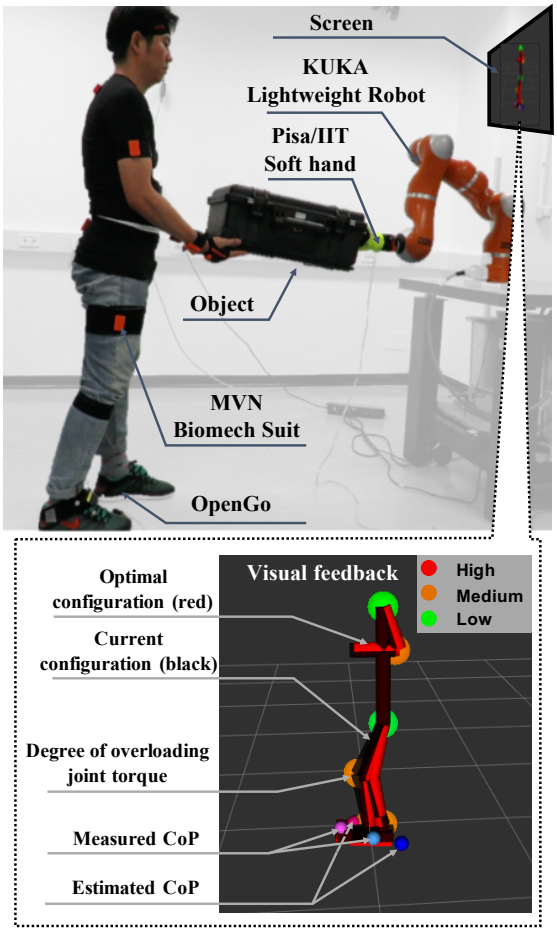

Figure 6.3: *Overview of the experimental setup. All the sensors and devices involved in the experiment are shown on the top. The visual feedback provided to the subject performing the HRC task is displayed on the bottom.*

joint torques estimated in the corresponding instants are represented as spheres superimposed on the human stick model and color-coded to denote their level (see Section 5.1). The first graph presents the trajectory that the robot end-effector followed to assist the subject during the task, both in time (left chart) and space (right chart). The second graph presents the numeric values of the estimated overloading torques $|\Delta\boldsymbol{\tau}|$ in the human main joints: left hip (LH), left knee (LK), left ankle (LA), right hip (RH), right knee (RK), right ankle (RA), elbow (E) and shoulder (S), respectively. The overloading joint torques in the left and right arm had similar values because the arms moved symmetrically to hold the external object, thus the results for the right arm only are provided. It can be noted that starting from the initial configuration (A) to the optimised one (C) $|\Delta\boldsymbol{\tau}|$ tend to significantly decrease in all the joints throughout the experiment. Specifically, the overall percentage of decrement was around 72.6% on average (56.1% in the arms, 92.2% in the left leg and 35.3% in the right leg).[3]. In addition, to provide a benchmark of the effective effort required to the subject during the task, the whole-body muscle activity was recorded with nine sEMG sensors. Specifically, anterior del-

[3]Overloading torque reduction percentage in the shoulder: 62.4%, elbow: 45.8%, left hip: 91.4%, left knee: 91.8%, left ankle: 93.4%, right hip: 40.5%, right knee: 7.8%, right ankle: 43.5%.

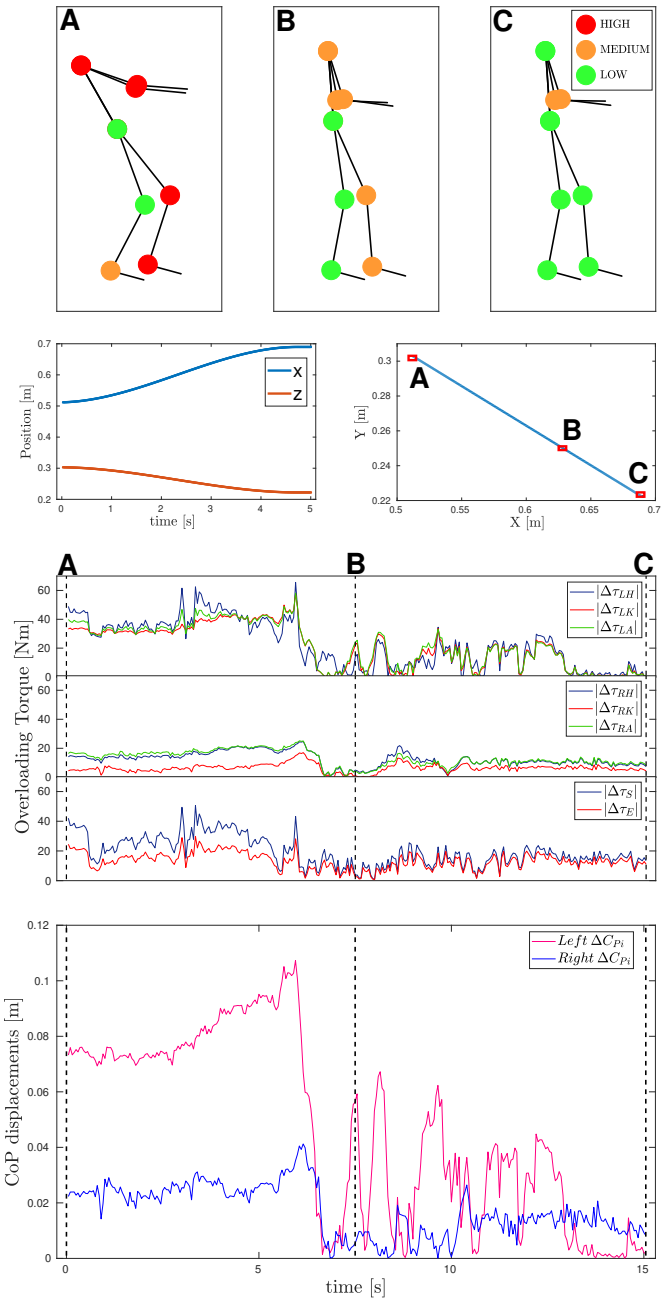

Figure 6.4: *Results of the human-robot load sharing task experiment. The sequence of the pictures on the top shows the progress of the experiment: un-optimised state (A), transition (B) and optimised state (C). The first plot shows the robot optimal trajectory both in space (left chart) and time (right chart). The second plot shows the calculated overloading joint torques. The third plot shows the displacements between the estimated and measured feet CoP for the right foot and for the left foot.*

toid (AD), biceps (BC), L5 paraspinals (L5), right and left vastus lateralis (R.VL and L.VL), right and left rectus femoris (R.RF and L.RF), and right and left tibialis anterior (R.TA and L.TA) were the selected muscles. The reduction rates of the EMG signals (filtered and normalised) were computed and resulted in 70.9% in the AD, 8.6% in the BC, 27.9% in L5, 62.3% on average for the right leg and 72.3% on average for the

left leg. Finally, the lower plot of Fig 5.5 shows the displacements between the feet CoP measured by the sensor insoles and the feet CoP estimated by the proposed synergistic method. It was worth noticing that passing from configuration (A) to (C) this displacement decreases both for the right foot and for the left foot.

Discussion

By observing the degree of the overloading joint torques represented by the color-coded markers in the first row of Figure 6.4, it can be noticed that, throughout the task, the external forces were redistributed among the joints so as to reach the human optimal configuration in phase (C). The fact that the elbow joint did not show the lowest level of joint overloading can be related to the condition, imposed by the task, of holding the heavy object. Correspondingly, as exhibited by the overloading joint torque values presented in the first plot, starting from the initial configuration (A) to the optimised one (C) $|\Delta\boldsymbol{\tau}|$ had a significant decrement in all joints, proving that the effect of the external load on human joints was reduced due to the robot reactive behaviour. The reduction rates demonstrated by the sEMG signals confirm that an effective reduction of the effort required to the subject was simultaneously achieved. Finally, the minimisation of the difference between $\mathbf{C}_P$ and $\hat{\mathbf{C}}_P$ provides further evidence of the method capability to make the human achieve more ergonomic configurations.

6.2.2 Using Fatigue Thresholds to Trigger the Robot Behaviour

A whole-body fatigue model has been presented in Section 4.3 to evaluate the cumulative effect of the overloading torque, induced on human body joints throughout time by light payloads. In [31], this fatigue model was originally proposed, and additionally integrated into the HRC framework addressed in this Chapter. In particular, the so-called overloading fatigue was adopted to set the timing for the optimisation procedure described in Section 6.1 and thus to trigger the collaborative robot assistance. By the time overloading fatigue exceeded a predefined threshold in a joint, the robot reacted and guided the subject towards a more ergonomic body configuration, to prevent further accumulation of fatigue.

The experimental analysis conducted to assess the integration of the overloading fatigue model into the HRC framework will be addressed in detail in this Subsection.[4]

Experimental setup

One female healthy subject (age: 27 years; mass: 57 kg; height: 171 cm) was recruited for the HRC experiment. The whole experimental procedure was carried out in accordance with the Declaration of Helsinki and the protocol was approved by the ethics committee Azienda Sanitaria Locale (ASL) Genovese N.3 (Protocol IIT_HRII_001). She was asked to wear the MVN Biomech suit (see Section 3.1.1), to hold a 1.5 kg spray gun with her dominant hand, and to paint a predefined area on a car bumper (the object which has to be painted for the purpose of the task). A KUKA LWR, provided with an impedance controller to ensure safety in HRC and equipped with a Pisa/IIT Softhand [200], was holding the car bumper. In Figure 6.5 the experimental setup is illustrated. Considering the area which needs to be painted - the yellow area on the car

[4] A video showing the whole procedure is available at `https://youtu.be/6Qw0Jz0EcdQ`.

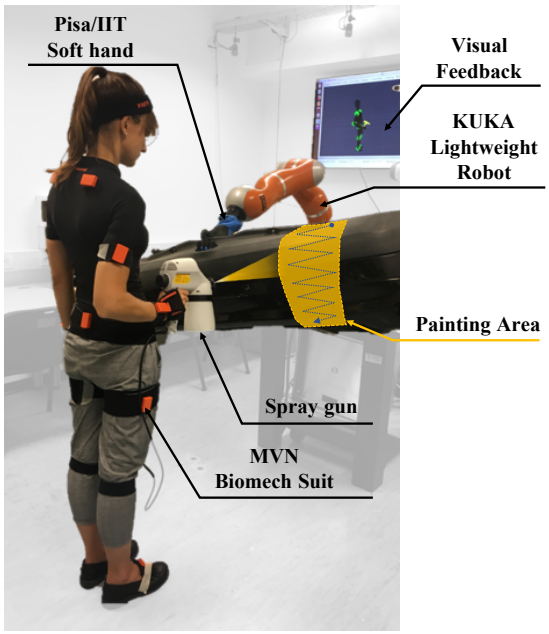

Figure 6.5: *Overview of the experimental setup. All the sensors and devices involved in the experiment are illustrated as well as the visual feedback provided to the subject during the experiment.*

bumper highlighted in the picture - the subject was expected to adopt a wide range of body postures to accomplish the task. Accordingly, different joints were supposed to accumulate fatigue during different stages. Consequently, for better results, the optimisation procedure had to occur multiple times throughout the experiment and to focus selectively case by case on the fatigued joint. Therefore, each time the overloading joint fatigue in a specific joint overcame a pre-defined threshold, the optimisation procedure described in Section 6.1 was triggered. As already mentioned, the ergonomic index selected to be minimised was the overloading joint fatigue. On the other hand, the constraints considered in the process were the joint angles boundary condition (6.2), the postural stability condition (6.3) and the human-robot shared space condition (6.4). As a result of the optimisation, the subject was induced to modify her body configuration by following the robot guidance so as to reach a more ergonomic loading condition. As a support tool to the robot assistance, the subject was provided with the visual feedback described in Section 5.1, showing the current body configuration and the current level of the overloading fatigue on the main joints.

Results

The results of the experimental analysis to evaluate overloading fatigue mitigation through HRC are shown in Figure 6.6. Figure 6.6a illustrates the four key moments of the experiment (i.e. stage 1, 2, 3, and 4). Some color-coded spheres are placed on the main joints of the subject to indicate the level of the overloading fatigue at that instant: high (red), medium (orange), and low (green) level (see Section 5.1). The trends of the normalised overloading fatigue in the main joints are presented in Figure 6.6b. Initially, the subject began to process a point on the top of the car bumper by assuming a body configuration which made the shoulder joint accumulate excessive fatigue, as shown in

the fourth line of the graph in Figure 6.6b. As soon as overloading fatigue overcame a threshold (stage 1), which is set to $1/2$ of the $\Delta\boldsymbol{\tau}_i^{max}$, the optimisation procedure was triggered and the subject was guided by the collaborative robot toward a more ergonomic body configuration, which led to a lower overloading torque in the shoulder and promoted the recovery phase (stage 2). In this case, the optimisation procedure was more focused on the upper body and resulted in a decrement of the overloading fatigue in the shoulder. In Figure 6.6d, the trajectory of the collaborative robot end-effector is shown: to make the subject reached the optimal body configuration, the car bumper was brought at a lower height at stage 2.

Subsequently, the subject started processing a point on the bottom of the car bumper by assuming a body configuration which, this time, made the lower body accumulate fatigue (stage 3), mainly in the hip joint, as shown in the first line of the graph in Figure 6.6b. Similarly, as soon as the overloading fatigue overcame the threshold, the optimisation procedure was triggered and the subject was guided by the collaborative robot toward a body configuration which led to a minor overloading torque in the lower body joints and initiated again the recovery mode (stage 4). In this case, the optimisation procedure was more concentrated in the lower body and made the overloading fatigue decrease in the hips, knees, and ankles. To this aim, the collaborative robot brought the car bumper at a higher height at stage 4 (see Figure 6.6d). Figure 6.6c illustrates the trends of the normalised overloading torque in the main joints.

Discussion

It is worth noticing that the values of the overloading torque, illustrated in Figure 6.6c, remained moderate (around the 50% of their maximum value) in all the joints throughout the entire duration of the experiment. In [129], where the HRC framework was originally proposed, the optimisation procedure was performed when the overloading torque reached a value close to the maximum one since heavy tools which generated high overloadings were considered. In this experimental analysis, a lightweight tool is considered and the overloading torques it induces on the joints are not so high. Hence, the optimisation procedure would not be initiated within the HRC framework original setting. In fact, as previously mentioned, the risk of joint injuries while supporting light payload is not related to the instantaneous loading they induce, but rather on their prolonged and repeated use over time. This is the reason why we developed an overloading fatigue model which accounts for the cumulative effect of the overloading torque throughout time and thus represents a good criterion to set the timing of the optimisation procedure when performing tasks with lightweight tool.

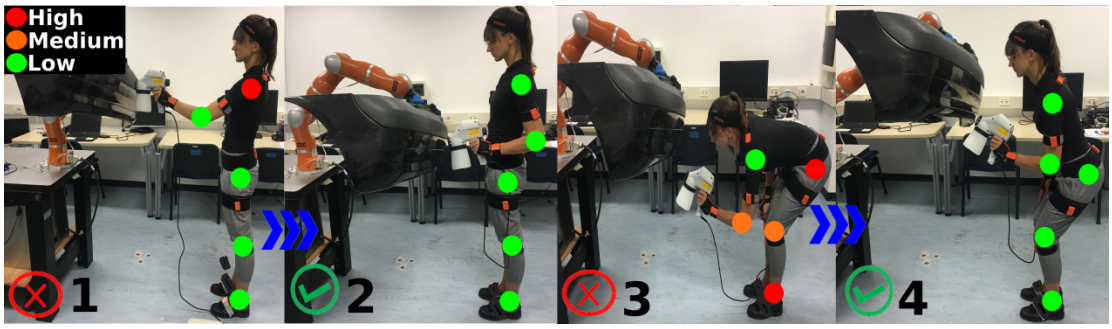

(a)

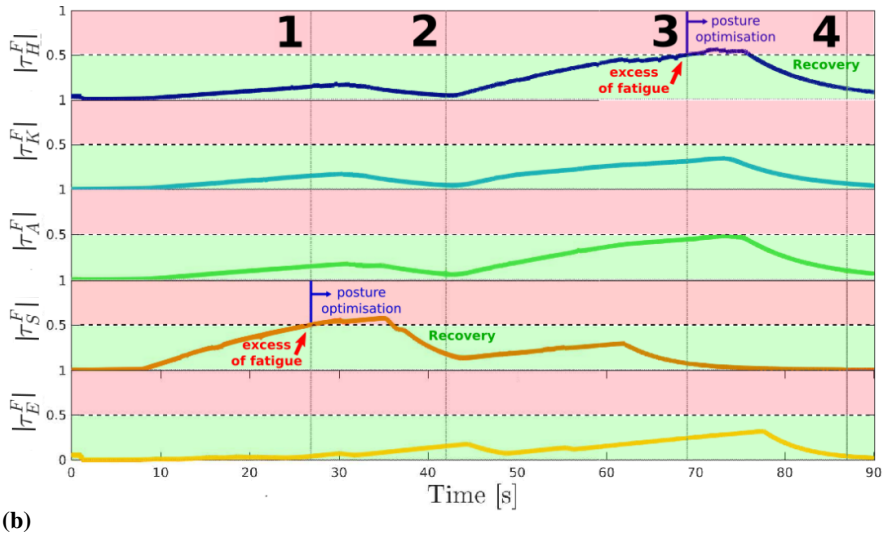

(b)

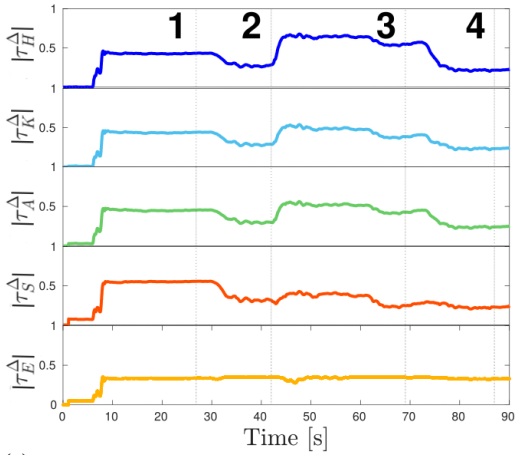

(c)

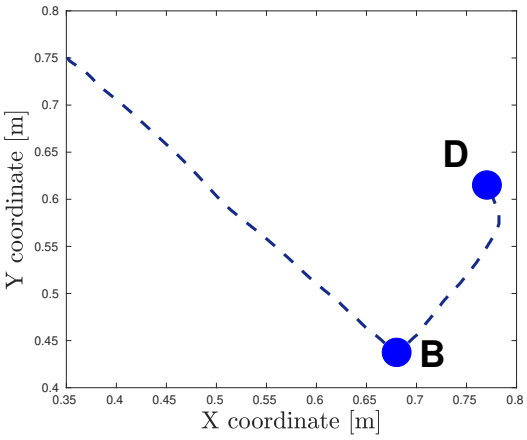

(d)

Figure 6.6: *Overloading fatigue mitigation through HRC: (a) Key moments of the HRC experiment. (b) overloading fatigue and (c) overloading torque in the hip(H), knee(K), ankle(A), shoulder(S) and elbow(E) joints for one subject performing the HRC experiment. (d) collaborative robot trajectory: the robot assistance promoted the recovery phase after fatigue in B and D.*

6.2.3 Multi-Human Mobile-Robot Collaborative Teams

The HRC framework tackled in this Chapter, has demonstrated its capability to mitigate the risk associated with joint mechanical overloading taking advantage of the assistance of a collaborative robot, which guides the human toward more ergonomic postures. Nevertheless, the proposed approach, as implemented so far, severely lacked flexibility due to the fixed base of the robot. As a result, its applicability in real industrial scenarios, including multiple workers that operate in a broad area, may be rather limited. To increase the potential of collaborative robotic technologies in the workplace, while meeting the requirements of frequently varying production processes, the concept of mobility must be integrated into the robot control framework (see Fig.6.7).

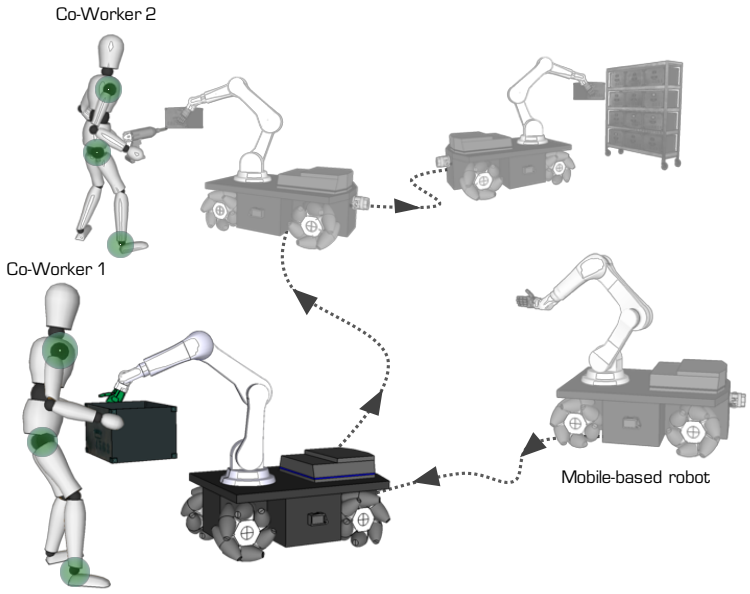

Figure 6.7: *The proposed multi-human mobile-robot control framework aims to improve workers' ergonomics by integrating an optimisation procedure into a mobile collaborative robot assistant.*

Accordingly, the first focus of [197] was to introduce a new MObile Collaborative robotic Assistant (MOCA), composed of a lightweight manipulator arm, an underactuated hand, and a mobile platform driven by four omni-directional wheels, which enables agile mobility in the work space and is provided with advanced interaction and manipulation features. Secondly, an ergonomics module to anticipate and mitigate the human risk factors by means of the optimisation procedure explained in Section 6.1 was integrated into the system, to ensure workers' well-being and the improvement of working conditions. The resulting control framework was able to ensure robot adaptation to multiple human workers' kinodynamic states and variable tasks while addressing their ergonomic requirements. An experimental analysis was conducted to evaluate the proposed strategy, simulating a simple manufacturing line that involves two subjects and the MOCA, and it will be presented in this Subsection.[5]

[5] A video showing the whole procedure is available at `https://youtu.be/Ug1Bpwo_eeo`.

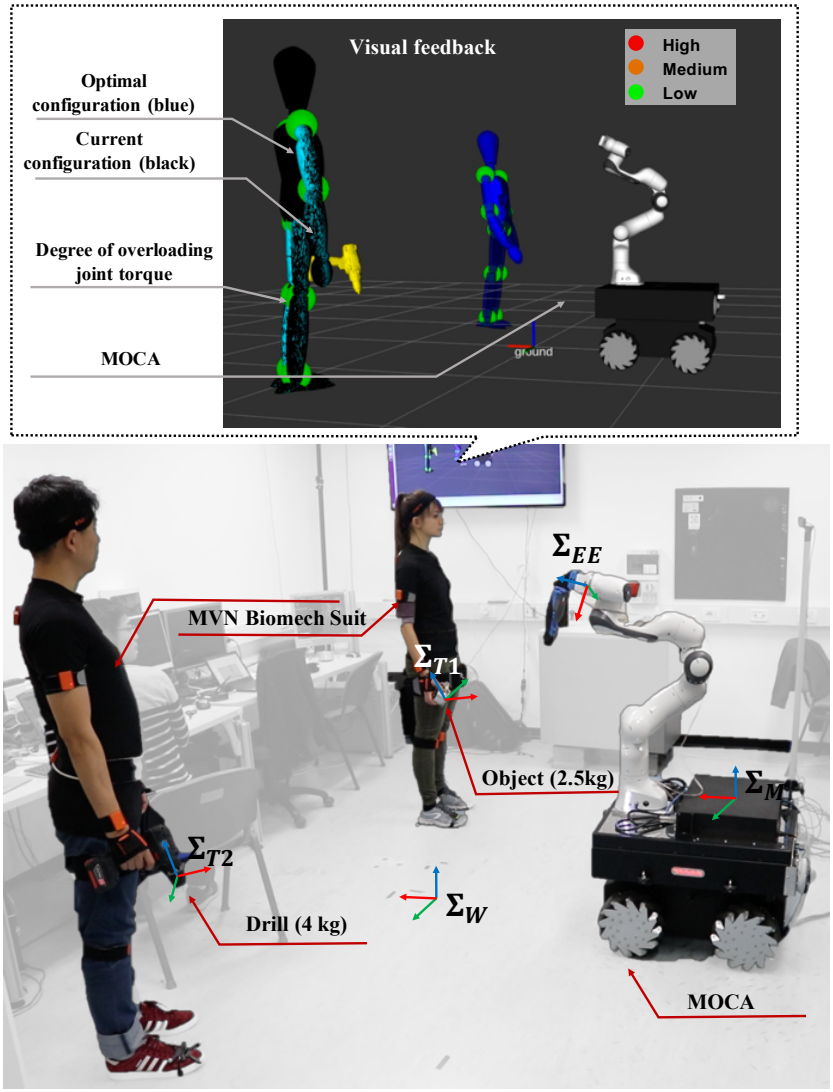

Figure 6.8: *Overview of the experimental setup: two subjects and MOCA were involved in the experiment (bottom). The visual feedback provided to the subjects during the experiment (top).*

Experimental setup

Two human healthy subjects (labeled as 1 [female] and 2 [male]) were recruited for the experimental session. Two different tasks were defined for them: subject 1 had to perform a handover task, passing an object to MOCA, while subject 2 had to perform a drilling task on the same object that was held by MOCA. The experimental setup of the experiment is illustrated in Fig. 6.8. The whole experimental procedure was carried out in accordance with the Declaration of Helsinki and the protocol was approved by the ethics committee Azienda Sanitaria Locale (ASL) Genovese N.3 (Protocol IIT_HRII_001). The actors involved were MOCA and the two human subjects. Each subject was asked to wear the MVN Biomech suit presented in Section 3.1.1. A global frame Σ_W was defined on the floor of the experimental area to localise in the shared work space the frame of each actor involved. Accordingly, both MOCA and the MVN Biomech suits worn by the human subjects were calibrated so as to set Σ_W as

their global frame. The local frames of subject 1, subject 2 and MOCA, were respectively defined as Σ_{T1}, Σ_{T2} and Σ_M. The experimental procedure included two stages: the handover task performed by subject 1 and the drilling task performed by subject 2. During the first stage, subject 1 held an object and MOCA approached her, assuming a configuration that drove her to adopt the optimal body posture for handing over the object to MOCA. Next, during the second stage, MOCA approached subject 2 offering him the object which he had to drill, in a way that he could assume the optimal body configuration to perform the task.

Both the human subjects in their respective stages had to accomplish their own task in the best working conditions considering the task constraints. Hence, for each subject, the optimal body configuration to perform the corresponding activity was estimated through the procedure described in Section 6.1. Since the conditions and requirements of the two tasks defined were different, different constraints were considered in the optimisation process. For subject 1, the optimisation constraints concerned the support polygon 6.3 and the shared work space 6.4 between the human subject and MOCA. For subject 2, the optimisation constraints concerned the human support polygon 6.3 and the human subject's manipulability 6.5.

Results

The results of the multi-human MOCA team experiment are illustrated in Figure 6.9. The optimised postures of each subject and the variations of MOCA configurations, provided by the visual feedback interface, are displayed in the first row of Figure 6.9a. The bottom plot illustrates the positions of the two subjects in the work space while performing their task and highlight the trajectories (position and orientation) that MOCA followed to guide them toward the optimal working conditions.

Figure 6.9b represents the whole sequence of tasks execution considering both the robot and the subjects' points of view. The first two plots illustrate the external interaction forces and positions, which were measured at MOCA end-effector w.r.t Σ_W. The variations of the overloading torques in the human main joints are depicted in the bottom graph of Figure 6.9b, for each subject during the execution of their respective task. For subject 2, also the value of manipulability throughout the experiment is provided. In the "homing phase", MOCA waited for the task of subject 1 to start. Then, as soon as optimisation procedure was performed, the locomotion phase was triggered and the robot was controlled to move towards the first optimised configuration so as to pick up the object from subject 1. When this task was finished, MOCA was notified about the task accomplishment: its end-effector was pushed by the subject with a force overcoming a pre-defined threshold ($F_y \geq 20N$). In this respect, it should be noted that the increment exhibited by the overloading joint torques at the end of the task was due to the human act of pushing the robot. Thereafter, the robotic arm (but not the mobile platform) came back to the homing configuration and MOCA waited for the next task to initiate. Similarly as before, when the optimisation procedure was performed, the locomotion phase started and the robot was controlled to move towards the second optimised configuration for offering the object to subject 2, which had then to operate on it. During the drilling task, the manipulability of the subjects maintained a high value, around 83.45%, meaning that the manipulability ellipsoid became nearly isotropic (see the bottom of the right graph in Figure 6.9b).

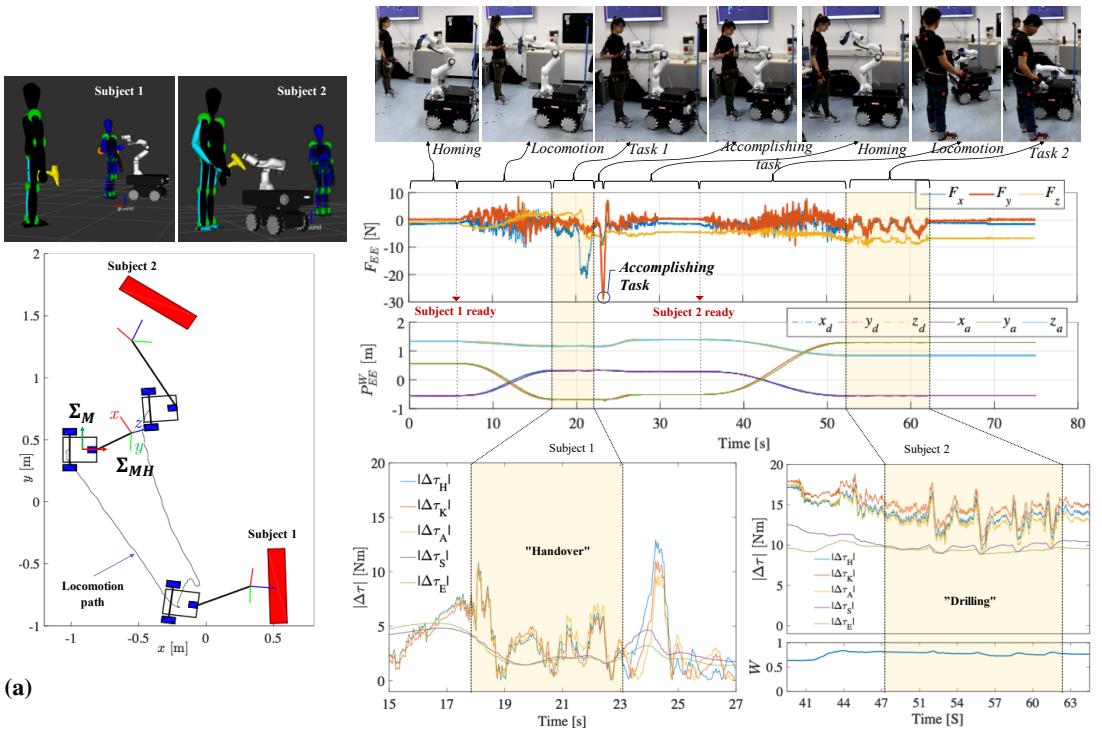

Figure 6.9: *Experimental results of the the multi-human mobile robot collaboration framework in the execution of simple manufacturing tasks. (a) The trajectory of the mobile platform during the execution of two tasks by the subjects (bottom) and the visual feedback provided to the subjects (top). (b) The interaction forces and the position of MOCA end-effector are illustrated in the first two rows, respectively, and the overloading joint torques and manipulability (only subject 2) estimated by the ergonomics module for each subject are illustrated in the bottom.*

Discussion

The proposed HRC framework was able to mitigate the physical load for multiple humans performing different tasks in a broad working area, introducing a considerable improvement in the applicability of the robotics solutions within the industrial environment. The salient feature of the strategy is the mobility of the collaborative robot which, combined with the capability of the ergonomics module to address workers' health, can meet the demands of the numerous unstructured and unergonomic workplaces which dot the current manufacturing scenario.

CHAPTER 7

Conclusions

The thesis herein presented introduced a novel online human ergonomics monitoring system, which adopted an exhaustive set of indexes to account for multiple ergonomic risk factors (e.g. unfavourable postures, mechanical overloading of the body tissues, repetitive movements, etc.) and thus enabled to assess workers' physical exposure to the major determinants of WMSDs. The proposed ergonomic indexes were combined with intuitive feedback interfaces (i.e. visual or vibrotactile) to enhance workers' awareness about their kino-dynamic states and the associated level of hazard. Therewith, they were integrated within a HRC framework to guide and assist the humans toward more convenient body configurations and loading conditions to execute their working activities. Such an improved attitude was achieved by taking advantage of an online optimisation procedure that minimised the ergonomic indexes according to the task and environment constraints thus mitigating the corresponding risk factor.

To adapt to workers' physical characteristics and individual demands, the framework proposed in this thesis was grounded on a subject-specific model of the human body. In fact, the majority of the dynamics-related ergonomic indexes included in the monitoring system relied on the SESC technique, which enabled to obtain the subject-specific BSIPs of the human. Such parameters could then be adopted to achieve the estimation of the whole-body CoP. With the aim to extend the human model adopted in this thesis and broaden its potential applications in real industrial scenarios, two approaches were proposed.

First, a learning technique to estimate the feet CoP and GRFs on the basis of the whole-body CoP and total GRF was developed. As a matter of fact, the SESC method allowed to represent the human biomechanical system as a planar serial chain that includes only one GRF. By exploiting the ability of artificial neural networks to implicitly detect complex nonlinear relationships between variables, the upgrade of this reduced model

to a bipedal one was accomplished. As demonstrated by the corresponding experimental validation, the proposed learning approach thereby allowed the tracking of human states in a wider work space.

Next, a novel method to approximately detect the contact point when an external load is exerted on the human body was introduced. The proposed approach relied on a torque equilibrium condition on the human sagittal plane integrated with a statistical analysis approach to increase the accuracy of the estimation. Its capability to provide a rather accurate and quick online estimation of the contact point was demonstrated both in a simulation study and in an experimental analysis conducted on human subjects. Consequently, this method permitted to avoid a-priori assumptions when tracking the human dynamic states, further tailoring the human model adopted in this thesis to the varying interaction conditions featuring workers' activities.

In view of achieving an extensive and thorough analysis of the whole range of risk factors associated with occupational activities, a human ergonomics monitoring system was outlined in this thesis. Such a tool consisted in a comprehensive set of indexes that encompassed not only the kinematics of workers' actions but put also particular attention to dynamic aspects (i.e. forces or torques acting on and inside the body), which may assume a significant role in contributing to WMSDs. For all the indexes proposed, a definition and justification were provided, specifying the ergonomic risk factor that each of them sought to address.

To validate the proposed ergonomics monitoring system, an experimental analysis was conducted on twelve subjects considering three different tasks, which represented typical occupational activities in manufacturing industries and, additionally, were associated to different potential risk factors to the development of WMSDs. Among the kinematics-related indexes, the joint displacement was identified as the most beneficial tool in assessing physical exposure due to its capability to detect unfavourable body postures. As regards dynamics-related variables, a specific index was found that better explained the physical load required in each considered task, evaluated by the outcome of the sEMG analysis. Specifically, to account for the mechanical overburden of the body structures during the lifting/lowering of heavy objects, the overloading joint torque index demonstrated to be the more promising novel index. Considering a task in which all the components of the interaction forces at the hand/tool interface are relevant, like the drilling task, the joint compressive forces index proved to be more predictive of the risk associated. Finally, to account for fatigue accumulation while executing repetitive and monotonous prolonged activities like painting, the overloading joint fatigue index gave proof to be more informative. It was also noted that the potential of the remaining indexes must be investigated more deeply considering more dynamically varying activities.

In addition, a comparison was made with the ergonomic risk scores resulting from the EAWS, which are a well-recognised tool to evaluate workers' physical exposure. It is noteworthy that EAWS are conceived for industrial environments and thus several assumptions were made to contextualise the experimental analysis in a real workplace, however, some advantages of the proposed framework compared to them were detected. In fact, EAWS happened to be subject-specific only to a certain extent and could be conducted only in an off-line by trained experts. Furthermore, they seemed to lack the full assessment of the dynamics aspects of the working activities. For these reasons, the

integration of EAWS with the proposed human ergonomics monitoring system would allow a more comprehensive and thorough analysis of the whole range of risk factors associated with occupational tasks, taking equally into account the relative kinematics and dynamics aspects and addressing workers' specific requirements.

With the aim to improve humans' risk-awareness, providing them with information about the degree of hazard associated with their activities, two feedback solutions were proposed in this thesis. The related interfaces were able to communicate the magnitude of an ergonomic index (selected among the ones constituting the proposed monitoring system) for which three levels were defined -high, medium, low- to categorise the extent of the corresponding risk factor addressed.

Firstly, a graphical interface was presented which took advantage of the ROS 3D visualizer RViz. By means of a dedicated screen, it was able to illustrate to the user both kinematic and dynamic meaningful information. The first was represented through a virtual simplified model of the human body while the second was expressed in terms of a dynamics-related ergonomic index. The selected index was illustrated with spheres superimposed on the human body model, located in the main joints, and its level was color-coded to denote a high (red), medium (orange) or low (green) risk. This traffic light scheme enabled a straightforward interpretation and ease of use of the interface, which proved to be an intuitive mean to alert workers about their physical exposure. In fact, it was adopted as a part of several experimental analysis within the context of this thesis and successfully employed to convey the level of the overloading joint torque and fatigue indexes during their respective investigations. Nevertheless, the proposed graphical interface had the severe disadvantage of requiring the users to focus on a specific spot, potentially interfering with the smooth execution of their activities.

Such a limitation was overcome by the second feedback strategy proposed: a vibrotactile device called ErgoTac that acted as a sensory substitution modality. ErgoTac offered the huge benefit of being wearable and wireless thus it could assist the users within a broad area allowing them to act freely in the work space. The level of the selected ergonomic index in this case (the overloading joint torque) was reported by means of a different vibration intensity of the device. An experimental study on ten human subjects was performed to validate the approach. While performing a lifting task with a heavy object, the subjects were required to reconfigure their body posture by following the vibrotactile feedback guidance so as to reduce the effort on the joints. The results, supported by statistical analysis, demonstrated the potential of ErgoTac in assisting the workers in their occupational activities.

Ultimately, a HRC framework was proposed as a solution to address workers' ergonomic demands in today's SMEs, which are featured by frequently varying work flows and unstructured work stations. Taking into account a specific ergonomic index, wherever its level of risk was medium/high, an optimisation procedure was employed to estimate a more ergonomic human body configuration by minimising the selected index according to certain constraints. Then, the human subjects could be facilitated to achieve such an optimal condition by following the guidance of a collaborative robot thus mitigating the effect of the risk factor associated. The main objective of the proposed HRC framework in this thesis was to introduce and evaluate its feasibility as well as flexibility, demonstrating robot's ergonomic collaboration with, and work in close proximity to, human co-workers. Hence, diverse applications were presented, which

can be tackled not only considering a fixed collaborative robot with a single co-worker but also a mobile robotic platform with multi co-workers.

First, the proposed synergistic model to estimate the feet CoP and GRF was deployed to enable the online estimation of the overloading joint torque index for human bipedal models and investigated in a human-robot load sharing task. An experimental analysis was conducted on one subject as a proof of concept, supported by an sEMG analysis. The corresponding findings provided evidence of the framework capability to reduce effort on human joints, during double-support, due to the robot reactive behaviour. Next, the proposed overloading fatigue model was exploited in the HRC framework as a trigger mechanism for the optimisation procedure. By the time fatigue exceeded a pre-defined threshold in any joint, the optimal body configuration was estimated by minimising the overloading joint torque index and the human was guided by the collaborative robot assistance to avoid the accumulation of further fatigue. Also in this case, the experimental validation of the method proved the capability of the HRC framework to mitigate the risk associated with the mechanical overloading of the human joints. However, repetitive and prolonged tasks with light-weight tools were addressed in this study showing additionally the HRC system adaptability to different occupational activities along with the flexibility of the optimisation procedure timing. Last, the case study of a multi-human and mobile-robot collaborative team was investigated. The HRC framework, as implemented so far, severely lacked flexibility due to the fixed base of the robot. As a result, its applicability in real industrial scenarios, including multiple workers that operate in a broad area, was rather limited. Hence, to increase the potential of collaborative robotic technologies in the workplace, the robotic platform MOCA was introduced, featured by agile mobility and advanced interaction and manipulation features. The optimisation procedure was integrated into its control system, enabling MOCA to mitigate the risk of excessive effort in the human joints in terms of overloading torque, for multiple workers performing different tasks. An experimental analysis was conducted simulating a simple manufacturing line where two human subjects performed a handover and drilling task, respectively, collaborating with MOCA. The effectiveness of the task-dependent optimisation was validated by means of the sEMG measurements, torque variations, and considerations on the manipulability aspect. The proposed strategy then demonstrated its key strength in the applicability to the real industrial environments, which demand for high flexibility in the few-of-a-kind production processes.

One of the main limitations of the proposed framework to assess and improve human ergonomics lies in the sensor technologies employed for the tracking of human kino-dynamic states. All the devices adopted in this thesis are rather expensive and sophisticated. Hence, a considerable initial investment to purchase the equipment is required as well as the resources necessary to cover the costs of maintenance, which may not be affordable by many SMEs. Moreover, highly trained and skilled technical staff is needed to ensure their effective operation. In addition, although the sensor systems adopted (i.e. Xsens suit, OpenGo sensor insoles) are wearable and lightweight, the attachment of devices directly to the subjects may still result in discomfort and possibly lead to changes or even limitation in workers' behaviour, especially for a prolonged time. Accordingly, in future works more affordable and convenient systems will be investigated as an alternative, as for instance low-cost vision system (i.e. Kinect, Robo-

Ception, RealSense) combined with machine learning algorithms, which are becoming more and more widespread as a motion-capture system. As mentioned in Section 3.1.1, such technologies lack accuracy and suffer from visibility limitations but the continuous technological innovations in this field seek to tackle these issues.

The proposed human ergonomics monitoring system showed promising capabilities to address different risk factors to the development of WMSDs while assessing multiple working activities. However, there are many possibilities for further developments. First, as already mentioned, some of the ergonomic indexes introduced should be deeper investigated considering more dynamically varying tasks and more articulated experimental conditions. Next, novel indexes could be added, which address other risk factors across the extensive list of possible determinants for musculoskeletal conditions. Last, feasible strategies to combine the proposed monitoring system with well-recognised tools to assess workers' ergonomics (e.g. EAWS) should be conceived, with the aim to enable an exhaustive and thorough analysis of the whole range of risk factors associated with work, considering all the essential related aspects.

Concerning the feedback interfaces, future studies will focus on the improvement of the proposed solutions. The screen-based visual feedback system will be converted into a fully-fledged GUI. The latter will allow the user to select a specific ergonomic index to be displayed, to adapt the feedback features depending on the task and its relative conditions and to store and make available meaningful information about the users' parameters, but also about the results of ergonomics analysis. On the other hand, the main shortcoming of the ErgoTac device is that no instructions regarding the correct direction of motion can be provided to the users. A possible solution would be adopting a higher number of vibrotactile devices (e.g., in antagonistic configurations) to orient movements toward an optimal path. However, this may excessively augment the cognitive load of the users. In this regard, an interesting development of this interface would include the investigation of the optimal number of devices and the influence of the person's own perception in recognising the risk level.

Finally, considerable scope for improvement is envisaged for the HRC framework. So far the optimisation procedure could be adopted with one ergonomic index at a time. Thus, a major and beneficial improvement in this respect would be the development of a multi-objective optimisation technique, which allows the simultaneous minimisation of multiple ergonomic indexes. In such a way, multiple ergonomic risk factors would be addressed at once and higher flexibility and re-configurabilty would be given to the robot control system. The latter would then be able to automatically handle different tasks without the need to be reprogrammed.
Additional novel constraints could be considered for the revised version of the optimisation procedure, taking into account different aspects in the execution of the task or in the workplace environment conditions.

On the other hand, the intelligence of robots, which allows understanding the environmental conditions and co-workers' intentions by using perception systems, will be employed to further improve the versatility of the HRC framework in real industrial settings. Some preliminary works following this aspect were attempted. In [37], the framework showed that a mobile-based collaborative robot was able to navigate towards human partners for serving the ergonomic collaboration behaviour. Meanwhile,

it was also able to distinguish obstacles such as the coexisting humans or fixed objects by using navigation strategies in the robot control system.[1] In [35], in the ergonomic HRC framework, a vision system was included that enabled to track the human intention: which tool/part is intended to be manipulated, if the worker is left or right-handed, or moves within the work space. Consequently, the cobot was able to keep addressing workers' ergonomic demands in a flexible way.

The final objective in this respect is to transform the HRC framework in a modular system whose components (i.e. ergonomics module, vision module, navigation module, manipulation module. etc.) can be rearranged and combined in multiple ways to ensure the best results in the improvement of humans' health and working conditions.

[1] A video showing the whole procedure is available at `https://youtu.be/vorn4GwCT2g`.

CHAPTER 8

Ringraziamenti

A conclusione di questo elaborato, vorrei dedicare qualche riga a tutti coloro che mi sono stati vicini in questo percorso di crescita personale e professionale.

In primo luogo, un sentito grazie va ai miei relatori, il Dr. Arash Ajoudani e la Prof.ssa Elena De Momi, per il costante sostegno e le preziose indicazioni che mi hanno fornito durante il dottorato. Un grazie particolare al Dr. Wansoo Kim, per la sua disponibilità e precisione nel darmi sempre consiglio.

Ringrazio immensamente i miei genitori e i miei fratelli, per avermi sempre incoraggiato nei miei progetti e per essere il mio punto di riferimento.

Un infinito grazie alle mie amiche, che mi sono sempre state vicine, sia per ascoltare i miei dubbi che per festeggiare i traguardi raggiunti. Un grazie particolare a Meri, la mia compagna di studi e avventure.

Ringrazio di cuore il mio ragazzo Francesco, per i consigli accorti e il suo immancabile supporto.

Ringrazio infine i miei colleghi dell' HRII Lab di IIT, per tutto l'appoggio e la collaborazione ma anche per i momenti di spensieratezza passati insieme. Un grazie particolare a Pietro ed Edoardo, questi anni non sarebbero stati gli stessi senza di voi.

Related Scientific Publications

This thesis has led to the following scientific publications:

JOURNALS:

Marta Lorenzini, Wansoo Kim, Elena De Momi, and Arash Ajoudani. *A synergistic approach to the real-time estimation of the feet ground reaction forces and centers of pressure in humans with application to human-robot collaboration.* IEEE Robotics and Automation Letters, 3(4): 3654-3661, 2018. (Chapter 3 and 6)

Wansoo Kim, **Marta Lorenzini**, Kağan Kapıcıoğlu, and Arash Ajoudani. *Ergotac: A tactile feedback interface for improving human ergonomics in workplaces.* IEEE Robotics and Automation Letters, 3(4): 4179-4186, 2018. (Chapter 5)

Wansoo Kim, **Marta Lorenzini**, Pietro Balatti, Phuong D.H. Nguyen, Ugo Pattacini, Vadim Tikhanoff, Luka Peternel, Claudio Fantacci, Lorenzo Natale, Giorgio Metta, and Arash Ajoudani. *Adaptable workstations for human-robot collaboration: A reconfigurable framework for improving worker ergonomics and productivity* IEEE Robotics and Automation Magazine, 26(3):14-26, 2019.

Marta Lorenzini, Wansoo Kim, Elena De Momi, and Arash Ajoudani. *An online method to detect and locate an external load on the human body with applications in ergonomics assessment.* Sensors, 20(16): 4471, 2020. (Chapter 3 and 4)

CONFERENCES:

Marta Lorenzini, Wansoo Kim, Elena De Momi, and Arash Ajoudani. *A learning-based approach to the real-time estimation of the feet ground reaction forces and centres of pressure in humans.* Sixth National Congress of Bioengineering, 2018.

Marta Lorenzini, Wansoo Kim, Elena De Momi, and Arash Ajoudani. *A new overloading fatigue model for ergonomic risk assessment with application to human-robot*

collaboration. IEEE International Conference on Robotics and Automation, pages 1962-1968, 2019. (Chapter 4 and 6)

Marta Lorenzini, Wansoo Kim, Elena De Momi, and Arash Ajoudani. *A real-time graphic interface for the monitoring of the human joint overloadings with application to assistive exoskeletons.* International Symposium on Wearable Robotics, pages 281-285. Springer, 2018. (Chapter 5)

Wansoo Kim, **Marta Lorenzini**, Balatti Pietro, Wu Yuqiang, and Arash Ajoudani. *Towards ergonomic control of collaborative effort in multi-human mobile-robot teams.* IEEE/RSJ International Conference on Intelligent Robots and Systems, pages 3005-3011, 2019. (Chapter 6)

Marta Lorenzini, Fusaro Fabio, Balatti Pietro, Elena De Momi, Mastrogiovanni Fulvio, Kim Wansoo, and Arash Ajoudani. *Toward a synergistic framework for human-robot coexistence and collaboration (hrc2).* Institute for Robotics and Intelligent Machines Conference, pages N-A, 2019.

Bibliography

[1] EU-OSHA European Agency for Safety and Health at Work. Introduction to work-related musculoskeletal disorders. https://osha.europa.eu/sites/default/files/publications/documents/en/publications/factsheets/71/Factsheet_71_-_Introduction_to_work-related_musculoskeletal_disorders.pdf, 2007. Available on line.

[2] World Health Organization. Icd-11: International classification of diseases 11th revision. https://icd.who.int/en, 2019. Available on line.

[3] L Punnett and DH Wegman. Work-related musculoskeletal disorders: the epidemiologic evidence and the debate. *Journal of electromyography and kinesiology*, 14(1):13–23, 2004.

[4] B Vellas, D Scrase, GA Rosenberg, S Andrieu, I Araujo de Carvalho, and LT Middleton. *WHO Guidelines on Community-Level Interventions to Manage Declines in Intrinsic Capacity: The Road to Prevention Cognitive Decline in Older Age*. Springer, 2018.

[5] SL James, D Abate, KH Abate, SM Abay, C Abbafati, N Abbasi, H Abbastabar, F Abd-Allah, J Abdela, A Abdelalim, et al. Global, regional, and national incidence, prevalence, and years lived with disability for 354 diseases and injuries for 195 countries and territories, 1990–2017: a systematic analysis for the global burden of disease study 2017. *The Lancet*, 392(10159):1789–1858, 2018.

[6] N Lezin and S Watkins-Castillo. The impact of musculoskeletal disorders on americans opportunities for action, executive summary of the burden of musculoskeletal diseases in the united states: prevalence, societal and economic cost. *Bone and Joint Initiative*, 2016.

[7] A Parent-Thirion. Fourth european working conditions survey. http://www.eurofound.europa.eu/pubdocs/2006/98/en/2/ef0698en.pdf, 2007. Available on line - Office for official Publications of the European Communities.

[8] E Occhipinti, D Colombini, D Alhaique, E Badellino, A Baratti, M Calamita, A. Goggiamani, D. Magosso, B. Manfredi, E. Mattace Raso, G. Ombuen, U. Osnato, A. Ossicini, and A. Papale. *I disordini muscuoloscheletrici lavorativi: la causa, l'insorgenza, la prevenzione,la tutela assicurativa*. INAIL, 2012.

[9] BR da Costa and ER Vieira. Risk factors for work-related musculoskeletal disorders: a systematic review of recent longitudinal studies. *American journal of industrial medicine*, 53(3):285–323, 2010.

[10] IL Nunes and PM Bush. Work-related musculoskeletal disorders assessment and prevention. *Ergonomics - A Systems Approach*, 2012.

[11] P McCauley-Bush. *Ergonomics: foundational principles, applications, and technologies*. CRC Press, 2011.

[12] EU-OSHA European Agency for Safety and Health at Work. Work-related musculoskeletal disorders: Back to work. http://osha.europa.eu/en/publications/reports/7807300, 2007. Available on line.

[13] S Bevan, T Quadrello, R McGee, M Mahdon, A Vavrovsky, and L Barham. Fit for work? musculoskeletal disorders in the european workforce. the work foundation. https://pdfs.semanticscholar.org/321b/5778628aee547fbf44e9be9329027155a976.pdf, 2009. Available on line.

[14] Agency for Healthcare Research, U.S. Department of Health Quality, and Human Services. Medical expenditures panel survey (meps). `www.meps.ahrq.gov/mepsweb/`, 1996-2011. Available on line.

[15] R McGee, S Bevan, and T Quadrello. Fit for work? musculoskeletal disorders and the canadian labour market (report 2). `https://www.cgib.ca/linkedpages/CCDPM_report2_jul2011.pdf`, 2011. Available on line.

[16] E Schneider, S Copsey, and X Irastorza. *OSH [Occupational safety and health] in figures: work-related musculoskeletal disorders in the EU-facts and figures*. Office for Official Publications of the European Communities, 2010.

[17] GC David. Ergonomic methods for assessing exposure to risk factors for work-related musculoskeletal disorders. *Occupational medicine*, 55(3):190–199, 2005.

[18] N Moray. Culture, politics and ergonomics. *Ergonomics*, 43(7):858–868, 2000.

[19] G Li and P Buckle. Current techniques for assessing physical exposure to work-related musculoskeletal risks, with emphasis on posture-based methods. *Ergonomics*, 42(5):674–695, 1999.

[20] MG Mehrabi, AG Ulsoy, and Y Koren. Reconfigurable manufacturing systems and their enabling technologies. *International Journal of Manufacturing Technology and Management*, 1(1):114–131, 2000.

[21] RH Westgaard. Work-related musculoskeletal complaints: some ergonomics challenges upon the start of a new century. *Applied ergonomics*, 31(6):569–580, 2000.

[22] A Ajoudani, AM Zanchettin, S Ivaldi, A Albu-Schäffer, K Kosuge, and O Khatib. Progress and prospects of the human–robot collaboration. *Autonomous Robots*, 42(5):957–975, 2018.

[23] I El Makrini, K Merckaert, D Lefeber, and B Vanderborght. Design of a collaborative architecture for human-robot assembly tasks. In *International Conference on Intelligent Robots and Systems (IROS)*, pages 1624–1629. IEEE, 2017.

[24] B Vanderborght. Unlocking the potential of industrial human-robot collaboration. Technical report, European Commission, Directorate-General for Research and Innovation, 2019.

[25] O Khatib, K Yokoi, O Brock, K Chang, and A Casal. Robots in human environments: Basic autonomous capabilities. *The International Journal of Robotics Research*, 18(7):684–696, 1999.

[26] D Kulić and E Croft. Pre-collision safety strategies for human-robot interaction. *Autonomous Robots*, 22(2):149–164, 2007.

[27] C Esteves, G Arechavaleta, and J-P Laumond. Motion planning for human-robot interaction in manipulation tasks. In *Mechatronics and Automation, 2005 IEEE International Conference*, volume 4, pages 1766–1771. IEEE, 2005.

[28] B Matthias and T Reisinger. Example application of iso/ts 15066 to a collaborative assembly scenario. In *ISR 2016: 47st International Symposium on Robotics; Proceedings of*, pages 1–5. VDE, 2016.

[29] M Lorenzini, W Kim, E De Momi, and A Ajoudani. A synergistic approach to the real-time estimation of the feet ground reaction forces and centers of pressure in humans with application to human–robot collaboration. *IEEE Robotics and Automation Letters*, 3(4):3654–3661, 2018.

[30] M Lorenzini, W Kim, E De Momi, and A Ajoudani. A learning-based approach to the real-time estimation of the feet ground reaction forces and centres of pressure in humans. In *Sith National Congress of Bioengineering*, 2018.

[31] M Lorenzini, W Kim, E De Momi, and A Ajoudani. A new overloading fatigue model for ergonomic risk assessment with application to human-robot collaboration. In *International Conference on Robotics and Automation (ICRA)*, pages 1962–1968. IEEE, 2019.

[32] M Lorenzini, W Kim, E De Momi, and A Ajoudani. An online method to detect and locate an external load on the human body with applications in ergonomics assessment. *Sensors*, 20(16):4471, 2020.

[33] W Kim, M Lorenzini, K Kapıcıoğlu, and A Ajoudani. Ergotac: A tactile feedback interface for improving human ergonomics in workplaces. *IEEE Robotics and Automation Letters*, 3(4):4179–4186, 2018.

[34] M Lorenzini, W Kim, E De Momi, and A Ajoudani. A real-time graphic interface for the monitoring of the human joint overloadings with application to assistive exoskeletons. In *International Symposium on Wearable Robotics*, pages 281–285. Springer, 2018.

[35] W Kim, M Lorenzini, P Balatti, P DH Nguyen, U Pattacini, V Tikhanoff, L Peternel, C Fantacci, L Natale, G Metta, et al. Adaptable workstations for human-robot collaboration: A reconfigurable framework for improving worker ergonomics and productivity. *IEEE Robotics & Automation Magazine*, 26(3):14–26, 2019.

[36] W Kim, M Lorenzini, P Balatti, Y Wu, and A Ajoudani. Towards ergonomic control of collaborative effort in multi-human mobile-robot teams. In *IEEE/RSJ International Conference on Intelligent Robots and Systems (IROS)*, pages 3005–3011. IEEE, 2019.

[37] M Lorenzini, F Fusaro, P Balatti, E De Momi, F Mastrogiovanni, W Kim, and A Ajoudani. Toward a synergistic framework for human-robot coexistence and collaboration (hrc2). In *Institute for Robotics and Intelligent Machines Conference (I-RIM)*, pages N–A, 2019.

[38] M Bortolini, M Gamberi, F Pilati, and A Regattieri. Automatic assessment of the ergonomic risk for manual manufacturing and assembly activities through optical motion capture technology. *Procedia CIRP*, 72:81–86, 2018.

[39] AJ van der Beek and MH Frings-Dresen. Assessment of mechanical exposure in ergonomic epidemiology. *Occupational and environmental medicine*, 55(5):291–299, 1998.

[40] J Winkel and SE Mathiassen. Assessment of physical work load in epidemiologic studies: concepts, issues and operational considerations. *Ergonomics*, 37(6):979–988, 1994.

[41] RH Westgaard and J Winkel. Guidelines for occupational musculoskeletal load as a basis for intervention: a critical review. *Applied ergonomics*, 27(2):79–88, 1996.

[42] L Ma, D Chablat, F Bennis, W Zhang, and F Guillaume. A new muscle fatigue and recovery model and its ergonomics application in human simulation. *Virtual and Physical Prototyping*, 5(3):123–137, 2010.

[43] GWJ Andreas and E Johanssons. Observational methods for assessing ergonomic risks for work-related musculoskeletal disorders. a scoping review. *Revista Ciencias de la Salud*, 16(SPE):8–38, 2018.

[44] E Nigel Corlett and RP Bishop. A technique for assessing postural discomfort. *Ergonomics*, 19(2):175–182, 1976.

[45] B Shackel, KD Chidsey, and Pat Shipley. The assessment of chair comfort. *Ergonomics*, 12(2):269–306, 1969.

[46] G Borg, G Ljunggren, and R Ceci. The increase of perceived exertion, aches and pain in the legs, heart rate and blood lactate during exercise on a bicycle ergometer. *European journal of applied physiology and occupational physiology*, 54(4):343–349, 1985.

[47] I Kuorinka, B Jonsson, A Kilbom, H Vinterberg, F Biering-Sørensen, G Andersson, and K Jørgensen. Standardised nordic questionnaires for the analysis of musculoskeletal symptoms. *Applied ergonomics*, 18(3):233–237, 1987.

[48] SJ Bigos, M C Battié, DM Spengler, LD Fisher, WE Fordyce, TH Hansson, AL Nachemson, and MD Wortley. A prospective study of work perceptions and psychosocial factors affecting the report of back injury. *Spine*, 16(1):1–6, 1991.

[49] CE Dickinson, K Campion, AF Foster, SJ Newman, AMT O'rourke, and PG Thomas. Questionnaire development: an examination of the nordic musculoskeletal questionnaire. *Applied ergonomics*, 23(3):197–201, 1992.

[50] C Wiktorin, L Karlqvist, J Winkel, and Stockholm MUSIC I Study Group. Validity of self-reported exposures to work postures and manual materials handling. *Scandinavian journal of work, environment & health*, pages 208–214, 1993.

[51] CG Drury and BG Coury. A methodology for chair evaluation. *Applied Ergonomics*, 13(3):195–202, 1982.

[52] T Cox and C Mackay. The measurement of self-reported stress and arousal. *British journal of psychology*, 76(2):183–186, 1985.

[53] REINO UNIDO. Health and safety executive (hse) cost benefit analysis (cba) checklist, 2009.

[54] WM Keyserling, M Brouwer, and BA Silverstein. A checklist for evaluating ergonomic risk factors resulting from awkward postures of the legs, trunk and neck. *International Journal of Industrial Ergonomics*, 9(4):283–301, 1992.

[55] N Moray. Models and measures of mental workload. In *Mental workload*, pages 13–21. Springer, 1979.

[56] A Burdorf and J Laan. Comparison of methods for the assessment of postural load on the back. *Scandinavian journal of work, environment & health*, pages 425–429, 1991.

[57] VZ Priel. A numerical definition of posture. *Human Factors*, 16(6):576–584, 1974.

[58] EN Corlett, SJ Madeley, and I Manenica. Posture targeting: a technique for recording working postures. *Ergonomics*, 22(3):357–366, 1979.

[59] O Karhu, P Kansi, and I Kuorinka. Correcting working postures in industry: a practical method for analysis. *Applied ergonomics*, 8(4):199–201, 1977.

[60] L McAtamney and EN Corlett. Rula: a survey method for the investigation of work-related upper limb disorders. *Applied ergonomics*, 24(2):91–99, 1993.

[61] M Christmansson. The hama-method: a new method for analysis of upper limb movements and risk for work-related musculoskeletal disorders. In *Proceedings of the 12th Triennial Congress of the International Ergonomics Association/Human Factors Association of Canada, August, Toronto*, pages 173–175, 1994.

[62] K Kemmlert. Plibel-the method assigned for identification of ergonomic hazards. In *Handbook of Human Factors and Ergonomics Methods*. CRC Press, 2006.

[63] G Li and P Buckle. A practical method for the assessment of work-related musculoskeletal risks-quick exposure check (qec). 42(19):1351–1355, 1998.

[64] S Hignett and L McAtamney. Rapid entire body assessment (reba). *Applied ergonomics*, 31(2):201–205, 2000.

[65] SH Rodgers. Muscle fatigue assessment: functional job analysis technique. In *Handbook of human factors and ergonomics methods*, pages 130–141. CRC Press, 2004.

[66] D Niosh. Occupational health guidelines for chemical hazards, 1981.

[67] American Conference of Governmental Industrial Hygienists. Tlvs: Threshold limit values for chemical substances and physical substances in the workroom environment with intended changes for 1981., 1981.

[68] D Kee and W Karwowski. Luba: an assessment technique for postural loading on the upper body based on joint motion discomfort and maximum holding time. *Applied ergonomics*, 32(4):357–366, 2001.

[69] SC Monnington, CJ Quarrie, AD Pinder, and LA Morris. Development of manual handling assessment charts (mac) for health and safety inspectors. *Contemporary Ergonomics*, pages 3–8, 2003.

[70] SH Snook and VM Ciriello. The design of manual handling tasks: revised tables of maximum acceptable weights and forces. *Ergonomics*, 34(9):1197–1213, 1991.

[71] E Occhipinti. Ocra: a concise index for the assessment of exposure to repetitive movements of the upper limbs. *Ergonomics*, 41(9):1290–1311, 1998.

[72] K Schaub, G Caragnano, B Britzke, and R Bruder. The european assembly worksheet. *Theoretical Issues in Ergonomics Science*, 14(6):616–639, 2013.

[73] I Shaikh, Y Kim, S Jayaram, U Jayaram, and H Choi. Integration of immersive environment and rula for real-time study of workplace related musculoskeletal disorders in the upper limb. In *International Design Engineering Technical Conferences and Computers and Information in Engineering Conference*, volume 36991, pages 1163–1171, 2003.

[74] SC Puthenveetil, CP Daphalapurkar, W Zhu, MC Leu, XF Liu, JK Gilpin-Mcminn, and SD Snodgrass. Computer-automated ergonomic analysis based on motion capture and assembly simulation. *Virtual Reality*, 19(2):119–128, 2015.

[75] N Vignais, M Miezal, G Bleser, K Mura, D Gorecky, and F Marin. Innovative system for real-time ergonomic feedback in industrial manufacturing. *Applied ergonomics*, 44(4):566–574, 2013.

[76] B Busch, G Maeda, Y Mollard, M Demangeat, and M Lopes. Postural optimization for an ergonomic human-robot interaction. In *2017 IEEE/RSJ International Conference on Intelligent Robots and Systems (IROS)*, pages 2778–2785. IEEE, 2017.

[77] SJ Ray and J Teizer. Real-time construction worker posture analysis for ergonomics training. *Advanced Engineering Informatics*, 26(2):439–455, 2012.

[78] H Haggag, M Hossny, S Nahavandi, and D Creighton. Real time ergonomic assessment for assembly operations using kinect. In *2013 UKSim 15th International Conference on Computer Modelling and Simulation*, pages 495–500. IEEE, 2013.

[79] P Plantard, HPH Shum, A Le Pierres, and F Multon. Validation of an ergonomic assessment method using kinect data in real workplace conditions. *Applied ergonomics*, 65:562–569, 2017.

[80] G Van de Perre, I El Makrini, BB Van Acker, J Saldien, C Vergara, L Pintelon, P Chemweno, R Weuts, K Moons, R Dewil, et al. Improving productivity and worker conditions in assembly part 1: a collaborative architecture and task allocation framework. In *IROS Workshop on Robotic Co-workers 4.0: Human Safety and Comfort in Human-Robot Interactive Social Environments, Location: Madrid, Spain*. IEEE, 2018.

[81] A Malaisé, P Maurice, F Colas, and S Ivaldi. Activity recognition for ergonomics assessment of industrial tasks with automatic feature selection. *IEEE Robotics and Automation Letters*, 2019.

[82] SL Delp, FC Anderson, AS Arnold, P Loan, A Habib, CT John, E Guendelman, and DG Thelen. Opensim: open-source software to create and analyze dynamic simulations of movement. *IEEE transactions on biomedical engineering*, 54(11):1940–1950, 2007.

[83] M Damsgaard, J Rasmussen, ST Christensen, E Surma, and M De Zee. Analysis of musculoskeletal systems in the anybody modeling system. *Simulation Modelling Practice and Theory*, 14(8):1100–1111, 2006.

[84] E YS Chao, RS Armiger, H Yoshida, J Lim, and N Haraguchi. Virtual interactive musculoskeletal system (vims) in orthopaedic research, education and clinical patient care. *Journal of Orthopaedic Surgery and Research*, 2(1):2, 2007.

[85] A Murai, K Kurosaki, K Yamane, and Y Nakamura. Musculoskeletal-see-through mirror: Computational modeling and algorithm for whole-body muscle activity visualization in real time. *Progress in biophysics and molecular biology*, 103(2-3):310–317, 2010.

[86] E Forster. *Predicting muscle forces in the human lower limb during locomotion*. PhD thesis, Universität Ulm, 2004.

[87] M Millard, T Uchida, A Seth, and SL Delp. Flexing computational muscle: modeling and simulation of musculotendon dynamics. *Journal of biomechanical engineering*, 135(2), 2013.

[88] LJ Bhargava, MG Pandy, and FC Anderson. A phenomenological model for estimating metabolic energy consumption in muscle contraction. *Journal of biomechanics*, 37(1):81–88, 2004.

[89] AV Hill. The heat of shortening and the dynamic constants of muscle. *Proceedings of the Royal Society of London. Series B-Biological Sciences*, 126(843):136–195, 1938.

[90] Y Nakamura, K Yamane, Y Fujita, and I Suzuki. Somatosensory computation for man-machine interface from motion-capture data and musculoskeletal human model. *IEEE Transactions on Robotics*, 21(1):58–66, 2005.

[91] F Fraysse, R Dumas, L Cheze, and X Wang. Comparison of global and joint-to-joint methods for estimating the hip joint load and the muscle forces during walking. *Journal of biomechanics*, 42(14):2357–2362, 2009.

[92] K Ayusawa, G Venture, and Y Nakamura. Identifiability and identification of inertial parameters using the underactuated base-link dynamics for legged multibody systems. *The International Journal of Robotics Research*, 33(3):446–468, 2014.

[93] DA Winter. Human balance and posture control during standing and walking. *Gait & posture*, 3(4):193–214, 1995.

[94] IP Herman. *Physics of the human body*, chapter Chapter 1 Terminology, the standard human, and scaling. Springer, 2007.

[95] S Stroeve. Impedance characteristics of a neuromusculoskeletal model of the human arm i. posture control. *Biological cybernetics*, 81(5-6):475–494, 1999.

[96] M IV Mientjes, RW Norman, RP Wells, and SM McGill. Assessment of an emg-based method for continuous estimates of low back compression during asymmetrical occupational tasks. *Ergonomics*, 42(6):868–879, 1999.

[97] J Village, M Frazer, M Cohen, A Leyland, I Park, and A Yassi. Electromyography as a measure of peak and cumulative workload in intermediate care and its relationship to musculoskeletal injury: an exploratory ergonomic study. *Applied ergonomics*, 36(5):609–618, 2005.

[98] D Kumar, KS Rudolph, and KT Manal. Emg-driven modeling approach to muscle force and joint load estimations: Case study in knee osteoarthritis. *Journal of Orthopaedic Research*, 30(3):377–383, 2012.

[99] M Gagnon and G Smyth. Muscular mechanical energy expenditure as a process for detecting potential risks in manual materials handling. *Journal of Biomechanics*, 24(3):191–203, 1991.

[100] A Sušić, T Jurčević Lulić, and F Veljović. Ergonomic evaluation of task execution: Surface electromyography in muscular activity screening. *Periodicum biologorum*, 112(1):33–38, 2010.

[101] CJ De Luca, LD Gilmore, M Kuznetsov, and SH Roy. Filtering the surface emg signal: Movement artifact and baseline noise contamination. *Journal of biomechanics*, 43(8):1573–1579, 2010.

[102] D Farina and R Merletti. A novel approach for precise simulation of the emg signal detected by surface electrodes. *IEEE transactions on biomedical engineering*, 48(6):637–646, 2001.

[103] European Commission. The 2018 ageing report: Economic and budgetary projections for the eu member states (2016-2070). *Institutional Paper No. 79. Luxembourg: Publications Office of the European Union*, 2018.

[104] AG Marin, MS Shourijeh, PE Galibarov, M Damsgaard, L Fritzsch, and F Stulp. Optimizing contextual ergonomics models in human-robot interaction. In *2018 IEEE/RSJ International Conference on Intelligent Robots and Systems (IROS)*, pages 1–9. IEEE, 2018.

[105] P Maurice, V Padois, Y Measson, and P Bidaud. Human-oriented design of collaborative robots. *International Journal of Industrial Ergonomics*, 57:88–102, 2017.

[106] Project sophia: Socio-physical interaction skills for cooperative human-robot systems in agile production. `https://project-sophia.eu/`. Available on line.

[107] Project ergo-lean: Rethinking human ergonomics in lean manufacturing and lean industry. `https://ergolean.eu/`. Available on line.

[108] W Kim, J Lee, N Tsagarakis, and A Ajoudani. A real-time and reduced-complexity approach to the detection and monitoring of static joint overloading in humans. In *Rehabilitation Robotics (ICORR), 2017 International Conference on*, pages 828–834. IEEE, 2017.

[109] S Ivaldi, L Fritzsche, J Babič, F Stulp, M Damsgaard, B Graimann, G Bellusci, and F Nori. Anticipatory models of human movements and dynamics: the roadmap of the andy project. In *Digital Human Models (DHM)*, 2017.

[110] L Rapetti, Y Tirupachuri, G Nava, C Latella, K Darvish, and D Pucci. Partner-aware humanoid robot control: from robot-robot collaboration to human-robot collaboration and ergonomy control. In *Workshop on Progress in Ergonomic Physical Human-Robot Interaction at IEEE/RSJ International Conference on Intelligent Robots and Systems*, 2019.

[111] S Cotton, AP Murray, and P Fraisse. Estimation of the center of mass: from humanoid robots to human beings. *IEEE/ASME Transactions on Mechatronics*, 14(6):707–712, 2009.

[112] K Aminian and B Najafi. Capturing human motion using body-fixed sensors: outdoor measurement and clinical applications. *Computer animation and virtual worlds*, 15(2):79–94, 2004.

[113] D Roetenberg, H Luinge, and P Slycke. Xsens mvn: Full 6dof human motion tracking using miniature inertial sensors. *Xsens Motion Technologies BV, Tech. Rep*, 1, 2009.

[114] AK Bourke, KJ O'Donovan, and G Olaighin. The identification of vertical velocity profiles using an inertial sensor to investigate pre-impact detection of falls. *Medical Engineering & Physics*, 30(7):937–946, 2008.

[115] TB Moeslund, A Hilton, and V Krüger. A survey of advances in vision-based human motion capture and analysis. *Computer vision and image understanding*, 104(2-3):90–126, 2006.

[116] E van der Kruk and MM Reijne. Accuracy of human motion capture systems for sport applications; state-of-the-art review. *European journal of sport science*, 18(6):806–819, 2018.

[117] M Field, D Stirling, F Naghdy, and Z Pan. Motion capture in robotics review. In *2009 IEEE International Conference on Control and Automation*, pages 1697–1702. IEEE, 2009.

[118] A Patrizi, E Pennestrì, and PP Valentini. Comparison between low-cost marker-less and high-end marker-based motion capture systems for the computer-aided assessment of working ergonomics. *Ergonomics*, 59(1):155–162, 2016.

[119] V Camomilla, R Dumas, and A Cappozzo. Human movement analysis: The soft tissue artefact issue. *Journal of Biomechanics*, 2017.

[120] Xsens Technologies. *MVN User Manual*. Xsens Technologies, 2015.

[121] Kistler Group. Kistler type 9260aa data sheet. `http://www.helmar.com.pl/helmar/plik/pdf/9260aa3__000_729e_04_nn3819.pdf`, 2009. Available on line.

[122] A González, M Hayashibe, V Bonnet, and P Fraisse. Whole body center of mass estimation with portable sensors: Using the statically equivalent serial chain and a kinect. *Sensors*, 14(9):16955–16971, 2014.

[123] G Venture, K Ayusawa, and Y Nakamura. Real-time identification and visualization of human segment parameters. In *2009 Annual International Conference of the IEEE Engineering in Medicine and Biology Society*, pages 3983–3986. IEEE, 2009.

[124] B Espiau and R Boulic. On the computation and control of the mass center of articulated chains. *Rapport de Recherche Inria*, 1998.

[125] MB Popovic, A Goswami, and H Herr. Ground reference points in legged locomotion: Definitions, biological trajectories and control implications. *The International Journal of Robotics Research*, 24(12):1013–1032, 2005.

[126] PR Bélanger, P Dobrovolny, A Helmy, and X Zhang. Estimation of angular velocity and acceleration from shaft-encoder measurements. *The International Journal of Robotics Research*, 17(11):1225–1233, 1998.

[127] A González, M Hayashibe, E Demircan, and P Fraisse. Center of mass estimation for rehabilitation in a multi-contact environment: A simulation study. In *Systems, Man, and Cybernetics (SMC), 2013 IEEE International Conference on*, pages 4718–4723. IEEE, 2013.

[128] J Carpentier, M Benallegue, N Mansard, and J Laumond. Center-of-mass estimation for a polyarticulated system in contact - a spectral approach. *IEEE Transactions on Robotics*, 32(4):810–822, 2016.

[129] W Kim, J Lee, L Peternel, N Tsagarakis, and A Ajoudani. Anticipatory robot assistance for the prevention of human static joint overloading in human–robot collaboration. *IEEE Robotics and Automation Letters*, 3(1):68–75, 2018.

[130] DA Winter. Human balance and posture control during standing and walking. *Gait & posture*, 3(4):193–214, 1995.

[131] B Michael and M Howard. Eliminating motion artifacts from fabric-mounted wearable sensors. In *2014 IEEE-RAS International Conference on Humanoid Robots*, pages 868–873. IEEE, 2014.

[132] J Ziegler, H Kretzschmar, C Stachniss, G Grisetti, and W Burgard. Accurate human motion capture in large areas by combining imu-and laser-based people tracking. In *International Conference on Intelligent Robots and Systems (IROS)*, pages 86–91. IEEE, 2011.

[133] M Kok, JD Hol, and TB Schön. Using inertial sensors for position and orientation estimation. *arXiv preprint arXiv:1704.06053*, 2017.

[134] JM Wang, DJ Fleet, and A Hertzmann. Gaussian process dynamical models for human motion. *IEEE transactions on pattern analysis and machine intelligence*, 30(2):283–298, 2007.

[135] NL Johnson, S Kotz, and N Balakrishnan. *Continuous univariate distributions*. John Wiley & Sons, Ltd, 1995.

[136] G Gao. Statistical modeling of sar images: A survey. *Sensors*, 10(1):775–795, 2010.

[137] TW Anderson and DA Darling. A test of goodness of fit. *Journal of the American statistical association*, 49(268):765–769, 1954.

[138] MA Stephens. Edf statistics for goodness of fit and some comparisons. *Journal of the American statistical Association*, 69(347):730–737, 1974.

[139] VJ Easton and JH. McColls. Statistics glossary v1.1. `http://www.stats.gla.ac.uk/steps/glossary/`. Available on line.

[140] C Bulpitt. Confidence intervals. *Lancet*, 1(8531):494–7, 1987.

[141] BJ Stephens and CG Atkeson. Dynamic balance force control for compliant humanoid robots. In *Intelligent Robots and Systems (IROS), 2010 IEEE/RSJ International Conference on*, pages 1248–1255. IEEE, 2010.

[142] S Lee and A Goswami. A momentum-based balance controller for humanoid robots on non-level and non-stationary ground. *Autonomous Robots*, 33(4):399–414, 2012.

[143] L Righetti, J Buchli, M Mistry, and S Schaal. Control of legged robots with optimal distribution of contact forces. In *Humanoid Robots (Humanoids), 2011 11th IEEE-RAS International Conference on*, pages 318–324. IEEE, 2011.

[144] S Hyon, JG Hale, and G Cheng. Full-body compliant human–humanoid interaction: balancing in the presence of unknown external forces. *IEEE Transactions on Robotics*, 23(5):884–898, 2007.

[145] U Lugrís, J Carlín, R Pàmies-Vilà, JM Font-Llagunes, and J Cuadrado. Solution methods for the double-support indeterminacy in human gait. *Multibody system dynamics*, 30(3):247–263, 2013.

[146] L Ren, RK Jones, and D Howard. Whole body inverse dynamics over a complete gait cycle based only on measured kinematics. *Journal of biomechanics*, 41(12):2750–2759, 2008.

[147] T Sim, H Kwon, SE Oh, S Joo, A Choi, Hyun M Heo, K Kim, and JH Mun. Predicting complete ground reaction forces and moments during gait with insole plantar pressure information using a wavelet neural network. *Journal of biomechanical engineering*, 137(9), 2015.

[148] HS Choi, CH Lee, M Shim, JI Han, and YS Baek. Design of an artificial neural network algorithm for a low-cost insole sensor to estimate the ground reaction force (grf) and calibrate the center of pressure (cop). *Sensors*, 18(12):4349, 2018.

[149] K Hornik. Approximation capabilities of multilayer feedforward networks. *Neural networks*, 4(2):251–257, 1991.

[150] S Karsoliya. Approximating number of hidden layer neurons in multiple hidden layer bpnn architecture. *International Journal of Engineering Trends and Technology*, 3(6):714–717, 2012.

[151] L Fortini, M Lorenzini, W Kim, E De Momi, and A Ajoudani. A real-time tool for human ergonomics assessment based on joint compressive forces. In *2020 International Conference on Robot & Human Interactive Communication (RO-MAN)*. IEEE, 2020.

[152] M Whitmore, J Boyer, and K Holubec. *NASA-STD-3001, Space Flight Human-System Standard and the Human Integration Design Handbook*. NASA, 2012.

[153] World Health Organization et al. Protecting workers' health series no. 5. preventing musculoskeletal disorders in the workplace; 2003, 2016.

[154] DM Jessop and MTG Pain. Maximum velocities in flexion and extension actions for sport. *Journal of human kinetics*, 50(1):37–44, 2016.

[155] WS Marras, SA Lavender, SE Leurgans, FA Fathallah, SA Ferguson, Gary AW, and SL Rajulu. Biomechanical risk factors for occupationally related low back disorders. *Ergonomics*, 38(2):377–410, 1995.

[156] JB Malchaire, NA Cock, A Piette, R Dutra Leao, M Lara, and F Amaral. Relationship between work constraints and the development of musculoskeletal disorders of the wrist: a prospective study. *International Journal of Industrial Ergonomics*, 19(6):471–482, 1997.

[157] WS Marras and RW Schoemarxlin. Wrist motions in industry. *Ergonomics*, 36(4):341–351, 1993.

[158] A Bhattacharya, M Mueller, and V Putz-Anderson. Traumatogenic factors affecting the knees of carpet installers. *Applied Ergonomics*, 16(4):243–250, 1985.

[159] KA Grant, PW Johnson, and TL Galinsky. Evaluation of an accelerometric activity monitor as an exposure assessment tool in ergonomic studies. *Applied Occupational and Environmental Hygiene*, 10(5):461–466, 1995.

[160] J Jovic, A Escande, K Ayusawa, E Yoshida, A Kheddar, and G Venture. Humanoid and human inertia parameter identification using hierarchical optimization. *IEEE Transactions on Robotics*, 32(3):726–735, 2016.

[161] SH Hyon. Compliant terrain adaptation for biped humanoids without measuring ground surface and contact forces. *IEEE Transactions on Robotics*, 25(1):171–178, Beb 2009.

[162] H Jeong, K Yamada, M Kido, S Okada, T Nomura, and Y Ohno. Analysis of Difference in Center-of-Pressure Positions between Experts and Novices during Asymmetric Lifting. *IEEE Journal of Transl. Eng. in Health and Medicine*, 4:1–11, 2016.

[163] JC E Van Der Burg, JH Van Dieën, and HM Toussaint. Lifting an unexpectedly heavy object: The effects on low-back loading and balance loss. *Clinical Biomechanics*, 15(7):469–477, 2000.

[164] DE Anderson, ML Madigan, and MA Nussbaum. Maximum voluntary joint torque as a function of joint angle and angular velocity: model development and application to the lower limb. *Journal of biomechanics*, 40(14):3105–3113, 2007.

[165] JZ Liu, RW Brown, and GH Yue. A dynamical model of muscle activation, fatigue, and recovery. *Biophysical journal*, 82(5):2344–2359, 2002.

[166] DD Wood, DL Fisher, and RO Andres. Minimizing fatigue during repetitive jobs: optimal work-rest schedules. *Human factors*, 39(1):83–101, 1997.

[167] D Imbeau, B Farbos, et al. Percentile values for determining maximum endurance times for static muscular work. *International Journal of Industrial Ergonomics*, 36(2):99–108, 2006.

[168] BP Bernard and V Putz-Anderson. Musculoskeletal disorders and workplace factors; a critical review of epidemiologic evidence for work-related musculoskeletal disorders of the neck, upper extremity, and low back. *DHHS (NIOSH) Publication*, 1997.

[169] L Peternel, W Kim, J Babič, and A Ajoudani. Towards ergonomie control of human-robot co-manipulation and handover. In *Humanoid Robotics (Humanoids), 2017 IEEE-RAS 17th International Conference on*, pages 55–60. IEEE, 2017.

[170] V Balasubramanian and S Jayaraman. Surface emg based muscle activity analysis for aerobic cyclist. *Journal of bodywork and movement therapies*, 13(1):34–42, 2009.

[171] MA Nussbaum. Static and dynamic myoelectric measures of shoulder muscle fatigue during intermittent dynamic exertions of low to moderate intensity. *European journal of applied physiology*, 85(3-4):299–309, 2001.

[172] S Thongpanja, A Phinyomark, P Phukpattaranont, and C Limsakul. Mean and median frequency of emg signal to determine muscle force based on time-dependent power spectrum. *Elektronika ir Elektrotechnika*, 19(3):51–56, 2013.

[173] G Björing and G Hägg. Musculoskeletal exposure of manual spray painting in the woodworking industry-an ergonomic study on painters. *International Journal of Industrial Ergonomics*, 26(6):603–614, 2000.

[174] L Ren, RK Jones, and D Howard. Predictive modelling of human walking over a complete gait cycle. *Journal of biomechanics*, 40(7):1567–1574, 2007.

[175] IH Chen, KN Kuo, and TP Andriacchi. The influence of walking speed on mechanical joint power during gait. *Gait & Posture*, 6(3):171–176, 1997.

[176] J Yang, RT Marler, H Kim, J Arora, and K Abdel-Malek. Multi-objective optimization for upper body posture prediction. In *10th AIAA/ISSMO multidisciplinary analysis and optimization conference*, page 4506, 2004.

[177] JR Potvin and RW Norman. Quantification of erector spinae muscle fatigue during prolonged, dynamic lifting tasks. *European journal of applied physiology and occupational physiology*, 67(6):554–562, 1993.

[178] H Shin and J Kim. Measurement of trunk muscle fatigue during dynamic lifting and lowering as recovery time changes. *International journal of industrial ergonomics*, 37(6):545–551, 2007.

[179] HB Maynard, GJ Stegmerten, and JL Schwab. *Methods-Time Measurement*. McGraw-Hill, 1948.

[180] G Caragnano and R Bonfiglioli. The ergo-uas system and a new design approach: Overview and validation. In *Congress of the International Ergonomics Association*, pages 787–792. Springer, 2018.

[181] CF Estill, LA MacDonald, TB Wenzl, and MR Petersen. Use of accelerometers as an ergonomic assessment method for arm acceleration a large-scale field trial. *Ergonomics*, 43(9):1430–1445, 2000.

[182] R Azuma, Y Baillot, R Behringer, S Feiner, S Julier, and B MacIntyre. Recent advances in augmented reality. *IEEE computer graphics and applications*, 21(6):34–47, 2001.

[183] M Gášová, M Gašo, and A Štefánik. Advanced industrial tools of ergonomics based on industry 4.0 concept. *Procedia engineering*, 192:219–224, 2017.

[184] J Egger and T Masood. Augmented reality in support of intelligent manufacturing–a systematic literature review. *Computers & Industrial Engineering*, 140:106195, 2020.

[185] H Shakarkan and N Arshadi. Transportation research part f: Traffic psychology and behaviour. *J. Educ. Psychol*, 14:129–148, 2007.

[186] S Condino, M Carbone, R Piazza, M Ferrari, and V Ferrari. Perceptual limits of optical see-through visors for augmented reality guidance of manual tasks. *IEEE Transactions on Biomedical Engineering*, 67(2):411–419, 2019.

[187] JH Abbott. A novel approach to managing graduated return to spinal loading in patients with low back pain using the spineangel® device: a case series report. *NZ Journal of Physiotherapy*, 36(1):22, 2008.

[188] Y Li, WR Jeon, and CS Nam. Navigation by vibration: Effects of vibrotactile feedback on a navigation task. *International Journal of Industrial Ergonomics*, 46:76–84, 2015.

[189] DA Ross and BB Blasch. Evaluation of orientation interfaces for wearable computers. In *Wearable Computers, The Fourth International Symposium on*, pages 51–58. IEEE, 2000.

[190] K Bark, P Khanna, R Irwin, P Kapur, SA Jax, LJ Buxbaum, and KJ Kuchenbecker. Lessons in using vibrotactile feedback to guide fast arm motions. In *World Haptics Conference (WHC), 2011 IEEE*, pages 355–360. IEEE, 2011.

[191] AU Alahakone and SMN Senanayake. A real-time system with assistive feedback for postural control in rehabilitation. *IEEE/ASME Transactions on Mechatronics*, 15(2):226–233, 2010.

[192] M Aggravi, G Salvietti, and D Prattichizzo. Haptic assistive bracelets for blind skier guidance. In *Proceedings of the 7th Augmented Human International Conference 2016*, pages 1–4, 2016.

[193] S Brumagne, L Janssens, E Janssens, and L Goddyn. Altered postural control in anticipation of postural instability in persons with recurrent low back pain. *Gait & posture*, 28(4):657–662, 2008.

[194] P Hlavackova, J Fristios, R Cuisinier, N Pinsault, M Janura, and N Vuillerme. Effects of mirror feedback on upright stance control in elderly transfemoral amputees. *Archives of physical medicine and rehabilitation*, 90(11):1960–1963, 2009.

[195] RW Cholewiak and AA Collins. Sensory and physiological bases of touch. *The psychology of touch*, pages 23–60, 1991.

[196] SE Mathiassen, T Möller, and M Forsman. Variability in mechanical exposure within and between individuals performing a highly constrained industrial work task. *Ergonomics*, 46(8):800–824, 2003.

[197] W Kim, M Lorenzini, P Balatti, Y Wu, and A Ajoudani. Towards ergonomic control of collaborative effort in multi-human mobile-robot teams. *The IEEE/RSJ International Conference on Intelligent Robots and Systems (IROS)*, 2019.

[198] E Rueckert, J Čamernik, J Peters, and J Babič. Probabilistic Movement Models Show that Postural Control Precedes and Predicts Volitional Motor Control. *Scientific reports*, 6:28455, jun 2016.

[199] T Yoshikawa. Manipulability of Robotic Mechanisms. *The Intl. Journal of Robotics Research*, 4(2):3–9, jun 1985.

[200] A Ajoudani, SB Godfrey, M Bianchi, MG Catalano, G Grioli, N Tsagarakis, and A Bicchi. Exploring teleimpedance and tactile feedback for intuitive control of the pisa/IIT soft hand. *IEEE Transactions on Haptics*, 7(2):203–215, 2014.